Converged wireline and wireless signal distribution in optical fiber access networks

Prince, Kamau

Publication date:
2010

Document Version
Publisher's PDF, also known as Version of record

TECHNICAL UNIVERSITY OF DENMARK

Converged Wireline and Wireless Signal Distribution in Optical Fiber Access Networks

Kamau Prince

DTU Fotonik
Department of Photonics Engineering

July 2010

"The mathematical sciences particularly exhibit order, symmetry, and limitation; and these are the greatest forms of the beautiful."

– Aristotle

"Concepts that have proven useful in ordering things easily achieve such authority over us that we forget their earthly origins and accept them as unalterable givens. Thus they might come to be stamped as 'necessities of thought,' 'a priori givens,' etc. The path of scientific progress is often made impassable for a long time by such errors. Therefore it is by no means an idle game if we become practiced in analysing long-held commonplace concepts and showing the circumstances on which their justification and usefulness depend, and how they have grown up, individually, out of the givens of experience. Thus their excessive authority will be broken. They will be removed if they cannot be properly legitimated, corrected if their correlation with given things be far too superfluous, or replaced if a new system can be established that we prefer for whatever reason."

– Einstein

Abstract

This thesis presents results obtained during the course of my doctoral studies into the transport of fixed and wireless signaling over a converged optical access infrastructure. In the formulation, development and assessment of a converged paradigm for multiple-services delivery via optical access networking infrastructure, I have been able to demonstrate increased functionalities that may be achieved with existing optical technologies and mature, commercially-available optoelectronic devices. I have developed novel systems for extending the range of optical access systems, and have repeatedly demonstrated the re-purposing of standard digital devices in supporting new base-band and radio-frequency communication systems.

Highlights of this research include significant extension of known bounds on free-running, long-wavelength (1.55 μm) VCSEL transmission at 10 Gbps, through the implementation of field-deployable chromatic dispersion compensation fibers; the implementation of continuously-variable true-time delay of WiMAX signaling for an adaptive antenna system, and the development of simple schemes for UWB signal generation and transmission in a long-reach optical access network link. Other key results include the pioneering demonstration of simultaneous error-free transmission of converged baseband and standards-compliant multi-protocol RF wireless signaling via a 78 km optical access link; as well as the demonstration of a new method for implementing all-optical signal downconversion for long-reach optical transmission of baseband and RF wireless signals.

This thesis additionally includes a formal development of the converged service-delivery paradigm that has guided the design and implementation of the work done within this project.

Resumé

Denne afhandling præsenterer resultaterne af mine ph.d.-studier i transport af faste og trådløse signaler over en fast optisk netværk infrastruktur. Vi har udviklet nye systemer til at udvide den praktiske vifte af optiske signalsystemer, og har gentagne gange vist, at brug af standard digitale enheder kan støtte applikationer med nye base-bånd og radio-frekvens-systemer.

Højdepunkter i denne forskning omfatter udvidelse af kendte grænser for fri-løb, lang bølgelængde (1.55 μm) VCSEL transmission med 10 Gbps, gennemførelsen af kontinuerligt variabel sand-tidsforsinkelse af WiMAX signaler til et adaptivt antennesystem, og udvikling af simple ordninger for UWB signalgenerering og transmission. Andre vigtige resultater omfatter den banebrydende demonstration af samtidig fejlfri transmission af forskellige signaler via et 78 km optiske link, og demonstration af helt optisk signal nedkonvertering for optisk transmission med lang rækkevidde.

Denne afhandling indeholder en formel udvikling af det paradigme om konvergeret service aflevering, der har ligget til grund for udformningen og gennemførelsen af det arbejde, der udføres inden for dette projekt.

Acknowledgements

I would first like to thank my thesis advisor, Professor Idelfonso Tafur Monroy, for allowing me the opportunity to pursue doctoral studies within the Metro Access and Short Range Systems group, and for providing essential guidance and feedback during the course of my studies at DTU Fotonik.

I am also grateful to Associate Professor Ernesto Ciaramella, for accepting me into his research group at the Scuola Superiore Sant'Anna in Pisa, Italy, and for allowing me to work in the optical research laboratories of the Consorzio Nazionale Interuniversitario per le Telecomunicazioni (CNIT) in that city. I must also express my gratitude to Marco Presi and family, for invaluable guidance and support throughout (and after) my stay in Italy. I would also like to thank Giampiero Contestabile, Isabella Cerrutti, Luca Valcarenghi, Luca Ascari, Marco Secondini, and other esteemed members of the CNIT/Sant'Anna research community, for welcoming me into the group, and for providing timely advice and assistance during my candidature. This applies equally well for *calcetto*, access to hidden gems in Tuscany and the South, and for providing me with invaluable support during some of the less well-lit days of my candidature. (*A Morrona e Terriciola, grazie di tutto!!*)

I am grateful to the august researchers at DTU Fotonik, including Mrs. Beata Zsigri, and Anders Clausen, Jorge Seoane, Timothy Gibbon, Xianbin Yu, Jesper Jensen and Darko Zibar for sharing in such a fantastic research environment - I will treasure memories of the convival and competitive atmosphere. Thanks also for continually striving to provide clear answers to my never-ending stream of questions (and babble). I must also thank Mrs. Hua Ji, and Antonio Caballero, Roberto Rodes, and Yongsheng Cao, my office mates at DTU Fotonik, for their tolerance and counsel through coffee addictions and sleepless weekends; and also for encouraging me to seek professional therapy as required. During my first few months at DTU, I was privileged enough to share an office and a few experiments with Víctor Torres-Company, then a visiting PhD scholar; I am proud to acknowledge the influence of his thoroughness, creativity and enthusiasm in developing my own approach to scientific research.

Much of the work realized during my candidature would not have been possible without access to first-rate laboratory equipment: I must therefore thank my forbears at DTU Fotonik and Sant'Anna, for having built up such impressive research

facilities, and for training me in its proper care and use. (Sometimes however, eagerness outweighed caution - my profound apologies.) I am also grateful for having been allowed access to some of the latest signal quality evaluation systems commercially available, and being simultaneously able to strengthen professional relationships with other scientists in the field.

I am profoundly indebted to Christophe Peucheret and Martin Schubert, for their patience in reading through early drafts of this thesis, and providing timely and invaluable feedback. (Sincerest apologies for having buried vague threads of logic in such cumbersome text; thanks for helping me pick them out from the chaff.) I must additionally thank the senior researchers at the former COM.DTU research group, especially Professor Palle Jeppesen, for his sage counsel on varied aspects of research, life and tennis. Many thanks also to Professor Leif Oxenløwe, for providing ready access to refreshing feedback, frank (and often eye-opening) discussions and an infinite supply of fresh espresso. Respects.

I will always be thankful for having met the Administrative group at DTU Fotonik, especially Ms. Lone Bjørnstjerne, Ms. Britt Boding, Ms. Anja Sohn Henriksen and Ms. Vivi Brackley. I've been overwhelmingly happy (and extremely grateful) to know where to turn when, say, my work permit application has mysteriously stalled, or when I needed to convince the beloved Tax Department that I'm not living the high life on the Italian Riviera (please don't tax me at the billionaire rate). Thanks for all the million little things.

Thanks to my darling Anastasia Permyakova, for enriching my life with your grace, forbearance and understanding.

I am also deeply indebted for the stellar support and encouragement always provided by my adoptive family: thanks again Martin, Elaine, Alex, Stephan, Evarist, Jure, Jana, Neil and Alexey for the criticism, food, laughs, drama, music and understanding.

And finally, I must thank my family, especially my parents, Mrs. Maureen Webster and Lloyd Prince, and my brother, Shomari Prince; for continually supporting my desire to seek knowledge and adventure, and to try a less-familiar path through the world. I will remain forever grateful for your encouragement and repeated advice to continue testing my abilities and striving for best results.

April 2010.

Contents

List of Figures

List of Tables

Abbreviations

3G	**T**hird-**g**eneration mobile telephone technologies
4G	**F**ourth-**g**eneration mobile telephone technologies
802.11	WLAN standards (IEEE 802.11 a/b/g/n)
802.16	WiMAX standards (including IEEE 802.16 d/e/j)
AAS	**A**daptive **A**ntenna **S**ystem
AWG	**A**rrayed **W**aveguide **G**rating
CATV	**C**ommunity **A**ntenna **T**ele**v**ision (**Ca**ble **TV**)
CO	**C**entral **O**ffice (node)
CP	**C**ustomer **P**remises (node)
CPE	**C**ustomer **P**remises **E**quipment
dB	**d**eci**B**el, logarithmic unit of relative measurement
DBA	**D**ynamic **B**andwidth **A**llocation
DFB	**D**istributed **F**eed-**b**ack
DL	**D**own**l**ink
DSL	**D**igital **S**ubscriber **L**ine
DSO	**D**igital **S**torage **O**scilloscope
EMI	**E**lectro-**M**agnetic **I**nterference
FWHM	**F**ull-**W**idth at **H**alf-**M**aximum (bandwidth)
HDTV	**H**igh **D**efinition **T**ele**v**ision
IEE	**I**nstitute of **E**lectrical **E**ngineers (U.K.-based)
IEEE	**I**nstitute of **E**lectrical and **E**lectronic **E**ngineers (U.S.A.-based)
ITU	**I**nternational **T**elecommunications **U**nion
ITU-T	**T**elecommunication Standardization Sector of the **ITU**

LAN	**L**ocal **A**rea **N**etwork
laser	**l**ight **a**mplification by **s**timulated **e**mission of **r**adiation
LTE	3GPP **L**ong-**T**erm **E**volution, a mobile networking standard
maser	**m**icrowave **a**mplification by **s**timulated **e**mission of **r**adiation
MQW	**M**ultiple-**Q**uantum-**W**ell
OBPF	**O**ptical **B**and-**P**ass **F**ilter
OAN	**O**ptical **A**ccess **N**etwork
OCDMA	**O**ptical **C**ode **D**ivision **M**ultiple-**A**ccess
OEO	**O**ptical-**E**lectrical-**O**ptical (signal conversion)
OTDM	**O**rthogonal **T**ime **D**ivision **M**ultiplexing
PON	**P**assive **O**ptical **N**etwork
PSTN	**P**ublic **S**witched **T**elephony **N**etwork
QAM	**Q**uadrature **A**mplitude **M**odulation
RN	**R**emote **N**ode
RoF	**R**adio **o**ver **F**iber
RF	**R**adio-**f**requency
TDM	**T**ime **D**ivision **M**ultiplexing
TTD	**T**rue-**T**ime **D**elay
UL	**U**p**l**ink
UMTS	**U**niversal **M**obile **T**elecommunications **S**ystem
UWB	**U**ltra **W**ide**b**and wireless RF signaling technology
WDM	**W**avelength **D**ivision **M**ultiplexing
WiFi	**Wi**reless **Fi**delity (IEEE 802.11 WLAN compliance)
WiMAX	**W**orldwide **I**nteroperability for **M**icrowave **Acc**ess
WLAN	**W**ireless **LAN**
xDSL	Generic designator for **DSL** technology

Symbols

$A_\Delta(t)$	Time-varying signal ampitude	V
D	fiber dispersion parameter	ps/nm·km
$f_\Delta(t)$	RF waveform carrier frequency	Hz
P_1	1 dB compression power point	W
P_3	Third-order intercept power point	W
λ_0	vacuum wavelength	nm
$\phi_\Delta(t)$	(modulated) phase	rads^{-1}

For my family;

always encouraging me to stop being precious
and get on with it.

Summary of Original Work

This thesis is based on the following journal publications:

Paper A K. Prince, I. Tafur Monroy, J. Seoane and P. Jeppesen, "All-optical envelope detection for radio-over-fiber links using external optical injection of a DFB laser," *Optics Express*, vol. 16, no. 3, pp. 2005–2014, Feb. 2008.

Paper B K. Prince and I. Tafur Monroy, "All-optical envelope detection and fiber transmission of wireless signals by external injection of a DFB laser," *IEEE Photon. Technol. Lett.*, vol. 20, no. 15, pp. 1317–1319, Feb. 2008.

Paper C V. Torres-Company, K. Prince and I. Tafur Monroy, "Fiber transmission and generation of ultrawideband pulses by direct current modulation of semiconductor lasers and chirp-to-intensity conversion," *Optics Letters*, vol. 33, no. 3, pp. 222–224, Feb. 2008.

Paper D V. Torres, K. Prince and I. Tafur Monroy, "Ultrawideband pulse generation based on overshooting effect in gain-switched semiconductor laser," *IEEE Photon. Technol. Lett.*, vol. 20, pp. 1299–1301, Aug.1, 2008.

Paper E K. Prince, J. B. Jensen, A. Caballero, X. Yu, T. Gibbon, D. Zibar, N. Guerrero, A. V. Osadchiy and I. Tafur Monroy, "Converged wireline and wireless access over a 78-km deployed fiber long-reach WDM PON," *IEEE Photon. Technol. Lett.*, vol. 21, pp. 1274–1276, Sept. 1 2009.

Paper F K.Prince, M. Presi, A. Chiuchiarelli, I. Cerutti, G. Contestabile, I.Tafur Monroy and E. Ciaramella, "Variable delay with directly-modulated

R-SOA and optical filters for adaptive antenna radio-fiber access," *J. Lightwave Technol.*, vol. 27, pp. 5056–5064, Nov. 2009.

Paper G A. V. Osadchiy, K. Prince, and I. Tafur Monroy, "Converged delivery of WiMAX and wireline services over an extended reach passive optical access network," *Optical Fiber Technology*, vol. 16, pp. 182 – 186, April 2010.

Paper H K. Prince, M. Ma, T. B. Gibbon, C. Neumeyr, E. Rönneberg, M. Ortsiefer and I. Tafur Monroy, "10.7-Gb/s passive optical network uplink with uncooled, free-running, directly-modulated 1550-nm VCSEL and inverse dispersion fiber." In preparation for submission to Journal of Optical Networking, April 2010.

Other scientific reports published during this project:

1. N. Guerrero Gonzalez, K. Prince, D. Zibar, and I. Tafur Monroy, "Reconfigurable digital receiver for optically envelope detected half cycle BPSK and MSK radio-on-fiber signals." In preparation for journal submission.
2. K. Prince and I. Tafur Monroy, "Multi-band all-optical halfwave rectification, transmission and down-conversion." In preparation for journal submission.
3. M. Presi, R. Proietti, K. Prince, G. Contestabile and E. Ciaramella, "A 80 km reach fully passive WDM-PON based on reflective ONUs,"*Optics Express*, vol. 16, no. 23, pp. 19043-19048, Nov. 2008.
4. K. Prince, M. Ma, T.B. Gibbon and I. Tafur Monroy, "Demonstration of 10.7 Gb/s transmission in 50-km PON with uncooled free-running 1550-nm VCSEL." To be presented at *Conference for Lasers and Electro-Optic Society & Quantum Electronics and Laser Science Conference (CLEO/QELS)*, (San Jose, CA, USA) May 2010. Paper ATuA2.
5. T. B. Gibbon, K. Prince, C. Neumeyr, E. Rönneberg, M. Ortsiefer, and I. Tafur Monroy, "10 Gb/s 1550 nm VCSEL transmission over 23.6 km single mode fiber with no dispersion compensation and no injection locking for WDM PONs," in *Proceedings Optical Fiber Communication/National Fiber Optic Engineers Conference (OFC/NFOEC)*, (San Jose, CA, USA) March 2010. Paper JThA30.
6. M. Presi, K. Prince, A. Chiuchiarelli, I. Cerutti, G. Constabile, I. Tafur Monroy and E. Ciaramella, "Adaptive antenna system for OFDMA WiMAX

radio-over-fiber links using a directly modulated R-SOA and optical filtering" in *Proceedings of the Optical Fiber Communication Conference and Exposition and the National Fiber Optic Engineers Conference (OFC/NFOEC)*, (San Diego, CA, USA), March 2009. Paper JWA74.

7. J. Seoane, I. Tafur Monroy, K. Prince and P. Jeppesen, "Local-oscillator-free wireless-optical-wireless data link at 1.25 Gbit/s over a 40 GHz carrier employing carrier preservation and envelope detection," in *Proceedings of the Conference on Optical Fiber Communication/National Fiber Optic Engineers Conference (OFC/NFOEC)*, (San Diego, California, USA), Feb. 2008. Paper OThD4.

8. K. Prince, I. Tafur Monroy, "Converged fixed and radio-over-fiber link employing optical envelope detection and optically injected DFB laser," in *Proceedings of the Conference on Optical Fiber Communication/National Fiber Optic Engineers Conference (OFC/NFOEC)*, (San Diego, California, USA), Feb. 2008. Paper OThD7.

9. K. Prince, A. V. Osadchiy and I. Tafur Monroy, "WiMAX radio-on-fibre in 118-km long-reach PON with deployed fibre," in *Proceedings of the 35th. European Conference on Optical Communication (ECOC)* (Vienna, Austria) Sept. 2009. Paper 2.4.1.

10. M. Presi, R. Proietti, K. Prince, G. Contestabile and E. Ciaramella, "A novel line coding pair for fully passive long reach WDM-PONs," in *Proceedings of the 34th. European Conference on Optical Communication (ECOC)*, pp. 43-44, Sept. 2008, (Brussels, Belgium). Paper Th.1.F.1.

11. K. Prince, A. V. Osadchiy and I. Tafur Monroy, "Full-duplex transmission of 256-QAM WiMAX signals over an 80-km long-reach PON," in *Proceedings of the 22nd. Annual Meeting of the IEEE Photonics Society* (LEOS), (Belek-Antalya, Turkey), October 2009. Paper WS1.

12. K. Prince, A. Chiuchiarelli, M. Presi, I. Tafur Monroy and E. Ciaramella, "All-optical delay technique for supporting multiple antennas in a hybrid optical - wireless transmission system," in *Proceedings of the 21st. Annual Meeting of the IEEE Lasers & Electro-Optics Society (LEOS)*, (Newport Beach, CA, USA), pp. 85 - 86, Nov. 2008. Paper MJ3.

13. I. Tafur Monroy, K. Prince, J. Seoane and X. Yu, "Optically envelope detected QAM and QPSK RF modulated signals in hybrid wireless-fiber systems," in *Microwave & Optical Technology Letters*, vol. 51, no. 3, pp. 864-866, March 2009.

14. I. Tafur Monroy, N. Guerrero Gonzales, A. Caballero Jambrina, K. Prince, D. Zibar, T. B. Gibbon, X. Yu and J. B. Jensen "Convergencia de sistemas de comunicación ópticos e inalámbricos," (Converged wireless and optical communication systems). Optica Pura y Aplicada, vol. 42, no. 2, pp. 83-90, June 2009.

15. I. Tafur Monroy, K. Prince, A.V. Osadchiy, N. Guerrero Gonzalez, A. Caballero Jambrina, D. Zibar, T. B. Gibbon, X.Yu and J. B. Jensen, "Converged wireline and wireless signal transport over optical fibre access links," in *Proceedings of the 14th. Opto-Electronics and Communications Conference (OECC)*, pp. 1-2 (Hong Kong), July 2009. Paper TuB6.

16. I. Tafur Monroy, R. Kjær, J. Seoane, F. Öhman, K. Yvind, K. Prince and P. Jeppesen, "Long reach PON links for metro and access convergence," in *Proceedings of the Asia-Pacific Optical Communications (APOC)*, (Wuhan, China), pp. 6783-6794, Nov. 2007.

17. K. Prince, D. Zibar, X. Yu and I. Tafur Monroy, "Optical coherent and envelope detection for photonic wireless communication links," in *Proceedings of the 6th. workshop on FTTH, Wireless Communications and their interaction*, organized by the Network of Excellence ISIS, (Stockholm, Sweden), June 2008.

Book Chapters

- V. Torres-Company, K. Prince, X. Yu, T. B. Gibbon, and I. Tafur Monroy, "Ultrawideband-over-fiber technologies with directly-modulated semiconductor lasers," in *Optical fibre, new developments* (C. Lethien, ed.), ch.17, pp. 407–424, INTEH, 2009. ISBN: 978-953-7619-50-3.

- J. B. Jensen, I. Tafur Monroy, K. Prince and N. Guerrero Gonzalez, "Building the photonic bridge: bringing people together with technology," in: *Beyond optical horizons: today and tomorrow with photonics*, pp. 41-53, 2009 DTU Fotonik, (Copenhagen, Denmark).

Other Reports

- "Forskere samler fire signaltyper i ét fiber," by Mie Stage. Ingeniøren Magazine (Denmark), 29 Jan. 2010, p. 4.
- "Fiber skal give Wimax øget rækkevidde," by Mie Stage. Ingeniøren Magazine (Denmark), 29 Jan. 2010, p. 4.
- K. Prince, "Every day we face another set of challenges," in *Beyond optical horizons: today and tomorrow with photonics*, p. 54, 2009. DTU Fotonik (Copenhagen, Denmark).

Chapter 1

Introduction

Telecommunications networks grew from the needs of voice carriers to provide connectivity between subscribers. This old paradigm has been upended within the last twenty years: increasing demand for broadband data connectivity (for access to the World Wide Web and the Internet) is currently a significant driver in the development of global communications networks at every level. Within the access environment, market de-regulation (and the resulting competition) has also reduced the costs associated with last-mile broadband network connectivity.[1] Network operators are therefore being encouraged to implement efficient higher-bandwidth technologies and exploit economies of scale in the provision of broadband data access.

During this project, trends have been observed which indicate a rapid expansion in the data bandwidth requirements of access networks, as increasing number of users demand enhanced connectivity to a burgeoning selection of online activities and services. Such trends may be seen, for example, in the recent surge in popularity of so-called mobile "smartphones," which provide access to multiple data services in addition to traditional mobile telephony, and which support several wireless signaling protocols. Indeed, users now expect ubiquitous broadband network connectivity to a suite of data services including electronic messaging, Internet connectivity, and location-specific services and applications, regardless of their current location or mobility. At the same time, competition between service providers in the network access environment has produced significant decline in the per unit cost of data provisioning. Network providers are therefore being forced to implement robust, cost-effective new systems to increase coverage levels without

increasing the complexity of access network infrastructure. As network operators scramble to fulfill the appetite for increased connectivity, two technologies are becoming increasingly attractive: optical-fiber based technology, and wireless *radio-frequency* (RF) communications systems.[2,3]

Optical access networks are penetrating deeper into the customer premises environment with the increased deployment of optical last-mile networks. Optical networking infrastructure provides a low-attenuation high-capacity data transport channel with a useful lifetime spanning several generations of signaling technology. Simultaneously, wireless *radio-frequency* (RF) networks are implementing advanced signaling schemes and densely-packed *base station transceiver* (BTS) access points, in order to satisfy user demand. Doing so will require additional data bandwidth to interconnect these BTS nodes to provide wireless clients with increased data delivery rates. The convergence of fixed and mobile access platforms offers significant opportunity for network operators to satisfy user demand by simultaneously leveraging the data transport capacity of the optical infrastructure and the mobility support of wireless access networking. The transparent optical infrastructure may also be exploited for the simultaneous provisioning of multiple RF signaling formats for simultaneously providing coverage for multiple networks via a single BTS; and obviate the need for additional infrastructure deployment to support areas with increased traffic patterns. In an appropriately-designed system, the *optical access network* (OAN) infrastructure should decouple access point infrastructure from the signaling protocol and thus provide a signal transport medium capable of supporting several generations of fixed and wireless access across its usable lifetime.

Several solutions have been presented in the literature for the simultaneous delivery of specific fixed and wireless signals through the use of tailored distribution systems. While such solutions have been successfully applied to their respective niches, significant need exists for the definition of a transparent converged access networking framework. This framework would then be applied for the provision of a multi-protocol access networking environment, and would provide transparent support for new and developing technologies over the life of the OAN infrastructure. This framework aims to provide platform-agnostic access signal delivery via low-loss, high-capacity optical infrastructure. It implements extended-range delivery of current- and next-generation signal delivery beyond the bounds of current

implementations. This framework may be defined by the following key characteristics: implementation of an optical access network which consolidates signal processing functions within the central office (CO) node, wherever possible; transparent protocol-agnostic wireline and wireless signal delivery; and the implementation of mature, proven, low-complexity devices at nodes away from the CO.

1.1 Thesis Contributions and Outline

During the course of this project, several aspects of this framework have been developed. This has led to the successful implementation of signal transport required to support current-generation converged access networks via suitably designed OAN implementations. Report has been made of the simultaneous transport of such access signaling via passive optical networks (PON), and evaluations of end-to-end delivery through optical and wireless transmission environments. This thesis therefore presents the key concepts of the converged service delivery framework and provides experimental and theoretical support for its key attributes.

A brief review of the history of optical networking technology is presented in Chapter 3; this will provide an awareness of the trends and technologies that have influenced the development of the OAN since first trials in the U.K. and U.S.A. Several of these trends will continue to be influential for the foreseeable future, and an awareness of these issues will allow for the development of pertinent solutions. An assessment of current *passive optical network* (PON) implementations is presented, with technical details including operating wavelengths used and link spans supported by the current definitions of PON standards; this is followed by an examination of current directions of interest for next-generation PON development. The development of the framework for converged access systems continues in Chapter 3, with an introduction of wireless radiowave transmission. A mathematical model for RF signal transmission through a wireless fading environment is developed. This is followed by an assessment of channel impairments introduced by the transmission of RF-modulated lightwave signals through a long-reach OAN, and a review of key demonstrations of RF signal distribution over optical access infrastructure. The framework is formally presented in Chapter 4, along with two example scenarios. Chapter 5 details the application of the framework for the provision of baseband optical signal transport, RF signal delivery, and converged services provisioning over current-generation access optical network infrastructure.

The contributions of the body of work accomplished within this project are then highlighted; concluding remarks are presented in Chapter 6.

Chapter 2

Optical Access Networks

Recent surges in the demand for broadband data connectivity to the end user have strained the capacity of the previous generation of data access networks, and encouraged a shift towards fiber-based signal transport. Current-generation, copper-based systems are presenting a "bottleneck" to faster end-user connectivity,[4] while the maintenance of the aging copper plant is reducing networks' profitability[5] and further investment has reached the point of diminishing returns.[5–7] On the economic side, market deregulation has produced increased competition in the access environment, and increased bandwidth provisioning has been used as a market differentiator between service providers seeking to attract and retain customers.[8] Fewer subscribers opt for broadband-over-CATV and xDSL access, instead preferring optical[8] network connectivity. Network operators have therefore been motivated to develop and implement fiber-based access networks and systems to cater to the next generation of access users.

It is a timely recognition that Charles Kao received the Nobel Prize in 2009 for his role in the development of optical fiber, the medium supporting optical signaling networks. Interestingly, the other Nobel Prize in that year went to the inventors of the CCD image sensor, the engine powering the digital image capture technology that has motivated much of the recent explosion in demand for broadband networking and high-speed Internet connectivity.

This chapter reviews key stages in the development of optical communications technology in Section 2.1. More detailed treatments of pioneering work in this

field are recommended[9–13] for additional knowledge. Section 2.2 reviews current-generation optical access networking, with a review of fiber in the last mile, and the multiple access technologies used in shared-medium fiber-to-the-home (FTTH) implementations. The *passive optical network* (PON) topology is described in Section 2.3, and important features of current-generation PON standards are also presented. Section 2.4 highlights significant recent results of access network research. The chapter concludes in Section 2.5 with an overview of baseband optical access networks, which will form the foundation for this converged signal delivery framework.

2.1 Background

The transmission of high-speed data signals over long distances requires a coherent, high-frequency transmitter. Monochromatic signal sources exploiting the phenomenon of stimulated photon emission[14,15] were physically realized at microwave frequencies in 1955[16] with the *maser*. Its extension[17] to optical frequencies was denoted the "optical maser" or *laser*, and was first demonstrated in ruby[18] crystal and He-Ne[19] gas. The introduction of solid-state semiconductor[20] devices operable at room temperature[21–23] heralded the dawn of the modern optical communications era. Laser diodes may be directly modulated with the message signal, or operated in continuous-wave mode and externally modulated with the use of electro-absorption[24] or interferometric[25,26] effects; the electroabsorption modulator[27] (EAM) and Mach-Zehnder interferometer modulator (MZM) have been readily applied for this purpose. Optical amplifiers also utilize stimulated emission to produce gain and are applied in long-reach links instead of OEO signal conversion. Optical gain was also observed in an optically-pumped fiber laser,[28] and this is exploited in the *erbium-doped fiber-amplifier* (EDFA).[29,30] Stimulated emission within a semiconductor laser cavity is used in the *semiconductor optical amplifier* (SOA).[31] The modern photodetector exploits the photovoltaic effect across a PN silicon junction, first observed in 1940;[32] fabrication of a high-speed photodiode followed in 1962.[33]

Waveguiding of electromagnetic (EM) radiation within a dielectric material was described in 1961,[34] although fused silica fiber was not considered to be a viable medium until it was shown in 1966[35] that attenuation due to impurities could be significantly reduced. Fiber attenuation levels of 20 db/km,[36] and then

4 dB/km[37,38] were reported by 1972. Further refinements also reduced attenuation due to impurity absorption.[39] The earliest optical fiber installations utilized the *first window* wavelengths in the 850 nm range, where optical fibre has low attenuation. Further research opened a *second window* for transmission near 1300 nm[40], and then a *third window* around 1550 nm.[41] Transmission in longer-wavelength bands provided low attenuation, allowing optical link extension[42,43] and relaxed the requirements on the deployment of optical-electrical-optical (OEO) signal regenerators.

With a monochromatic laser signal source, *single-mode* optical fiber (SMF)[44] demonstrated superior transmission characteristics[45] to *multimode* fiber (MMF), due to the the elimination of modal noise[46] effects. SMF has become the standard medium used in access network and long-haul optical communications links. Dispersion-induced pulse broadening is a key mitigating factor in long-range optical transmission. The use of SMF eliminated modal dispersion, leaving chromatic dispersion (CD) and polarization-mode dispersion (PMD) as the major limiting factors; both are affected by waveguide geometry. While an optical fiber may be designed with a particular CD profile, PMD is due to fiber irregularities introduced during manufacture.[47]

CD management has been made possible since by the introduction of *dispersion-compensating fiber* (DCF),[48] *dispersion-shifted fiber* (DSF)[49] and *non-zero dispersion shifted fiber* (NZDSF).[50] DCF has high unit attenuation, high bending losses and a higher nonlinearity coefficient than SMF; it is typically installed in controlled CO environments. An *inverse dispersion fiber* (IDF)[51,52] has been designed with a dispersion profile opposite to standard G.652 SMF, but with a comparable unit attenuation. IDF also has physical dimensions compatible with G.652 SMF, making it attractive for field deployment (via splicing onto existing fiber) as a dispersion management alternative to DCF or NZDSF. It is therefore a good candidate for developing extendended-range optical access networks and also reduces the dispersion penalty in such extended networks.

2.1.1 Pioneering OAN Implementations

Last-mile optical access networks were first seriously proposed by John Fulenweider at the 1972 International Wire and Cable Symposium.[11,53,54] He appreciated the increased bandwidth and compactness of optical cabling and observed that it

would reduce cable bulk in the access loop, while also providing a high-bandwidth data channel into the customer premises. Although the associated costs made the scheme impractical at the time, his ideas were received with interest at the conference. Fiber optic communication links were first installed in the UK in September 1975,[55] and near Boston in the USA in April 1977.[56] Network operators quickly realized the additional advantages of low-attenuation and EMI immunity offered by optical fiber transport.[57] The first full-service optical communication link was commissioned in May 1977, over 2.4 km (1.5 miles) in Chicago, U.S.A.

The Japanese Ministry of International Trade and Industry commenced trials of multiple-access optical fiber networking in 1978, with the world's first demonstration of optical access networking in a small town near Osaka, Japan. Dubbed the Higashi-Ikoma "Highly Interactive Optical Visual Information System" (Hi-OVIS), it saw the interconnection of 158 homes and 10 public buildings with a 400 km optical access network[58–60] operating at a wavelength of 0.83 μm.[61] Each node was equipped with video camera, television, keyboard and microphone, which allowed the delivery of interactive content to subscribers. This project allowed the assessment of novel interactivity concepts, including home shopping, virtual meetings, distance education and tele-commuting;[62] it was executed in two phases, between 1978-1983 and between 1984-1987. More detailed accounts have also been presented.[10,11,55,63]

2.2 Current-Generation Access Networks

The earliest record of lightwave modulation for telecommunications signaling was of a system patented in 1880[64] to implement free-space transmission of a voice-modulated sunbeam. Recent interest in broadband data access to the Internet and the World Wide Web has encouraged the development of higher-rate optical signaling technologies for last-mile access networks. Significant developments will be reviewed in this section.

2.2.1 Fiber in the Last-Mile

Consider an optical access network (OAN) providing connectivity between central office (CO) and customer premises (CP) nodes within an arbitrary geographic

area. Following standard nomenclature of the ITU-T[65] and IEEE[66] optical access working groups, the *optical line terminal* (OLT) is denoted as the optical interface equipment, located within the CO premises, which communicates with customer equipment via the installed optical fiber. On the customer side, if the optical interface equipment is located within the CP, it is referred to as the *optical network termination* (ONT). If the OAN interface equipment is instead installed between CO and CP, it is referred to as the *optical network unit* (ONU); connectivity is provided to customer premises equipment (CPE) via *network termination equipment* (NTE) located at the CPE. Communications between ONU and NTE may be implemented with copper-based (xDSL or CATV modem) technology, for example. The boundaries of the OAN are therefore at the OLT and the ONT or ONU. It may additionally be possible to consider a *remote node* (RN) within the OAN, at which signal processing or amplification may be implemented as required.

OAN layouts may be described by the umbrella acronym *fiber to the* X (FTTX), in which the 'X' describes how closely OAN approaches the CP. Contemporary variants of FTTX include:[67]

- *Fiber-to-the-home* (FTTH): This option requires an ONT for each customer, placed at the CP, and hence requires the least complexity .
- *Fiber-to-the-building/basement* (FTTB): An ONU is placed within each *multiple dwelling unit* (MDU) or high-rise office building.
- *Fiber-to-the-curb* (FTTC): This is similar to FTTB, although the ONU here serves multiple buildings within a neighborhood.
- *Fiber-to-the-node* (FTTN): The ONU serves multiple users over a wider coverage area; and includes intermediate-range *hybrid fiber-coax* (HFC) schemes.

FTTH is an attractive deployment option in densely-populated urban areas[68,69] and in "green-field" scenarios (i.e. without any pre-existing infrastructure). This technology simplifies outside plant requirements and provides the best upgradeability path for future network growth. It therefore represents the most 'future-proof' access technology. As the OAN provides a transparent, protocol-agnostic transport medium into each CP, it may readily support future signaling technologies; this allows network establishment costs to be more easily recovered over the expected life of the optical plant, which may span several generations of signaling technology.

In FTTB, last-hop network connectivity from the ONU to each CP is established with a suitable short-range technology; xDSL-based links over twisted-pair copper cabling has proven popular. This option is suitable for regions with a high density of potential network customers.

FTTN is the simplest option for fiber deployment in a "brown-field" environment, as it allows the exploitation of pre-existing copper plant. In this case, location of the NTE closer to the CP would reduce copper loop length in the last mile; this would therefore make it feasible to increase the per-user bandwidth by implementing broadband xDSL or CATV signaling. Doing so would enable the network operator to exploit the residual service life of pre-existing copper plant.

2.2.2 Multiple-Access Technologies used in FTTH

The first demonstration of a shared transparent optical access infrastructure was first published in 1986.[70] This has since evolved into the modern FTTH topologies used in current-generation OAN implementations. Key medium-access schemes applied in the multi-user PON environment will quickly be reviewed.

- *Time-Division-Multiplex* (TDM) systems provide a shared physical access medium, in which each ONT/ONU is assigned a time-slot channel for implementing transmissions. Optical signaling may be implemented via a single defined wavelength, or the system may operate without wavelength selectivity. *Ranging* protocols may be used to compensate for varying transmision delays from dispersed ONT/ONU, and transmission *guard band* time intervals may be implemented to addtitionally separate signaling from individual ONT/ONU.[71] All transceivers must operate at similar signaling speeds, so bandwidth increases generally require forklift upgrades across the network.

- *Wavelength-Division-Multiplex* (WDM) systems were first demonstrated in 1988.[72] Although the physical medium is shared among transceivers, communications channels are logically separated by transmission wavelength. The additional complexity of supporting wavelength-selective hardware is traded off against the flexibility of implementing arbitrary bandwidth or signaling

schemes on each wavelength: wavelength-based routing in the nethis separation provides additional privacy to user transmissions. The ITU has approved coarse WDM (CWDM) channelization, with inter-channel separation of 20 nm; and dense WDM (DWDM) schemes with less channel separation.

- *Optical Code-Division-Multiple-Access* (OCDMA) systems were described in 1989.[73,74] All users share a common infrastructure and individual transmissions are encoded with user-unique keys, which provide privacy as well as robustness against transmission impairments.

- *Subcarrier Multiplexing* (SCM) was initially developed by the CATV industry for video distribution;[75,76] although the potential for broadband data networking was quickly realized.[77] Multiple signals streams are electrically multiplexed in the frequency domain: the composite FDM signal thus obtained is used to intensity modulate a single optical carrier. Independence between signal streams is thus preserved and overall spectral efficiency of the system is increased.

- *Orthogonal Frequency Division Multipexing* (OFDM) is similar to wireless OFDM signaling[78–80] and has been shown to provide enhanced dispersion tolerance for high-bandwidth data transmissions.[81,82]

2.3 Passive Optical Network (PON)

The PON has been in development at British Telecom since the latter half of the 1980's.[70,83] This network scheme aims to achieve an economically-viable extension of optical infrastructure into the access network. Its development therefore represents significant progress towards the realization of a fully-optical broadband communications access network. In the PON scheme, network connectivity to distributed client nodes is provided via a shared optical infrastructure which links them to a centralized CO. The CO serves as an interface between this optical access network and core or metro-level networks; it provides aggregation and routing functionalities for traffic flows between these levels of the network hierarchy as required for data flows between high-speed highly-multiplexed core network linkages and the distributed lower-speed access network linkages.

The key defining characteristic of the PON concept is the transparent sharing of the installed fiber plant across several network subscribers in a point-to-multipoint layout implementing (ideally) passive external plant infrastructure. It was developed as a means of sharing a common optical plant among several users and thus providing a good balance between per-user bandwidth and overall system cost. The shared-medium access this implemented requires support for multi-user medium-access signaling to avoid cross-talk and collision issues, and provide a reasonable level of privacy and data security within the network. The PON has been widely implemented in the U.S.A.[67] and Asia.[84]

2.3.1 PON Standards Development

Early PON implementations utilized TDMA-based channelization,[71] although alternative multiple-access schemes have been utilized in subsequent PON generations. The *Full Service Access Network* (FSAN)[65] and IEEE have assumed responsibility for defining PON standards; key points of PON access standards are quickly reviewed.

Early TDMA PON implementations developed into the *ATM-PON* (A-PON) standard,[67,85,86] formally defined in FSAN recommendation G.983.1[85] in March 2003. It implemented native support for the ATM cell format, as an extension from SONET signaling already in use along the optical backbone. The standard supported both single- and dual-fiber operation with transceivers operable in the wavelength (λ) ranges of 1.3 μm (1260 nm-1360 nm) and 1.5 μm (1480 nm-1580 nm). WDM was used to separate *uplink* (UL) and *downlink* (DL) data-streams traveling along a single fiber; in an OAN, the UL is considered to be the data flow towards the CO, and the DL denotes data flow away from the CO. Long wavelength transmission is preferred, and a wavelength of 1.3 μm may be used in a single-fiber implementation. In a dual-fiber implementation, 1.5 μm may be used for the DL, with 1.3 μm used for UL transmissions.

The *Broadband PON* (B-PON) was originally defined by FSAN in November 2001[87] and provided additional wavelengths for video overlay as well as support for *dynamic bandwidth allocation* (DBA). An alternative, the *Ethernet PON* (E-PON) was essentially developed in parallel and was defined in IEEE standard 802.3ah,[88,89] first released in 2002: it provided direct support for native Ethernet packet transmission over the OAN, with standard Ethernet electrical interfaces

at both ends of the network. Higher data rates were implemented for *Gigabit PON* (G-PON). This was defined in FSAN recommendations G.984,[90–94] originally released in March 2003. The standard supports backward-compatibility with optional transmission of gigabit-Ethernet (GbE) packet streams, s well as ATM packet transmission. The *Ten-Gigabit PON* (such as the ITU-T 10G-PON, or IEEE 10G-EPON[95]) represents the latest formal definition of the PON series, and was codified in IEEE standard 802.3.av[96] in September 2009.[97] The 10G-EPON has also been shown to support backward-compatibility with GE-PON.[98] Ongoing efforts are being made[99] to characterize the technology required to implement hundred-gigabit connectivity in the access environment. All PON defnitions assume an SMF transmission medium. Key attributes of PON standards' definitions are presented in Table 2.1.

TABLE 2.1: PON standards overview.

	Unit	A-PON	B-PON	E-PON	G-PON	10G-EPON
Latest revision	-	1998	2001	2008	2009	2009
Max. Length	km	20	20	20	20 (10)	20
ONU split	-	32	32	16	32 (64)	32
λ range	μm	1.3/1.5	1.3/1.5	1.3/1.5	1.3/1.5	1.3, 1.5, 1.6
No. of λ	-	2	32	11	-	-
Gross DL rate	Mbps	1,244	622	1,250	2,488	10,312
Gross UL rate	Mbps	155	155	1,250	2,488	10,312

Although GPON transceivers were required to support 20 km transmission at a data rate of 1.25 Gbps,[90] the line rate has been increased to 2.4 Gbps and provisions have been made in the standard for link extensions[90,91] to 60 km. An *enhancement band* has been defined[94] to allow for WDM extensions to the standard.

2.4 Current Research

There has been much interest in extending the limits of the passive optical network; in terms of increasing the number of supported users per PON segment, the maximum PON length, and by also increasing the data rates supported. A solution which provides an effective balance between these three aims will therefore be expected to strongly influence the layout and technologies used in as-yet-undefined

next-generation PON (XG-PON)[100] schemes. Each new technology develops from previous generations and implementations; one is therefore required to examine the current body of literature to gain insight into the development of new development trends. Additionally, breakthrough technologies showcased in influential "hero experiments," may also significantly affect the course of research and industrial developments over generations of technology. Examination of these key reports will therefore develop a richer understanding into the processes shaping the direction within this field of research.

2.4.1 Optoelectronic Devices

In the hierarchy of communications technologies, the most advanced systems are often initially used in military applications or core networking systems: then, as learning-curve effects produce increased availability and experience, these technologies often get integrated into future-generation access systems. Insight into the capabilities of future access systems may be obtained by examining the state of cutting-edge optical transceiver technologies that are currently available.

The fastest directly-modulated laser had a modulation speed of 44 GHz[101] and a resonance frequency of 72 GHz. The fastest report of a directly-modulated VCSEL operated at 50 GHz.[102] The fastest-operating external modulator is capable of 100 Gbps[99] operation. The fastest PIN photodiode operated at120 GHz;[103] and the fastest hybrid optoelectronic receiver was reported at 107 Gbps.[104]Indium-phosphide technology allows the integration of optoelectronic devices onto a single chip; the fastest InP RF amplifiers were reported at 110 GHz.[105] Good reviews of high-speed optoelectronic device development also appear in the literature.[106,107]

For future WDM systems, the availability of high–port-count *arrayed waveguide grating* (AWG) devices may influence network layout or spectral requirements. AWG systems have been reported[108] with 240 channels at a channel spacing of 100 GHz. With respect to bi-directional transceivers, a photonic transmit-receive module[109] operating between $1 - 10$ GHz, as well as a 60 GHz device capable of bidirectional 155 Mbps operation[110] have both been presented. Optical access systems will likely continue to be driven by cost and power consumption issues: uncooled device technology is therefore attractive in last-mile applications. Uncooled lasers operating at 10 Gbps have been reported[111] at temperatures up to 70°C. Another system, utilizing an optically injected device[112] operating at 155 Mbps,

was demonstrated over a 70°C operating range. An overview of the state of the art in optoelectronic devices appears in Table 2.2.

TABLE 2.2: Current records in optoelectronic device technology.

Device	Record
DFB laser[101]	44 GHz
Uncooled DFB[111]	10GHz, 70°C
VCSEL[102]	50 GHz
EAM[99]	50 GHz
PIN Photodetector[103]	120 Gbps
InP amplifier[105]	110 GHz

2.4.2 PON Reach Extension Research

Although field trials for next-generation XG-PON schemes[113] delivering UL/DL data retes of 10/2.5 Gbps have recently been reported, there have also been other suggestions for PON evolution,[114] to support increased numbers of users/segment, and for longer-range coverage. Range extension could be achieved with mid-span amplification,[115] Raman amplification[116] or protocol transponders.[117] The integration of WDM,[118] hybrid WDM-TDM[119] or optical CDMA[120–123] technologies also provide viable candidate paths for OAN development.

WDM-PON systems[124–126] have been readily examined by the research community since the first reported evaluation in 1988.[72] Assessments have been made into the possibility of wavelength re-use for bi-directional signaling, and the crosstalk impairments[127] introduced by reflections in the system. AWG multiplexers have been readily been demonstrated to accommodate the increased number of channels required by developing DWDM systems: athermal operation, extended operating range (from −30°C to +70°C) and 50 GHz channel spacing have already been demonstrated.[128–130] Research projects such as the "Stanford University Access" (SUCCESS)[119,131] and "Scalable Advanced Ring Dense Access Network Architecture" (SARDANA)[132,133] are seeking to extend the range of hybrid WDM-TDM PON systems for next-generation access networks.

The maximum range of a WDM PON is constrained by optical attenuation and dispersion effects, as well as nonlinear phenomena: these also influence the power levels and wavelength separation used within the system. CD-uncompensated

WDM transmission of of eight WDM channels modulated at 10 Gbps over 45 km of SMF[134] has been reported. The most simultaneously-transmitted 10 Gbps WDM signals (32 channels)[135] has been sent over 20 km SMF. The highest number of ONU per PON segment (1024)[132] was achieved with asymmetric data rates of 10/2.5 Gbps (DL/UL). The longest reach WDM system (115 km with DCF[136]) was also reported with reported 10/2.5 Gbps (DL/UL) data rates. Bitrates of 44 Gbps[137] and 108 Gbps[138] have recently been reported for single optical carrier access systems.

In systems with colorless ONU, a reflective SOA (RSOA) was used at the ONU in an 80 km system[139] operating at a data rate of 1.25 Gbps. Colorless ONU implementing quantum-dash injection locked FP laser devices[140,141] have also been reported. It is anticipated that the capacity of such injection-locked schemes will increase as more experience is gained in the fabrication of these quantum dash devices. Software algorithms have also been applied to overcome device limitations in access scenarios, allowing 10 Gbps signaling with a 1.5 GHz bandwidth RSOA[142,143] implemented at the ONU.

Subcarrier-multiplexed PON (SCM-PON) systems were originally developed for video signal distribution[77] in CATV HFC networks, although soon[144] used for data transmission. A WDM system utilizing SCM was demonstrated by Kang et al.[145] with colorless RSOA at the ONU; the system achieved UL/DL data transmission rates of 622/100 Mbps.

2.5 Conclusions

Development of converged optical transport of fixed and wireless network signaling will ideally be accomplished with an awareness of previously-installed generations of optical access networks. Key steps in the development of the optical access network have therefore been examined, as well as the enabling technologies involved. Recent trends in the development of next-generation optical access networks were also evaluated, which has revealed significant desire for the implementation of wavelength-selectivity in future optical access networking systems.

Strong suggestion has been made for the implementation of *colorless* (wavelength-independent) systems that will be operable across wavelength-sensitive infrastructures. Maximum advantage will be obtained with the re-use of as much of the

infrastructure from baseband optical networks as possible: this will also allow for easy harmonization with existing standards and allow smooth upgrade from current-generation systems to converged schemes.

Radio access technologies and radio over fiber developments will next be presented, in order to clarify the issues and imperatives in the development of converged access networks.

Chapter 3

Converged Access Networks

Multiple-access mobile communications schemes were initially designed for voice transmissions and implemented analog modulation schemes. These pioneer technologies lowered psychological barriers for mobility-enabled connectivity, and the concept of ubiquitous communications entered the lexicon of common usage. Over the last few years, wireless network users, operators and designers alike have further embraced the concept of ubiquitous connectivity. In the current wireless access paradigm, users have grown to expect (and are often rewarded by) seamless, uninterrupted access to online services, including streaming multimedia, online gaming, and online social networking and productivity tools via hand-held terminals that operate across several wireless access networking schemes.

This chapter examines phenomena affecting the transmission of signals through the wireless transmission environment in Section 3.1. Section 3.2 provides an overview of the technologies implemented by network designers to provide a reasonable level of broadband communications through this unstable transmission medium. Concepts relating to the transmission of wireless RF signaling over optical fiber are introduced in Section 3.3. Highlights of recent demonstrations of radio over fiber signal delivery, as well as converged baseband and RF signal delivery over optical access infrastructure is presented in Section 3.4. The chapter concludes in Section 3.5 with a quick overview of the key points considered within the development of the converged architecture.

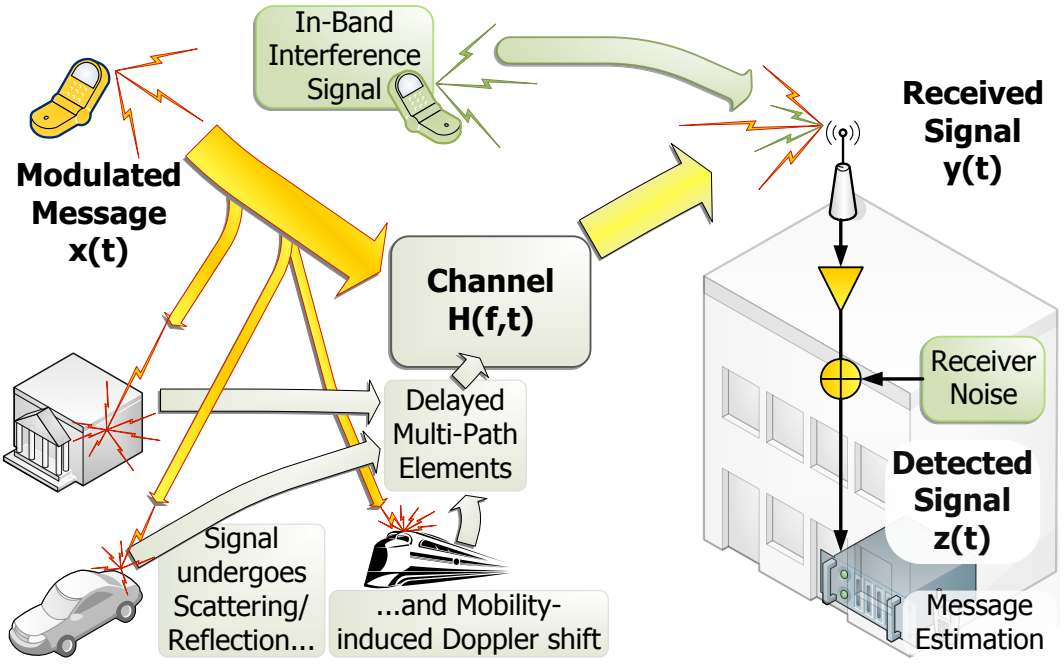

(a) Conceptual diagram

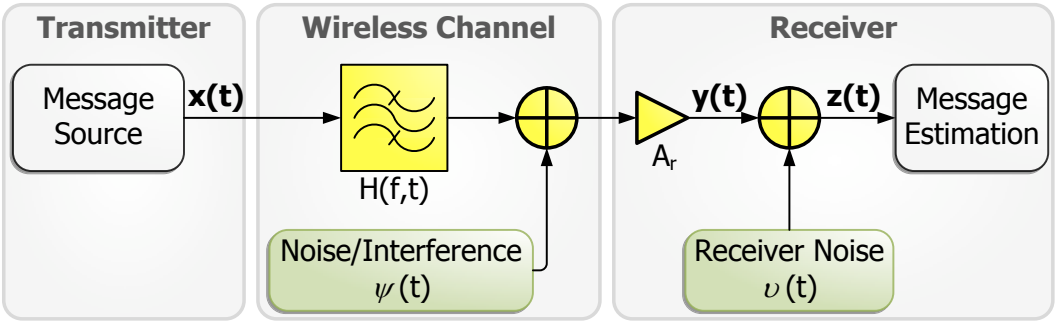

(b) Signal flow diagram

FIGURE 3.1: Wireless RF transmission scheme operating in the presence of interference in a rich scattering environment. The time-variant frequency-selective channel, channel noise/interference and receiver noise are modeled with statistical processes $\mathcal{H}$, $\boldsymbol{\Psi}$ and $\boldsymbol{\Upsilon}$ respectively, yielding realizations denoted $H(f,t)$, $\psi(t)$ and $\upsilon(t)$. Concept (a) and signal flow (b) diagrams shown.

3.1 Wireless Radiowave Transmission

Phenomena affecting communications within the mobile wireless communications environment are examined to provide insight that will aid the development of converged fixed and wireless optical access networking schemes. A representative wireless communications link is shown in Figure 3.1(a), and the signal flow diagram is presented as Figure 3.1(b). Wireless radio-frequency (RF) communications between an active transmitter and its associated receiver are considered. The transmission is assumed to occur within a rich scattering environment, and

transceiver locations are not assumed to be fixed for the duration of the transmission.

The transmitter accepts an input data stream containing information signals to be transmitted over the wireless link; this message is *up-converted* in frequency for passband transmission over the wireless link. Up-conversion processes use RF modulation techniques that accept an input message signal $m(t)$ and vary the amplitude, frequency and/or phase of a higher-frequency carrier wave $c(t) = A_c Cos(f_c(t) + \phi_c)$. Neglecting DC terms, the RF upconverted signal radiated from the transmitter may be represented as $x(t)$:

$$x(t) \equiv A_\Delta(t) \cdot Cos\left(f_\Delta(t) + \phi_\Delta(t)\right) \tag{3.1}$$

The time-varying amplitude, frequency and phase of the modulated signal $x(t)$ are represented by $A_\Delta(t)$, $f_\Delta(t)$ and $\phi_\Delta(t)$ respectively; selection of modulation scheme will determine how these coefficents vary with $m(t)$. The signal $x(t)$ is transmitted over the wireless channel, and the reverse process of *down-conversion* takes place at the receiver. Complete, error-free message recovery is possible since up-conversion and down-conversion processes do not distort the information content of the transmitted message.

The propagating signal may be delayed and distorted during transmission over the wireless link. This may be represented mathematically as filtering by a stochastic process $\mathcal{H}$, which yields a sequence of instantaneous realizations $H(f,t)$. Each realization may in turn be represented by a set of frequency- and time-dependent amplitude and delay coefficients. For *narrowband* signals in which the message bandwidth is within the channel *coherence bandwidth*, it is often convenient to assume dominant *flat fading* processes and neglect the frequency-dependence of the channel response function $\mathcal{H}$. In this case, the channel gain $H(t)$ may be considered as a linear filter with coefficients $h_i(t-\tau_i)$, as shown in Equation (3.2).

$$H(t) = h_0(t) + h_1(t-\tau_1) + h_2(t-\tau_2) + \cdots + h_i(t-\tau_i) + \ldots \tag{3.2}$$

Wide-band signals undergoing *frequency-selective fading* may be treated by subdivision of overall signal bandwidth into a group of narrowband frequency subchannels experiencing similar gain conditions. Without any loss of generality,

each sub-channel may conveniently be defined to lie within the channel coherence bandwidth. Causality allows terms $h_{i<0}$ to be neglected with no loss of generality.

In the presence of nonzero transmission delay $p > 0$, the expression of Equation (3.2) would be modified to incorporate the time-shift in the reception of the symbol of interest. All filter tap coefficients for delay less than channel propagation delay (i.e. $\tau_i < p$) would thus be forced to zero ($h_i|_{\forall \tau_i < p} = 0$) and all subsequent terms would be p-shifted in time. This time-shift may therefore be ignored by associating h_0 with the instant of reception of the first message component, and proceed with no loss of generality. At the receiver, the signal of interest is recovered at the air interface (with an appropriate antenna) in addition to other signals also be propagating in the wireless environment. If these signals lie within the bandwidth occupied by $x(t)$ they contribute energy as channel *noise* and *interference* which affects transmission system performance. The recovered signal of interest may be represented as the convolution of transmitted signal and channel response, i.e. $H(t) * x(t)$.

The propagating signal may also be reflected at surface interfaces (building walls, vehicles, etc.) within the transmission environment; these scattered signal components may eventually propagate to the receiver antenna and produce additional interference. The additional distance travelled along these divergent signal paths, as well as imperfect scattering and reflection at each object interface, attenuates the energy of divergent signal elements arriving at the receiver. Scattering terms which contribute signal energy below the receiver sensitivity will not affect the performance of the transmission system under consideration and may be neglected. Channel noise and interference effects may be modelled through the use of a statistical process $\mathbf{\Psi}$, yielding time realizations $\psi(t)$. The receiver input $y(t)$, is therefore the sum of the signal of interest and channel noise/interference components.

$$y(t) = H(t) * x(t) + \psi(t) \tag{3.3}$$

At the receiver, the incoming wireless signal $y(t)$ is amplified prior to signal down-conversion and signal processing for information recovery; noise is also introduced by the receiver circuits. Receiver noise may be modeled as being drawn from a time-varying statistical process $\mathbf{\Upsilon}$, producing instantaneous realizations υ(t); the receiver output is denoted $z(t)$. If A_r denotes the amplitude shift corresponding to receiver gain, the receiver output may be described as:

$$z(t) = A_r\Big(H(t) * x(t)\Big) + A_r \cdot \psi(t) + \upsilon(t) \tag{3.4}$$

The baseband signal obtained after downconversion and appropriate demodulation contains a version of the original message signal, scaled by channel effects, $H(t)$, in addition to contributions from channel ($\psi(t)$) and receiver ($\upsilon(t)$) noise.

Digital transmission allows simplification of transmission scheme analysis; the transmitted signal $x(n)$ would be constrained to a fixed constellation, the channel transfer function may be approximated to $H(n) = \sum_{k=0}^{\infty} h_k(n-k)$. Here, $H(n)$ is a linear-time-variant filter, and $h_{k\neq 0}$ is used to characterize *inter-symbol interference* (ISI), in which delayed signal energy is received during the processing of another data symbol. In practical systems, the channel has finite memory and terms h_k quickly converge to zero as k increases; causality forces $h_k|_{\forall k<0} = 0$. Under these conditions, Equation (3.4) usually collapses to a form:

$$z(n) = A_r \cdot h_0(n) \cdot x(n) + A_r \sum_{k=1}^{\infty} h_k(n) \cdot x(n-k) + A_r \cdot \psi(n) + \upsilon(n) \tag{3.5}$$

In Equation (3.5), the first term denotes the symbol of interest and the second represents contributions of ISI. The third term of Equation (3.5) represents transmission interference and channel noise effects, and the fourth represents receiver noise. Receiver noise is usually characterized by a zero-mean Gaussian process $\mathcal{N}$ with a flat power spectral density σ^2, hence $\mathcal{N} \sim \mathbb{N}(0, \sigma^2)$. This noise process yields time realizations $\eta(n)$. The receiver SINR is given by Equation (3.6).

$$SINR_r = \frac{\Big(A_r \cdot h_0(n) \cdot x(n)\Big)^2}{\Big(A_r \sum_{k=1}^{\infty} h_k(n) \cdot x(n-k) + A_r \cdot \psi(n) + \eta(n)\Big)^2} \tag{3.6}$$

The signal to noise ratio (SNR) is more commonly applied when interference effects are negligible (i.e. when $h_k \ll 1; \forall k \neq 0$). For digital modulation schemes operating in the AWGN channel, it is known that the *bit-error rate* (BER) may be related to the SNR per bit;[146] more complex modulation schemes allow greater spectral efficiency, but are often more sensitive to added noise. Channel coding[147–150] has also been used to provide robustness against noise and transmission link quality

variation, but this comes at the expense of transceiver complexity. Wireless transmission scheme design may thus be optimized to satisfy the desired performance and receiver complexity requirements for a particular application.

3.1.1 Wireless Channel Effects

Significant features of the wireless channel filter process $\mathcal{H}$ are attenuation, multi-path and *Doppler* effects. Doppler effects are strongly associated with mobility within the transmission environment and distort the spectral profile of the received signal. Attenuation has been determined to vary with path length, frequency (f_Δ) and atmospheric moisture (humidity, fog and rain) levels.[151–153] The path-dependent variations have been well-studied; classic results are presented in Figure 3.2: Figure 3.2(a) was reported by Altshuler[151] and Figure 3.2(b) reported by Straiton[153], after work by van Vleck.[154,155]

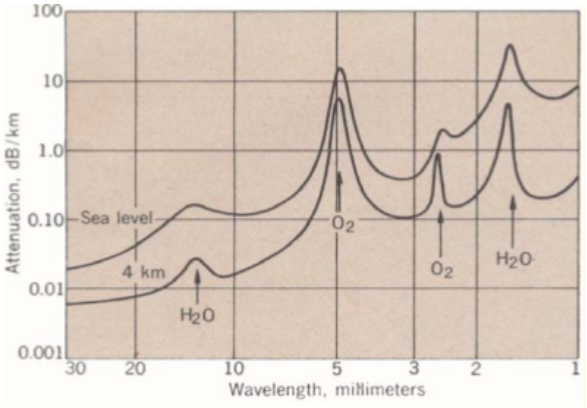

(a) Air attenuation[151]

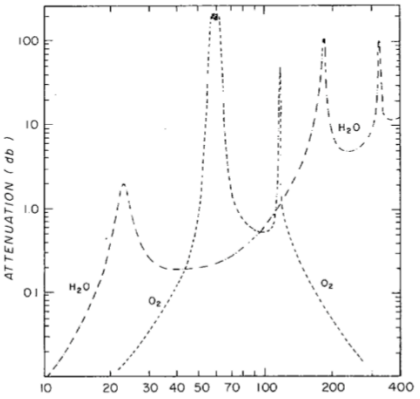

(b) Gas absorption spectra[153]

FIGURE 3.2: (a) Spectral profile of air attenuation, at sea level and 4 km elevation, from Altshuler;[151] (b) H_2O and O_2 attenuation spectra, from Straiton.[153] Frequency (GHz) is plotted on the horizontal axis of (b).

Additionally, in practical systems, multi-path phenomena can also cause energy from a given symbol to arrive at the receiver with non-uniform time delay, as described in Equation (3.2). The direct path between transceivers gives the shortest transmit delay and is usually associated with highest received signal energy, although it may sometimes be obscured by obstacles (buildings, vehicles, etc.) along the transmission path. RF signals may additionally be scattered and reflected at object boundaries within the transmission environment, allowing the delayed reception of energy from a particular transmitted symbol; the phase offset associated

with the reception of a signal propagating along the i^{th} radio path causes interference effects to be observed at the receiver input. If the i^{th} scattered component is received before reception of a given symbol is complete, then the resulting interference will distort the received signal, affecting the receiver signal-to-noise ratio (SNR). If the i^{th} scattering component is instead received after the receiver has already processed its associated symbol, then interference will be observed in a subsequently-processed symbol, this gives rise to ISI as shown in Equation (3.5).

In the literature, the channel development process is often described in terms of its statistical properties. Its *coherence time* describes the timescale during which $H(f,t)$ undergoes little variation; its coherence bandwidth describes the frequency range within which $H(f,t)$ yields similar attenuation. Additionally, depending on the rate at which $\mathcal{H}$ evolves, the wireless environment may be described as being dominated by *fast fading* or *slow fading* processes. The literature is rich with the assessment of wireless transmission schemes in which multi-path effects and time-varying, frequency selective channel fading effects are significant;[156] a thorough treatment was presented by Simon.[157]

3.2 Wireless Access Networking Technologies

The spread of the Internet has encouraged interest in wireless networking connectivity, for access to new telephone and data services. Modern wireless telecommunications networks have thus been developed to serve increasing numbers of users with enhanced data access speeds. Signal coverage is typically implemented with a cellular layout: the total coverage area is divided into discrete *cells* in which a *base transceiver station* (BTS) provides signaling required to facilitate communications connectivity to client *radio access unit* (RAU) devices. Depending on external factors, including geography and subscriber activity patterns, network operators may optionally implement smaller-scale "microcells" and "picocells," in addition to larger "macro-cell" coverage areas in order to provide adequate coverage and support the offered load of the network. Overlap regions may be implemented between adjacent cells to facilitate hand-off functionalities required for user mobility within the geographical coverage area.

Successive generations of technology, including *second-generation* (2G) mobile cellular systems like the Global System for Mobiles (GSM), and *third-generation* (3G)

technologies including Universal Mobile Telecommunications System (UMTS), have been developed to cater for increasing numbers of subscribers.[158,159] The development of broadband wireless access networks has split into two main areas: on one hand, short-range, high-throughput technologies like *ultra-wideband* (UWB) *personal area network* (PAN), and *wireless fidelity* (WiFi) *wireless local area networking* (WLAN) technologies including the "alphabet soup" of IEEE 802.11 (including 802.11n[160–162]) signaling protocols. On the other hand are technologies that provide longer-range connectivity with mobility support but with lower aggregate bitrates, like *fourth-generation* (4G) cellular platforms of mobile *Worldwide Interoperability for Microwave Access* (WiMAX)[163–167] and 3GPP *long-term evolution* (LTE)[168–170] signaling. Point-to-point free space optic links have also been proposed for last-mile wireless access: reports have been made of short-range demonstrations,[171–173] but the application of this technology in wireless access networking will not be considered in this report.

If the classic layered network protocol schema is used, significant progress may be observed at all hierarchical levels in the development of modern mobile wireless RF voice and data networks. At the physical layer, successive generations of wireless access network systems have implemented advanced modulation technologies to maximize spectral efficiency and provide increasing data bandwidth to a growing number of network subscribers. Wireless RF signaling is however constrained by limitations on radiated power levels and spectral occupancy; mobile access terminals have also been designed for conservative power consumption. Network designers have met these competing criteria by developing a suite of signaling technologies to implement feasible broadband wireless networks. Key enabling technologies supporting current-generation wireless access networks include the following:

- *Time-division-duplexing* (TDD) and *frequency-division-duplexing* (FDD), allow bidirectional transmission to be implemented between transceiver pairs via channelization in the time- or frequency domains; both have been implemented in digital wireless schemes since GSM.
- *Spread-spectrum* transmission enables the spreading of a data signal across a frequency band much larger than the message bandwidth, and provides increased noise and crosstalk immunity. It may implement *frequency hopping* (FHSS) or *direct sequence* (DSSS) signalingl. This technology has been implemented in CDMA-based telephony systems including IS-95 and UMTS.

- *Orthogonal frequency division multiplexing* (OFDM) is a specialization of *discrete multi-tone* (DMT) transmission, in which the message is transmitted via a number of closely spaced RF subchannels. Sub-channel spacing is selected for orthogonality to be maintained between subchannels. OFDM allows a low symbol rate to be implemented for a given data rate and is resistant to time spreading and multipath effects produced by transmission over a wireless channel. Additionally, the implementation of a cyclic prefix provides robustness to ISI effects. The *fast Fourier transform* (FFT) and its inverse (IFFT) are typically implemented to reduce the computation load of converting between digital data and the transmitted analog waveform.

- *Ultra-wideband* (UWB) modulation implements high-speed, low power spectral density (PSD) signaling spread across a wideband communications channel: the low PSD reduces interference to other narrowband communications protocols.[174,175] Unlicensed UWB signaling has recently been fomalized by the FCC[176] and ETSI.[177] UWB has been proposed as a wireless personal area networking (W-PAN) enabling technology and may be implemented with impulse-radio (IR-UWB), direct-sequence (DS-UWB) or OFDM (OFDM-UWB) signaling. The development of DS-UWB standardization has stalled, although OFDM-UWB[178,179] is now an ISO standard.[180]

- *Adaptive antenna systems* (AAS) requiring multiple transceiver antennas have recently been introduced in newer RF access schemes including the IEEE 802.11n,[160–162] WLAN standard, as well as the *Worldwide Interoperability for Microwave Access* (WiMAX) signal platforms.[163,164,181,182] Such systems exploit spatial characteristics of the wireless transmission environment to implement radiowave *beam-steering* in an AAS. They also take advantage of statistical variations in channel quality through the implementation of *multiple-input multiple-output* (MIMO) techniques like *space-time coding* (STC), which simultaneously increases transmission capacity and provide multipath robustness and range extension.[183–186] Combined MIMO-OFDM transmissions have also been implemented for enhanced spectral efficiencies.

- *Adaptive modulation schemes* are also defined in modern RF access standards, which allow connectivity to be established for varying channel conditions, so that a trade-off is dynamically implemented between signaling throughput and wireless channel quality. This compensates for time-varying

channel capacity and allows for user mobility support within the wireless coverage area. Modulation rate may be adjusted to guarantee a desired quality of service and this adaptation may be implemented on a per-symbol basis in a single-channel scheme. Multi-channel transmission systems may also implement adaptation across sub-channels to compensate for frequency-selective fading.

Continuous-level signaling waveforms are used for message transmission via wireless communications access networks. Newer RF access schemes will also encode information in statistical correlation of phase or frequency shifts across wideband frequency channels. Both of these developments will increase the susceptibility of the wideband transmitted signals to frequency-dependent variation in channel quality. On the other hand, adaptive filtering and signaling processing techniques implemented (e.g. FFT/IFFT, STC and DSSS/FHSS operations) will provide additional robustness to the wireless transmissions, without compromising link throughput.

RF engineers typically assess the following link characteristics when evaluating the performance of a radiowave transmission system: gain, noise figure, spur-free dynamic range, *compression-free dynamic range* (CDR) and *third-order intercept* (P_3). Reports by Ackerman[187,188] and Cox[189–191] have done much to explain optical transmission of radiowave passband signals in terms of analog RF transmissions; they subsequently presented more thorough analyses[189,192] of the impact of optical link design on these parameters. Linearity may be assessed using a two-tone injection test in which two sinusoidal signals of equal magnitude are applied to the system and the input power is increased until the onset of nonlinear system response. For a multi-tone transmission system, it is useful to assess system response with tone separation equal to the channel spacing.

Since these concepts are not immediately accessible within optical communications, they are briefly illustrate by an examination of linearity results obtained from a colorless bi-directional radio over fiber distribution system developed during this project.[193–195] Using a two-tone injection procedure[196–198] with equal-amplitude 5.8 GHz signals separated by 2 kHz, input RF power was varied and system response was observed. Figure 3.3 presents the output signal RF power at each of the the fundamental (square) frequencies, as well as the output power due to each of the the third-order intermodulation (IM) products (circle) and fifth-order intermodulation products. This system supported narrowband transmission,

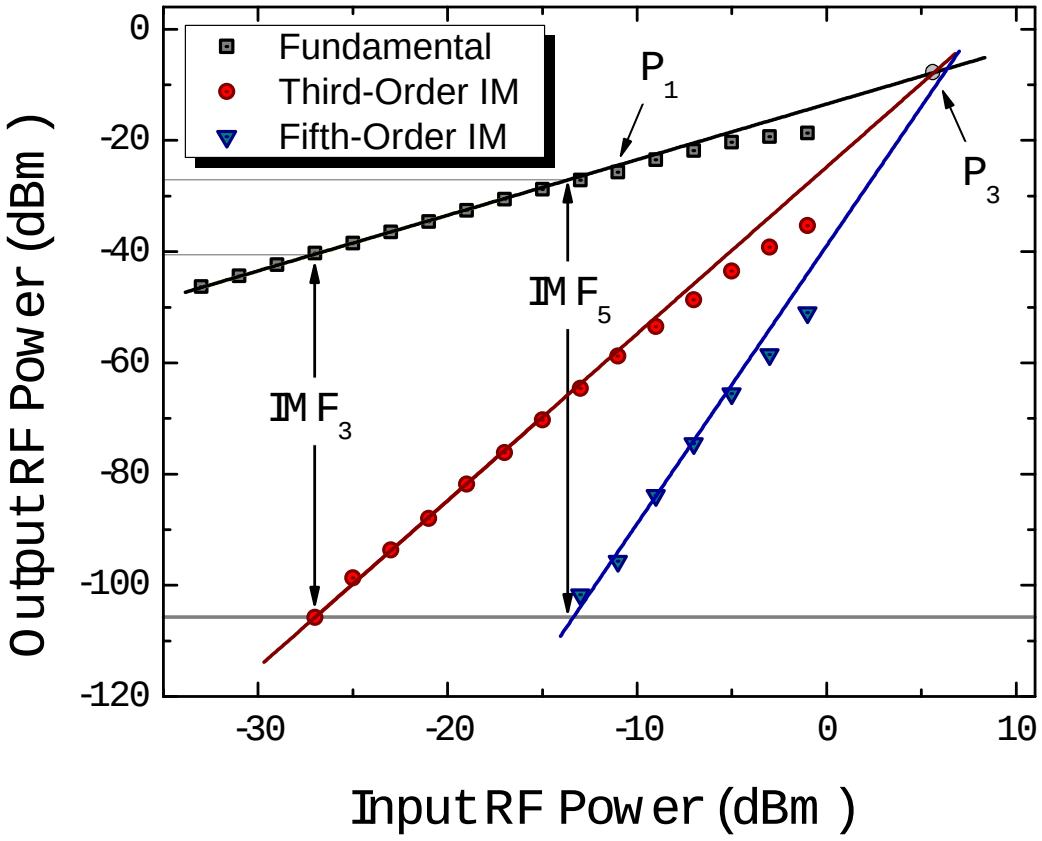

FIGURE 3.3: Results of two-tone injection test on the downlink of a 5.8 GHz radio over fiber signal delivery scheme developed for WiMAX transmission.[193,194] Graph shows system response at fundamental (square) frequencies, as well as third-order (circle) and fifth-order (triangle) IM products. Third-order intercept (P_3) and 1 dB compression point (P_1) also shown. Tone separation: 2 kHz; RF spectrum analyzer resolution bandwidth: 10 Hz.

and implemented 20 MHz FWHM duplexers at the antenna; second order (and all even higher-order) IM products did not appear at the output to the ONU antenna. System linearity was thus constrained by third-order IM distortion, the spurious-free dynamic range (IMF_3) of the system was evaluated at 65 dB/Hz$^{2/3}$; the fifth-order intermodulation-free range (IMF_5) was similarly evaluated at 78 dB/Hz$^{2/3}$. The 1 dB gain compression point (P_1) occurred at an input power of -11 dBm, and P_3 was observed at $+5.5$ dBm input power; system CDR was at 79 db/Hz$^{2/3}$.

3.3 Radio Signaling over Optical Fiber Links

The previous section examined the time and frequency-dependent variations in the effective channel transfer function of a free-space RF communication link, as

well as the technologies being used to overcome time and frequency-dependent variations in wireless channel quality. Since optical fiber presents a stable channel to the well-confined propagating lightwaves, channel quality variations typically occur at a much slower rate than the broadband signaling speeds typically applied. Indeed, the most significant processes causing time-variation in the optical channel occur due to the macro environment effects including fiber expansion due to ambient temperature changes or changes in fiber shape due to twisting or swaying in aerial cable installations. In long-haul terrestrial or transoceanic installations spanning thousands of kilometers, the accumulated effects of such processes may yield significant channel variations over a short time; within the access environment, the conservative loop lengths (< 100 km) typically yield variations that are negligible across the time-scale of the signaling rates used. Dispersion remains as the key effect encountered by lightwaves propagating along optical fiber; the optical channel response may thus be approximated by a time-invariant filter function.

Consider a system in which wireless signaling is routed over an optical access network. Two possible scenarios are shown in Figure 3.4; the main figure shows wireless network connectivity provided within a mobile "cell" coverage area, in either a macro-coverage environment (green area), or in a "micro-cell" within a cutomer premises (brown area). The inset shows a broadband wireless bridge in which an optical communications link provides an alternate switching path for RF signaling going between two network nodes.

In a radio over fiber system, an RF signal is to be transported from a CO to an ONU, via the OAN. At the ONU, the RF signal may be amplified or radiated by a suitable antenna. For consistency, the RF signal of interest is denoted $x(t)$, as previously defined in Equation (3.1); it modulates an optical signal at wavelength λ_0. This modulated lightwave then propagates over a fiber with length L, and dispersion parameter D.

It is well known[199] that EM fields of a propagating wave interact with the molecules of the propagation medium, and that the molecular susceptibility of a material becomes non-linear at high field intensities; propagating waves may thus interact non-linearliy with the medium (and hence with each other), producing significant *non-linear* scattering (and mixing) effects that can affect optical lightwave communication systems. Experiences from baseband data transmission have allowed the establishment of safe operating power levels, and inter-channel wavelength spacing,

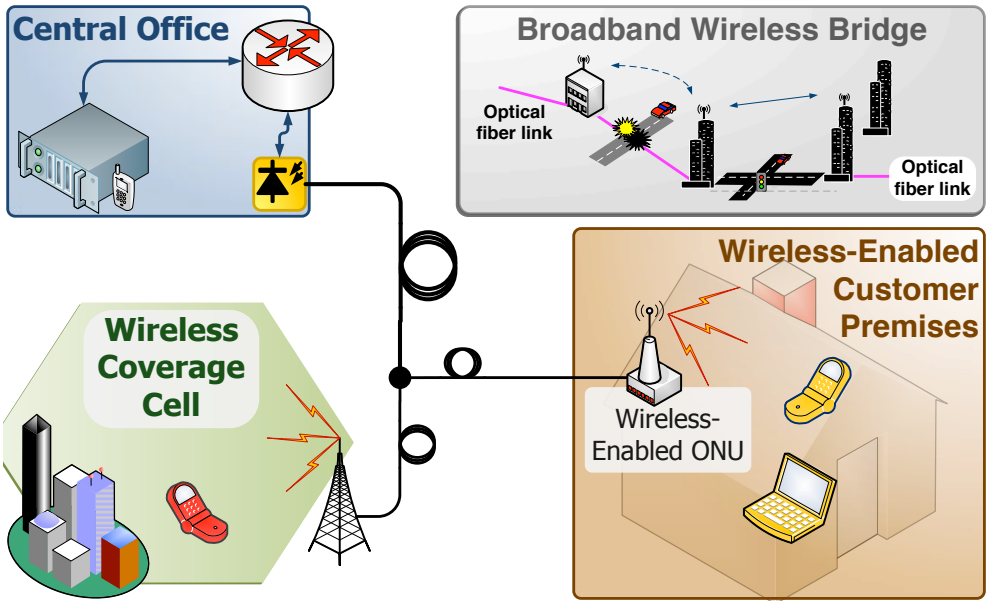

FIGURE 3.4: System configuration in which wireless signals are transported over an OAN. potential applications include macro-scale cell provisioning, picocellular coverage within CP area, or broadband wireless bridge (inset).

at which these nonlinear effects become negligible, and the optical channel may be treated as a linear time-invariant (LTI) filter with finite taps. Consideration must also be taken with the use of optical amplification techniques to compensate for transmission losses; optical SNR at the receiver will also impact the SNR of the photodetected RF signal.[200]

Within the optical channel, propagating signals experience distortion due to attenuation and dispersion. Fiber attenuation has been well-stabilized within the optical transmission windows and varies very slowly over the lifetime of the installed cable. Dispersion within single-mode fiber primarily manifests as polarization-mode dispersion (PMD) and chromatic dispersion (CD). PMD is due to birefringence within the fiber and introduces statistical variation in the propagation delay experienced by the lightwave bearer propagating along two orthogonal states of polarization within the fiber. The effects of PMD have been reduced with the development of fibers with reduced birefringence and improvements in optical cable installation procedures. Chromatic dispersion introduces wavelength-dependent propagation delay in the propagation time of an optical waveform, and is a function of waveguide geometry and material, as well as operating wavelength.

3.3.1 Radio over Fiber (RoF) Transmission Schemes

A straightforward method of distributing radiowave signals over an optical access network is to implement *intensity-modulation* of the optical carrier and utilize *direct-detection* at the receiver: such IMDD systems re-use standard techniques developed for baseband optical communications systems. These systems may be characterized my the frequency at which the RF waveform is is modulated before being transmitted over the optical link. In an *RF over Fiber* (RFoF) system, the analog RF waveform at frequency f_Δ is directly applied to the modulator and recovered from the remote PD. With *intermediate frequency over fiber* (IFoF) transmission, the analog waveform is modulated at a lower intermediate frequency ($f_\text{I} < f_\Delta$), transmitted over the optical link, and then remotely upconverted to the desired frequency f_Δ by post-detection modulation at the receiver. The transmission of the signal waveform at baseband over the optical link and remote upconversion from baseband to f_Δ is known as *baseband over fiber* (BBoF). Thorough treatments of these phenomena have been presented in the literature.[201–204]

IMDD radio over fiber systems are susceptible to frequency-dependent dispersion-induced fading effects; IFoF and BBoF schems are more robust to this fading than RFoF. RFoF however focuses most system complexity at the transmitter, the receiver performs only optoelectronic conversion and possibly signal amplification. Frequency up-conversion at the receiver in IFoF and BBoF schemes will require precision oscillators and RF mixers at the wireless-enabled ONU.

3.3.2 RF Power Fading

Dispersion-induced fading affects IMDD radiowave distribution schemes. Fiber dispersion causes the three components (the optical carrier and both sidebands) of the modulated optical spectrum to propagate at slightly different speeds; phase decorrelation thus produced leads to interference between components of the received signal at the photodiode output. This results in a reduction of post-detector RF power and increased phase noise.[205,206] A thorough evaluation of the effect of chromatic dispersion in RFoF links was presented by Gliese;[207] PMD effects were analyzed by Schmuck.[208]

It has been shown that an optical wave centered at (vacuum) wavelength λ_0 ideally modulated at an RF frequency f_Δ, propagating along a length l of optical fiber

with dispersion parameter D and detected with an ideal PIN photodiode, produces an post-PD RF power P_{RF,f_Δ} (at frequency f_Δ) that varies as shown in[206] Equation (3.7), where c_0 denotes the speed of light in a vacuum.

$$P_{\mathrm{RF},f_\Delta} \propto \cos\left(\pi \frac{l \cdot D}{c_0} \lambda_0^2 f_\Delta^2\right) \tag{3.7}$$

Dispersive fading phenomena result in a periodic power vs. length profile at a given operating frequency. Since fading is observed when three optical components are dispersed, various schemes have been proposed[205] to overcome this impairment in IM-DD RoF transmissions; these include carrier suppression,[209] sideband filtering[206,210,211] and optical phase conjugation.[212] WDM systems have also been proposed which exploit AWG periodicity[213] or an optical interleaver at the receiver[214] to eliminate the undesirable spectral component of the optical signal.

Evaluation of the transmission lengths L_{NULLL} associated with significant impairment due to dispersion-induced fading may be done by:[215]

$$L_{\mathrm{NULL}} = \frac{N c_0}{2 D \lambda_0^2 f_\Delta^2}, \qquad N = 1, 3, 5, \cdots \tag{3.8}$$

The fading power loss associated with SMF transmission of four RF frequencies was evaluated, and is presented in Figure 3.5 for 100 km. The figure shows the fading effect observed as a function of propagation length at 2 GHz (blue), 5 GHz (red), 20 GHz (green) and 60 GHz (brown, dashed). Low penalty is associated with 2 GHz transmissions over 100 km SMF. This indicates that dispersive penalty is not a major impairment for IMDD signaling in the RF spectrum occupied by current-generation mobile telephone networks such as GSM and UMTS. At 5 GHz, less than 10 dB fading power loss is incurred over 100 km, which is of the order of fiber attenuation (typically 0.2 dB/km[43]). This indicates that key WLAN protocols may be supported by IMDD RoF backhaul. Such technologies include WiFi (IEEE 802.11a/b/g/n) signaling at 2.4 GHz and 5 GHz, and mobile WiMAX at 3.5 GHz. IMDD transmission of 20 GHz RF signals over SMF will be associated with significant power penalty due to dispersion; the first null is observed within 10 km of SMF. Transmission of 60 GHz signals is significantly affected by IMDD transmission over modest lengths ($L \leq 5$ km) of SMF.

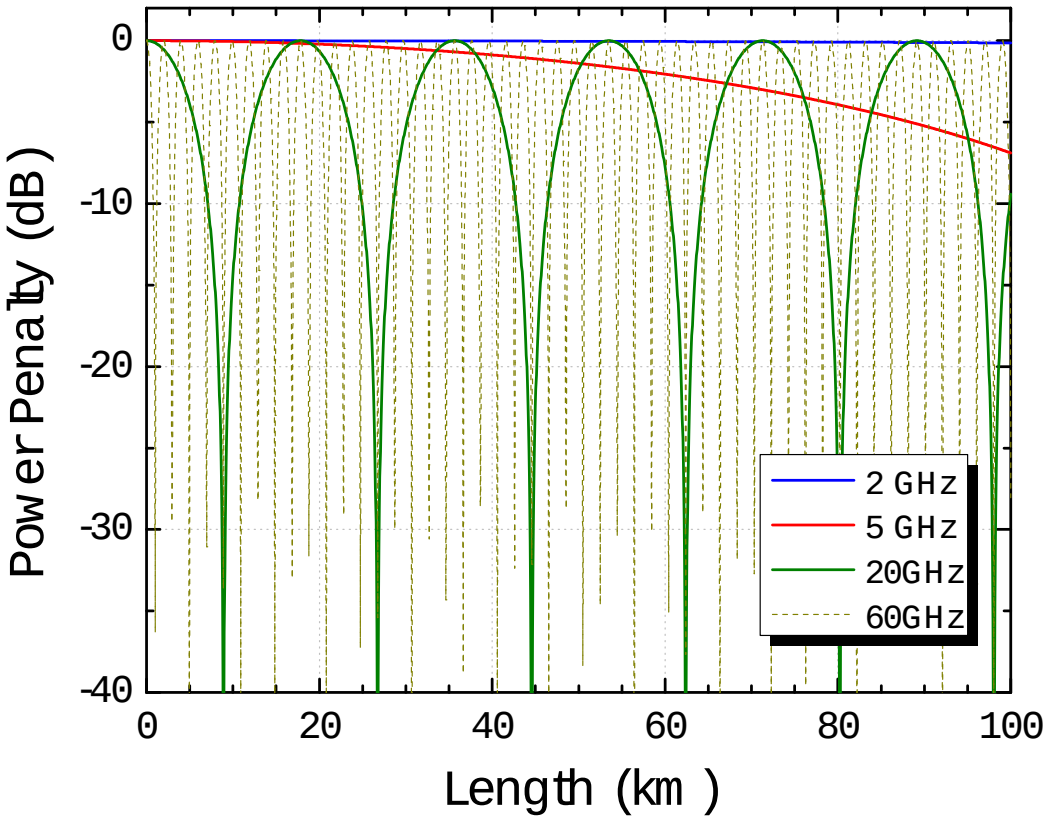

FIGURE 3.5: Dispersion-induced fading power loss as a function of fiber length for IMDD radio signals over SMF, at carrier frequencies of 2 GHz (solid blue line), 5 GHz (red), 20 GHz (green) and 60 GHz (dashed brown line).

The results of Figure 3.5 indicate the feasibility of implementing IMDD techniques for long-reach ($L \sim 100$ km) OAN backhaul of wireless RF signaling for carrier frequencies up to 5 GHz. The passband RF signaling could thus be remotely generated at the CO and transparently conveyed to the wireless-enabled ONU, thus simplifying the requirements of field-deployed nodes within the OAN. RF signaling at higher carrier frequencies will be significantly affected by dispersive fading if directly modulated onto the lightwave carrier in an IMDD system. Support for high-frequency RF signal delivery via a long-range OAN will therefore require engineering effort to overcome this impairment and simultaneously reduce the requirements at the CPE.

3.4 Previous Research

Progress has been reported in increasing the bit-rate and frequency supported over an IMDD radio over fiber link through the use of optical spectral shaping

to mitigate dispersion-induced fading during transmission. The use of optical techniques in the processing of RF signals, e.g. for optical beam steering[216] in radar applications, has also been investigated. The interested reader is directed towards the literature for comprehensive reviews of microwave photonics[217] and long-haul RF signal transmission[218] issues. Recent results obtained in RoF signal transmission, as well as the simultaneous transport of fixed and wireless signaling, will now be reviewed.

3.4.1 RoF demonstrations

High-fidelity RF signal transmission remains as a goal for radio over fiber system designers: improved linearity transmission has been demonstrated with the use of electrical pre-distortion[219,220] of the transmitted waveform, optical suppression[221] of inter-modulation distortion, and the use of high-linearity[222,223] transmitters and receiver equalization.[224] Optical distribution of RF signals has been demonstrated for frequency ranges that have been reserved for wireless communications. Most applications have targeted antenna remoting applications, although air-link experiments have also evaluated the effect of end-to-end signal delivery. Key results obtained are presented below:

- *GSM* signaling has been demonstrated at 900 MHz and 1.8 GHz.[225]
- *UMTS* IMDD demonstrations were also presented over SMF[225,226] fiber. UMTS-compliant WCDMA signals were reported[227] with a VCSEL source in an MMF link.
- *WiFi WLAN*: Full-duplex 2.4 GHz IEEE 802.11g signal distribution has been demonstrated[228] in a distributed antenna scheme with 32 radio access units.
- *WiMAX* signaling with 64-QAM constellation was demonstrated[226] over 400 m MMF. With SMF, IEEE 802.16d signaling at 3.5 GHz was reported[229] over 5 km; WiMAX signal transport via the SuperMAN architecture has also been discussed in detail.[230]
- *WCDMA* signaling with 500 MHz bandwidth, modulated on a 6 GHz carrier was transmitted[231] over 5 km SMF.

- *HiperAccess*: Transmission of 18 GHz 16-QAM signaling at 5 Mbps was also demonstrated[232] over 100 km SMF.

- *UWB*: 4 Gbps IR-UWB transmission[233] via 100 m MMF and 4 m of air; as well as bi-directional transmission of 3.125/2 Gbps (DL/UL) over 50 km SMF and a 1.85 m air, have both been described. Assessments of UWB signal transport in the PON environment have also been presented.[234]

- LMDS: Transmission over 21 km SMF and 2.5 m air transmission was reported[235] with a 33 GHz RF signal, using a suppressed optical carrier scheme; the carrier suppression eliminated fading effects. An optical heterodyne system was also demonstrated[236] over 90 km SMF, and allowed a low-complexity envelope detector to be implemented at the remote antenna unit.

- *60 GHz* schemes are also generating increased interest.[237,238] N'goma et al. reported[239] a QPSK OFDM radio over fiber system with a supported data rate of 14 Gbps. The data rate was increased to 21 Gbps 8-QAM OFDM signaling[240] using a 60 GHz RF carrier and transmitted via 500 m SMF and 10 m air link. Gomes et al. reported[226] 12.5 Gbps after fiber and 40 m free-space transmission with a carrier-suppressed NRZ-OOK scheme. Injection-locked VCSEL transmitters have also been applied[241] at this frequency. Optical carrier suppression and envelope detection allowed the distribution of a 63 GHz, 1.25 Gbps ASK signal over 23 km SMF.[242]The most-known ONUs (1,024) in a 60 Ghz distribution system was also reported at this frequency. OFDM-UWB systems at 60 GHz have also been demonstrated[243] to allow 1 Gbps data transmission speeds.

- *120 GHz* at 10 Gbps transmission was demonstrated[244,245] by NTT researchers with fiber followed by 200 m air link.

- *280-400GHz* transmission at 2 Gbps over a 50 cm wireless link was recently demonstrated[246] by a team at NTT. The report mentions that a collimated RF beam was obtained, suggesting the possibility of extending the wireless transmission length.

3.4.2 Converged Wireless and Optical Signal Systems

Dual-band systems for providing simultaneous fixed and RF wireless signal delivery have also been reported, but the majority of reports present results obtained with narrowband RF systems.[247–249] SCM systems have been reported to allow three RF signals and baseband data[250] to be delivered via a single optical carrier. Systems-level evaluations have also been presented, for 3G integration with G-PON.[251] An optical carrier suppressed system was also shown to allow[252] 2.1 Gbps data transmission on 63 GHz and 21 GHz RF carriers over 50 km SMF. The longest-range simultaneous delivery of RF and baseband data was reported[253] for 2.5 Gbps and 40 GHz digital video broadcast (DVB) signaling over 400 km.

Highly linear RoF systems which support simultaneous signal delivery across a wider RF frequency range are attractive for converged access networking; such systems are starting to appear more frequently in the literature. Wideband multiprotocol RoF signal delivery to a distributed antenna scheme has recently been examined,[254] and polarization multiplexing been used for 25-km transmission of UWB and WiMAX signals.[255]

3.5 Conclusions

This chapter examined key phenomena affecting the transmission of RF signaling through the free-space communications channel, making key note of the frequency and time dependence of the wireless channel transfer function $\mathcal{H}$. The rapid development of fading processes (relative to the signaling rate) have motivated the use of advanced signal transmission techniques in wireless RF communications networks, in order to provide reliable communications over the statistically-varying wireless channel. Wireless fading processes were contrasted with the relatively slow channel development encountered along an optical fiber, in which the well-confined lightwave carrier is mainly affected by fiber dispersion effects. At low frequencies, dispersion effects are not significant over typical OAN installations, by virtue of the short transmission lengths implemented ($\sim$ 100 km), allowing the stable, low-attenuation transport of an RF waveform over an OAN. Low-frequency (below 5 GHz) and high-frequency (above 20 GHz) signaling bands have been defined, allowing the proposal of schemes for IMDD transmission of input signals within these bands, for transport over long-range OAN.

Chapter 4

Framework for Converged Services Delivery via Optical Access Network

Current-generation optical access networks employing a point to point or PON configuration provide connectivity to network subscribers via passive field-deployed outdoor optical infrastructure and low-complexity customer premises equipment. Such installations are being installed further into the wider access environment, ultimately leading to a full-penetration FTTH access network layout. Current-generation optical systems, while offering significantly larger bandwidth than that offered by competitor technologies, are still a far way from exploiting the full capacity of the optical fiber installation. It is therefore obvious that significant opportunities exist for providing the high-bandwidth data backhaul required for supporting current and future generations of wireless RF access networks.

The merging of fixed and wireless access architectures is being proposed through the application of a converged access framework for providing broadband multi-protocol data access to network subscribers. Such framework would be defined for a transparent backhaul of RF signaling from the wireless environment to an intelligent CO node and would therefore support full-service RF wireless coverage areas within the customer premises environment. Additionally, the framework would exploit the distributed network points of presence to reduce the traffic loading on centralized BTS installations, and thereby increase the load-bearing capacity of

the offered wireless network through the segmenting of the wireless access environment. This framework will support the delivery of fixed and wireless network services at the customer premises (CP) interface, which is connected via an ONU (located at the CO) via some intermediate remote node (RN). For the following discussion, the ITU-T definition of ONU and OLT is relaxed to allow the consideration of a wireless-enabled ONU, which provides transparent fixed and multi-protocol wireless access coverage.

At each access node, CPE and wireless WAP units would therefore interface directly with a *wireless enabled ONU* which would deliver the required signaling for supporting multiple fixed-line and wireless access standards. From the wireless RF perspective, the wireless-enabled ONU would incorporate the signaling functionalities of a typical BTS. However, the transparent optical infrastructure would allow the integration of BTS signal processing functionality at the CO, allowing ONU design simplification. The wireless enabled ONU could therefore be standardized across implementations, although additional RF amplification and antenna equipment may be optionally added to increase the coverage area as required. Additionally, OAN transparency directly promotes the implementation of protocol-agnostic RF wireless signal delivery via the converged network infrastructure.

Several possible applications exist in which this network convergence framework would be especially attractive, and the concept for converged service provision in urban and rural application scenarios will be presented, and then a brief conclusion.

4.1 Urban Deployment Scenario

In an urban deployment of Figure 4.1, for example, the converged fixed/wireless access network would exploit the FTTH network layout to support multi-protocol fixed wireless access within the immediate CP area. In addition to the traditional broadband FTTH service delivery, small-scale wireless-enabled customer premises applications are anticipated, with the OAN providing signaling backhaul for these micro-cells. In the wireless-enabled CP, for example, simultaneous broadband Internet access provision to fixed-location computing equipment via fixed-line and wireless signal formats is envisioned, possibly including pico-cellular range of WiFi, LTE, WiMAX or UWB signaling. The same infrastructure could also facilitate

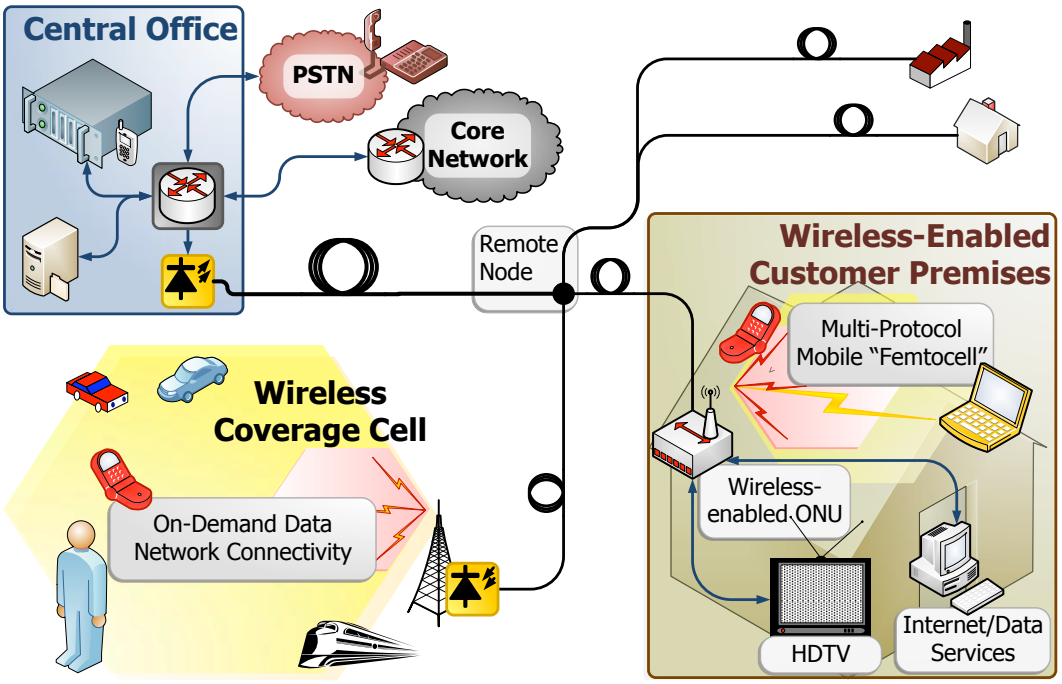

FIGURE 4.1: Converged access: urban scenario. Simultaneous provisioning of broadband fixed-line signaling and multi-protocol wireless network coverage is implemented via a shared optical infrastructure and wireless-enabled customer premises equipment (CPE). Transparent OAN enables multi-protocol short-range "femtocell" and regular "cell" wireless coverage.

larger-scale wireless coverage cells, in which on-demand data network connectivity is provided to multi-protocol (including 3G, LTE, or other) wireless devices roaming within the coverage area. It would therefore be possible for network operators to exploit the bandwidth of the optical access infrastructure as required, by dynamic wavelength routing or other adaptive schemes, to cater to trends in usage patterns across the wireless network without the need for additional infrastructure deployment.

4.2 Rural Deployment Scenario

Within the suburban/rural deployments as shown in Figure 4.2, it is anticipated that subscriber density would not require the establishment of a local CO node; but that network connectivity services for customers within a given area could be trunked from a CO in a nearby metropolis, via a long-range OAN infrastructure. FTTH would not be an immediately attractive option for deployment, so

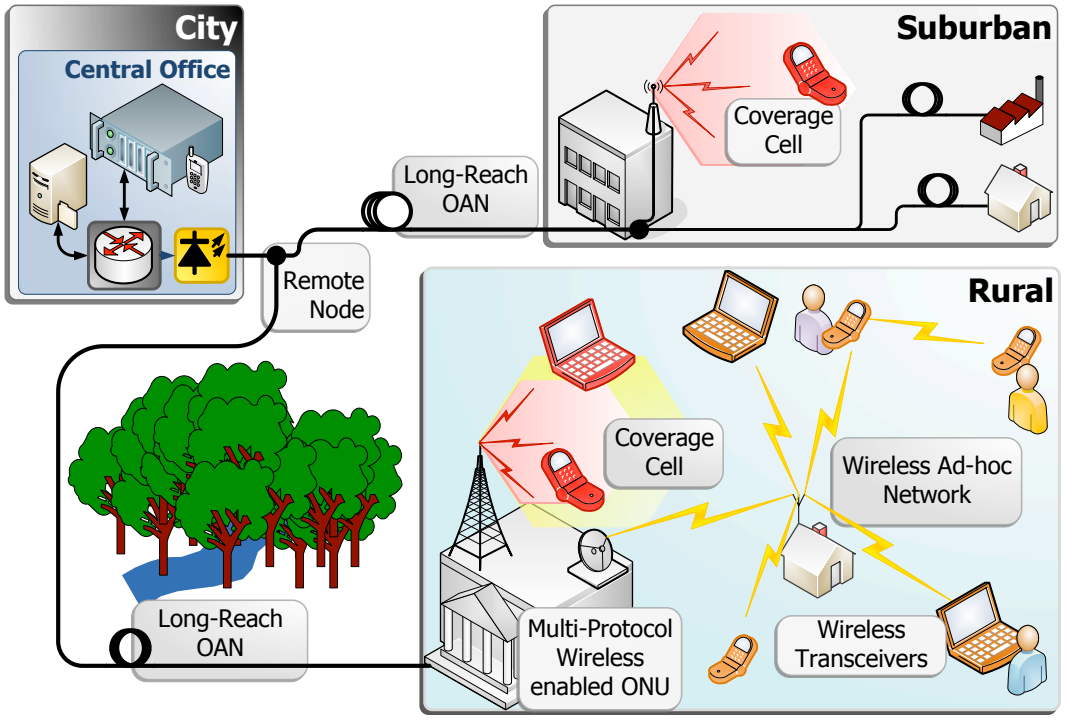

FIGURE 4.2: Converged access: suburban/rural scenario. Simultaneous provisioning of broadband fixed-line signaling and multi-protocol wireless network coverage is implemented via a shared OAN infrastructure and wireless-enabled CPE. Arbitrary *ad hoc* RF wireless access may also be implemented.

scenarios have been identified in which the converged service delivery via long-reach optical access infrastructure would prove advantageous over an all-copper alternatve. Long-range wireless multi-protol services delivery would be a powerful incentive for the installation of FTTN (or other FTTx) infrastructure. It is anticipated that suburban deployments would allow point-to multipoint WiMAX, WiFi, and other last-mile RF access solution for service delivery over a given area.

Additional RF amplifier and antenna equipment required for the radio coverage area could then be co-located with a wireless-enabled CPE, which would thus operate as the optical-to-air interface for the last-hop RF link. The PON infrastructure would also allow fixed-line connectivity to be established to the (urban) CO from other large enterprises over the lifetime of the installed cable, as the need arises, without requiring infrastructure upgrades. In the rural scenario, a similar point-to-multipoint last-hop wireless solution to the suburban case is anticipated, supporting WiFi, WiMAX or other technologies. It is also anticipated that client nodes outside the service range of typical broadband RF access systems may additionally be connected via some ad-hoc wireless networking solution. Connectivity

between this wireless network and the CO could then be established via a multi-protocol remote relay point, which would then interface signaling between wireless and optical media.

4.3 Conclusion

The framework for the converged support of fixed and wireless signal transport via a common optical access network was presented in this chapter. The next chapter will present the application of this framework in the provision of fixed and wireless access services over a common optical infrastructure.

Chapter 5

Thesis Contributions

This chapter presents the key contributions realized during this project, categorized as follows: a treatment of baseband signaling in the optical access environment is presented first, in Section 5.1. Section 5.2, relates progresses made with all-optical UWB wireless signal generation, as well as the novel implementation of tunable all-optical true time delay (TTD) for supporting an adaptive antenna system providing full 360° wireless RF beam-steering of standards-compliant WiMAX radiowave signals. Section 5.3 presents an architecture for supporting pass-band and baseband signaling over a common OAN infrastructure; this scheme exploits cross-gain modulation within an injection-locked MQW DFB laser and avoids the dispersion penalty otherwise associated with IMDD transmission of radiowave signals over a dispersive optical medium. Section 5.4 presents the insights gleaned during a record-setting world-first delivery of multiple-protocol baseband and radiowave signaling via a single field-deployed optical fiber: simultaneous error-free transmission over eight WDM channels was demonstrated, modulated with NRZ-DQPSK, WiMAX, UWB and phase-modulated BPSK radio over fiber signals. At each step, key insights gained during the evaluations will be outlined.

5.1 Baseband Signal Transport

Intensity-modulated baseband signaling has been used as a legacy modulation format since the development of the earliest optical communications networks.

It is anticipated that baseband networks will continue to be deployed in future optical access networks, due to the simplicity of the required receiver structure. During the course of this project, support has been demonstrated for baseband optical signaling access networks, in experiments that have advanced the state of the art in low-complexity high-rate signaling. Uncooled, directly modulated silicon laser devices have been applied in optical access networks operating at baseband data rates up to 10.7 Gbps, and which achieve record transmission distances over field-deployable optical transmission fiber.

Prior to the start of this research, VCSEL devices had been suggested for low-cost FTTH installations,[256,257] but it was understood that the modulation response of such devices made them unsuitable for long-reach OAN implementations. *Optical injection locking* (OIL) had been proposed as a method of reducing[258] or tuning[259,260] the chirp of the optical signal source, to achieve transmission lengths typical of long-reach PON; but at the cost of added transmitter complexity. VCSEL devices capable of direct-modulation at 10 Gbps, without OIL or temperature stabilization, were obtained for experimental trials. These devices were provided within EU Project GigaWaM,[261] which intends to develop WDM-based long-reach FTTH networking within Europe. The optical output from these devices was characterized, the eye diagram and output optical spectrum is presented in Figure 5.1(a) and Figure 5.1(b), respectively. Laser bias and input signal conditions were optimized for maximum eye Q-factor; this was achieved at a bias of 11.5 mA and an average output optical power of −0.5 dBm, an extinction ratio of 5.88 dB and an output eye SNR of 7.5 dB were obtained. These values correspond with the waveform observed in in Figure 5.1(a). The optical spectrum for this device is presented as Figure 5.1(b); it was observed to vary within 1 nm over the course of the experiments.

The performance of this device was assessed for the uplink of an optical access network, and the results were presented results in Paper G. Stable, error-free (BER = 10^{-9}) transmission was obtained over 40 km of uncompensated SMF at a modulation rate of 10.7 Gbps, with a receiver input power level of approximately −19 dBm. This represents the furthest-known demonstration of a free-running 1550 nm VCSEL directly-modulated at 10 Gbps. Optical bandpass filtering was used to remove out-of-band ASE from the photodiode input st the pre-amplified receiver; no offset filtering or other chirp-to-intensity conversion was required for system operation, although it was clear during the analysis that there was some

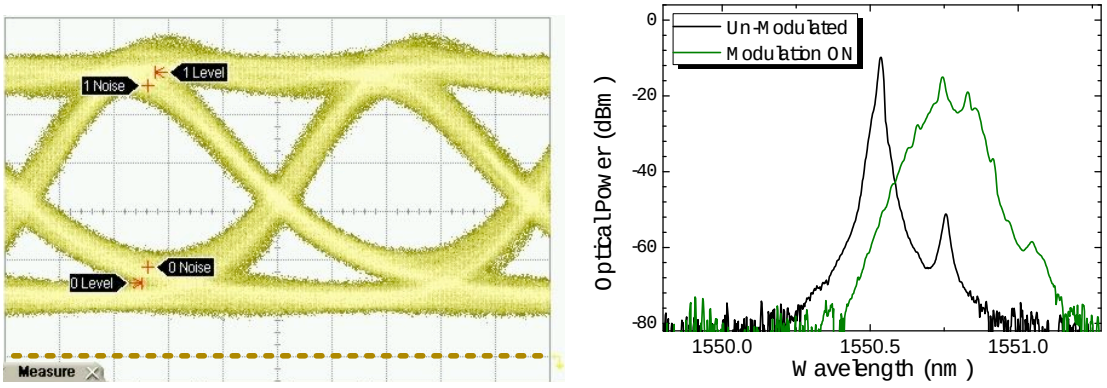

(a) 10.7 Gbps Eye. (b) Optical Spectrum (OSA resolution: 0.01 nm)

FIGURE 5.1: VCSEL output for direct modulation at 10.7 Gbps; (a) eye diagram and (b) optical spectrum. Extinction ratio of 5.8 dB, eye SNR of 7.5 and average optical power of −0.5 dBm obtained at 11.5 mA bias. From PAPER G.

advantage that would be obtained by such selective filtering. The system was characterized for *optical bandpass filter* (OBPF) passband centering on the received signal spectrum, which allowed maximum received signal energy through to the photreceiver.

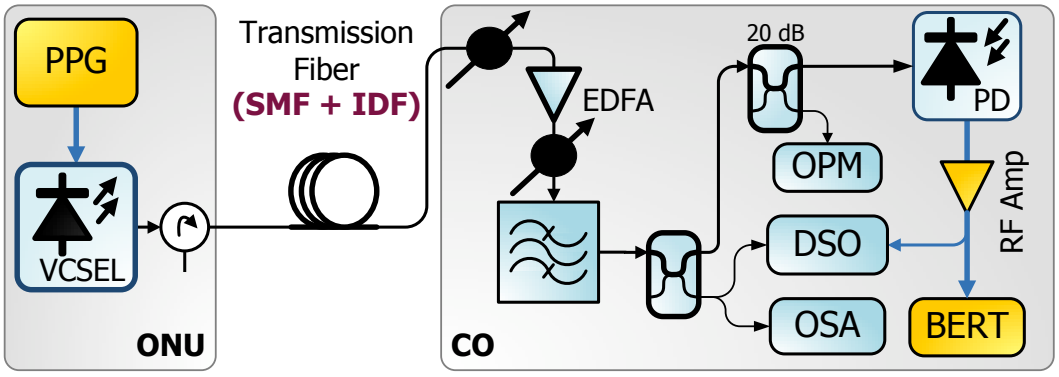

FIGURE 5.2: Uncooled free-running VCSEL in uplink of 99.7 km OAN, transmission span comprised matched spans of G.652 SMF and inverse dispersion fiber (IDF). The pre-amplified receiver allowed passive link operation. BERT, bit-error rate test set; DSO, digital storage oscilloscope; OPM, optical power monitor; PPG, pulse pattern generator. From PAPER G.

This network was extended by the deployment of matched spans of SMF and IDF, using the setup shown in Figure 5.2, and note was made of the evolution of the optical signal at key points throughout the network. Observations were made of the effectiveness of IDF in reducing net dispersion penalty of the long-reach PON installation, as well as extending the range of the passive infrastructure.

Evaluations were done of 10 Gbps transmission over 23.6 km of uncompensated SMF,[262] as well as matched-span SMF + IDF links of 50 km[263] and 99.7 km passive fiber plant (with no mid-span amplification). Advanced results, including power sensitivity analyses and eye diagram characterizations are presented in Paper G.

5.2 Transparent RF Signal transport via Optical Access Network

5.2.1 UWB over Long-Reach PON

In 2007, UWB signal generation and delivery was a hot research technology being developed for next-generation wireless applications including PAN connectivity, electronic tagging or positioning. Interest was primarily focused on potential applications in two unlicensed spectral bands: the first was between $3-10$ GHz, in addition to 7 GHz-wide allocation close to 60 GHz. In an IR-UWB system, a Gaussian singlet or doublet pulse[264] may be designed to satisfy the spectral mask required for FCC-compliant[176] indoor UWB signaling. Unfamiliarity with this particular waveform motivated an interest in the research community to evaluate a simple, repeatable signal generation unit that could be modulated for high speed data transmission. At the time, there was particular interest in reducing the complexity of the UWB signal generator, since there was yet no optimized method for electrical generation of the pulse shapes required. Prior art solutions exploited optical dispersion in fiber, cross-gain modulation (XGM) in an SOA or OEO conversion of a chirped laser signal with filtering in the electrical domain. Demonstration was made of two all-optical methods for generating UWB signaling that required a single commercially - available directly-modulated DFB laser source. UWB signals were produced, which were compliant with the active specification, and these results have been reported in Paper C and Paper D.

Paper C reported on the use of a directly-modulated DFB laser that was biased far from threshold. The adiabatic chirp of the laser output was exploited by using an OBPF to shape the laser output pulse in the optical domain: an UWB signal at a repetition rate of 390.6 MHz was obtained after photodetection. In this experiment, tuning an OBPF with a Gaussian passband profile such that the laser output spectrum fell within the linear region of the OBPF passband profile

was found to yield best results. An optical amplifier was implemented at the transmitter to increase the available power in the system, allowing transmission over 20 km NZDSF.

Paper D demonstrates an alternative approach for generating UWB signals. A directly-modulated DFB was biased close to threshold, and the modulated optical output signal from the laser was optically bandpass filtered. This filtering removed the high-frequency oscillatory terms associated with the under-damped relaxation oscillations observed in the laser output. A 10-GHz phototodiode was implemented at the receiver, to recover the UWB-compliant waveform in the electrical domain. Since the optical filtering reduced the available optical power, a boost EDFA was utilized at the transmitter to improve the power budget of the system. This waveform was successfully transmitted over a long-reach access link, achieving standards-compliant signaling without dispersion compensation. An in-line amplifier was required to achieve 118 km (88 km SMF and 30 km NZDSF) optical transmission. Paper D additionally reported the longest distance achieved in optical delivery of a UWB-compliant waveform. These results indicate the feasibility of centralized UWB signal generation and distribution via long-reach uncompensated OAN systems.

This work has advanced the state of the art in all-optical UWB signal generation and delivery. Paper C has been selected for re-publication[265] in the Virtual Journal of Ultrafast Science, an edited compilation of links to articles on focused areas of frontier research; it is published by the American Physical Society and the American Institute of Physics in cooperation with numerous other societies and publishers. This work has also attracted interest from the wider engineering community, the authors have recently accepted an invitation to contribute to a new textbook on novel technologies in optical signaling.[266]

5.2.2 All-Optical support for Adaptive Antenna System

During this project, the growing use of multi-antenna transceiver systems within newer wireless access standards[160,163,181] was identified, and it was noted that RoF research was not providing adequate support for novel multi-antenna transceiver systems. A potential application of such an adaptive antenna system was examined, and it was determined that the capability for provisioning all-optical control of the wireless beam launched from such a multiple-antenna wireless access point

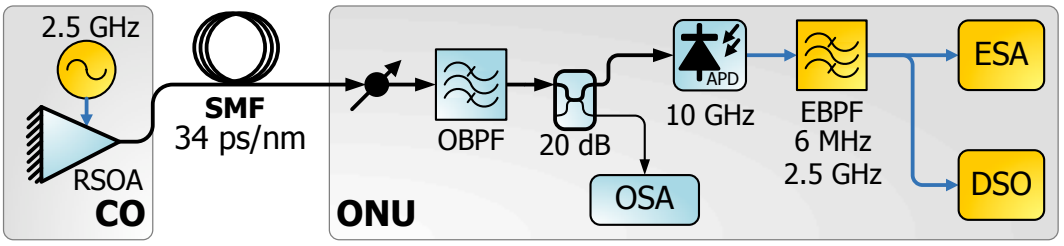

(a) Initial Characterization

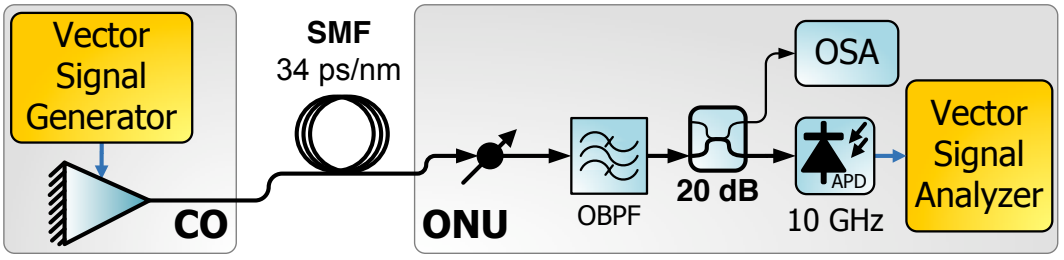

(b) Advanced System Evaluation

FIGURE 5.3: All-optical continuously-variable true time delay for adaptive antenna system; (a) delay characterization with 2.5 GHz tone; (b) evaluation of complex-modulated RF signals. OAN implemented 2 km SMF($D = 34$ ps/nm). EBPF, RF bandpass filter; ESA, RF spectrum analyzer. (From PAPER F).

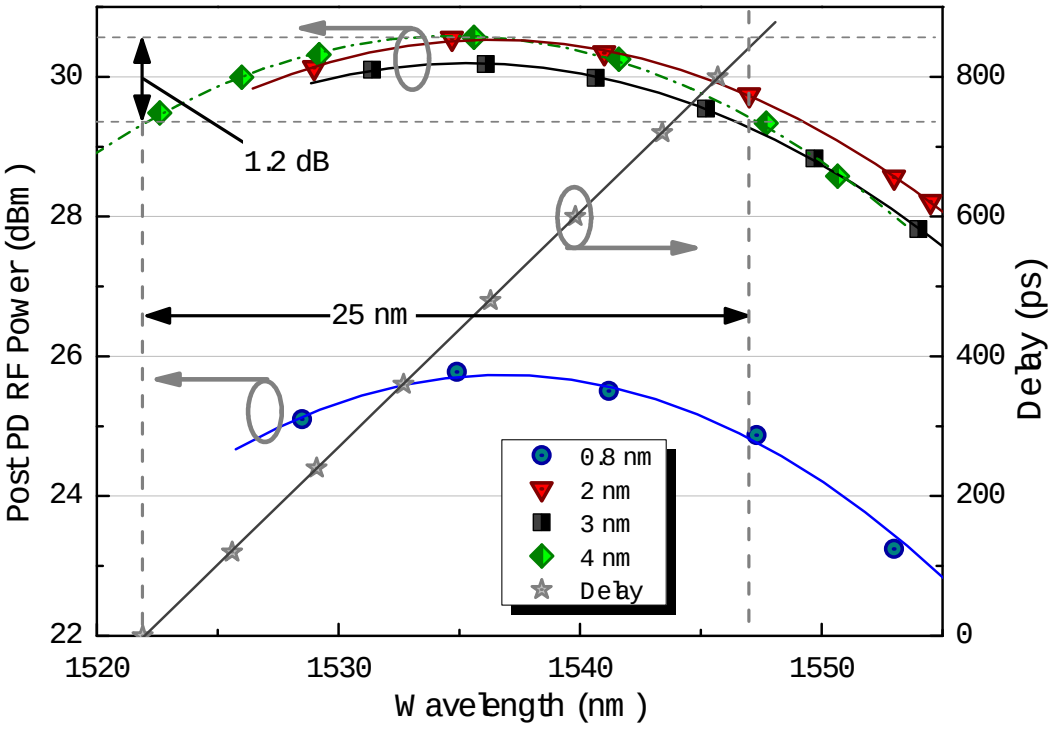

FIGURE 5.4: RF output power (left axis) and TTD (right axis) variation with OBPF central wavelength (horizontal axis), for OBPF FWHM of 0.8 nm, 2 nm, 3 nm and 4 nm; the setup is shown in Figure 5.3(a). (From PAPER F).

would be very attractive from a systems engineering point of view. The key requirement of such an AAS is the ability to control the relative delay between wireless signals radiated from elements of an antenna array; the wireless beam thus obtained would have a tunable launch angle. Such systems also find applications in radar and radio telescope applications.[217] Since the first application of optical technology in the provision of true time delay of an RF signal,[216] proposals have implemented active switching devices implementing discrete delay intervals (therefore supporting a finite number of wireless launch angles),[267,268] or require specialized optical components.[269]

Subsequent work resulted in a low-complexity all-optical control mechanism for continuously-variable steering of the launched RF beam from the WAP: the system utilized the wideband optical output of an un-seeded RSOA, as well as the chromatic dispersion of the optical access infrastructure and tunable optical bandpass filtering to implement the differential delay required. The system requires antenna-coupled photodiodes at the wireless-enabled ONU to implement the all-optical beam-steering solution. Adjustment of the source wavelength would be used to vary the launch timing from each element of the ONU antenna array.The TTD provided by the system was characterized with the setup shown in Figure 5.3(a), and evaluated of WiMAX transport functionality was done using the setup shown in Figure 5.3(b). Complex-modulated RF signals may be characterized by an *error-vector magnitude* (EVM)[270] metric; wireless RF access standards therefore specify minimum EVM requirements for standards compliance. The *vector signal generator* (VSG) and *vector signal analyzer* (VXA) test set equipment allowed direct evaluation of the EVM of the RF signal after transmission. The source datastream for the modulator was a pseudo-noise sequence (PN-23), generated internally by the VXA.

The optical transmitter was an unseeded commercially-available directly modulated RSOA with 1.5 GHz electrical bandwidth; linear modulation was successfully obtained for narrowband,[271] as well as OFDMA wide-band[272] WiMAX-compliant signaling with carrier frequencies of 2.5 GHz and 2.4 GHz, respectively. Paper F presents a thorough report on this system, and details the mechanisms exploited for system operation. This paper also provides a report on the gain and linearity characteristics of the wireless signal delivery mechanism for implementing adaptive-antenna functionality.

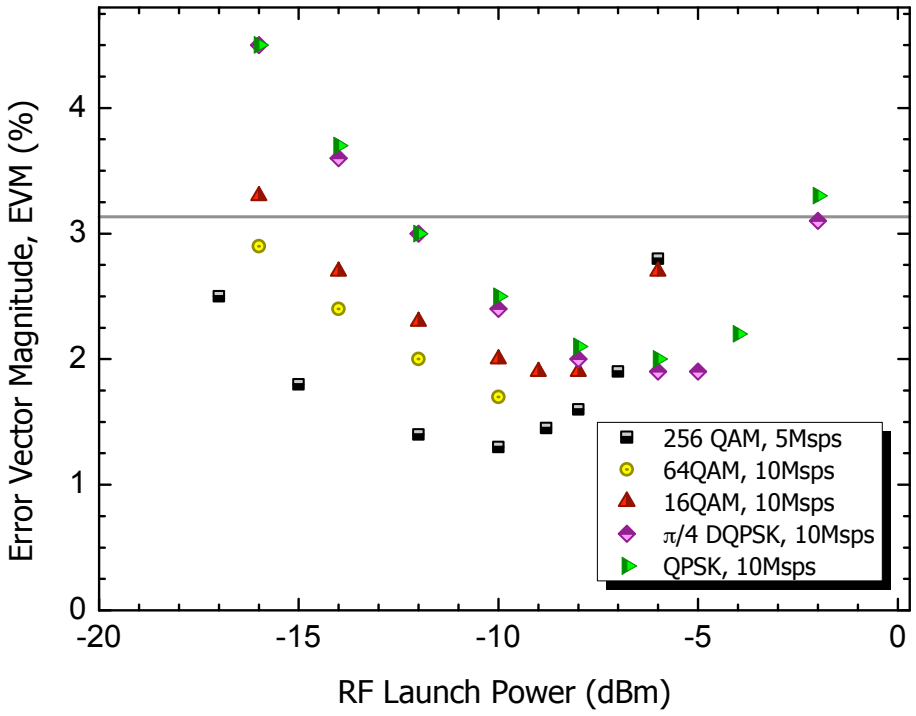

FIGURE 5.5: EVM variation with RF launch power for various modulation schemes; 256-QAM, 64-QAM, 16-QAM, QPSK, and $\pi/4$ DQPSK. Results evaluated under identical conditions using setup shown in Figure 5.3(b); 2 nm OBPF at 1540 nm. 3.1% WiMAX threshold for 64-QAM shown. (Unpublished)

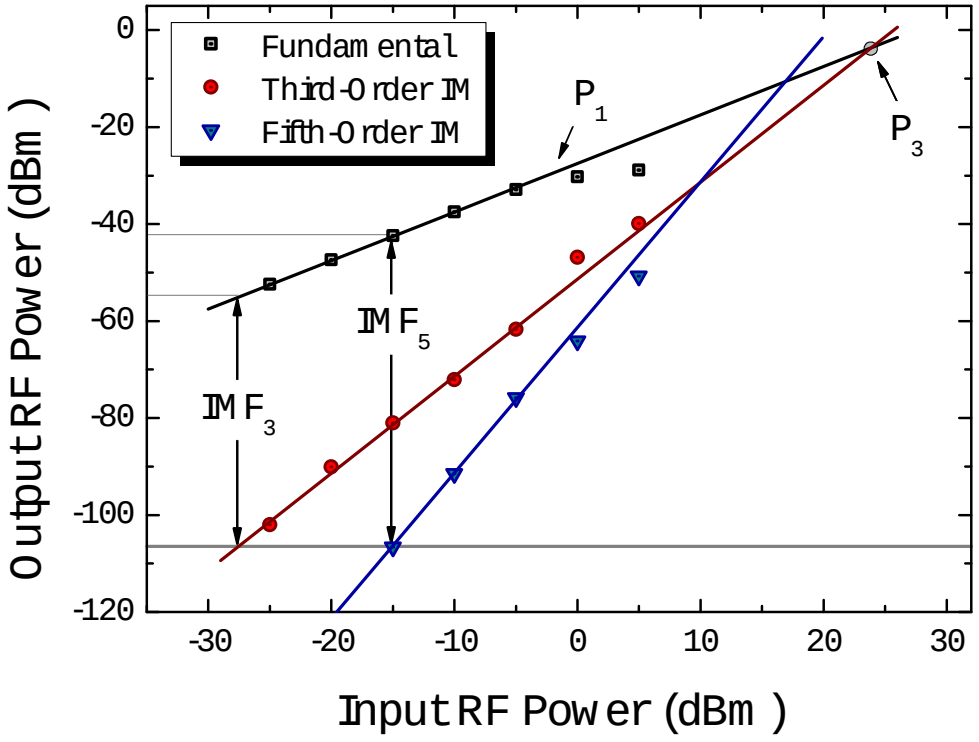

FIGURE 5.6: Linearity results of two-tone evaluation of TTD scheme showing fundamental, as well as third- and fifth-order intermodulation products. Inter-modulation (IM) free results shown (IMF_3=53 dB/Hz$^{2/3}$ and IMF_5=65 dB/Hz$^{2/3}$); system rejected even-order IM terms. From PAPER F.

Figure 5.4 reports the power penalty associated with OBPF detuning across the RSOA output spectrum, and the associated TTD. Un-published results from this experiment, shown in Figure 5.5, demonstrate support for several other modulation formats and modulation rates; clear eye diagrams and standards-compliant error vector magnitude (EVM) results were obtained with 256-QAM signals in the laboratory - such signal rates are above the highest mandated levels specified in the WiMAX standard, but demonstrated the applicability of this system for supporting future generations of wireless RF transport signals. EVM was assessed as a function of launch RF power and optical receiver power, for complex-modulated RF signals modulated on the 2.5 GHz carrier. Figure 5.5 presents the results for 256-QAM signaling at five *million symbols per second* (Msps), equivalent to 45 Mbps, as well as 64-QAM at 10 Msps (80 Mbps), 16-QAM at 10 Msps (50 Mbps), and $\pi/4$ DQPSK and QPSK at 10 Mbps (20 Mbps). These results show multi-protocol RF signal transport via this AAS scheme, which makes it suitable for AAS implementations requiring adaptive modulation rates. No additional hardware was required at the ONU to support multi-protocol signaling.

A two-tone injection test at a channel separation of 200 kHz was performed to assess the linearity of the RF delivery scheme; the results are presented in Figure 5.6. It was observed that only odd-order intermodulation products appeared at within the system bandwidth; the system successfully rejected second- and higher even-order intermodulation products at the output. System linearity was therefore constrained by third-order intermodulation product, and spur free-dynamic range (IMD_3) of 53 db/$Hz^{2/3}$ was evaluated. The 1 dB compression point (P_1) was close to, but less than 0 dBm input power and the third-order intercept (P_3) was close to +23 dBm input power.

5.3 RF Signal Downconversion and Delivery

A method for performing all-optical frequency downconversion of a passband intensity-modulated RF waveform was also demonstrated. In this scheme, a propagating RF wireless signal may be half-wave rectified by an appropriately-biased EAM and frequency downconverted by optical injection of a commerically-available DFB laser. This scheme was demonstrated with acommercially-available,

uncooled, multiple-quantum-well DFB device, and the results obtained were presented in PAPER A and PAPER B. Report has also been made on the use of optical envelope detection to frequency down-convert complex-modulated signaling.[273]

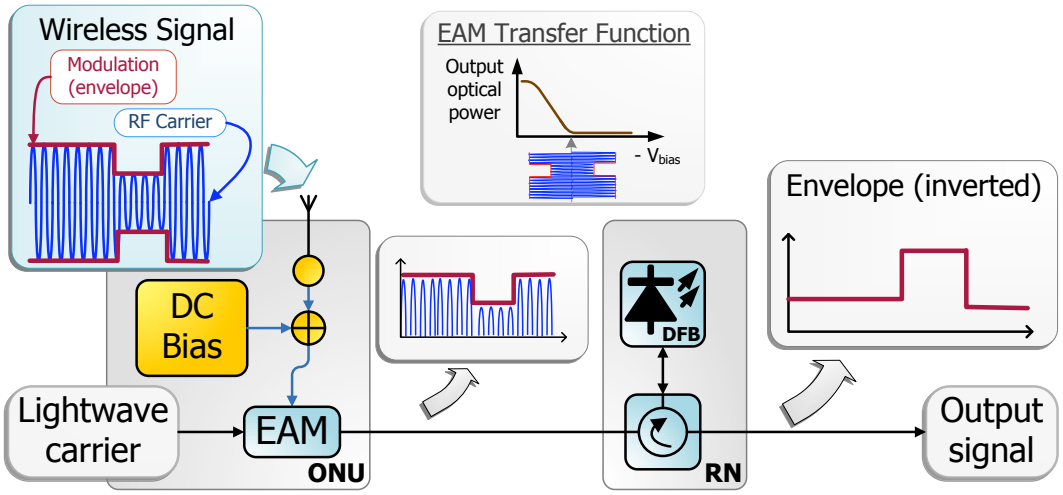

FIGURE 5.7: Showing the steps in all optical frequency downconversion; halfwave rectification in appropriately-biased EAM, followed by envelope detection from optical injection. EAM transfer function shown in inset, with applied RF signal at half-wave bias point. Taken from PAPER A.

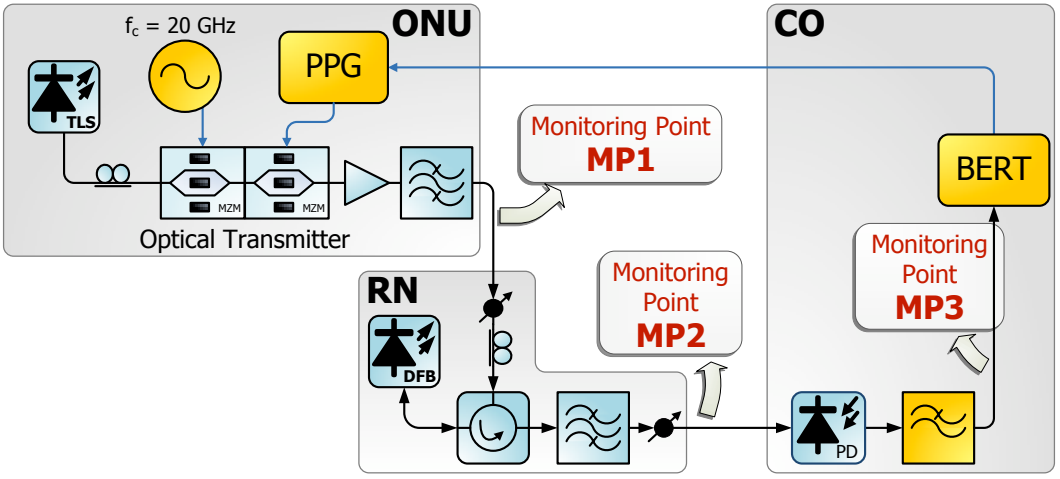

FIGURE 5.8: Demonstration of all-optical RF signal downconversion: system implemented Bessel LPF after photodetector (at CO). PPG, pulse pattern generator; TLS, tunable laser source; BERT, bit-error rate test set; MZM, Mach-Zehnder interferometer modulator. Taken from PAPER A. Transmission over a long-reach OAN was subsequently assessed with 20 km SMF between CPE and RN, and 50 km of transmission fiber between RN and CO.

As reported in PAPER A, this scheme for all-optical signal downconversion is presented as Figure 5.7. The scheme achieved frequency downconversion of the halfwave-modulated 20 GHz ASK input waveform, allowing error-free recovery of the data signal without use of RF signal processing equipment. By eliminating the

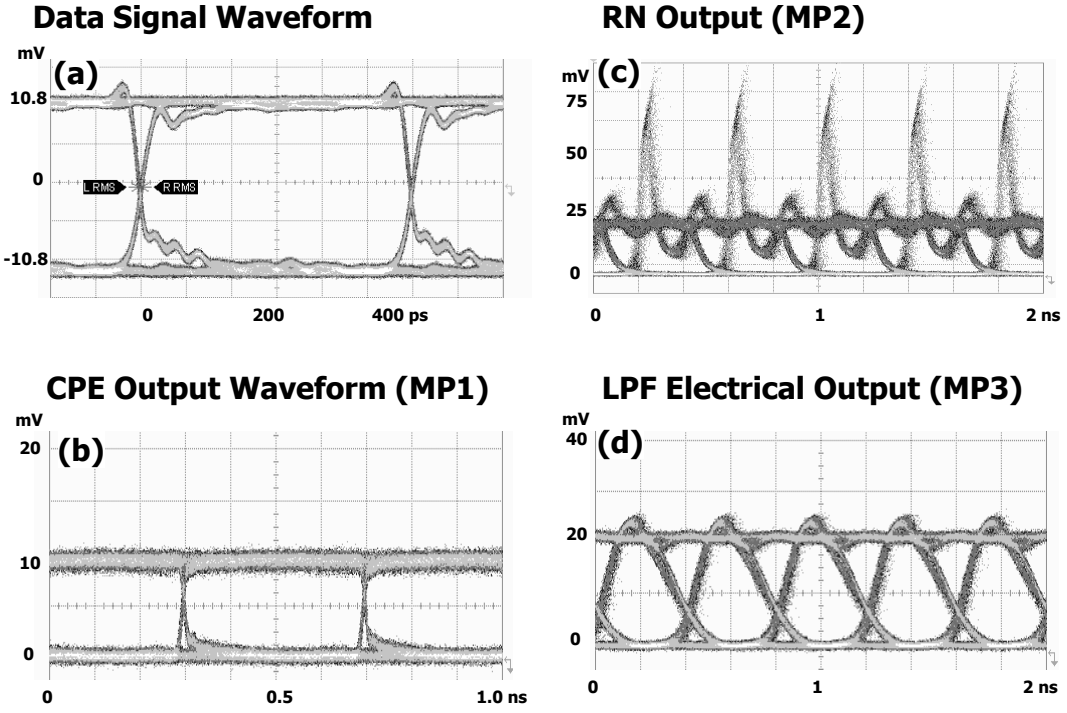

FIGURE 5.9: Evolution of baseband signal transmission propagating through signal downconversion and system. Taken from PAPER A.

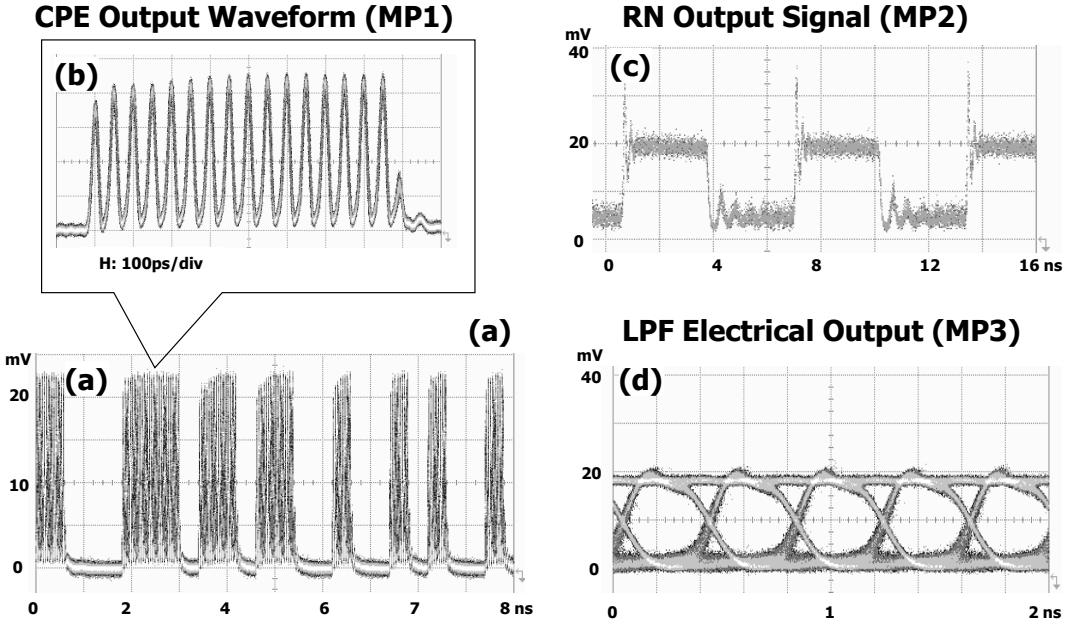

FIGURE 5.10: Evolution of RF Signal transmission propagating through system. Taken from PAPER A.

need for RF oscillator and mixer equipment, this system allows optical backhaul of the input microwave signal with a significantly simpler layout than would have been required with a conventional signal downconversion and transmission scheme. This method of performing the required frequency downconversion in the optical domain also allows the deployment of robust,

System operation was demonstrated with a half-wave optical intensity-modulated signal emulating a 20 GHz carrier wave ASK modulated at 2.5 Gbps. The DFB output contained the information from the source waveform, but resembled an NRZ-OOK baseband signal. Samples of the injected and output waveforms are presented in Figure 5.8. The electrical signal fron the receiving antenna allows modulation of the lightwave carrier; this optical signal is injected into the DFB laser at the RN. Within the injected laser device, cross-gain modulation effects transferred information from the injected lightwave onto the laser output; when the electrical source waveform was incoming wavefomsamples of the injected the laser output was of the form of an NRZ-OOK modulated signalof the incoming signal waveform onto the laser output. The DFB device exhibited relaxation oscillations at a frequency of approximately 5 GHz; this was apparent in the overshoot observed in the optical output waveform, as well as limiting the maximum data rate supported by the system. The underdamped response of the DFB to the optical injection signal required electrical low-pass filtering at the output of the photodetector at the CO; the optimal bandwidth of this LPF varied with the data rate used.

Paper B reports the application of this scheme in a long-reach optical access link, consisting of 20 km SMF between the wireless-enabled CPE and the RN, and an additional 50 km between RN and CO. Conversion of the input intensity-modulated RF waveform to a baseband signal format at the RN, which was closer to the CP than the CO, eliminated most of the fading penalty that would have been incurred with direct transmission of the 20 GHz carrier. It was also noted that envelope detection and transmission over the optical link would have also suffered from the dispersive fading: if nonlinear effects are neglected, halfwave RF waveform transformation produces spectral components at multiples of the RF carrier frequency, each of which would have incurred fading penalty, dependent on the frequency range occupied. This system provided a transmission penalty of less than 1.7 dB receiver penalty at a BER of 10^{-9}. Review of Figure 3.5 indicates

that 20 GHz transmission over 20 km SMF is associated with significant dispersive fading penalty; however this transmission distance exceeds the first null of the dispersion penalty response. Although acceptable transmission quality may occur at these lengths, engineering principle suggests that sound system implementation would avoid this variation in penalty by location of the RN as close to the CPE as feasible: all-optical signal downconversion would overcome the dispersive penalty. The notable advantage of this system is that it removes the influence of this periodic fading penalty without requiring electrical signal processing in the RN or CPE nodes; indeed, the uncooled, injection-locked DFB implemented at the RN provides additional optical energy to the transmitted signal, allowing implementation in a long-reach PON environment, for example, without requiring external optical amplification.

5.4 Converged Signaling over OAN

This work has demonstrated that engineering design techniques may be used to support converged access signaling over a simple optical access network. Paper A reported on the support for baseband signal transmission with this optically-injected RN device. Transmission of a 2.5 Gbps NRZ-OOK modulated input waveform through the system was achieved without any required changes to the infrastructure. Since the optimal cut-off frequency of the post-detector LPF implemented at the CO varied with the data rate used, it was possible to upgrade the system to transmit at 5.5 Gbps by implementing a 4.5 GHz LPF after the photodetector.

5.4.1 WiMAX over Long-reach OAN

WiMAX technology has been developed to bridge the niche between low-mobility, high throughput WLAN systems, and high-mobility enabled technologies providing lower data rates. it has been defined in IEEE standards that allow fixed-node communications[181] as well as multiple-access systems[163,164] that support greater user mobility. Key requirements of the WiMAX standard is the support for high-rate modulation formats, with mandated support for BPSK, QPSK, 16-QAM and 64-QAM and optional support for 256-QAM.

Support for WiMAX intensity-modulated radio-over-fiber systems has been investigated with the use of commercially-available colorless optical transceivers, key results have been presented in Paper G. Devices originally optimized for digital data transmission have been operated in an analog regime; a 10 GHz MZM was implemented at the ONU and a 40 GHz EAM was implemented at the CO. Wireless signal transmission was assessed within the Danish unlicensed spectrum around 5.8 GHz, frequency separation was used to separate uplink and downlink channels (5725 MHz and 5800 MHz), allowing the evaluation of bidirectional transmission in optical and wireless domains. The system was designed for simplification of ONU equipment; signal generation equipment was installed only at the CO, and RF low-noise amplifiers and RF duplexers were implemented after photodetection at the ONU, to condition signal levels before wireless transmission. The system was optimized for best linearity.

Paper G presents the bidirectional transmission of 256-QAM modulated signaling for WiMAX transmissions at data rates of 100 Mbps (downlink) and 64 Mbps (uplink) over 80 km optical fiber;[194] this scheme utilized a single optical wavelength and implemented colorless transceivers. This manuscript additionally presented the results of bi-directional 64-QAM transmission in this system, to demonstrate compliance with the current definitions of the WiMAX standard. The colorless transceivers and single-wavelength operation suggested interoperability in a WDM transmission scheme, which was investigated in a coordinated experiment for multi-service delivery via a WDM optical infrastructure: this was a groundbreaking experiment that combined expertise from significant areas of optical access networking technologies. A brief review of key results will be presented in the next section.

5.4.2 Converged Signal Delivery via OAN

Paper E reports an assessment of the performance of a WiMAX radio over fiber scheme operating in a real-world testbed including 78.8 km of installed optical cable, which was part of a Danish commercial optical communications network. Signals from other optical access technologies were WDM multiplexed onto the same fiber: in addition to the WiMAX signal, there four channels modulated with NRZ-DQPSK, two channels with a coherently-detected BPSK RoF signal, and one channel was modulated with IR-UWB. The equipment layout is shown in

Figure 5.11; this was the first known demonstration of such diverse signaling over field-deployed optical infrastructure.

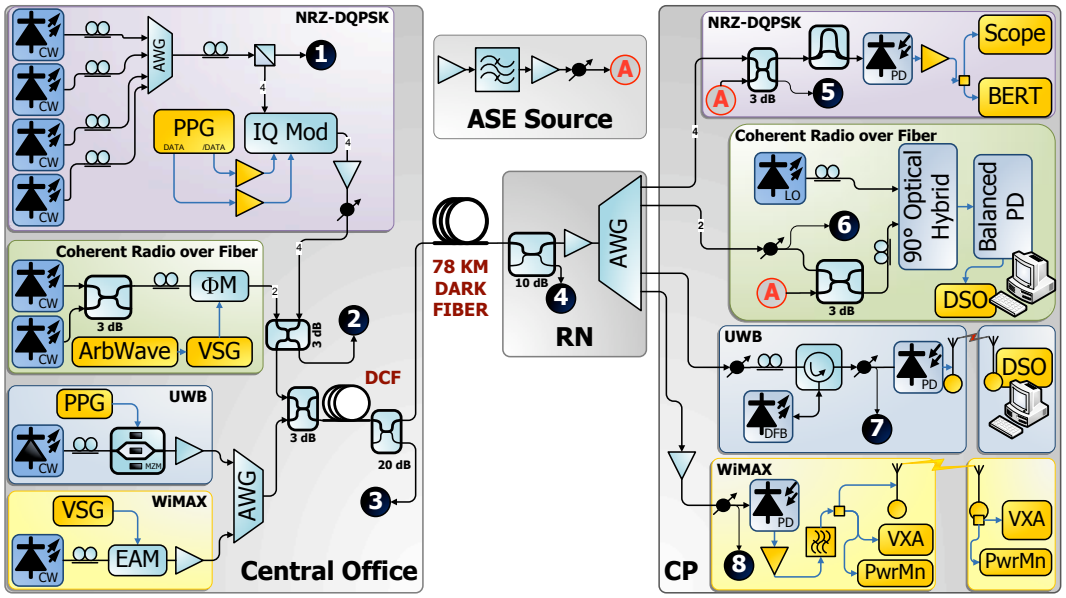

FIGURE 5.11: System layout for converged-services delivery via optical access network. PPG, pulse pattern generator; ArbWave, arbitrary waveform generator; VSG, vector signal generator; VXA, vector signal analyzer; PwrMn, RF power monitor; AWG, array waveguide grating WDM multiplexer; ASE, amplified spontaneous emission; BERT, bit error rate test set. From PAPER E.

WDM channel spacing of 200 GHz was utilized, because of the unavailability of AWG devices with narrower channel separation. Due to equipment constraints, it was not possible to simultaneously evaluate bidirectional transmission on any of the eight WDM channels used. Direct assessment was made of single-channel operation on all services, as well as system performance with simultaneous WDM transmission.

For the WiMAX channel, a short range bi-directional wireless link was implemented within the laboratory, although longer-range wireless evaluations were precluded during the equipment loan period because of unfavorable weather. Since WiMAX is a licensed wireless RF access technology, the communications link was monitored to ensure that the transmissions in the unlicensed 5 GHz transmission band did not encounter interference from other sources. Assessment was made of optical and wireless transmission on the performance of the WiMAX service.

Converged signaling for fixed and wireless access networking over a shared optical infrastructure was successfully demonstrated. All services were successfully

carried, error free, by the shared optical infrastructure and wireless transmission environment (for UWB and WiMAX).

5.5 Conclusions

Work done within this project has demonstrated support for transparent delivery of multiple signaling formats via current-generation optical access infrastructure. Reports have been presented on the application of uncooled, low-complexity directly modulated VCSEL devices in extending the range of passive optical networking. Standards-compliant UWB signal generation, transport and delivery via passive optical access network infrastructure has also been reported. Finally, it was shown that long-reach WDM technology being developed for next-generation optical access networks can support the converged signaling required to support fixed and wireless services delivery.

Paper A

K. Prince, I. Tafur Monroy, J. Seoane and P. Jeppesen, "All-optical envelope detection for radio-over-fiber links using external optical injection of a DFB laser," *Optics Express*, vol. 16, no. 3, pp. 2005–2014, Feb. 2008.

All-optical envelope detection for Radio-over-Fiber links using external optical injection of a DFB laser

Kamau Prince, Idelfonso Tafur Monroy, Jorge Seoane, and Palle Jeppesen

COM•DTU, Department of Communications, Optics & Materials, Technical University of Denmark, DK-2800, Kgs. Lyngby, Denmark
kpr@com.dtu.dk

Abstract: We outline a novel method performing all-optical envelope detection of radio-frequency signals for radio-over-fiber links. A high frequency modulated signal with a slower-varying envelope is injected into a DFB laser which, due to gain suppression effects, recovers only the envelope of the optical signal. We characterize the DFB gain suppression effect in terms of injected signal wavelength and power level requirements. System performance is assessed, including experimental bit-error rate results; these illustrate successful envelope detection for a 20 GHz carrier with ASK modulation operating at 2.5 Gbit/second. Preliminary results at 5.5 Gbit/s show significant potential for application in hybrid optical-wireless communications networks.

OCIS codes: (060.0060) Fiber optics and optical communications; (060.2330) Fiber optics communications; (060.5625) Radio frequency photonics.

References and Links

1. A. Hirata, T. Nagatsuma, T. Kosugi, H. Takahashi, R. Yamaguchi, F. Nakajima, T. Furuta, H. Ito, H. Sugahara, and Y. Sato, "120-GHz-band millimeter-wave photonic wireless link for 10-Gb/s data transmission," IEEE Trans. Microwave Theory Tech. **54**, 1937-1944 (2006).
2. I. Tafur Monroy, J. Seoane, and P. Jeppesen, "All-optical envelope detection for wireless photonic communication," in *Proceedings of 33rd European Conference and Exhibition on Optical Communication* (ECOC, Berlin, 2007), pp 173-174.
3. A. Nirmalathas, D. Novak, C. Lim, R.B. Waterhouse, D. Castleford, "Fiber networks for wireless applications," in *Proceedings of IEEE Lasers and Electro-Optics Society 2000 Annual Meeting* (LEOS, Puerto Rico, 2000) pp. 35-36
4. G. Agrawal and N. Dutta, *Semiconductor Lasers, 2nd ed.*, (Van Nostrand Reinhold, New York, 2003).
5. B. R. Koch, J. S. Barton, M. Masanovic, Z. Hu, J. E. Bowers and D. J. Blumenthal, "Monolithic mode-locked laser and optical amplifier for regenerative pulsed optical clock recovery," IEEE Photon. Technol. Lett. **19**, 641-643 (2007).

1. Introduction

Continuing trends of increasing speed and coverage in the mobile communications services marketplace indicate further deployment of higher-capacity communications technologies well into the foreseeable future. A major hurdle in the development of these networks will be the realization and implementation of reliable low-cost network interface nodes between high-bandwidth wireless networks and the fixed core communications infrastructure. As an example of ongoing development trends, envelope detection of a 10 Gbit/s amplitude shift key (ASK) modulated 110 GHz carrier wave employing microwave components was recently reported in [1]. It is anticipated that backhaul infrastructure for cellular and broadband wireless networks will converge with that of fixed broadband networks in the near future.

All-optical envelope detection allows easy integration of microwave wireless communications schemes with fixed optical access links such as fiber-to-the-customer-

#89805 - $15.00 USD Received 19 Nov 2007; revised 14 Jan 2008; accepted 25 Jan 2008; published 29 Jan 2008

premises (FTTCP) infrastructure. Although most existing wireless communication systems employ heterodyning methods for radio-frequency (RF) down-conversion and detection, envelope detection of microwave signals has recently received attention due to its simplicity. Furthermore, simple, robust base station design and construction is an important requirement for the development of high bandwidth, high carrier-frequency wireless communications networks as these are characterized by smaller coverage cell size and therefore require that more base transceiver stations (BTS) be deployed over a given area. The authors have also reported successful envelope detection of a 3.25 Gbit/s signal stream, ASK modulated onto a 38 GHz carrier, by employing all-optical half-wave rectification followed by slow-bandwidth photodetection [2], to yield the downconverted baseband signal in the electrical domain.

In this paper, we report on an all-optical envelope detection approach employing external injection of a half-wave-rectified optical pass-band signal into a multi-quantum well (MQW) DFB laser which delivers the corresponding down-converted baseband signal in the optical domain. We propose to deploy this device at an intermediate point of an optical access network, to perform optical signal processing required to convert RF-over-Fiber (RFoF) signaling to baseband, and thus avoid the dispersion penalty incurred when RF carrier frequency signals are transmitted over the optical network [3]. The all-optical envelope detection simultaneously eliminates the requirement for more complex coherent detection systems at RF transceiver nodes. This all-optical scheme would therefore be integrable with a wireless network BTS connected to a FTTCP link, and presents the added benefit of lowering system complexity, representing potential cost savings for network implementation and maintenance. All-optical envelope detection was successfully performed with a 5.5 Gbit/s ASK system operating at 20 GHz carrier frequency.

2. Principle of operation

We consider the case of a base station employing optical envelope detection as depicted in Fig. 1. The ASK-modulated microwave signal received by the antenna drives an electro-absorption modulator (EAM), biased such that all-optical half-wave rectification is achieved [2]. This signal was directly injected into the active region of the DFB laser device and the resulting DFB output was evaluated to assess its suitability for data transport.

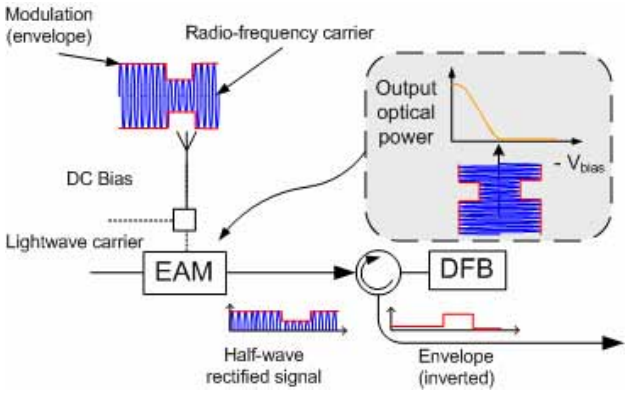

Fig. 1. All-optical envelope detection of wireless signals. EAM: electro-absorption modulator. DFB: distributed feed-back laser. V_{bias}: bias voltage

It is well known [4, 5] that introducing photons into an active laser cavity results in decreased output optical power at the lasing wavelength due to gain suppression. This effect may be described as a cross-gain modulation (XGM) and has typically been regarded as a pernicious feature of laser operation: it is traditionally mitigated with optical isolation at the laser output. We instead seek to exploit this optical XGM effect in the development of a novel all-optical envelope detection scheme. Optical injection of a distributed Bragg reflector laser

#89805 - $15.00 USD Received 19 Nov 2007; revised 14 Jan 2008; accepted 25 Jan 2008; published 29 Jan 2008

had previously been reported to perform high-speed optical packet detection with payload duration between 8 ns and 300 ns [5]. We instead wished to directly integrate the all-optical detection phenomenon directly into the data stream and evaluated the potential for replacing conventional optical signal conditioning circuitry with an appropriately biased DFB device.

3. Experimental setup

The experimental setup used for characterizing the gain suppression effect of an optical injected DFB laser for all-optical envelope detection is presented in Fig. 2. The core of this system is the external optical injected device, in this case implemented with a multiple-quantum well (MQW) InGaAs DFB device. This DFB laser is a commercially available, fiber pigtailed coax packaged device, with no optical isolation at the output; it is operated without temperature or wavelength stabilization circuitry. The central emitting wavelength λ_C was observed to lie around 1551 nm. A sample of the measured optical spectrum is presented in Fig. 3. The DFB laser used in these experiments was biased above threshold and optical signals injected into the active medium. The XGM effect caused laser output to be suppressed or allowed depending on the injected optical signal envelope. Since the laser response is slow compared to the radio-frequency carrier but faster than the source data rate, the resulting DFB output waveform therefore followed the inverted envelope of the optical source signal.

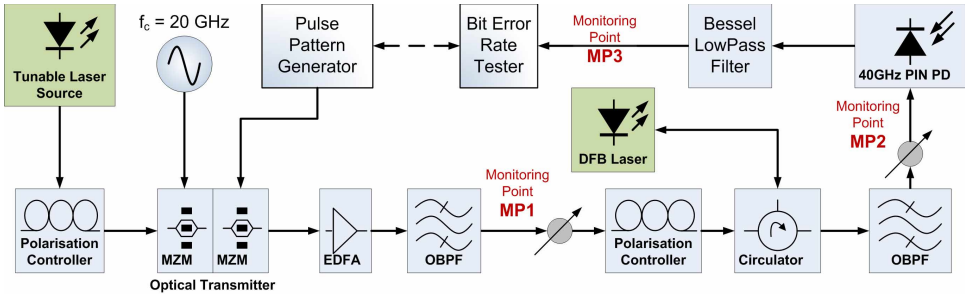

Fig. 2. Layout of the experimental setup. OBPF means optical band pass filter, MZM means Mach-Zehnder Modulator. Signal monitoring point (MP) locations are also shown.

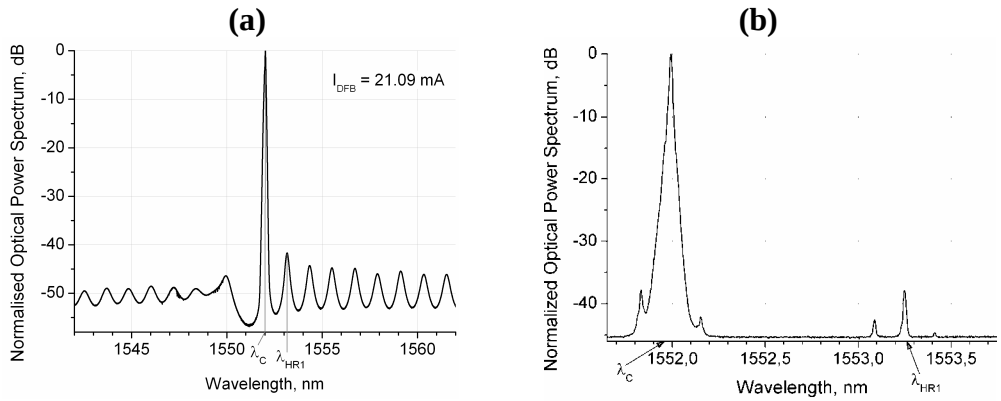

Fig. 3. Measured optical emission spectrum of the DFB laser used for external optical injection. The vertical axes have been normalized for convenient comparison. The peak wavelength λ_C was found to be close to 1551 nm; the first right side mode peak (λ_{HR1}) at 1553 nm. Higher side modes were observed at a periodic spectral separation of approximately 1.2 nm. The figure on the right indicates the spectrum observed at MP2 when the 2.5 GHz ASK signal is injected into the DFB at λ_{HR1} and filtered by the OBPF.

#89805 - $15.00 USD Received 19 Nov 2007; revised 14 Jan 2008; accepted 25 Jan 2008; published 29 Jan 2008

For experimental purposes, the optical transmitter was implemented by a pair of cascaded Mach-Zehnder interferometer modulator (MZM) units. The first MZM imposed the 20 GHz radio-frequency (RF) carrier. The second MZM imposed ASK modulation onto this optical carrier: the driving electrical signal was obtained from the pulse pattern generator. For RFoF input, the optical signal generated by the cascaded MZM is the same type obtained when an EAM device is used to perform half-wave rectification of an input RF passband signal [2]. This facilitated the evaluation of system response to baseband (by disabling the 20 GHz carrier wave) and passband RFoF (by enabling this carrier) signaling as required to emulate input from various types of terminal node equipment. A variable optical attenuator was used to set the value of the average optical power level injected into the DFB laser via an optical circulator. An optical band-pass filter (OBPF) was inserted after the EDFA to reduce system noise; the second OBPF allowed selection of the DFB emitting wavelength. Photodetection was implemented using a 40 GHz photodiode. The resulting electrical signal was filtered using a 1.8 GHz Bessel lowpass filter. Post-detector bit-error-rate performance was assessed using a bit-error-rate tester. Optical power splitters allowed monitoring and measurement of the signal at various Monitoring Points (shown). Polarization control was used to optimize system performance. Further work is required to optimize material selection and laser device design to reduce the polarization sensitivity of the cross-gain modulation effect at the core of this system and hence increase its attractiveness for practical implementation.

4. Results

First, we report on the experimental assessment of the DFB laser response to external injected optical signals with various wavelengths and power levels when operating at different driving current levels (*static operation characterization*). In this way, a suitable operating point was determined for the operation of the DFB as envelope detector. We then assessed the dynamic behavior of the system (*data signal response*) using PRBS of varying lengths and report on the bit-error rate measurements for the following cases:

- Baseline case: evaluation made of the performance of the ASK-modulated source, without the optically injected DFB system.
- Baseband performance of the DFB system: the ASK-modulated system operated with the 20 GHz carrier disabled.
- Envelope detection performance: the source signal is ASK modulated onto a 20 GHz carrier.

We also evaluated the signal BER sensitivity under the following conditions:

- Varying received power levels at the photodetector (MP2), with fixed injected power into the DFB,
- Varying injected optical power levels into the DFB, at a fixed average power at the photodetector (MP2).

Analysis was also done to determine the wavelength-dependency of the XGM effect exploited. Our observations are presented below.

4.1 Characterization of static operation

By disabling the two MZI modulators we consider the static case for different values of the tunable laser source emitting wavelength and input optical power level into the DFB. An example of the measurements results for the DFB output power and lase mode wavelength (λ_C) are presented in Fig. 4.

Four settings of the driving current were considered; all bias points selected were above the device threshold current value of 15 mA. Observations were made of the effect of operating point proximity to threshold and how this affected DFB output power and spectrum. Optical filtering was applied to remove signals at the operating wavelength of the tunable

#89805 - $15.00 USD Received 19 Nov 2007; revised 14 Jan 2008; accepted 25 Jan 2008; published 29 Jan 2008

laser (TL). The DFB output power was measured when λ_{TL} was varied over a wide range of wavelengths around λ_C.

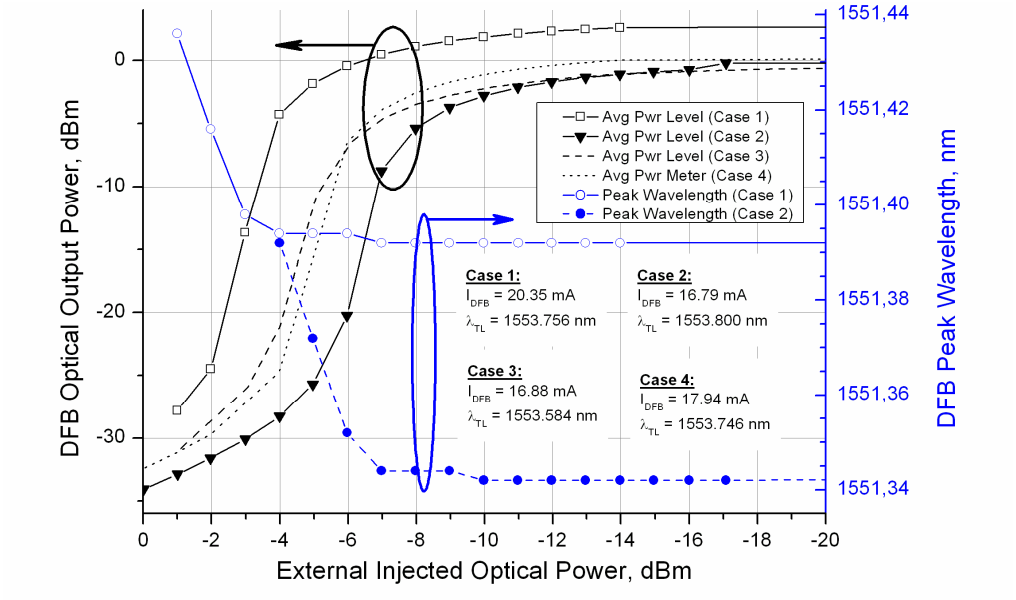

Fig. 4. Relationship between input optical power and DFB laser output power (black) and lasing wavelength (circles, blue) at various operating points (color online).

It was found that the device input/output relationship exhibited a sharper response to variations to external optical input power when the TL was aligned with one the spectral peaks observed in Fig. 3, and this response was greatest when the TL operating wavelength was greater than λ_C. At TL operation with wavelength below λ_C, more injected power was required to produce a similar extinction of the DFB output. From the static measurement results seen in Fig. 4, the following trends were observed:

- No hysteresis was observed in the relationship between input & output optical power
- For P_{TL}< -18 dBm, negligible variation in DFB output to change of P_{TL}
- For P_{TL} > -8 dBm, increased slope was observed for the DFB output optical power versus P_{TL} relationship
- For P_{TL} increasing above -6 dBm, DFB peak wavelength was observed to increase
- For P_{TL} < -8 dBm, the BL output wavelength of the DFB remained constant.

4.2 Data signal response

Consider an active transmission system implementing ASK modulation of a 20 GHz carrier, presenting optically halfwave rectified signals previously described [2]. We applied this 2.5 Gbit/s ASK-modulated output waveform to the DFB as shown in Fig. 2 and observed the signal characteristics of the test system. The power meter/variable attenuator at MP1 (see Fig. 2) was used to maintain a constant average optical power level injected into the DFB laser. Eye diagrams are presented as Figs. 5 - 6.

Figure 5 shows the signal propagation through the system with the carrier disabled: this corresponds to a baseband transmission scenario. The output from the optical transmitter (MP1) is presented in Fig. 5(b); the optical signal output from the DFB laser (MP2) is shown in Fig. 5(c); and the electrical waveform obtained after photodetection and low-pass filtering (MP3) is presented as Fig. 5(d).

#89805 - $15.00 USD Received 19 Nov 2007; revised 14 Jan 2008; accepted 25 Jan 2008; published 29 Jan 2008

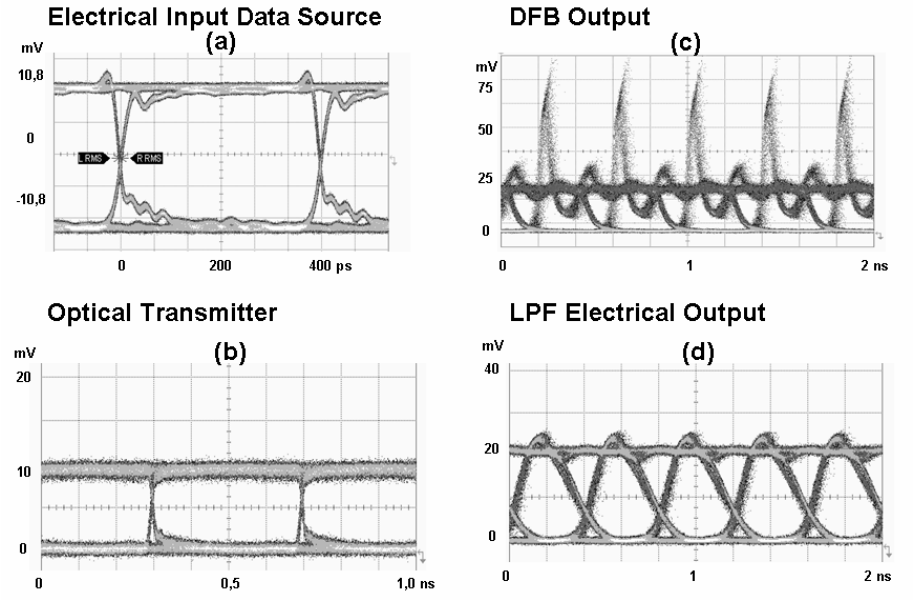

Fig. 5. Results were obtained for baseband system operation, without the 20 GHz carrier. We note the shape of the driving 2.5 Gb/s data source signal (a); the output waveform from the optical transmitter (Measuring Point, MP1) (b); the corresponding DFB output (MP2) (c), and the resulting electrical waveform obtained after 40 Ghz photodetection and filtering with a 1.8 GHz Bessel LPF (MP3) (d)

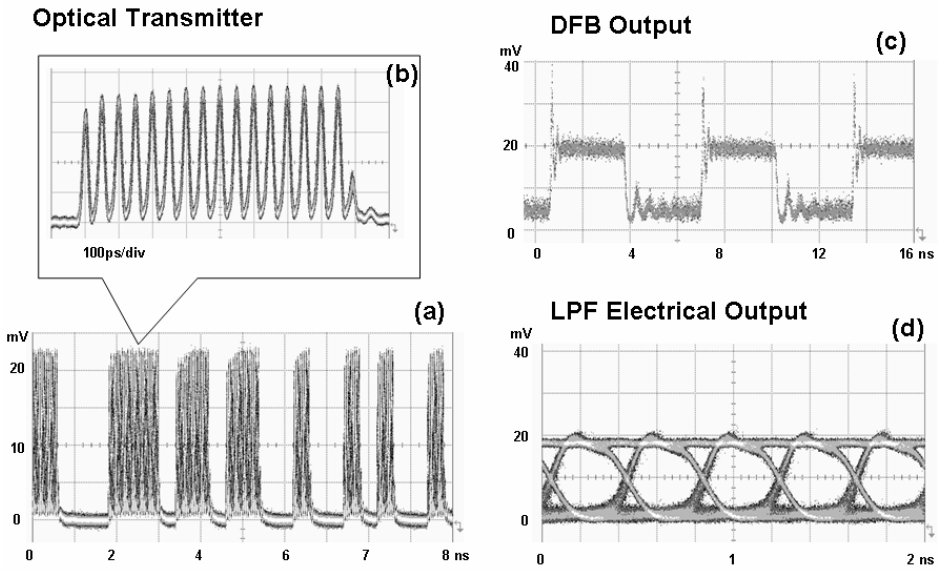

Fig. 6. Showing signal waveforms at various points in the system in response to a 20 GHz halfwave rectified ASK modulated signal input. The driving data waveform is identical to that of Fig. 5. We present details of the optical transmitter output waveform with different time resolutions (MP1) (a,b). The DFB output (MP2) and the output obtained by photodetection of this signal with a 40 GHz photodiode and filtering of the electrical signal obtained with a 1.8 GHz Bessel lowpass filter (MP3) are also shown as (c) and (d) respectively.

#89805 - $15.00 USD Received 19 Nov 2007; revised 14 Jan 2008; accepted 25 Jan 2008; published 29 Jan 2008

Figure 6 presents the results obtained with ASK transmission using a 20 GHz carrier. The driving data source waveform is similar to that presented in Fig. 5; this information is not presented twice. We instead present a sample of the waveform from the optical transmitter (MP1), shown in Fig. 6(a). Figure 6(b) presents a more detailed view of this waveform, corresponding to a data transmission sample. The DFB output in response to this driving input is presented as Fig. 6(c); and the results obtained from photodetection and application of the lowpass filter (LPF) as previously described is shown in Fig. 6(d).

From Fig. 6, we observed that the output of the optical transmitter is characteristic of an optical halfwave rectified signal, such as would be obtained at the output of an all optical wireless signal detector [2], shown in Fig. 1. The DFB output waveform exhibits the overshoot and relaxation oscillations associated with the switching of this device. We have observed improved rise and fall times of the DFB laser output: in response to an input signal having rise time of 22.2 ps, the minimum rise time of the DFB output is 14.6 ps. We additionally noted the removal of DFB output overshoot and high-frequency oscillations at MP3. Logic inversion was observed between the electrical input signal waveform and the DFB output. It is straightforward that application of appropriate bias to the EAM at the system input corrects for this effect and preserves signal logic during system transmission.

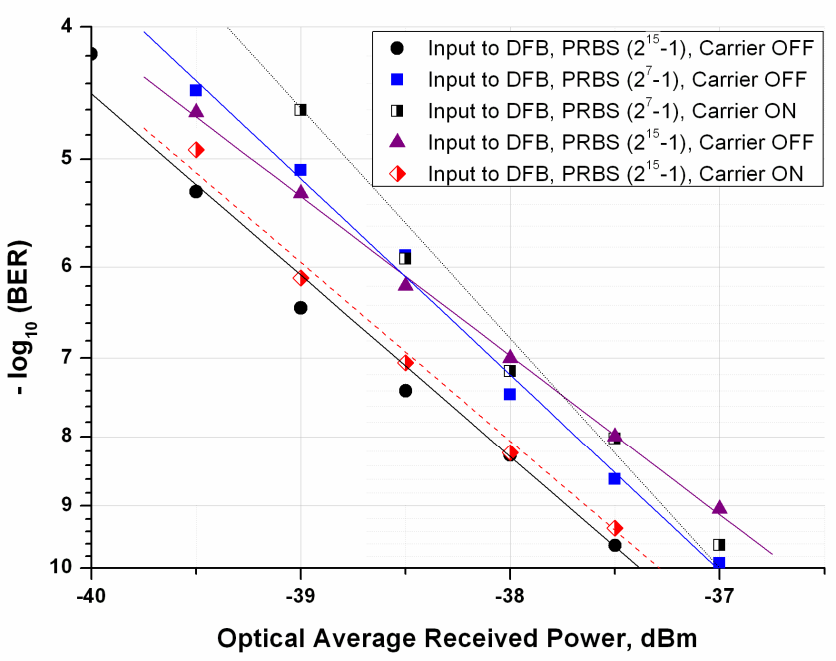

Fig. 7. BER sensitivity for fixed P_{TL} = -7.5 dBm and fixed DFB bias current of 21.10 mA. The baseline performance (black line) is very close to the best performance with the envelope detection of the 20 GHz carrier, 2.5 Gb/s ASK passband signal (red). (Color online)

4.3 BER sensitivity to received power

We evaluated bit-error rate (BER) sensitivity to receiver power with baseband and 20 GHz halfwave rectified input signal for fixed injected power level to the DFB and fixed DFB bias. Based on previous observations, the wavelength of the tunable source was set to λ_{HR1} as this operating point corresponds to the maximum response of the DFB to the injected signal. The electrical data pattern consisted of PRBS of lengths $(2^7 - 1)$ and $(2^{15} - 1)$ bits.

It may be seen from Fig. 7 that the optical transmitter signal yields a receiver BER sensitivity of 10^{-9} at approximately -37.7 dBm average received optical power. We consider

#89805 - $15.00 USD Received 19 Nov 2007; revised 14 Jan 2008; accepted 25 Jan 2008; published 29 Jan 2008

this the baseline scenario for evaluation of the signal quality effects introduced by the optically-injected laser system. Results for BER sensitivity analysis with the DFB are presented in Table 1 for baseband (carrier off) and passband (ASK modulation of 20 GHz carrier) system operation. With a PRBS of length (2^{15}-1) bits, we observed that the system sensitivity (at 10^{-9} BER) increased by 0.6 dB when the 20GHz carrier wave was activated in the ASK injected optical signal. With PRBS of length (2^{7}-1) bits, we observed that the system performance with envelope detection of the input optical signal was associated with a BER sensitivity degradation of 0.1 dB, relative to the sensitivity of the optical signal into the DFB. The worst-case receiver power penalty associated with inserting the optically-injected system is less than 1 dB relative to the baseline situation at this BER. This value may be considered to lie within tolerable experimental error limits.

These results indicate that negligible performance penalty is associated with insertion of the optically injected DFB system at the bias point and optical injected power selected. For DFB bias current close to 21.1 mA, the results of Fig. 4 indicate that optical power levels above the threshold P_{TL} = -4 dBm cause deviation of DFB output wavelength away from λ_C. We noted that the selection of average optical injection power level P_{TL} = -7.55 dBm into the DFB provided 3.5 dB operating margin before the onset of this wavelength shift.

Table 1. Receiver sensitivity at BER = 10^{-9} for various PRBS with 20 GHz carrier ON or OFF[a]

2,5Gb/s ASK. 20 GHz Carrier?	PRBS length	Receiver sensitivity for BER=10^{-9}
Off	2^7-1	-37.3
On	2^7-1	-37.2
Off	2^{15}-1	-37.0
On	2^{15}-1	-37.6

[a] Optical injection of baseband signal corresponds to scenario with *20 GHz Carrier off* and the emulated halfwave rectified signal is represented by *20 GHz Carrier on.*

4.4 BER sensitivity to optical power level into DFB, P_{TL}

We then assessed the relationship between receiver sensitivity and injected optical power level P_{TL} into the DFB when the system performed all-optical envelope detection of a 2.5 Gbit/s waveform ASK-modulated onto a 20 GHz carrier. For this assessment, the DFB bias current was fixed at I_{DFB} = 21.10 mA: the corresponding results are presented in Fig. 8. From Fig. 8, the following trends can be observed:

- For values of P_{TL} below -7.5 dBm, system sensitivity increased with increasing P_{TL}
- The best sensitivity was obtained in the range $-7.5\,dBm \le P_{TL} \le -4.5\,dBm$,
- For $-4.5\,dBm \le P_{TL} \le -4.0\,dBm$, the 10^{-10} sensitivity result is degraded, but the sensitivities at 10^{-9} and 10^{-8} BER display negligible variation.
- Values in the range P_{TL} > -4 dBm produced rapid deterioration in system performance. No usable results are available for this range.

We note that a sensitivity of less than -37 dBm for a target BER of 10^{-10} may be achieved for:

$$-8.0\,dBm \le P_{TL} \le -4.2\,dBm \quad (1)$$

4.5 Assessment of wavelength dependency of XGM effect produced by optical injection

We characterized the wavelength dependency of the injection locking effect used in this system. The first assessment was performed by maintaining a constant input power into the DFB and varying the injected signal wavelength. The response of the DFB was evaluated in

#89805 - $15.00 USD Received 19 Nov 2007; revised 14 Jan 2008; accepted 25 Jan 2008; published 29 Jan 2008

terms of the output power level and the output spectrum. We observed very similar response of the DFB device when the wavelength of the injected light corresponded to any of the spectral peaks in the range indicated in Fig. 2. This suggested that the envelope detection effect exploited throughout this paper is applicable across a wider range of input wavelengths. The DFB response to injected signal was negligible (i.e. no gain compression was observed) when the wavelength of the injected signal coincided with any of the minima (valleys) of the spectral curve as shown in Fig. 2.

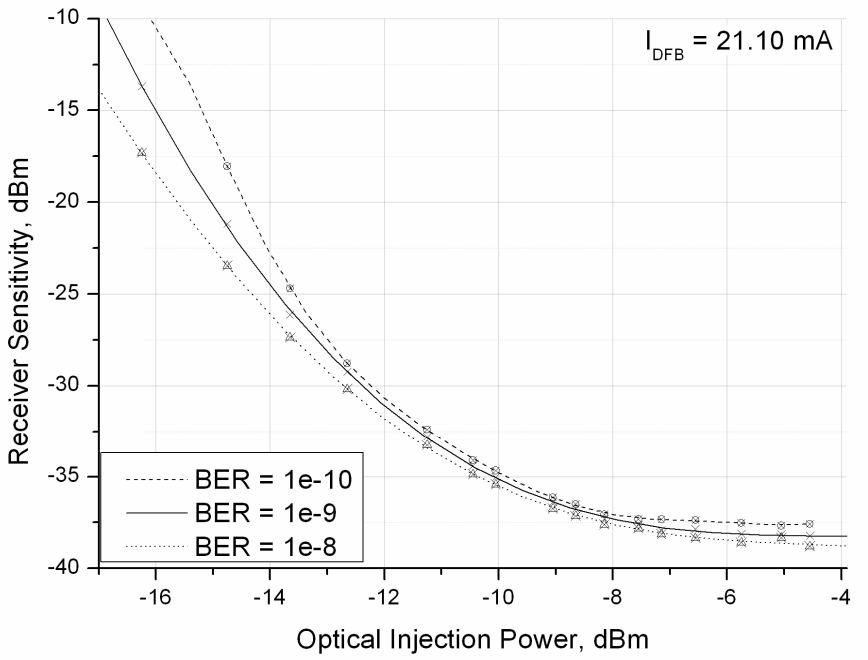

Fig. 8. Sensitivity analysis of DFB system (for I_{DFB} = 21.10 mA). These results were obtained when the injected signal was at a wavelength $\lambda_{TL} = \lambda_{HR1}$

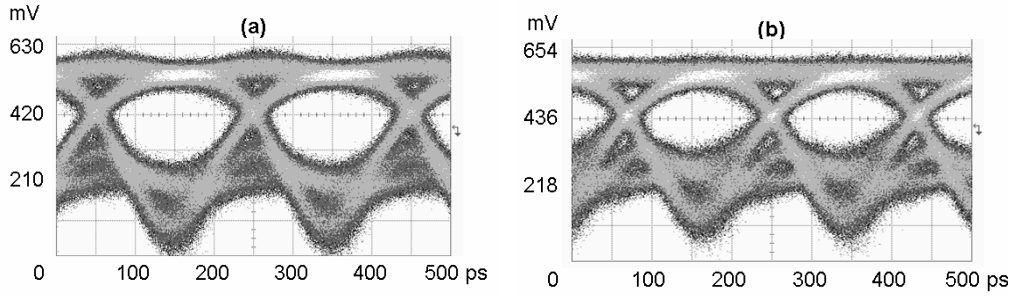

Fig. 9. Showing the eye diagrams obtained at system output with increased data rates of 4 Gbit/s (a) and 5.5 Gbit/s (b). A 4.5 GHz Bessel LPF was implemented after photodetector.

We then assessed the DFB response to an optical signal at an intermediate point between one of the peaks and valleys indicated in Fig. 3(a), to evaluate the power penalty incurred by operating the optically-injected system with misalignment between the injected signal and the DFB spectrum. For this analysis, we considered operation near the sixth harmonic wavelength greater than λ_C, denoted λ_{HR6}.

#89805 - $15.00 USD Received 19 Nov 2007; revised 14 Jan 2008; accepted 25 Jan 2008; published 29 Jan 2008

We observed the sixth peak at a wavelength of λ_{HR6} = 1559.116 nm, the corresponding power output was -56.08 dBm. We selected $\lambda_{TL} = \lambda_{HR6}$ and P_{TL} = -7.55 dBm and noted the minimum receiver sensitivity at target BER = 10^{-9}. We varied λ_{TL} around λ_{HR6} (with this fixed value of P_{TL} injected into the DFB) and observed that the XGM-dependent attenuation of the DFB output was decreased (i.e. DFB output power increased) when λ_{TL} deviated away from λ_{HR6}.

In order to determine the power penalty paid at the optical injection source due to this wavelength detuning, the DFB output was assessed when $\lambda_{TL} - \lambda_{HR6} = \varepsilon \neq 0$. We selected an injection wavelength of λ_{TL} = 1559.240 nm (therefore ε = 124 pm) and varied P_{TL} until the receiver sensitivity returned to the value noted in the previous paragraph. Under these conditions, it was found that P_{TL} had to be increased by 1.7 dB to achieve the same receiver sensitivity. Analysis of the DFB spectrum shows that the difference in output power obtained at this pair of wavelengths is 1.5 dB. The power penalty of misaligned wavelength operation is therefore greater than output power difference by 0.2 dB, which is less than 14% of the difference in DFB output power.

4.6 Assessment of transmission at increased bit-rate

We implemented a 4.5 GHz Bessel LPF, increased the data rate through the system and evaluated eye diagrams obtained at MP3. Eye diagrams are presented in Fig. 9(a) for operation at 4 Gbit/s, and in Fig. 9(b) for 5.5 Gbit/s. Full system characterization was not evaluated for this test, although these results indicate potential to operate at higher bitrates.

5. Conclusion

We have presented experimental results demonstrating that gain suppression due to external optical injection of a DFB laser can be exploited to perform envelope detection of wireless signal in a radio-over-fiber communications scheme. A characterization of the DFB output signal as a function of optical injected power level and wavelength values has been presented, leading to the determination and characterization of a suitable operation point for this system.

We assessed the performance of the optically-injected device under static conditions in which the wavelength and power of the injected optical signal is slowly varied and present observations made of the corresponding DFB output power and spectrum. Advanced system characterization is also presented for system operation at 2.5 Gb/s under baseband and passband conditions. Data transmission was experimentally evaluated with (2^7-1) and (2^{15}-1) bit-length PRBS: passband conditions were evaluated using ASK modulated 20 GHz carrier.

With the all-optical envelope detection scheme evaluated, optical signals yielding receiver sensitivity better than -37 dBm were achieved at a target 10^{-10} bit error rate (BER) with an average optical injected power less than -7.5 dBm. The BER sensitivity of the optical signal output from the DFB very closely followed that of the data source. These encouraging results indicate that the proposed all-optical envelope detection for wireless signals may provide benefits for accelerated convergence of radio-over-fiber backbone as well as fixed broadband optical communications systems.

We note that this novel method for all-optical envelope detection, using an optically-injected laser device, has been successfully demonstrated to operate under conditions similar to those suitable for future radio-over-fiber applications. We observe that the simplicity of this scheme, as well as the wide range of operating conditions available, give this scheme significant potential for implementation in current and future systems.

Acknowledgments

The Danish Agency for Science, Technology and Innovation is acknowledged for supporting K. Prince through an International Ph.D. Scholarship.

#89805 - $15.00 USD Received 19 Nov 2007; revised 14 Jan 2008; accepted 25 Jan 2008; published 29 Jan 2008

Paper B

K. Prince and I. Tafur Monroy, "All-optical envelope detection and fiber transmission of wireless signals by external injection of a DFB laser," *IEEE Photon. Technol. Lett.*, vol. 20, no. 15, pp. 1317–1319, Feb. 2008.

All-Optical Envelope Detection and Fiber Transmission of Wireless Signals by External Injection of a DFB Laser

Kamau Prince, *Student Member, IEEE*, and I. Tafur Monroy, *Member, IEEE*

***Abstract*—We outline a novel method for all-optical envelope detection of wireless signals by exploiting cross-gain modulation effects in a distributed feedback laser operating with optical injection. We successfully demonstrate envelope detection of a 20-GHz carrier amplitude-shift-keying modulated signal at 2.5 Gb/s and its transmission over a 70-km optical fiber link. We present results including bit-error-rate measurements, signal waveforms, and receiver sensitivity penalties associated with envelope detection and fiber transmission.**

***Index Terms*—All-optical signal processing, envelope detection, optical access network, radio-frequency-over-fiber (RFoF).**

I. Introduction

OPTICAL communications technology has become established as the preferred option for implementing high-speed data transfer within the core and metropolitan network segments. More recently, the development of fiber-to-the-home networks [1] has allowed the delivery of high-bandwidth services directly to the end-user, encouraging the convergence of wired and wireless signal transport into a common optical fiber backbone infrastructure [2].

The cross-gain-modulation (XGM) effect observed when an optical signal from an external source is introduced into the active region of a semiconductor laser had previously been used to detect the presence of a data packet at an optical receiver port [3]. We have demonstrated the application of the XGM effect in a distributed feedback (DFB) laser to achieve all-optical envelope detection of wireless signals and have reported on experimental characterization of such a device to obtain all-optical envelope detection of an amplitude-shift-keying (ASK) modulated signal with 20-GHz carrier frequency, carrying data at speeds up to 5 Gb/s [4]. In this letter, we report on further investigation of the application of the detection scheme in an optical access network environment simultaneously supporting passband radio-frequency-over-fiber (RFoF) and baseband transmission via a 70-km converged wireline and wireless signal transport optical link.

Manuscript received February 8, 2008; revised May 7, 2008. This work was supported by an International Ph.D. Scholarship from the Danish Agency for Science, Technology and Innovation.

The authors are with DTU Fotonik, Technical University of Denmark, Kgs. Lyngby, DK-2800, Denmark (e-mail: kpr@com.dtu.dk).

Color versions of one or more of the figures in this letter are available online at http://ieeexplore.ieee.org.

Digital Object Identifier 10.1109/LPT.2008.926915

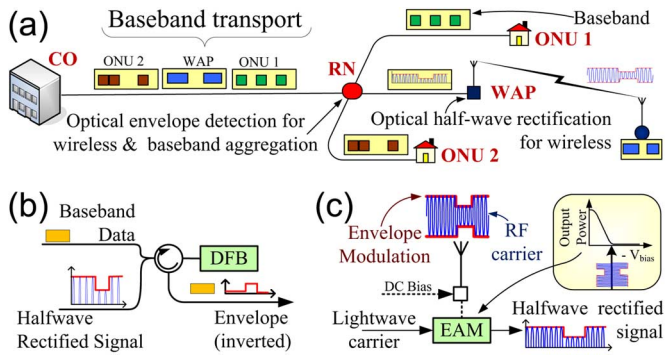

Fig. 1. Optical access network under consideration. (a) Data signals sent between CO and ONU and WAP nodes are distributed via intermediate RN. (b) Externally optical injected DFB laser at RN performs all-optical envelope detection of baseband and RoF signals. (c) ASK-modulated RF signal received at WAP, halfwave rectified by EAM and transmitted over optical network.

Section II contains a brief system description and a summary of the conditions under which the experimental study was made. Results are presented with samples of the signal waveforms as well as the receiver sensitivity obtained at various points within the network. The receiver sensitivity analysis, for a target bit-error rate (BER) of 10^{-9}, reveals that less than 1.7-dB receiver sensitivity penalty is associated with fiber transmission for a system operating at 2.5-Gb/s ASK modulation on a 20-GHz carrier.

II. System Description

We consider an optical communication network incorporating merged baseband and wireless communications services as shown in Fig. 1(a). Data signals between central office (CO) and optical network unit (ONU) and wireless access point (WAP) nodes are transported via an optical communications network, and distributed at some intermediate remote node (RN). Communication between the ONU and CO terminals is assumed to be formatted for baseband data transmission. WAP nodes interface to wireless access networks and we assume that the signaling between WAP and CO is formatted for RFoF transmission with the data being modulated onto an appropriate radio-frequency (RF) carrier wave as required for wireless data transmission between WAP and customer node(s). The RN comprises an optically injected DFB laser which transparently processes optical signals from WAP and ONU nodes, and forwards data content to the CO as shown in Fig. 1(b). This represents a significant simplification in signal processing requirements, and will reduce the overall network

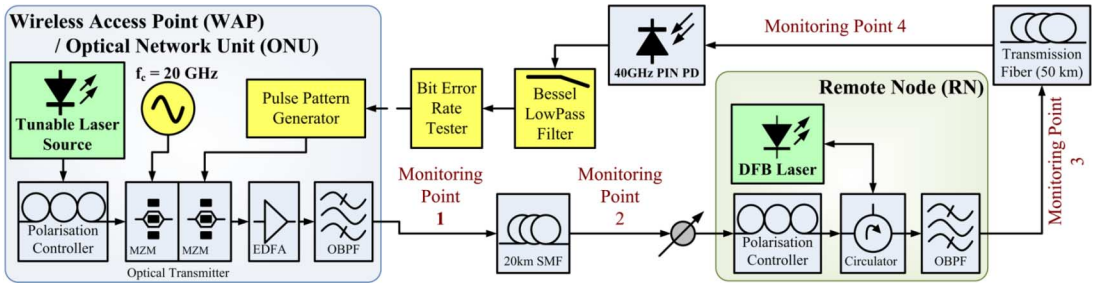

Fig. 2. Experimental setup showing the optical access uplink from WAP/ONU to CO. The RN transparently performs envelope detection and passes baseband traffic to CO via 50-km transmission fiber. Photodetection and further signal processing occurs at the CO. The transmission fiber was either SMF (dispersion: 17 ps/nm/km) or NZDSF (5 ps/nm/km).

costs. Optical half-wave rectification has been achieved by appropriately biasing an electroabsoption modulator (EAM) as shown in Fig. 1(c) [5].

A diagram of the experimental setup is presented as Fig. 2. For experimental purposes, the ASK RFoF/baseband nonreturn-to-zero (NRZ) signaling from the WAP/ONU was provided using a pair of cascaded Mach–Zehnder modulator (MZM) units. Baseband signaling was implemented by disabling the 20-GHz clock signal, this produced an output NRZ pulse stream in response to the digital data input. Activation of the clock input emulated a halfwave-rectified ASK signal at the output: this waveform was typical of that obtained at the output of an EAM-based RF-to-optical half-wave rectifier as shown in Fig. 1(c) and described in [5]. The overall system performance was assessed with the pulse-pattern generator and the BER test set.

Frequency down-conversion of the RFoF signal from passband to baseband is associated with greater robustness of the transmitted signal because of dispersion and power fading effects introduced when an RF signal with a high carrier frequency is sent via an optical network [2]: for example, 6-dB power penalty was observed for 155-Mb/s data transmission over 50-km single-mode fiber (SMF) when a 29-GHz RFoF signal was used [6] as opposed to a baseband waveform. We achieved frequency down-conversion using familiar optical components, without specialized RF electrical equipment at WAP or RN. At the RN, XGM effects associated with external optical injection of an active DFB laser were exploited to perform all-optical envelope detection of the ASK-modulated half-wave rectified input. The DFB used in this experiment was an uncooled multiple quantum-well coaxial fiber device: it operates without wavelength control. Since the optical gain in quantum-well devices is polarization-dependent, polarization controllers were used to optimize the XGM effect exploited for all-optical envelope detection. A laser device with bulk material would not require such controllers, as its optical gain is generally less polarization-dependent. A variable optical attenuator was used to maintain uniform injected power to the DFB.

A 20-km span of standard SMF was used between WAP/ONU and RN: 50 km of transmission fiber was used between CO and RN; this was alternately implemented with SMF (17-ps/nm/km dispersion at 1550 nm) or nonzero dispersion-shifted fiber (NZDSF), with 4-ps/nm/km dispersion. We assessed system performance with pseudorandom binary sequence (PRBS) data of lengths $2^7 - 1$ and $2^{15} - 1$ at a bit rate of 2.5 Gb/s for baseband and also RFoF signaling. The baseband traffic simulated data flows between CO and ONU, encoded in NRZ pulses. The RFoF signaling would be used for traffic flows to a wireless access network interfaced at the WAP, and was implemented with an optically halfwave rectified ASK modulated 20-GHz carrier wave [5]. Signal waveforms obtained at various points in the network were observed for these types of input. System performance was also assessed using a receiver sensitivity analysis at various monitoring points. For a target BER of 10^{-9}, the receive sensitivity power penalty incurred by end-to-end transmission via this system was less than 0.7 and 1.6 dB when NZDSF and SMF, respectively, was used for the 50-km access link.

III. Results

A. Signal Propagation Through Network

With this system, XGM was previously [4] maximized when the wavelength of the injected optical signal into the DFB coincided with one of the spectral side lobes of the DFB output spectrum and was higher than the lase wavelength, and with an average injected power level in the interval $[-4.2, -8.0]$ dBm. In this experiment, the DFB wavelength was approximately 1551 nm; the following results were obtained with a WAP/ONU laser wavelength of 1553 nm and an average injected power level of -7 dBm into the DFB at RN.

Sample optical waveforms at WAP and RN are presented as Fig. 3; Fig. 3(a) shows the waveform obtained at WAP output (MP1) and Fig. 3(b) is the corresponding waveform at RN input (MP2). Fig. 3(c) presents a 64-sample average of the waveform obtained at RN output (MP3): the eye diagram at MP3 is presented as Fig. 3(d). We clearly identify the optical halfwave rectified ASK signal from the WAP [in Fig. 3(a)]; note that it is attenuated at MP2 [Fig. 3(b)] and that the lowest part of the waveform during transmission of a "zero" bit does not return to the ground level indicated. In Fig. 3(c), a clear distinction can be made between RN output levels, indicating that the RN has performed envelope detection as desired. This waveform shows an underdamped response, having overshoot and transient oscillation at each rising edge, as consistent with relaxation oscillations typically observed at the output of a directly modulated DFB laser [7]. Some pattern dependence was observed in RN output,

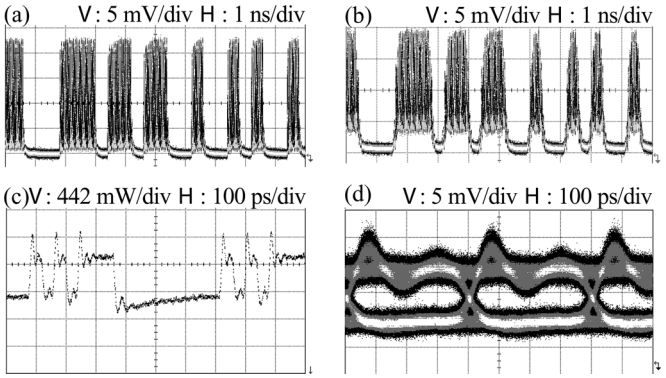

Fig. 3. (a) ASK modulated optical signal present at WAP output, Measuring Point 1 (MP1); (b) at input to RN after 20-km SMF (MP 2): (c) 64-average sample of waveform and (d) eye diagram at RN output (MP3).

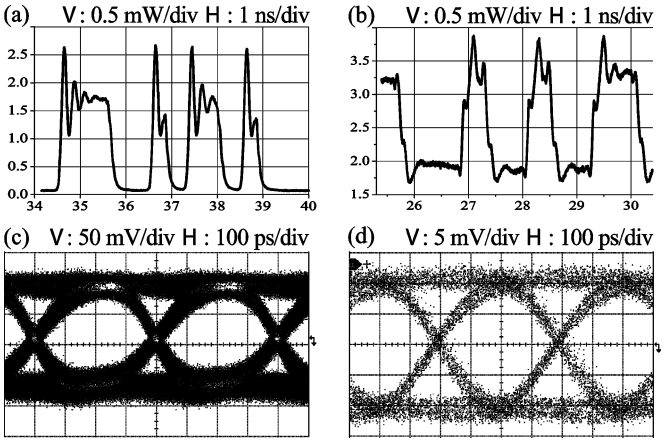

Fig. 4. Signal waveforms obtained at output of long-reach access link (MP4). [(a) and (b)] Sample detected signal observations and [(c) and (d)] post-LPF electric signal eye diagrams are presented when NZDSF and SMF, respectively, were implemented as the 50-km *transmission fiber*.

with minor level shift in response to a long run of "ones". The eye diagram obtained at MP3 [Fig. 3(d)] shows well-defined level transitions and a good opening. When the 50-km *transmission fiber* was implemented with NZDSF, the waveform presented in Fig. 4(a) was observed at MP4. We can see that the overshoot and high-frequency transient ripple were removed by electrical postphotodetection filtering using a Bessel low-pass filter (LPF) and the result is presented as Fig. 4(c). The corresponding waveforms obtained when SMF was used are presented as Fig. 4(b) and (d).

B. Receiver Sensitivity Assessment

We assessed the receiver sensitivity power penalty for a target BER of 10^{-9} at various points throughout the system under test: the results are presented in Fig. 5. At baseband, for a desired BER of 10^{-9}, a receive sensitivity power penalty of less than 0.1 dB was incurred through the use of the DFB to perform all-optical envelope detection in a back-to-back configuration. The penalty incurred at the end of the 20-km link between WAP/ONU and RN was less than 0.2 dB. Total power penalty incurred by end-to-end transmission over the network link under consideration was less than 0.7 dB for NZDSF transmission fiber and less than 1.6 dB for SMF.

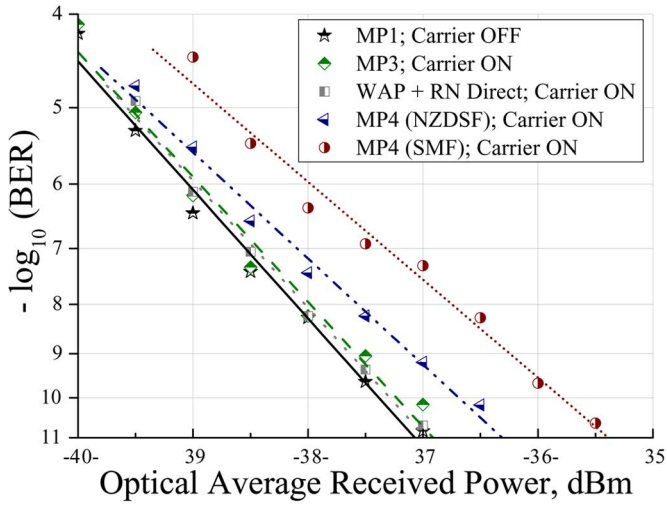

Fig. 5. Receiver sensitivity analysis of the access link system at various points, with a PRBS of length $2^{15}-1$. The baseline is at measuring point (MP) 1, with the 20-GHz carrier OFF. Carrier-ON receiver sensitivity at MP2 is also presented, and also for direct connection of WAP to RN (WAP + RN) without the 20-km SMF. Results obtained at the access link output are shown for 50-km *transmission fiber* of SMF and NZDSF type.

IV. Conclusion

We have successfully achieved signal transmission in a converged long-reach access link environment simultaneously supporting both baseband and RoF traffic streams at 2.5 Gb/s, using only common optical components and simple WAP, ONU, and RN node design. Successful all-optical envelope detection of an optical halfwave rectified ASK signal with 20-GHz carrier has simultaneously been demonstrated; RF signal frequency downconversion was thus achieved in the optical domain, without specialized electrical high-frequency RF components. Signal quality analysis at various network points has been presented in terms of measured BER, indicating that low receiver sensitivity penalties are associated with envelope detection in a DFB and fiber transmission. These results indicate the potential of the proposed scheme for converged wireless and baseband signal transport in a typical 2.5-Gb/s optical access network scenario.

References

[1] T. Koonen, "Fiber to the home/fiber to the premises: What, where, and when?," *Proc. IEEE*, vol. 94, no. 5, pp. 911–934, May 2006.
[2] A. Ng'oma, "Radio-over-fibre technology for broadband wireless communication systems" Ph.D. dissertation, Tech. Univ. Eindhoven, Eindhoven, The Netherlands, Jun. 2005 [Online]. Available: http://alexandria.tue.nl/extra2/200512106.pdf
[3] B. Koch, Z. Hu, J. Bowers, and D. Blumenthal, "All-optical payload envelope detection for variable length 40-Gb/s optically labeled packets," *IEEE Photon. Technol. Lett.*, vol. 18, no. 17, pp. 1846–1848, Sep. 1, 2006.
[4] K. Prince, I. T. Monroy, J. Seoane, and P. Jeppesen, "All-optical envelope detection for radio-over-fiber links using external optical injection of a DFB laser," *Opt. Express*, vol. 16, no. 3, pp. 2005–2014, 2008.
[5] I. T. Monroy, J. Seoane, and P. Jeppesen, "All-optical envelope detection for wireless photonic communication," in *Proc. ECOC*, Berlin, Germany, Sep. 2007.
[6] D. Novak, "Fiber optics in wireless applications," in *Proc. Opt. Fiber Commun. Conf. (OFC)*, Los Angeles, CA, Feb. 22–27, 2004, short course 217.
[7] G. P. Agrawal, *Fiber-Optic Communication Systems*. New York: Wiley, 2002, sec. 3.5.3.

Paper C

V. Torres-Company, K. Prince and I. Tafur Monroy, "Fiber transmission and generation of ultrawideband pulses by direct current modulation of semiconductor lasers and chirp-to-intensity conversion," *Optics Letters*, vol. 33, no. 3, pp. 222–224, Feb. 2008.

Fiber transmission and generation of ultrawideband pulses by direct current modulation of semiconductor lasers and chirp-to-intensity conversion

Víctor Torres-Company,[1] Kamau Prince,[2] and Idelfonso Tafur Monroy[2,*]

[1]*Departament de Física, GROC-UJI, Universitat Jaume I, 12071 Castelló, Spain*
[2]*Department of Communications, Optics and Materials, Technical University of Denmark, 2800 Kgs. Lyngby, Denmark*
**Corresponding author: itm@com.dtu.dk*

Received November 15, 2007; accepted December 15, 2007;
posted January 7, 2008 (Doc. ID 89697); published January 22, 2008

Optical pulses generated by current modulation of semiconductor lasers are strongly frequency chirped. This effect has been considered pernicious for optical communications. We take advantage of this effect for the generation of ultrawideband microwave signals by using an optical filter to achieve chirp-to-intensity conversion. We also experimentally achieve propagation through a 20 km nonzero dispersion shifted fiber with no degradation of the signal at the receiver. Our method constitutes a prospective low-cost solution and offers integration capabilities with fiber-to-the-customer-premise systems. © 2008 Optical Society of America

OCIS codes: 060.4510, 070.0070, 250.5960, 350.4010.

In the past few years, there has been a growing interest in the generation of ultrawideband (UWB) microwave signals. The UWB radio-frequency (RF) spectrum is regulated between the 3.1 and 10.6 GHz band with a power spectral density of −41.3 dBm/MHz [1]. Due to the high-data-rate capabilities, low power consumption, and immunity to multipath fading, these signals have an unprecedented opportunity to impact radio communication systems and promise as well substantial applications in radar, safety, and biomedicine. Although a large number of electronic devices for providing UWB pulses exist, optical technologies offer a viable alternative with several advantageous features. With optical approaches, the achieved bandwidth is usually limited only by the optoelectronic (O/E) conversion bandwidth. More important, all-optical UWB signal generation schemes constitute an ideal scenario for seamless integration of the distribution of wireless communications signals over optical fiber links.

Optical schemes to generate UWB signals include the use of a Fourier-transform geometry for shaping the power spectrum of an ultrashort light pulse [2–4]. The UWB signal is achieved by stretching the pulse in a fiber and by subsequent photodetection. In this way, a frequency-to-time mapping takes place. Later, an all-fiber variation was verified, achieving the generation of monocycle and doublet pulses only [5]. The same group also obtained UWB pulses by synthesizing a bandpass coherent microwave filter by combining an electro-optic phase modulator (EOPM) with fiber dispersion [6], acting globally as an electronic differentiator at low frequencies but implemented in the optical domain. More recently, some reported optical UWB signal generation approaches take advantage of the nonlinear optical properties of semiconductor optical amplifiers (SOAs) [7–9]. By exploiting cross-gain modulation [7], the output light of the SOA consisted of two reversed polarized pulses. By further adjusting the time delay between the two pulses with a pair of fiber Bragg gratings, monocycle pulses were achieved. This pulse waveform has also been generated based on the intensity overshooting effect [9] of optical dark pulses amplified by an SOA with unsaturated optical gain. Cross-phase modulation in an SOA, combined with an optical filter to provide chirp-to-intensity conversion, has proved to be an alternative way to generate UWB monocycles [8]. A similar chirp-to-intensity conversion approach was demonstrated with an EOPM combined with a fiber Bragg-grating filter [10].

In this Letter, we propose an efficient method to generate UWB pulses based on chirp-to-intensity conversion requiring a single optical source. Our experimental setup consists of a distributed feedback (DFB) laser whose driving current is modulated by the electrical data signal. When the laser is biased far from the threshold, the generated pulses are strongly frequency chirped. For a long time, this effect has been considered as pernicious for pulse propagation in optical fibers due to chromatic-dispersion issues [11]. However, by placing a spectral filter after the output of the DFB laser, a chirp-to-intensity conversion takes place. The resultant intensity waveform after photodetection has an RF spectrum that meets the regulations for being considered as UWB. With respect to previous reported approaches, our configuration offers an efficient solution in terms of power consumption, since there are no optical nonlinear processes involved requiring additional light sources or additional active optical devices. Our approach requires a single optical light source and avoids the use of external electro-optic modulation, so low complexity is inherent to this generation scheme. We have further verified the capability of the new technique for a fiber-to-the-home sce-

0146-9592/08/030222-3/$15.00

nario by propagating the signal through a 20 km nonzero dispersion shifted fiber (NZDSF). It is worth mentioning that a previous reported work [12] used a Fabry–Perot laser, current modulated for the generation of UWB signals. However, the frequency chirp was not used for achieving UWB signal generation. Instead, monocycle pulses were achieved by O/E conversion and subsequent differentiation of Gaussian intensity pulses in the electrical domain.

Our experimental setup is schematically depicted in Fig. 1. A DFB laser (NEL NLK5C5EBKA) with a central wavelength of 1550.10 nm is used as a light source. The bias current is fixed to −66.35 mA. A 12.5 Gbit/s electrical signal from a pulse pattern generator (Anritsu MP17633) with a peak-to-peak voltage of 0.250 V is used for direct current modulation. Figure 2 depicts the temporal pulse laser shape measured with a 20 GHz bandwidth photodiode at point A in Fig. 1. Because we are operating far from the threshold bias current the contribution of the frequency modulation is dominant versus the intensity modulation contribution. We profitted this chirp to achieve a monocycle pulse by placing a tunable optical bandpass filter (OBPF) with a Gaussian shaped transfer function at the output of the laser. Figure 3 shows the measured optical power spectrum at the output of the laser (solid curve), and the dashed–dotted curve represents the measured optical filter transfer function. The measurements have been taken with an optical spectrum analyzer (Ando OSA) with a resolution bandwidth of 0.01 nm. The plot represents the optimal placement of the OBPF, that is, when the laser spectrum lies at the linear slope of the OBPF transfer function. The average optical power level before the OBPF was measured to be 2.6 and −4.0 dBm at the input of the fiber, respectively.

Mathematically, frequency-chirp-to-intensity conversion can be denoted as follows. We can assume that the complex field of the frequency-chirped pulse is filtered by a linear optical filter $H(\omega)=A(\omega+\Delta\omega)$, where A is a real constant that determines the slope of the filter and $\Delta\omega$ denotes the vertical offset from the zero-crossing point. The temporal envelope at the output of the filter is given by

$$e_{\text{out}}(t) = jA[e'_{\text{in}}(t) - j\Delta\omega e_{\text{in}}(t)], \tag{1}$$

where the prime denotes temporal derivation and $e_{\text{in}}(t)$ is the input temporal envelope. We have taken

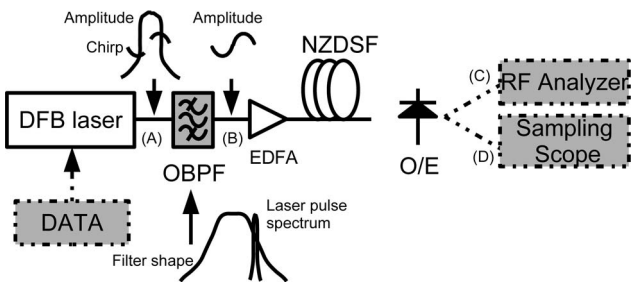

Fig. 1. Experimental setup. DFB, distributed feedback laser; OBPF, optical bandpass filter; O/E, optoelectronic conversion. NZDSF, nonzero dispersion shifted fiber; EDFA, erbium-doped fiber amplifier. Dotted lines, electrical connections.

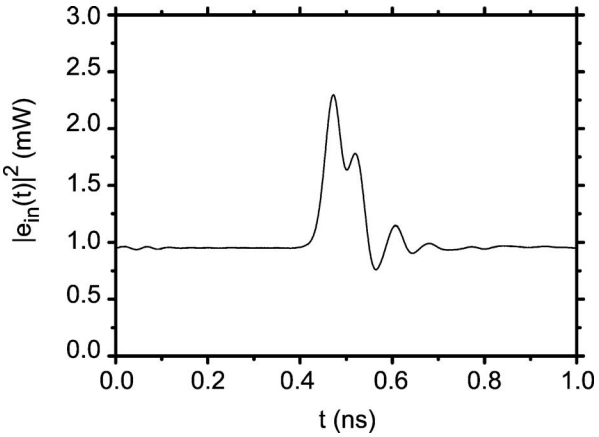

Fig. 2. Intensity pulse shape before the filter.

into account that $FT^{-1}[-j\omega E_{\text{in}}(\omega)]=e'_{\text{in}}(t)$, where $E_{\text{in}}(\omega)=FT[e_{\text{in}}(t)]$, with FT and FT^{-1} denoting Fourier and inverse Fourier transformation, respectively. We can always rewrite the input envelope as $e_{\text{in}}(t)=I_o^{1/2}(t)\exp[-j\Phi(t)]$, where $\Phi(t)$ and $I_o(t)$ denote the phase and intensity modulations, respectively. We now assume that the frequency modulation dominates with respect to the intensity modulation, but its contribution value is less than the corresponding frequency offset of the filter, i.e., $|I'_o(t)| \ll |\Phi'(t)| \ll \Delta\omega$. With this assumption, and after some straightforward algebra, the optical intensity at the output of the filter can be approximated to

$$I_{\text{out}}(t) \approx 2A^2\Delta\omega I_o(t)[\Phi'(t) + \Delta\omega/2]. \tag{2}$$

The above equation establishes that the light intensity at the output of the optical filter is essentially given by the frequency chirp of the input optical pulse. The derivation of Eq. (2) follows the approach in [8,10]. Note that Eq. (2) includes the contribution of both chirp and intensity modulations. However, since the laser is biased far from the threshold, the frequency modulation dominates over the intensity, and it is expected that the resultant intensity waveform after spectral linear filtering comes from the chirp.

At point B in Fig. 1, the optical signal is amplified by an erbium-doped fiber amplifier (EDFA) and

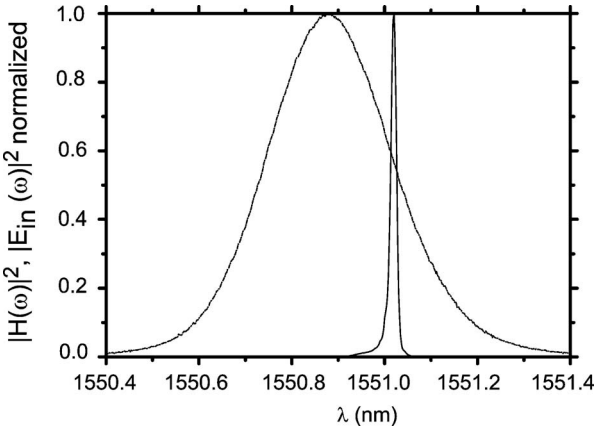

Fig. 3. Power spectrum of laser (solid curve) and OBPF (dashed–dotted curve).

propagated through 20 km of a NZDSF with a 4.5 dB loss and a 5 ps/nm/km dispersion. The intensity waveform at the output is O/E converted by a 10 GHz 3 dB bandwidth photodiode, which intrinsically assists in smoothing undesired high-frequency RF components that do not fall into the UWB range. The resultant electrical signal is measured in the RF domain by an electrical spectrum analyzer (Agilent E4407B9) with a resolution of 1 MHz, and in the time domain by a sampling oscilloscope (Agilent Infinium 86100A). The EDFA is adjusted so that the receiver gets an average optical input power of −0.5 dBm. Figure 4 shows the measured resultant UWB signal consisting of a monocyclelike pulse in time and frequency domains. For the frequency domain, we selected a repetition rate of 390.6 MHz (a "1" followed by 32 "0") so that the achieved spectral shape is properly sampled. As can be appreciated, the RF spectrum spreads over the UWB region. Due to the monocyclelike waveform, a nondisregarding low-frequency content still remains, which can be minimized by reducing the power into the photodiode with some extra attenuator.

In summary, a novel optical approach for the generation of UWB signals has been proposed and experimentally verified. It takes advantage of the frequency chirp of optical pulses generated by direct current modulation of semiconductor lasers. Essentially, chirp-to-intensity conversion is achieved by optical linear filtering of frequency-chirped optical pulses. We achieve a monocycle waveform that meets the UWB requirements. The proposed scheme is simple and compact since it avoids the use of any external electro-optic modulator and achieves high efficiency in terms of power consumption because nonlinear optical processes are involved.

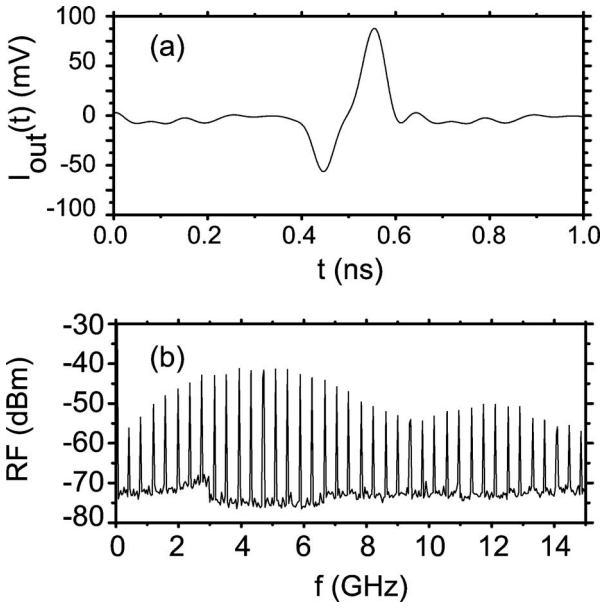

Fig. 4. UWB pulse achieved at the receiver: (a) intensity waveform and (b) RF spectrum.

This work has been partly funded by the Dirección General de Investigación Cientifica y Técnica, Spain and Fondos Europeos para el DEsarrollo Regional, under the projects FIS2007-62217 and SAUUL (Science and Applications of ultrafast ultraintense lasers) in the programme CONSOLIDER. V. Torres acknowledges financial support from a Formación de Profesorado Universitario grant from the Ministerio de Eduación y Ciencia. K. Prince acknowledges the Danish Agency for Science, Technology and Innovation International PhD Scholarship.

References

1. M.-G. Di Benedetto, T. Kaiser, A. F. Molish, I. Oppermann, and C. Politano, eds., *UWB Communication Systems: A Comprehensive Overview* (Hindawi, 2006).
2. J. Chou, Y. Han, and B. Jalali, IEEE Photon. Technol. Lett. **15**, 581 (2003).
3. I. S. Lin, J. D. McKinney, and A. M. Weiner, IEEE Microw. Wirel. Compon. Lett. **15**, 226 (2005).
4. J. D. McKinney, I. S. Lin, and A. M. Weiner, IEEE Trans. Microwave Theory Tech. **54**, 4247 (2006).
5. C. Wang, F. Zeng, and J. P. Yao, IEEE Photon. Technol. Lett. **19**, 137 (2007).
6. F. Zeng and J. P. Yao, IEEE Photon. Technol. Lett. **18**, 823 (2006).
7. Q. Wang, F. Zeng, S. Blais, and J. P. Yao, Opt. Lett. **31**, 3083 (2006).
8. J. J. Dong, X. L. Zhang, J. Xu, D. X. Huang, S. N. Fu, and P. Shum, Opt. Lett. **32**, 1223 (2007).
9. J. J. Dong, X. L. Zhang, J. Xu, and D. X. Huang, Opt. Lett. **32**, 2158 (2007).
10. F. Zeng and J. P. Yao, IEEE Photon. Technol. Lett. **18**, 2062 (2006).
11. G. P. Agrawal, *Fiber-Optic Communication Systems* (Wiley Interscience, 2002).
12. W. P. Lin and Y.-C. Chen, IEEE J. Sel. Top. Quantum Electron. **12**, 882 (2006).

Paper D

V. Torres, K. Prince and I. Tafur Monroy, "Ultrawideband pulse generation based on overshooting effect in gain-switched semiconductor laser," *IEEE Photon. Technol. Lett.*, vol. 20, pp. 1299–1301, Aug.1, 2008.

Ultrawideband Pulse Generation Based on Overshooting Effect in Gain-Switched Semiconductor Laser

Víctor Torres-Company, *Student Member, IEEE*, Kamau Prince, and Idelfonso Tafur Monroy

***Abstract*—We demonstrate an alternative procedure to achieve ultrawideband (UWB) radio-frequency (RF) doublet impulses. It is based on the overshooting effect appearing by biasing a semiconductor laser close to the threshold with a large-amplitude signal. Specifically, with an optical bandpass filter and an electrical low-pass filter, we easily obtain doublet-like impulses whose RF spectrum meets the UWB regulations. Furthermore, we have been able to propagate such signals through an optical fiber link of 118-km length. Though the technique is not flexible in terms of waveform generation, our method constitutes a reliable, easy, and low-cost alternative for RF UWB impulse generation.**

***Index Terms*—Microwave photonics, pulse propagation, ultrawideband (UWB).**

I. Introduction

ULTRAWIDEBAND (UWB) transmission is an emerging technology for wireless high-speed communications, offering services for radar, sensor networking, and biomedical applications, to name only a few. The UWB radio-frequency (RF) spectrum is regulated in the frequency band between 3.1 and 10.6 GHz. Mitigation of possible interference across different wireless technologies operating in the same sprectrum is implemented by enforcing a maximum transmission power spectral density (PSD) of -41.3 dBm/MHz [1]. There already exist some electronic devices that provide UWB-compliant pulses, but the radiation PSD restrictions limit their operating range to a few hundreds of meters.

However, photonics-based generation of signals with high RF bandwidth is a relatively easy task usually limited only by the photodiode bandwidth. But the key feature is that all-optical UWB pulse generation allows the signal distribution through fiber links, thus increasing the operating range of UWB networks by several orders of magnitude compared to their counterpart electrical approaches [2]. Typical optical schemes to generate UWB signals are based on the use of spectral shaping of ultrashort laser pulses and subsequent frequency-to-time mapping in an optical fiber [2]–[5]. There are other optical approaches for UWB signal generation that avoid the use of ultrashort-pulse laser sources [2]. For example, the chirp-to-intensity conversion effect in linear filters has been exploited by using optical phenomena such as cross-phase modulation in semiconductor optical amplifiers (SOAs) [6]; an electrooptic phase modulator [7]; or the inherent chirp produced by direct current modulation of a laser biased far from threshold [8]. Monocycle shapes can be created by means of the birefringence in polarization-maintaining fiber [9]. The use of nonlinear effects in SOAs to generate monocycle impulses has also recently been reported [10], [11]. This latest technique uses cross-gain modulation, in which the time delay between two reversely polarized pulses from the output of the SOA was adjusted with a pair of fiber Bragg gratings until the desired output waveform was obtained [10]. Finally, monocycle impulses have been generated based on the intensity overshooting effect of optical dark pulses amplified by an SOA with unsaturated optical gain [11].

In this letter, we propose and demonstrate an alternative method to generate UWB pulses based on a similar overshooting effect in a direct-modulated semiconductor laser. It should be noted that although we employ the same optoelectronic equipment as [8], the subjacent physical phenomenon is different, which has allowed us to achieve doublet UWB pulses, in contrast to the monocycle shapes from [8]. Doublet-like impulses are more efficient to satisfy the UWB regulation mask [5]. Our technique avoids the use of any external modulation, nonlinear phenomena, mode-locked lasers, and/or specially designed fiber Bragg gratings. Together with the approach in [8], we offer a simple low-cost solution for the generation of UWB doublet and monocycle impulses just by controlling the bias of current-modulated semiconductor lasers.

II. Heuristic Approach

The principle of operation is illustrated in Fig. 1(a). A semiconductor laser is current-modulated close to the threshold with a return-to-zero (RZ) electrical signal. In the large-signal modulation regime, the laser power overshoots at the rising edge due to relaxation oscillations and then reaches the steady state. Although prediction of the actual laser output pulse shape while operating under these conditions may be done by numerical solution of the laser rate equations, it suffices for our discussion to state that this overshooting effect is a general feature of gain-switched semiconductor lasers [12]. The resulting pulse is then filtered with an optical bandpass filter (OBPF). The role

Manuscript received January 21, 2008; revised April 29, 2008. This work was supported in part by the Dirección General de Investigación Cientifica y Técnica, Spain and FEDER, under the project FIS2007-62217. The work of V. Torres-Company was supported by an FPU fellowship from the MEC. The work of K. Prince was supported by an International Ph.D. scholarship from the Danish Agency for Science, Technology and Innovation.

V. Torres-Company is with the Department of Physics, Universitat Jaume I, Castello, 12071 Castelló, Spain (e-mail: vtorres@fca.uji.es).

K. Prince and I. T. Monroy are with the Department of Photonics Engineering, Technical University of Denmark, DK-2800 Lyngby, Denmark.

Color versions of one or more of the figures in this letter are available online at http://ieeexplore.ieee.org.

Digital Object Identifier 10.1109/LPT.2008.926905

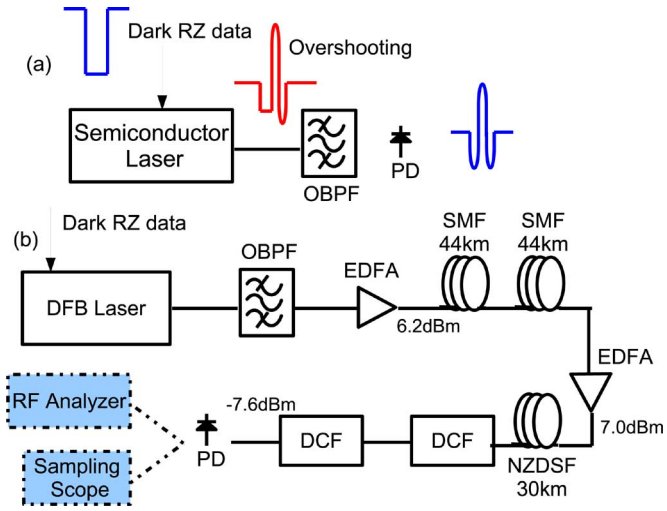

Fig. 1. (a) Principle for the generation of UWB impulses and (b) experimental setup for the generation and transport of UWB pulses. The average power levels before the different fiber stages are displayed in the figure. Acronyms are explained in the text.

of the filter is to smooth out the high-frequency optical components in order to eliminate the frequency oscillation in the intensity before achieving the steady state. We then detect the signal with a 10-GHz bandwidth photodiode, removing the high frequency components of the impulse RF signal that do not fall into the UWB range. We found that the resultant signal was then a doublet-like impulse waveform that met the UWB specification criteria.

III. Experimental Verification

The experimental arrangement for generation and distribution is drawn in Fig. 1(b). A direct-modulated distributed-feedback (DFB) laser (NEL NLK5C5EBKA), nominally specified for operation at 10 Gb/s, was used as the light source. The driving data signal was taken from the inverted data output of a bit pattern generator. We selected a bit rate of 12.5 Gb/s, and a peak-to-peak amplitude of 1.282 V. We adjusted the bit-pattern produced in order to regulate the duty cycle and frequency of the driving electrical signal applied to the DFB laser. We biased the laser at -35 mA, which is a value close to the lasing threshold of -30 mA. Fig. 2 shows the electrical RZ data pulse (blue dashed–dotted line) applied to the laser, and the output optical power (red solid line). The overshooting effect at the trailing edge of the pulse is apparent. The power oscillates at the relaxation oscillation frequency before achieving a steady state following the shape of the driving electrical signal. We measured the RF spectrum of this waveform with a 10-GHz bandwidth photodiode and verified that it was not UWB-compliant. However, we were able to produce the required pulse characteristics by passing this laser pulse through a conventional tunable OBPF with a Gaussian roll-off and having a full-width at half-maximum of 0.3 nm. In Fig. 3, we show the output laser spectrum (red solid line) and the OBPF power spectrum (red dashed–dotted line) placed in the optimal position to achieve the doublet shape. As we can see, the high-frequency optical components are smoothed. It should be mentioned that previously reported approaches for optical filtering of gain-switched lasers

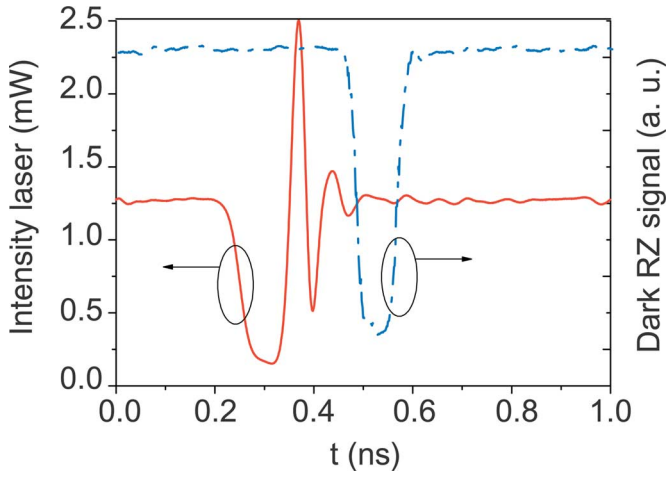

Fig. 2. Output overshot laser pulse (solid red line) and dark RZ modulating signal (dashed–dotted blue line).

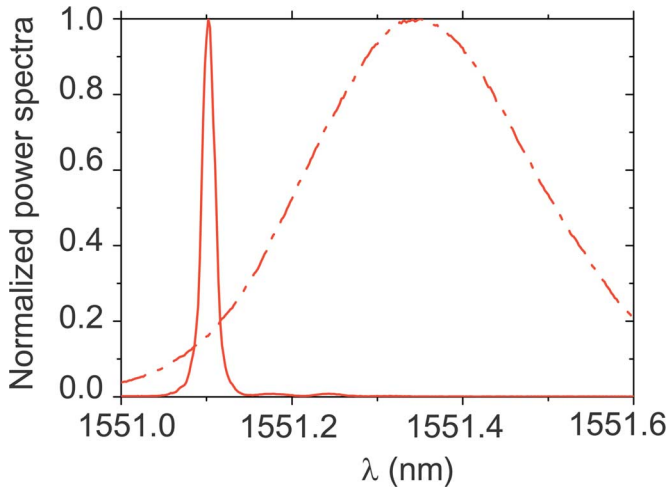

Fig. 3. Power transmission of OBPF (red dashed line) and power spectrum of the laser pulse (red solid line).

tried to avoid this overshooting effect and aimed to generate bell-shaped ultrashort waveforms [13], [14]. Our goal here is instead to optimize the intensity profile so that this waveform can be exploited for UWB RF signal generation. After the OBPF, we converted the optical signal into the electrical domain with a 10-GHz bandwidth photodiode, and succeeded in generating a doublet-like UWB impulse, as shown by the blue dashed–dotted line in Fig. 4(a). We can see how the OBPF has removed the oscillatory terms present in the overshot laser intensity pulse from Fig. 2. After optoelectronic conversion, the corresponding PSD is displayed in Fig. 4(c). The spikes are due to the fact that we introduced a data sequence of one "1" followed by 16 "0", so that the RF spectrum of a single UWB pulse is conveniently sampled at 0.78 GHz for illustration purposes. The temporal pulse duration will be the main limiting factor to achieve higher transmission rates.

IV. Transmission Fiber Link Results

In order to verify the usefulness of this method, we performed an additional experiment for propagating the signal through an optical fiber link. For this evaluation, the signal needed to

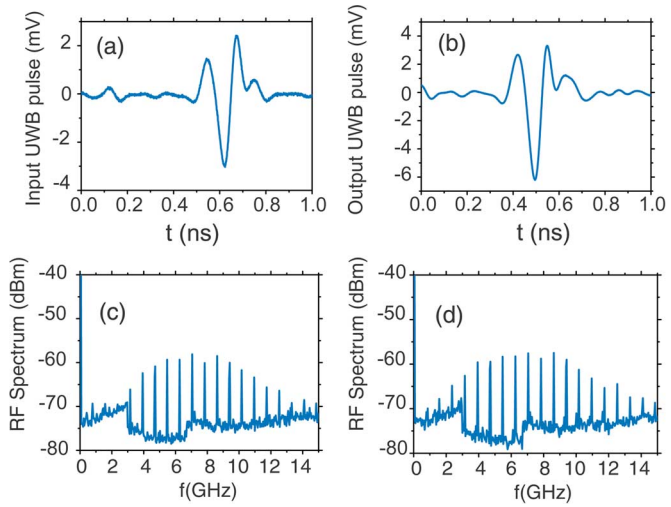

Fig. 4. Generated UWB signal in (a) time domain before transmission; (b) after propagation through the 118-km fiber link; (c) and (d) are the corresponding PSD, respectively.

be amplified after optical filtering and the optical–electrical converter was placed at the receiver. As indicated in Fig. 1(b), the fiber link is comprised of two stages. We first propagated the signal through two single-mode fiber (SMF) coils of 44-km length each. Then the optical signal was further amplified and propagated through 30 km of nonzero-dispersion-shifted fiber (NZDSF) as well 13 km of dispersion-compensating fiber (DCF), matched to the dispersion introduced by the SMF in the first stage. This constitutes a total optical link length of 118 km, which represents the largest distance ever reported for UWB signal distribution, to the best of our knowledge. The specific order of the different fibers is chosen in order to minimize possible nonlinear effects in the DCF module. Further investigation indicated that this proposed UWB transmission scheme is not dependent on this specific arrangement of optical fibers and dispersion compensation. The measured average power levels before the fiber modules are displayed in Fig. 1(b). The output optical pulse is detected with the 10-GHz bandwidth photodiode and measured simultaneously in the time domain with a sampling oscilloscope, and in the frequency domain with an electrical spectrum analyzer with a 1-MHz measurement resolution. The achieved signal is displayed in Fig. 4(b) and (c). It possesses a central frequency of 7 GHz and has a 10-dB bandwidth of 10.2 GHz, hence a fractional bandwidth of 146%. The pulse duration was measured to be 236 ps. Comparison of Fig. 4(a) and (b) indicates that there is no significant distortion of the UWB pulse during propagation. The slight discrepancy is attributed to low distortion in the NZDSF and amplified spontaneuous emission noise introduced by the erbium-doped fiber amplifiers. However, from Fig. 4(d), we conclude that the waveform still satisfies the UWB RF regulations.

V. Summary and Conclusions

In summary, we have demonstrated the generation of UWB doublet impulses with a direct-current-modulated semiconductor laser. The principle takes advantage of the overshooting effect in the gain-switching operating regime. Although our scheme does not offer flexibility in the achievable pulse waveform the technique is simple, reproducible, and highly efficient since it does not require any additional external modulation, SOA, or mode-locked laser. Together with the approach presented in [8], we offer the possibility to obtain UWB monocycle and doublet pulses just by direct modulation of semiconductor lasers and spectra filtering. In this setup, we have also achieved transmission over a 118-km fiber link without appreciable distortion of the waveform. The achieved pulse at the receiver has a 146% fractional bandwidth and 236-ps time duration.

References

[1] , M. -G. Di Benedetto, T. Kaiser, A. F. Molish, I. Oppermann, and C. Politano, Eds., *UWB Communication Systems: A Comprehensive Overview*. New York: Hindawi Publishing, 2006.

[2] J. P. Yao, F. Zeng, and Q. Wang, "Photonic generation of ultrawideband signals," *J. Lightw. Technol.*, vol. 25, no. 11, pp. 3219–3235, Nov. 2007.

[3] J. Chou, Y. Han, and B. Jalali, "Adaptive RF-photonic arbitrary waveform generator," *IEEE Photon. Technol. Lett.*, vol. 15, no. 4, pp. 581–583, Apr. 2003.

[4] I. S. Lin, J. D. McKinney, and A. M. Weiner, "Photonic synthesis of broadband microwave arbitrary waveforms applicable to ultra-wideband communication," *IEEE Microw. Wireless Compon. Lett.*, vol. 15, no. 4, pp. 226–228, Apr. 2005.

[5] M. Abtahi, M. Mirshafiei, J. Magné, L. A. Rusch, and S. LaRochelle, "Ultra-wideband waveform generator based on optical pulse-shaping and FBG tuning," *IEEE Photon. Technol. Lett.*, vol. 20, no. 2, pp. 135–137, Jan. 15, 2008.

[6] J. J. Dong, X. L. Zhang, J. Xu, D. X. Huang, S. N. Fu, and P. Shum, "Ultrawideband monocycle generation using cross-phase modulation in a semiconductor optical amplifier," *Opt. Lett.*, vol. 32, no. 10, pp. 1223–1225, May 2007.

[7] F. Zeng and J. P. Yao, "Ultrawideband impulse radio signal generation using a high-speed electrooptic phase modulator and a fiber-Bragg-grating-based frequency discriminator," *IEEE Photon. Technol. Lett.*, vol. 18, no. 19, pp. 2062–2064, Oct. 1, 2006.

[8] V. Torres-Company, K. Prince, and I. T. Monroy, "Fiber transmission and generation of ultrawideband pulses by direct current modulation of semiconductor lasers and chirp-to-intensity conversion," *Opt. Lett.*, vol. 33, no. 3, pp. 222–224, Feb. 2008.

[9] H. Chen, M. Chen, C. Qiu, J. Zhang, and S. Xie, "UWB monocycle pulse generation by optical polarisation time delay method," *Electron. Lett.*, vol. 43, no. 9, pp. 542–543, Apr. 2007.

[10] Q. Wang, F. Zeng, S. Blais, and J. P. Yao, "Optical ultrawideband monocycle pulse generation based on cross-gain modulation in a semiconductor optical amplifier," *Opt. Lett.*, vol. 31, no. 21, pp. 3083–3085, Nov. 2006.

[11] J. J. Dong, X. L. Zhang, J. Xu, and D. X. Huang, "All-optical ultrawideband monocycle generation utilizing gain saturation of a dark return-to-zero signal in a semiconductor optical amplifier," *Opt. Lett.*, vol. 32, no. 15, pp. 2158–2160, Aug. 2007.

[12] G. P. Agrawal, *Fiber-Optic Communication Systems*. New York: Wiley, 2002.

[13] M. Nakazawa, K. Suzuki, and Y. Kimura, "Transform-limited pulse generation in the gigahertz region from a gain-switched distributed-feedback laser diode using spectral windowing," *Opt. Lett.*, vol. 15, no. 12, pp. 715–717, Jun. 1990.

[14] T. Niemi, J. G. Zhang, and H. Ludvigsen, "Effect of optical filtering on pulses generated with a gain-switched DFB laser," *Opt. Commun.*, vol. 192, no. 3, pp. 339–345, Jun. 2001.

Paper E

K. Prince, J. B. Jensen, A. Caballero, X. Yu, T. Gibbon, D. Zibar, N. Guerrero, A. V. Osadchiy and I. Tafur Monroy, "Converged wireline and wireless access over a 78-km deployed fiber long-reach WDM PON," *IEEE Photon. Technol. Lett.*, vol. 21, pp. 1274–1276, Sept. 1 2009.

Converged Wireline and Wireless Access Over a 78-km Deployed Fiber Long-Reach WDM PON

Kamau Prince, *Student Member, IEEE*, Jesper Bevensee Jensen, Antonio Caballero, Xianbin Yu, Timothy Braidwood Gibbon, Darko Zibar, Neil Guerrero, Alexey Vladimirovich Osadchiy, and Idelfonso Tafur Monroy

***Abstract*—In this letter, we demonstrate a 78.8-km wavelength-division-multiplexing passive optical network supporting converged transport of 21.4-Gb/s nonreturn-to-zero differential quadrature phase-shift keying, optical phase-modulated 5-GHz radio-over-fiber, fiber and air transmission of 3.125-Gb/s pulse ultrawideband, and 256-quadratic-amplitude modulation wireless interoperability for microwave access.**

***Index Terms*—Coherent optical systems, converged access networks, ultrawideband (UWB) signaling, wireless interoperability for microwave access (WiMAX).**

I. Introduction

HYBRID optical/wireless access network architectures are considered a promising solution for large-scale deployment of broadband access as they combine the advantages of high capacity offered by optical access with the flexibility provided by wireless networks [1], [2]. Simultaneous transport of wireline and wireless types of signals, fulfilling power budget, dispersion, and other quality requirements for both signal types, over a common fiber infrastructure is an important aspect for hybrid optical wireless access networks.

We report on a converged wireless and wireline, wavelength-division multiplexing (WDM) passive optical network (PON) access link over a 78.8-km-long commercially deployed optical fiber in Copenhagen. We successfully implemented an eight-channel, single-fiber, WDM transmission system simultaneously supporting 85.6-Gb/s baseband via four 21.4-Gb/s nonreturn-to-zero (NRZ) differential quadrature phase-shift keying (DQPSK) channels, 500 Mb/s via two coherently detected phase-modulated radio-over-fiber (RoF) channels, 3.125 Gb/s via impulse radio ultrawideband (UWB), and intensity-modulated, direct-detected RoF link with quadratic-amplitude modulation (QAM) at 12 megabaud (MBd). Air transmission was demonstrated after fiber transmission for the UWB and WiMAX signals.

Manuscript received April 21, 2009; revised June 08, 2009. First published July 10, 2009; current version published August 19, 2009. This work was supported in part by the European Union FP7 Information Communication Technology (ICT)-ALPHA and in part by the ICT GigaWaM projects.

The authors are with the Department of Photonics Engineering, Technical University of Denmark, DK-2800 Kgs. Lyngby, Denmark (e-mail: kpri@fotonik.dtu.dk; jebe@fotonik.dtu.dk; acaj@fotonik.dtu.dk; xiyu@fotonik.dtu.dk; tbgi@fotonik.dtu.dk; dazi@fotonik.dtu.dk; nggo@fotonik.dtu.dk; avos@fotonik.dtu.dk; idtm@fotonik.dtu.dk).

Color versions of one or more of the figures in this letter are available online at http://ieeexplore.ieee.org.

Digital Object Identifier 10.1109/LPT.2009.2025699

II. System Layout

Fig. 1 shows a block diagram of the field trial and setup used in the experiment. The field-deployed fiber connects the Kongens Lyngby campus of the Technical University of Denmark (DTU) and facilities located in the suburb of Taastrup. The fiber is a G.652 standard single-mode fiber (SMF) type (16.5 ps/nm·km chromatic dispersion, 0.20 dB/km attenuation, polarization dispersion coefficient < 0.20 ps/$\sqrt{\text{km}}$). The total link loss was measured at 25 dB. The eight WDM channels employed were separated by 200 GHz, at standard International Telecommunication Union (ITU) wavelengths, denoted by $\lambda_1 = 1549.3$ nm through $\lambda_8 = 1560.0$ nm. Four wavelengths (λ_{5-8}) were used for NRZ-DQPSK: two $(\lambda_{2,4})$ for coherent RoF, λ_3 for UWB, and λ_1 for WiMAX. Launch power into the deployed fiber was set to 0 dBm for each of the eight channels. A dispersion-compensating fiber (DCF) was used at the transmitter; this also ensured decorrelated signals at the input to the transmission fiber. A preamplifier erbium-doped fiber amplifier (EDFA) overcame transmission losses before wavelength demultiplexing by arrayed waveguide grating (AWG). AWG spacing of 200 GHz was used due to equipment availability; we anticipate good system performance with closer spacing [3].

A. NRZ-DQPSK Baseband

The transmitter setup comprises four DFB lasers at wavelengths $\lambda_5 - \lambda_8$ multiplexed in an AWG and NRZ-DQPSK modulated using an inphase/quadrature (I/Q) modulator driven by two electrical pseudorandom bit sequences (PRBSs) of length $2^7 - 1$ bits and bit rate 10.7 Gb/s, resulting in a per-channel bit rate of 21.4 Gb/s at a symbol rate of 10.7 GBd. The $2^7 - 1$ bit pattern length was selected due to limitations of the bit error rate tester (BERT) functionality. Since we used phase modulation, no pattern dependency was expected from nonlinear effects in the transmission fiber. After transmission and wavelength demultiplexing, the NRZ-DQPSK signals were demodulated using a one-symbol delay Mach–Zehnder interferometer (MZI) and detected by a pair of balanced photodetectors (BPDs). The BER of each DQPSK tributary was measured independently, and we report the average obtained.

B. Coherent RoF

A 5-GHz RF carrier at $+8$ dBm was BPSK modulated at 250 Mb/s, and used to optically phase modulate signals at wavelengths of λ_2 and λ_4. At the receiver, the desired channel was optically mixed with a continuous-wave local oscillator (LO) signal, derived from a tunable laser source at 0 dBm output power, and coherently detected using a 90° optical hybrid with integrated photodetectors. The in-phase (I) and quadrature (Q)

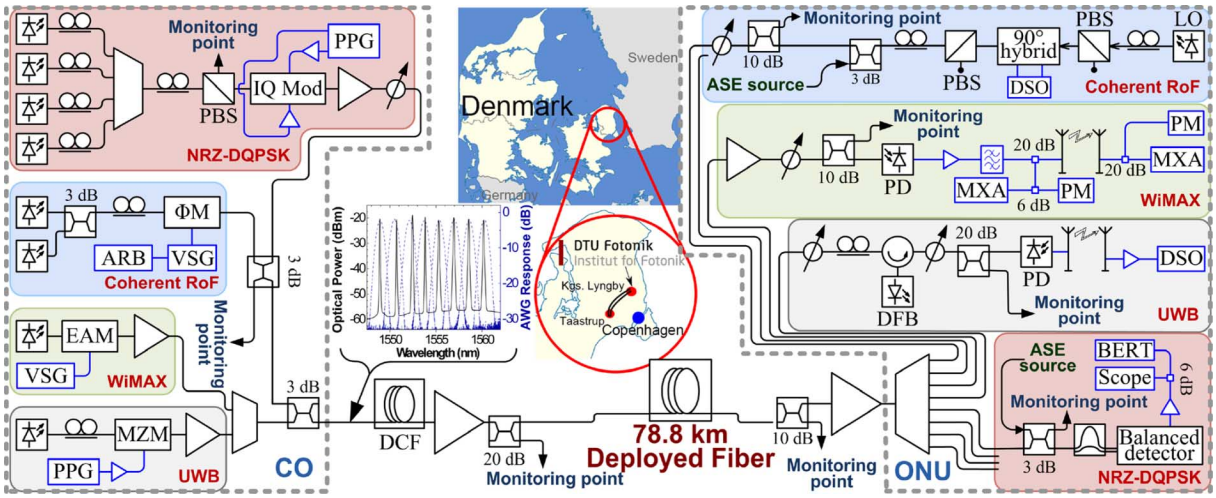

Fig. 1. Detail of the experimental setup. PPG: pulse pattern generator; PBS: polarization beam splitter; PM: optical phase modulator; ARB: arbitrary waveform generator; VOA: variable optical attenuator. ASE added to evaluate system OSNR sensitivity for phase-modulated signals: precompensating DCF-implemented decorrelation of RoF and NRZ-DQPSK signals. (Inset) Spectra of launched WDM optical signal (solid line) and AWG response (dashed line).

electrical signals were sampled at 40 GSa/s by a sampling oscilloscope (SO) with a 13 GHz bandwidth. The stored signals were processed offline using DSP algorithms described in [3] to perform signal demodulation and BER evaluation.

C. Impulse Radio UWB

A lightwave at λ_3 (1552.80 nm wavelength) was modulated by a 12.5-Gb/s pattern "1000" using a Mach–Zehnder modulator (MZM). An uncooled DFB laser was optically injected with the incoming signal from the fiber link. Under optical injection, cross-gain modulation and relaxation oscillations governing the dynamic response of the DFB shape its output signal [4]. The incoherent combination of the injected and DFB wavelengths after photodetection generated a pulse with a postdetection RF spectrum that is compliant with the impulse radio UWB mask. Air transmission of 40 cm was implemented. These UWB signals were sampled by a 40 GSa/s sampling scope with 13 GHz bandwidth, and processed offline using a DSP algorithm.

D. WiMAX

An electroabsorption modulator (EAM) fed by an optical carrier at λ_2 was modulated with a 256-QAM RF signal, centered at 5.8 GHz, obtained from an Agilent E4438C vector signal generator (VSG); a boost EDFA and a variable optical attenuator (VOA) controlled the launch power. A preamplified receiver was implemented with a 30-dB gain EDFA, an optical bandpass filter (BPF), and a 10-GHz PIN photodiode. The electrical signal obtained was amplified by 35 dB, filtered by 25 MHz RF duplexers for 5 GHz unlicensed ISM band operation, and radiated by a 12 dBi omnidirectional 5 GHz antenna. The wireless signal was detected with an identical antenna at 40 cm separation, and amplified and assessed with an Agilent 9020 MXA vector signal analyzer (VSA) with the 89 600 VSA signal analyzer software. We report error vector magnitude (EVM) sensitivity to RF source power at both ends of the wireless link for the single active wavelength and for all WDM transmitters active. We additionally assessed the performance with extra 40 km of uncompensated SMF, after DF and preamp and the postdetection eye diagram.

III. Results

A. NRZ-DQPSK Baseband

The BER of the four NRZ-DQPSK-modulated baseband channels back-to-back (B2B) and after fiber transmission is plotted in Fig. 2(a) with filled symbols/solid lines for the back-to-back case and hollow symbols/dashed lines for the transmitted. OSNR requirement for a BER of 10^{-9} was observed between 22 dB (λ_5) and 23.3 dB for λ_8. At λ_7, a penalty of 0.3 dB was observed after transmission; for all other channels, no penalty was measured. The eye diagrams before and after transmission shown in Fig. 2(b) show no transmission distortion, thus confirming good transmission properties.

B. Coherent RoF

A 250-MBd BPSK data signal modulating a 5-GHz RF carrier for each WDM channel was successfully recovered after transmission through the dark fiber with input power to the coherent receiver set to -15.77 and -16.77 dBm, respectively. In Fig. 2(b), the BER curves for back-to-back and after fiber transmission are computed as a function of OSNR values from 7 to 12 dB. We observed a receiver sensitivity penalty of 0.5 dB at λ_2 for BER at 10^{-3}, whereas a 2 dB penalty was observed in channel 4, which we believe was caused by partial misalignment of the source with the AWG passband.

C. Impulse Radio UWB

We generated 3.125-Gb/s ON–OFF key (OOK) modulation with $2^7 - 1$ PRBS; an example of "1110111" pattern and the resulting RF spectrum are shown in Fig. 3(a). The frequency spectra observed are compatible with the FCC (indoor) UWB mask. We used a sample size of 684 kilosamples, and a DSP algorithm was employed to calculate the BER offline. From the BER measurement curves, we observed less than 0.5 dB penalty between B2B and fiber transmission (for both single-channel and WDM transmissions).

D. WiMAX

We successfully transported 256-QAM signals at 12 MBd over the deployed fiber and an additional 40 km SMF with no

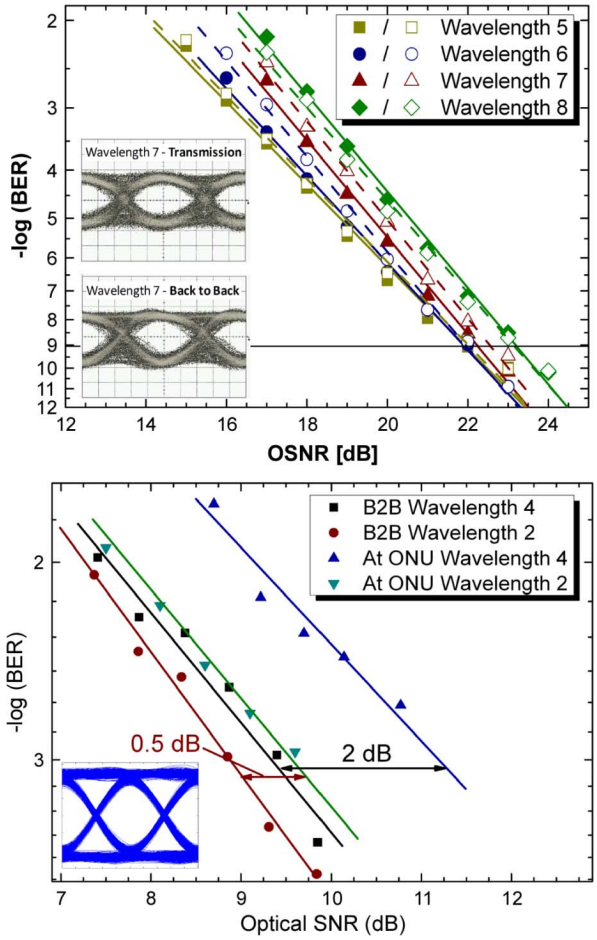

Fig. 2. BER results. (Top) 21.4-Gb/s NRZ-DQPSK. (Bottom) Coherent RoF. Sample eye diagrams are also shown.

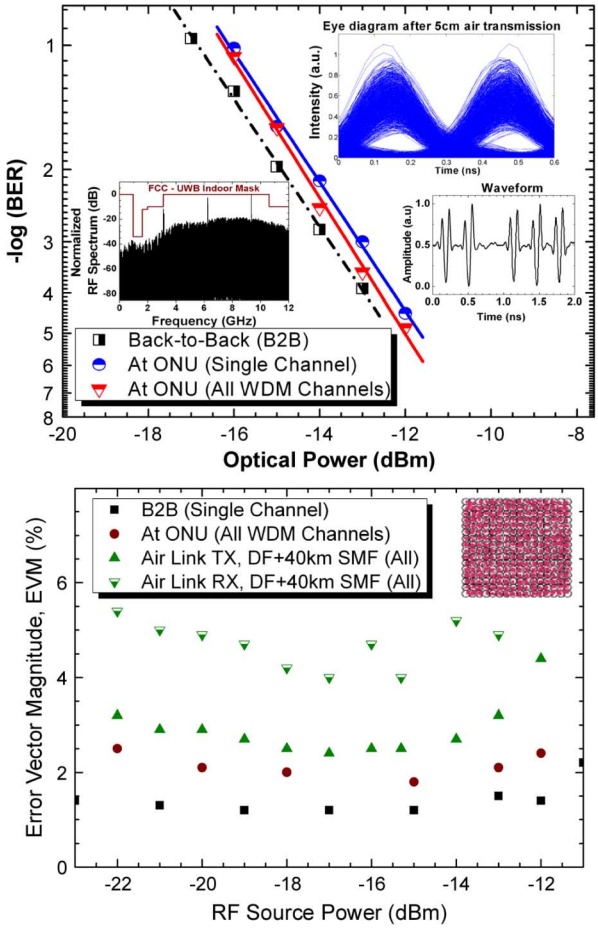

Fig. 3. (Top) BER results, RF spectrum, and eye diagrams obtained for 3.125-Gb/s UWB. (Bottom) WiMAX EVM sensitivity and constellation.

further optical amplification, with below 3% EVM at the remote transmit antenna, as shown in Fig. 3(b). System spur-free dynamic range was 74 dB/Hz$^{2/3}$.

IV. Conclusion

We successfully demonstrated combined transport over a single 78.8-km field-installed fiber of NRZ-DQPSK-modulated baseband access at 21.4 Gb/s per channel, coherent RoF at 250 Mb/s per channel, impulse-radio UWB at a record speed of 3.2 Gb/s, and a 256-QAM WiMAX signal at 12 MBd. For the UWB and WiMAX signals, air transmission was included after the fiber link. This is the first known demonstration of its kind, and it proves that the existing standard SMF based fiber infrastructure can support the seamless coexistence of various wireless and wireline signals for future converged broadband access networks. Prior results [5] also suggest the feasibility of WDM transmission with 100-GHz channel separation.

Acknowledgment

The authors would like to thank M. M. Nedergaard and D. Fryd of the Agilent Technologies Denmark for access to RF signal quality evaluation platforms, and N. Raun of GlobalConnect Denmark for access to the deployed fiber.

References

[1] S. Sarkar, S. Dixit, and B. Mukherjee, "Hybrid wireless-optical broadband-access network (WOBAN): A review of relevant challenges," *J. Lightw. Technol.*, vol. 25, no. 11, pp. 3329–3340, Nov. 2007.

[2] W.-T. Shaw, S.-W. Wong, N. Cheng, K. Balasubramanian, X. Zhu, M. Maier, and L. G. Kazovsky, "Hybrid architecture and integrated routing in a scalable optical-wireless access network," *J. Lightw. Technol.*, vol. 25, no. 11, pp. 3443–3451, 2007.

[3] D. Zibar, X. Yu, C. Peucheret, P. Jeppesen, and I. Tafur Monroy, "Digital coherent receiver for phase-modulated radio-over-fiber optical links," *IEEE Photon. Technol. Lett.*, vol. 21, no. 3, pp. 155–157, Feb. 1, 2009.

[4] X. Yu, T. B. Gibbon, D. Zibar, and I. Tafur Monroy, "A novel incoherent scheme for photonic generation of biphase modulated UWB signals," presented at the Opt. Fiber Commun. Conf. (OFC), San Diego, CA, Mar. 2009, Paper JWA60.

[5] J. Jensen, T. Torkle, C. Peucheret, and P. Jeppesen, "Transmission of WDM multilevel 8 × 30 Gbit/s single polarization RZ-D8PSK with a total capacity of 240 Gbit/s," presented at the 33rd Annu. Eur. Conf. Exhib. Opt. Commun. (ECOC), Berlin, Germany, Sep. 2007, Paper P097.

Paper F

K. Prince, M. Presi, A. Chiuchiarelli, I. Cerutti, G. Contestabile, I. Tafur Monroy and E. Ciaramella, "Variable delay with directly-modulated R-SOA and optical filters for adaptive antenna radio-fiber access," *J. Lightw. Technol.*, vol. 27, pp. 5056–5064, Nov. 2009.

Variable Delay With Directly-Modulated R-SOA and Optical Filters for Adaptive Antenna Radio-Fiber Access

Kamau Prince, Marco Presi, Andrea Chiuchiarelli, Isabella Cerutti, Giampiero Contestabile, Idelfonso Tafur Monroy, and Ernesto Ciaramella, *Member, IEEE*

***Abstract*—We present an all-optical adaptive-antenna radio over fiber transport system that uses proven, commercially-available components to effectively deliver standard-compliant optical signaling to adaptive multiantenna arrays for current and emerging radio technology implementations. The system is based on a directly-modulated reflective semiconductor amplifier (R-SOA) and exploits the interplay between transmission-line dispersion and tunable optical filtering to achieve flexible true time delay, with 2π beam steering at the different antennas. The system was characterized, then successfully tested with two types of signals defined in IEEE 802.16 (WiMAX) standard for wireless networks: a 90 Mbps single-carrier signal (64-QAM at 2.4 GHz) and a 78 Mbps multitone orthogonal frequency-division multiple access (OFDMA) signal. The power budget of this configuration supports a 4-element antenna array.**

***Index Terms*—Beamforming, mobile communications, optical access networks, radio over fiber (RoF) networks, WiMAX.**

I. Introduction

THE explosion of Internet traffic will be the key driver for the deployment of next-generation high-speed fixed and mobile data access networks [1]. We are going to see the massive introduction of the passive optical network (PON) and eventually its long-reach and wavelength-division multiplexed variants, with increased range and user data rates upward of 10 Gb/s [2], [3]. Convergence of optical and wireless access networks is required in order to provide seamless connectivity to mobile users. Additionally, next-generation wireless access networks should provide mobile connections to fast-moving users at much higher data rates than currently available. This would realistically be achieved with multiple-antenna transceivers and statistical signal processing [4]. Such technologies are being integrated into newer radiofrequency (RF) communications systems, including the worldwide interoperability for microwave access (WiMAX) (IEEE 802.16d [5] and IEEE802.16e *mobile WiMAX* [6]–[10]) and the IEEE 802.11n wireless LAN [11]–[13] standards.

We consider an RF communications scheme in which signaling from the central office (CO) propagates over an access network to remote wireless access point (WAP) units that radiate wireless RF signals to mobile customer terminals. High mobile user density may be supported by reducing the coverage area of each mobile cell. Therefore, radio over fiber (RoF) access will be a key supporting technology, allowing the flexible integration of low-loss optical transport and high-density radio access networks. It also allows reduction in the complexity of remote antenna equipment thanks to the remotization of RF processing. RoF systems should therefore evolve from today's commercially available schemes, optimized for single-antenna access, to new architectures implementing multiple-antenna transceivers [14], [15] and adaptive antenna systems (AAS) [16] which adjust the launch angle of the propagating wireless RF wavefront to maximize the receiver SNR at a wireless terminal as it moves through the coverage area. Active control of the differential delay between RF signal copies launched from each element of the WAP antenna array is, therefore, required for adaptively adjusting the beam-steering angle. In this way, the RoF access system can maximize the throughput to multiple mobile terminals while maintaining high spectral efficiency. Ideally, the differential delay of the RF signal launched from each element of the antenna array should be continuously tunable, to achieve continuous beam steering throughout the cell area. Fine-tune control of RF signal true-time delay (TTD) at each antenna element is therefore a key requirement for future RoF systems.

Previous steered-beam systems used spatial sampling of the interference pattern generated by injection-locked sources [17], optical-heterodyne-based phase compensation [18], switched delay elements [19], switching matrices [20], multiwavelength lasers [21] or a combination of multiple optical sources, multiple modulators and tunable birefringent materials [22] to vary the launch angle of the RF wave. Another early approach [23] used a tunable signal wavelength at the central office (CO), and fixed dispersion between photodetectors to control the relative signal delay. Demonstration of wavelength-dependent variable TTD has also been presented [24] using an externally-modulated wideband optical source chirped Fiber Bragg grating and optical tunable filter (OTF).

We present a novel and effective RoF system providing wideband RF signal delivery to an arrayed-antenna, based on well-known commercially available components. In this

Manuscript received January 27, 2009; revised May 12, 2009 and June 12, 2009. First published June 30, 2009; current version published September 17, 2009.

K. Prince and I. Tafur Monroy are with DTU Fotonik, Technical University of Denmark, 2800 Kgs. Lyngby, Denmark (e-mail: kpri@fotonik.dtu.dk; idtm@fotonik.dtu.dk).

M. Presi, A. Chiuchiarelli, I. Cerutti, G. Contestabile, and E. Ciaramella are with the Scuola Superiore Sant'Anna, 56124 Pisa, Italy (e-mail: marco.presi@sssup.it; andrea.chiuchiarelli@cnit.it; isabella.cerutti@sssup.it; g.contestabile@sssup.it; ernesto.ciaramella@cnit.it).

Color versions of one or more of the figures in this paper are available online at http://ieeexplore.ieee.org.

Digital Object Identifier 10.1109/JLT.2009.2026491

scheme, the beam-steering angle is controlled by adjusting OTF central wavelength at the photodetecter feeding each antenna. Our scheme allows for variable tuning of signal TTD by optical means, is transmission-protocol agnostic and natively supports a wide range of current and emerging wireless standards including IEEE 802.11, and IEEE 802.16d/e. Our scheme exploits a single, directly-modulated wideband optical SOA source, singlemode fiber (SMF) chromatic dispersion and optical filtering to implement the TTD required for the AAS functionality. The selective filtering of a broad-spectrum optical source allows us to achieve continuous delay in the electrical RF signal and reduces the impact of uncontrolled wavelength drifts: these can affect systems with tunable [23] or multiwavelength [21] sources; thus, it is inherently very stable. Our system uses only known, reliable components and is, therefore, simpler than previous proposals. It can be used to send different RF signals to each antenna element with the appropriate delay, thus natively supports space-time codes [26] or other multiple-input multiple-output (MIMO) systems [27].

We report the first known demonstration of support for multiple-antenna WiMAX and WiFi signal transmissions over optical media and demonstrate the reliable operation of our system in achieving the desired functionality while meeting or exceeding the applicable RF signal quality specifications. These results represent a natural progression from our previous report using an R-SOA with similar complex-modulation signaling [25]. Our system successfully operates across a wide range of RF communications frequencies, including 2.5 GHz (using a low-frequency R-SOA). We consider downlink performance with data flow from CO to WAP. We evaluated both single-channel 64-QAM IEEE 802.16d WiMAX with the highest data rate of 90 Mbps and multitone 72 Mbps IEEE 802.16e mobile WiMAX format with an uncoded 1024-subcarrier orthogonal frequency-division multiple access (OFDMA) signal also modulated at 64-QAM.

The paper is organized as follows. Section II introduces a theoretical description of the operating principle. Section III reports the small-signal system response, indicating jitter, gain linearity, delay response and sensitivity to OTF passband full width at half maximum (FWHM). In Sections IV and V, we present the results obtained with single-carrier WiMAX transmission, and multitone orthogonal frequency-division multiple access (OFDMA) WiMAX input, respectively. Concluding remarks are then presented.

II. Theoretical Analysis

As shown in Fig. 1(a), the CO transmitter implements an unseeded R-SOA which is directly-modulated by the message RF signal. This results in a broad-spectrum (>30 nm) modulated optical signal which is then propagated through the SMF between CO and wireless access point (WAP). The chromatic dispersion (D) of the SMF produces a wavelength-dependent delay in the broad-spectrum optical signal. At the WAP, the signal is split and sent to each antenna, equipped with a OTF and a photodiode (PD). By tuning each OTF, the photodetected RF signal has, therefore, an effective variable TTD and is ready to be radiated by the antenna. The relative TTD, Δt, obtained

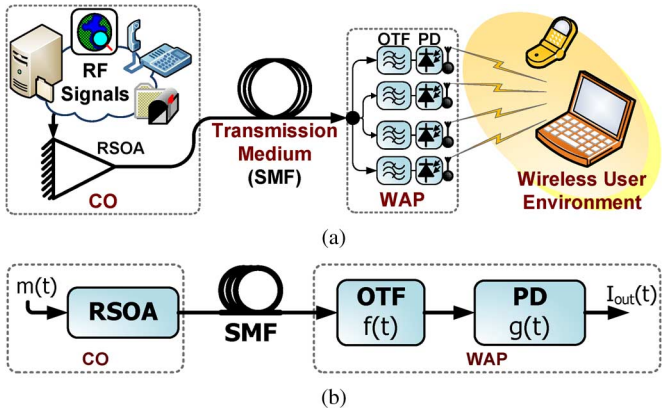

Fig. 1. (a) All-optical AAS-enabled RF over fiber scheme with directly-modulated R-SOA, dispersive transmission and OTF; and (b) block diagram.

after propagation through a SMF of length L, and optical filtering with wavelength detuning $\Delta\lambda$ is given by $\Delta t = D{\cdot}L{\cdot}\Delta\lambda$. We now analytically characterize the RoF signal.

A. Derivation of Output Current

Let $P_{\mathrm{ASE}}(\Omega)$ be the power spectral density of the ASE noise emitted by the R-SOA. Assuming the Optical Tuneable Filters (OTFs) have a Gaussian profile of variance σ around the tuneable central optical angular frequency Ω_0, the power contained in each slice is then given by

$$P_0(\Omega_0) = \frac{1}{2\pi}\int_{-\infty}^{\infty} P_{\mathrm{ASE}}(\Omega)e^{-\frac{(\Omega-\Omega_0)^2}{2\sigma^2}}d\Omega. \quad (1)$$

Assuming the ASE power spectrum to be constant over the OTF bandwidth centered at Ω_0, (1) can be approximated to

$$P_0(\Omega_0) = \frac{1}{2\pi}\int_{-\infty}^{\infty} P_{\mathrm{ASE}}(\Omega_0)e^{-\frac{(\Omega-\Omega_0)^2}{2\sigma^2}}d\Omega. \quad (2)$$

As the modulating waveform is constant with respect to the scale of the coherence time of the ASE noise, the average current obtained after the photodetection is given by the following convolution product [28]

$$\langle i(t)\rangle \approx m(t) * f(t) * g(t) \quad (3)$$

where $m(t)$ is the modulating signal, $g(t)$ is the postdetection filter impulse response and $f(t)$ is the Fourier transform of the function $F(\omega)$, given by

$$\frac{1}{2\pi}\int_{-\infty}^{\infty} P_{\mathrm{ASE}}(\Omega_0)e^{-\frac{(\Omega-\Omega_0)^2}{2\sigma^2}}e^{-i\omega\beta_2 z(\Omega-\Omega_0)}e^{-i\omega\beta_1 L}d\Omega. \quad (4)$$

In (4), ω is the electrical baseband angular frequency, β_1 is the inverse of the group velocity, β_2 is the group velocity dispersion and L is the fiber length. We remark here that β_1 and β_2 are both functions of the OTF central position Ω_0, i.e, $\beta_{1,2} = \beta_{1,2}(\Omega_0)$. As probe signal, we consider a pure RF tone with modulation index $m_0(|m_0| \ll 1)$ and amplitude A, i.e $A[1 + m_0 cos(\omega_0 t)]$. With the assumption that the photodiode bandwidth is larger

than the RF tone (such that $g(t) = \delta(t)$), the received current is found to be (see Section II-B)

$$i(t) \propto A\sigma + A\sigma \cdot m_0 \cos\left[\omega_0 \left(t - \beta_1(\Omega_0)L\right)\right] \cdot \exp\left(-\frac{(\beta_2\omega_0 L)^2\sigma^2}{2}\right). \quad (5)$$

To avoid heating effects, the DC term $A\sigma$ in (5) is removed by an AC coupled receiver and is, thus, neglected. From (5) it is evident that the OTF central frequency allows us to set a TTD given by $\beta_1(\Omega_0)L$ at the fiber output. Indeed at wavelengths around 1550 nm, in a single mode fiber β_1 has a linear relationship versus the optical carrier. On the other hand, the OTF bandwidth σ influences the output signal magnitude. For small σ values the optical power delivered to each avalanche photodiode (APD) increases linearly with the OTF bandwidth. For higher OTF bandwidths, the output signal outputs decreases exponentially. Physically, this corresponds to a fading effect due to the dispersion accumulated in the wavelength-dependent delay line, which dephases the optical frequencies spread within the OTF pass band. The optimal filter bandwidth $\sigma_{\max}$ which maximizes the output RF power is then found by setting $\partial i(t)/\partial\sigma = 0$, which results in

$$\sigma_{\max} = \frac{1}{\|\beta_2\omega_0 L\|}. \quad (6)$$

Substitution yields an optimal OTF FWHM of 3.2 nm.

B. Detailed Derivation

In (4), the term $e^{-i\omega\beta_1 L}$ is constant, so it can be put outside the integration, together with $P_{\mathrm{ASE}}(\Omega_0)$. The expression of $F(\omega)$ is then found after the substitution $\Omega \to \Omega - \Omega_0$, by applying the known self-reciprocal property of Gaussian functions with respect to the Fourier transform

$$\begin{aligned} F(\omega) &= \frac{1}{2\pi} P_{\mathrm{ASE}}(\Omega_0) e^{-i\omega\beta_2 L}\sqrt{2\pi}\sigma \exp\left(-\frac{(\beta_2\omega L)^2\sigma^2}{2}\right) \\ &= \frac{1}{\sqrt{2\pi}} P_{\mathrm{ASE}}(\Omega_0)\sigma \exp\left(-\frac{(\beta_2\omega L)^2\sigma^2}{2}\right) e^{-i\omega\tau} \\ &= F'(\omega)e^{-i\omega\tau}. \end{aligned} \quad (7)$$

In (7), we separated $F(\omega)$ into two parts: the odd function $F'(\omega)$ and a constant phase delay $e^{-i\omega\tau}$. Now, with the assumption $g(t) = \delta(t)$, (3) can be calculated with the aid of the convolution theorem. In order to do this, we first write the Fourier transform of the modulating signal $M(\omega)$

$$M(\omega) = \delta(0) + \frac{m_0}{2}\left[\delta(\omega_0) + \delta(-\omega_0)\right] \quad (8)$$

and then evaluate the product $M \cdot F$

$$\begin{aligned} \langle i(t)\rangle &= \int_{-\infty}^{\infty} \left(\delta(0) + \frac{m_0}{2}\left[\delta(\omega_0) + \delta(-\omega_0)\right]\right) F(\omega)e^{i\omega t}d\omega \\ &= \int_{-\infty}^{\infty} \left(\delta(0) + \frac{m_0}{2}\left[\delta(\omega_0) + \delta(-\omega_0)\right]\right) \\ &\qquad \times F'(\omega)e^{-i\omega\tau}e^{i\omega t}d\omega \\ &= F(0) + \frac{m_0}{2}\left(F'(\omega_0)e^{i\omega_0(t-\tau)} \right. \\ &\qquad \left. + F'(-\omega_0)e^{-i\omega_0(t-\tau)}\right) \end{aligned} \quad (9)$$

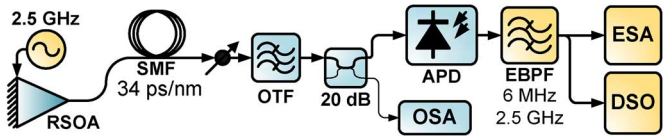

Fig. 2. Experimental setup for RF small-signal evaluation. VOA, variable optical attenuator; OTF, optical tunable filter; EBPF, electrical bandpass filter; OSA/ESA, optical/electrical spectrum analyzer; DSO, oscilloscope.

and since $F'(\omega)$ is odd (i.e., $F'(\omega) = F'(-\omega)$), we find

$$\langle i(t)\rangle = F(0) + m_0 F'(\omega_0)\cos\left(\omega_0(t-\tau)\right). \quad (10)$$

Equation (5) is then readily obtained from (10) by substituting the expression for $F'(\omega)$. For a differential path length between the CO and each PD equal to an AAS element spacing of $\lambda/2$ [29], [30], a TTD of 400 ps would be required for 2π steering at a frequency of 2.5 GHz.

C. Impact of OTF FWHM on System Performance

For fixed electrical input power to the system and small σ, the optical power delivered to each PD increases with OTF bandwidth, yielding a proportional increase in $|I_{out}(t)|$. At a fixed PD responsivity, when using large FWHM values the RF forward system gain (S_{21}) depends on filter FWHM, and therefore on σ.

Arbitrarily large output RF power cannot be obtained by increasing OTF bandwidth, as fading effects become increasingly apparent at the RoF system output. The dispersion accumulated during transmission results in a time-staggered wideband optical signal reception at the PD, and the use of large FWHM OTF produces a fading in the output RF signal. Considering the wideband optical source as a synchronized group of narrowly-spaced optical wavelengths, we observe that dispersive transmission causes the PD to receive each wavelength with a small relative delay. Narrow filtering selects only a few wavelengths and their optical fields interfere constructively. Large FWHM values result in a large number of received wavelengths at the PD, each arriving with a slightly different transmission delay. The interaction between out-of-phase signal components at each wavelength results in signal fading at the PD due to the slight phase mismatch and imperfect constructive interference. Increasing the FWHM would naturally increase this fading effect.

Another constraint on FWHM selection is imposed by relative intensity noise (RIN) effects, since the system is based on the modulation of an incoherent optical source with ASE noise output and selective filtering [31]. Narrow filtering therefore increases the system output RIN due to the spontaneous emission of the optical source. OTF FWHM should, therefore, be chosen large enough to achieve a balance between RIN and fading effects, with adequate forward system gain. The optimal FWHM for a Gaussian OTF was found in (6) to be 3.2 nm.

III. RF Small-Signal Characterization

We assessed the performance of our optical TTD system using the configuration presented in Fig. 2. Our analysis was informed by the excellent systems-level treatment of RoF systems presented in [36]. The R-SOA used had a datasheet-specified electrical bandwidth of 1.25 GHz, and was

directly intensity-modulated by a 2.5-GHz RF carrier. We used a commercially-available R-SOA providing 20 dB small-signal gain and 2 dBm output saturation power when operated at 20°C: a temperature-independent device [32] would be preferable for a real-world deployment. The broad-spectrum optical output of the R-SOA is centered at approximately 1549 nm, has around 20-nm FWHM, an average power of 3 dBm and a typical ASE ripple of 0.5 dB at peak. The modulated broad-spectrum optical signal was transmitted through 2.1 km standard SMF (1 dB insertion loss and 17 ps/nm·km· dispersion). This gave 35.7 ps/nm wavelength-dependent delay, producing 2π beam steering at 2.5 GHz with 11.2 nm OTF detuning.

The signal was passed through a variable optical attenuator (VOA), an OTF and onto an APD. This APD had 10 GHz electro-optical bandwidth, 0.5 W/A responsivity and an avalanche gain factor of 10. We used a postdetector electrical band-pass filter (EBPF) with a FWHM of 6 MHz, centered at 2.5 GHz, to reject out of band noise. We evaluated system performance for various OTF having passband FWHM of 0.8, 2, 3, and 4 nm, using spectrum analyzers (OSA, ESA) and digital storage oscilloscope (DSO).

A. Small-Signal Phase Noise/Jitter

The system was excited with a 2.5 GHz tone at -10 dBm: we observed negligible intensity noise at system output, and we evaluated jitter and single-sideband (SSB) phase noise performance [33], [34]. The results of SSB phase noise $S(f)$ assessments at system input and output are shown in Fig. 3(a) for various OTF implementations. For f_{offset} in the interval $[10, 10^6]$ Hz, the output signal phase noise closely followed the synthesizer characteristic, with less than 10 dB difference between the two over this range. For offset frequency in the interval $(10^3, 3\times 10^3)$ Hz, we noted an almost flat phase noise response. Between approximately 3 kHz and 10 MHz offset frequency, the phase noise decreased rapidly with increasing frequency offset. Above 10 MHz, the system phase noise remained below -150 dBc/Hz, which is comparable with the noise floor of the analyzer used. The postdetector RF filter accounts for the sharp roll-off observed in the phase noise characteristic for frequency offset greater than 3 MHz. The worst phase noise performance was obtained for the OTF with the highest bandwidths (3 and 4 nm), and the best results were obtained with 2 nm FWHM.

The integrated SSB jitter δ_t of a signal within frequency interval $[f_{\min}, f_{\max}]$ is given by [34]

$$\delta_t = \frac{1}{2\pi f_c}\sqrt{2\int_{f_{\min}}^{f_{\max}} S(f)df}. \tag{11}$$

We experimentally evaluated system input and output SSB jitter, from a minimum offset frequency $(f_{\min})$ of 100 Hz, up to $f_{\max}$ of 20 GHz, and present the results in Fig. 3(b). The selected $f_{\min}$ value ensured that the tails of the carrier signal would not be included in the calculation of the phase noise of the system, due to frequency resolution limitations of the ESA [33]. The best resolution of the device used was 316 Hz. From Fig. 3(b), we observed that all OTF implementations provide less than 1.5 ps integrated SSB jitter in the frequency interval $[10^3, 2\times 10^6]$ Hz:

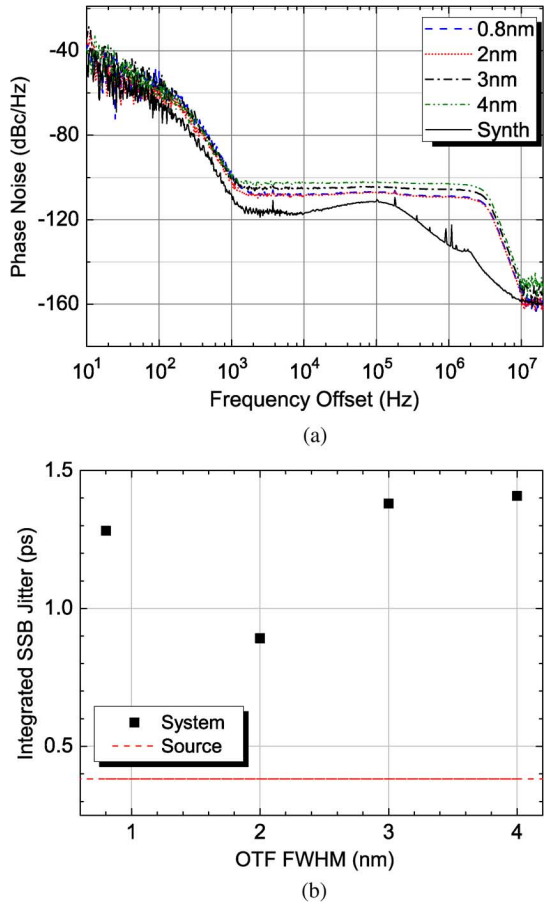

Fig. 3. (a) Phase noise; (b) jitter versus FWHM in the interval $[10^3, 2\times 10^6]$ Hz.

best jitter results were obtained with the 2 nm OTF. We assessed the carrier-to-noise ratio (CNR) for the output signal measured at 1 kHz offset frequency; all OTF produced CNR better than -100 dBc/Hz.

B. RF Gain Characteristics

As the best jitter and phase noise results were observed with the 2 nm OTF, we used this filter and assessed system linearity as a function of the input RF power [35]. Without the postdetector EBPF, we observed linear system response for source power levels between -30 dBm and $+10$ dBm. Inclusion of the postdetection RF bandpass-filter produced a shaped gain spectrum. We also observed that system gain was almost constant at -15 dB for input power below approximately -10 dBm, which is comparable with the literature [36]. Above this threshold, system gain begins to decrease steadily with increasing input power, resulting in loss of linearity. These results are presented in Fig. 4; similar trends were obtained for other OTF units evaluated.

C. System Linearity

We evaluated system-induced distortion by assessing second and third-order intermodulation according to [37] using two unmodulated carriers of equal magnitude separated by 200 kHz. We used the setup of Fig. 2, with 2 nm OTF; results were obtained at a resolution bandwidth of 316 Hz, the noise floor was at

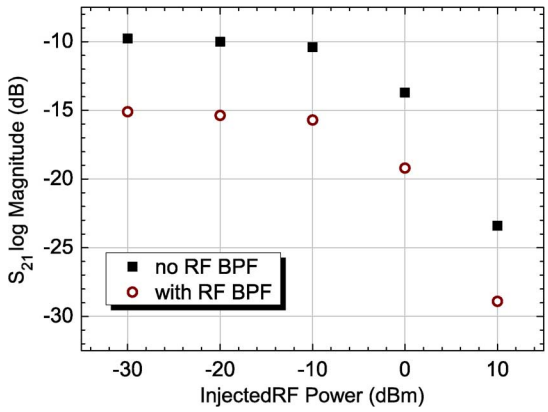

Fig. 4. System magnitude response (S_{21}) versus input RF power for 2 nm OTF.

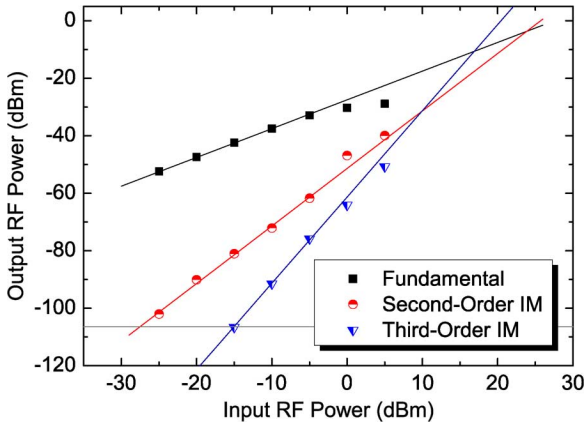

Fig. 5. Two-tone fundamental and intermodulation product (second- & third-order) output power as a function of input RF signal power. Dynamic range, $\mathrm{IMF}_3 = 65$ dB $\mathrm{Hz}^{2/3}$: tone separation, 200 kHz; meas. bandwidth, 316 Hz.

−106 dBm. The evolution of output fundamental and intermodulation (IM) terms with input RF signal power is shown in Fig. 5. The second-order free dynamic range (IMF_2) is 52dB $\mathrm{Hz}^{2/3}$ and the third-order free dynamic range (IMF_3), also called the spurious-free dynamic range (SFDR), is 65 dB $\mathrm{Hz}^{2/3}$. This is comparable with the values reported in [38] (for an amplified 120 km optical link operating at 5 GHz, with an EAM source), but less than the 106 dB $\mathrm{Hz}^{2/3}$ obtained using a DBR source without RF preamplification [39], or the 115 dB $\mathrm{Hz}^{2/3}$ obtained using a DFB with RF preamplification [40]. The 1 dB compression point of our system was at −4 dBm input power, which is suitable for short-range picocellular applications requiring low launch RF power levels: other authors [20] have previously reported +7 dBm output power level corresponding to a 1 dB compression point, but with a more complex architecture. We observed the second-order intercept point at an input power of +25 dBm and a third-order distortion intercept at +16 dBm.

D. Sensitivity to OTF Central Wavelength and Bandwidth

We assessed the variation of TTD with filter detuning across the operating band. This is reported in Fig. 6(a). The TTD was independent of OTF FWHM; however, the RF output power varied with FWHM: the maximum output RF signal was observed for the 2 nm-filter and the output RF power decreased at higher OTF bandwidth as also anticipated by (5). At any given

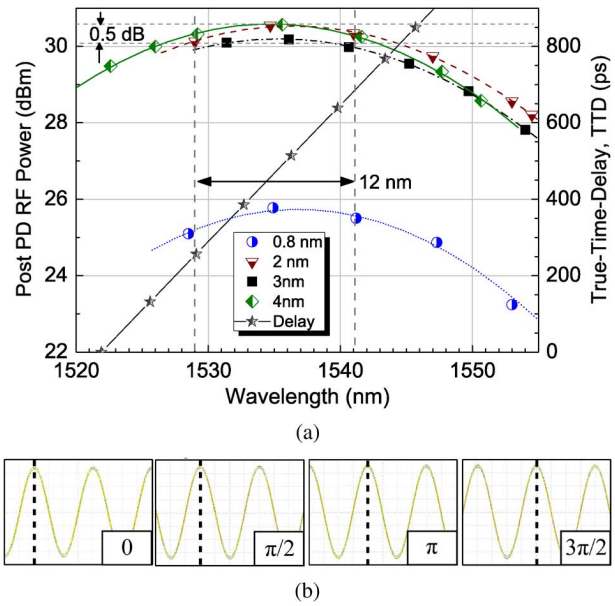

Fig. 6. (a) Output RF power and TTD versus detuning with various OTF for 2.5-GHz signal; (b) output signal at various TTD (across 12-nm detuning), with 2-nm OTF. (Vert. scale: 10 mV/div., power variation within 0.5 dB).

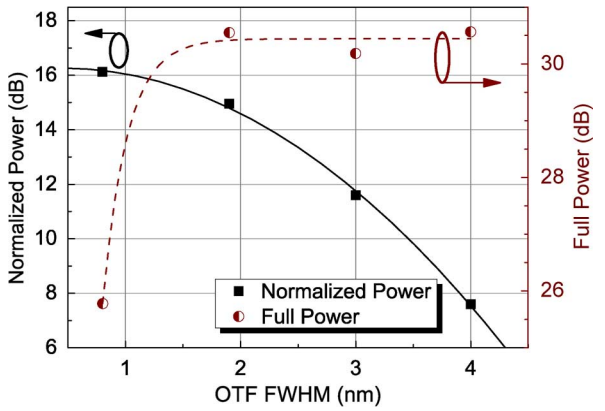

Fig. 7. Normalized system gain as a function of OTF FWHM; APD input power fixed at −30 dBm (solid), full optical power onto the APD (dashed).

wavelength, all filter implementations produced output power profiles proportional to the ASE noise power spectral density (PSD) at that wavelength. The detuning range of 12 nm (for full 2 π beam steering) had an associated power excursion within 1.2 dB; samples of the output signal amplitude for various TTD are presented in Fig. 6(b). System response was then evaluated for OTF implementations with varying FWHM. As the filters that we used had unequal insertion losses and unequal passband characteristics (Gaussian OTF were not available for all FWHM values evaluated), measurements were taken with maximum available optical power into the APD (i.e., with zero VOA attenuation), and also with VOA adjusted to maintain a constant −30 dB input average optical power into the APD: the results are presented in Fig. 7. For the case with controlled optical input power to the APD (solid line), we observed that the RF output power decreased with increasing OTF FWHM. We concluded that this test scenario isolated the RF fading phenomenon (by removing the gain associated with increased APD input power)

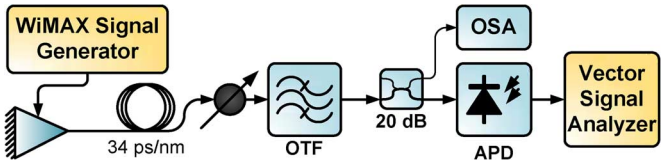

Fig. 8. System layout for WiMAX evaluation.

that was predicted in (5) and we clearly see that the output electrical RF signal is diminished with increased FWHM, and that the observations closely follow the trace predicted by theory (which is parabolic for a log scale). When maximum optical power was sent to the APD (dashed line), the output RF power was approximately 26 dBm for the 0.8 nm OTF; all other OTF units provided approximately 30.5 dBm. We believe that the discrepancy in OTF insertion loss and passband characteristic mask the trends predicted by (5), although there is a marked decrease in output power at low FWHM. Theory indicates a similar decrease in output RF power if the FWHM were further increased, but we were unable to evaluate these conditions.

IV. Single-Carrier WIMAX Signal Transmission

We evaluated system performance with single-carrier WiMAX IEEE 802.16d signals: the MAN SCa PHY [5] regulates single-carrier transmissions at frequencies below 11 GHz: 120 km AAS support is optional within the standard. It supports 16- and 64-QAM, allowing FDD and/or TDD with TDM(A) downlink and TDMA uplink, with a maximum allowable frame duration of 20 ms. The maximum allowable error vector magnitude (EVM) for 64-QAM signaling is 3.1% and the symbol-to-symbol timing jitter must be within 2%: power control is required, in 1 dB increments, although maximum transmit power levels are set by local authorities and there are no intermodulation specifications in the standard.

The test signal was obtained from an Agilent E4438C ESG generator. System EVM performance was characterized with a 26.5 GHz Agilent N9020A MXA signal analyzer. Our analysis was done for 64-QAM, which is the fastest modulation scheme required by the WiMAX standard. The layout is shown in Fig. 8. We used a carrier frequency of 2.4 GHz and symbol rate of 15 Msps (million symbols per second), equivalent to 90 Mbps. At this carrier frequency, $(\lambda/2 = 6.25\ \text{cm})$ antenna spacing required 417 ps TTD for 2π steering, this was achieved with 11.7 nm OTF detuning.

A sample of the received signal constellation is presented in Fig. 9(a); Fig. 9(b) presents EVM as a function of drive electrical RF power. RF power in the range $[-6, -14]$ dBm provided acceptable EVM: we note from Fig. 4 that this overlaps with the power required for good system linearity. We also assessed EVM variation with received optical power (at fixed wavelength and input RF power) and present the results in Fig. 9(c): we observed approximately 6 dB system margin to the EVM threshold. Observations of the variation of RMS EVM with OTF detuning is presented in Fig. 9(d), indicating 12 nm detuning associated with less than 0.2% EVM excursion: acceptable EVM was obtained across the entire operating range of the OTF.

Low EVM and output power variation with OTF detuning and the optical power margin, indicate the feasiblity of optical split

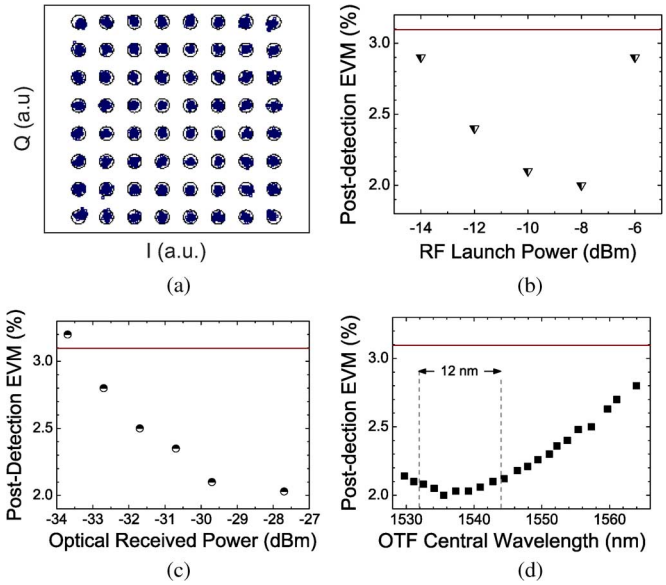

Fig. 9. Single-carrier 64-QAM WiMAX signal at 90 Mbps, (a) constellation; and output signal EVM as a function of (b) input RF power, (c) APD power, (d) OTF wavelength. 3.1% IEEE 802.16d WiMAX EVM threshold indicated.

and filtering at the WAP to implement a quad-antenna array configuration with low-loss splices: differential OTF wavelength selection would control the TTD delay at each antenna element and, hence, the angle of the launched RF wave. We then investigated system performance with a multicarrier OFDMA payload.

V. Multitone WIMAX Signal Transmission

IEEE 802.16e Mobile WiMAX [7] is heavily favored to become a dominant technology for supporting wireless data access services. It will require multiple transceiver antennas at WAP nodes for integrated AAS support: the MAN-OFDMA PHY [6] defines the air interface requirements. OFDMA signaling is implemented with up to 2048 subcarriers: for subscriber station and base station (or WAP), the relative constellation error (RCE) with an encoded (rate 3/4) 64-QAM transmission must be less than -30 dB. Maximum transmit power levels and intermodulation performance specifications are not mandated.

We used the setup shown in Fig. 8 to evaluate the transmission of mobile WiMAX OFDMA signals. Performance was assessed using the relative constellation error (RCE) obtained on the uncoded data subchannels, as defined in [6]. The generated OFDMA signal allowed a selection between a partial use of subchannels (PUSC) or a full use of subchannels (FUSC) format: we opted for PUSC and fixed 64-QAM modulation on all data subcarriers. We evaluated time-division multiplex system using a ratio of downlink/total frame duration $(T_{\text{DL}}/T_{\text{TOTAL}})$ of 99% and 50%. The test OFDMA signal had the following parameters: 2048 subcarriers, 20 MHz signal bandwidth, no FEC coding, 5 ms frame duration, 1/4 guard interval and a central frequency of 2.5 GHz. The maximum data throughput was 72.3 Mbit/s. Since R-SOA typically have a highly non-linear electro-optical transfer function, which is unsuitable for OFDMA signals, we optimized R-SOA bias-point and input RF power to operate the R-SOA in the quasi-linear region, in order to reduce intermodulation distortion between sub-carriers and obtain adequate SNR.

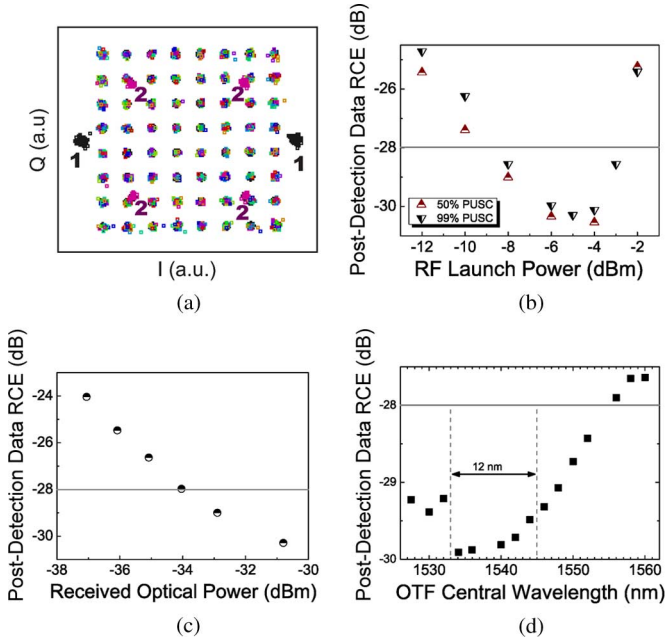

Fig. 10. 64-QAM, 2048-subcarrier, 99% downlink OFDMA IEEE 802.16e WiMAX frame, (a) constellation, BPSK pilot (1) and QPSK preamble (2): data RCE variation with (b) launch RF power, (c) received APD power and (d) OTF wavelength. RCE below −28-dB WiMAX threshold for 64-QAM.

Fig. 10(a) illustrates the constellation of the signal obtained at the APD output. It is possible to clearly distinguish between the BPSK pilots, the QPSK used in the packet preamble and the 64-QAM used in each burst of the WiMAX signal [6]. Fig. 10(b) shows the performance of OFDMA PUSC signals having 50% and a 99% downlink sub-frame duration. In both cases, the optimal RF driving power was approximately −5 dBm. The 99% represented more stringent requirements, so all subsequent evaluations were taken with this setting. The IEEE 802.16e RCE requirement of −28 dB for a 64-QAM coded (rate 3/4) signal was met for RF driving power levels in the range $[-9, -3]$ dBm. Fig. 10(c) reports the system performance in terms of received optical power. The sensitivity (measured at −28 dB RCE) determines the maximum number of antennas (i.e., the splitting ratio) supported by this system. It matches the IEEE 802.16e requirements when the received optical power level exceeds −34 dBm. In our case, modulated ASE experienced a 1-dB loss in the feeder and 22 dB at the OTF (20 dB due to OTF rejection). RCE variation with OTF detuning is reported in Fig. 10(d): IEEE 802.16e requirements are met in a detuning range wider than the 12 nm required for full beam steering: this range is associated with less than 1 dB RCE penalty. Due to the low power and RCE penalty with OTF detuning, and 3 dB optical power margin, a dual-antenna WAP is feasible for mobile WiMAX-compliant signaling: a higher output power device may allow additional antennas.

VI. Conclusion

We presented a radio-over-fiber system suitable for adaptive antenna systems based on spectrum-slicing of a directly-modulated R-SOA. We have successfully characterized the system, and evaluated it with single-tone and OFDMA WiMAX signals. This optical source can support four antennas in the single-tone implementation, and the use of an electrical preamplifier allows the transmission of an optical signal that can be distributed to two antenna elements. We note that operation with optimal input RF power levels implies low RF electrical power at the output of each photodiode driving the antenna array: a higher-powered optical source or low-noise RF amplification at the WAP could improve system gain while preserving the other advantages. In all cases, standard-compliant operation was obtained with the maximum modulation depth specified (64-QAM). The OTF tuning required to achieve full beam steering may safely be done with the delayed output still meeting performance criteria. Sample constellation diagrams demonstrated good signal transmission through our optical system.

Acknowledgment

The authors would like to thank M. Pagano and R. Sacchi of Agilent Technologies for technical support and the loan of the N9020A MXA signal analyzer and E4438C ESG generator.

References

[1] S. Cherry, "Edholm's law of bandwidth," *IEEE Spectrum*, vol. 41, no. 7, pp. 58–60, Jul. 2004.
[2] K. Grobe and J.-P. Elbers, "PON in adolescence: From TDMA to WDM-PON," *IEEE Commun. Mag.*, vol. 46, no. 1, pp. 26–34, Jan. 2008.
[3] C.-H. Lee, S.-M. Lee, K.-M. Choi, J.-H. Moon, S.-G. Mun, K.-T. Jeong, J. H. Kim, and B. Kim, "WDM-PON experiences in Korea (invited)," *J. Opt. Netw.*, vol. 6, no. 5, pp. 451–464, 2007.
[4] W. Konhäuser, "Broadband wireless access solutions—Progressive challenges and potential value of next generation mobile networks," *Wireless Pers. Commun.*, vol. 37, no. 3–4, pp. 243–259, 2006.
[5] *IEEE LAN/MAN Standards Cttee.*, IEEE Std.802.16-2004, Oct. 2004.
[6] *IEEE LAN/MAN Standards Cttee.*, IEEE Std. 802.16e-2005, Feb. 2006.
[7] K. H. Teo, Z. Tao, and J. Zhang, "The mobile broadband WiMAX standard [standards in a nutshell]," *IEEE Signal Process. Mag.*, vol. 24, no. 5, pp. 144–148, Sep. 2007.
[8] S. Cherry, "South Korea pushes mobile broadband," *IEEE Spectrum*, vol. 42, no. 9, pp. 14–16, Sep. 2005.
[9] C. Nam, S. Kim, and H. Lee, "The role of WiBro: Filling the gaps in mobile broadband technologies," *Technolog. Forecast. Social Change*, vol. 75, no. 3, pp. 438–448, Mar. 2008.
[10] S. J. Vaughan-Nichols, "Mobile WiMAX: The next wireless battle ground," *Computer*, vol. 41, no. 6, pp. 16–18, 2008.
[11] *Unapproved draft standard*, IEEE P802.11n/D4.00, Mar. 2008.
[12] R. Nee, V. K. Jones, G. Awater, A. Zelst, J. Gardner, and G. Steele, "The 802.11n MIMO-OFDM standard for wireless LAN and beyond," *Wireless Pers. Commun.*, vol. 37, no. 3–4, pp. 445–453, 2006.
[13] Y. Xiao, "IEEE 802.11n: Enhancements for higher throughput in wireless LANs," *IEEE Wireless Commun.*, vol. 12, no. 6, pp. 82–91, Dec. 2005.
[14] S. Alamouti, "A simple transmit diversity technique for wireless communications," *IEEE J. Sel. Areas Commun.*, vol. 16, no. 8, pp. 1451–1458, Aug. 1998.
[15] V. Tarokh and H. Jafarkhani, "A differential detection scheme for transmit diversity," *IEEE J. S. Ar. Cm.*, vol. 18, no. 7, pp. 1169–1174, 2000.
[16] J. Winters, "Smart antennas for wireless systems," *IEEE Pers. Commun.*, vol. 5, no. 1, pp. 23–27, Feb. 1998.
[17] M. Tamburrini, M. Parent, L. Goldberg, and D. Stillwell, "Optical feed for a phased array microwave antenna," *Electron. Lett.*, vol. 23, no. 13, pp. 680–681, June 1987.
[18] E. Toughlian and H. Zmuda, "A photonic variable RF delay line for phased array antennas," *J. Lightw. Tech.*, vol. 8, no. 12, pp. 1824–1828, Dec. 1990.

[19] W. Ng, A. Walson, G. Tangonan, J. Lee, and I. Newberg, "Optical steering of dual band microwave phased array antenna using semiconductor laser switching," *Electron. Lett.*, vol. 26, no. 12, pp. 791–793, June 1990.

[20] M. Piqueras, G. Grosskopf, B. Vidal, J. Herrera, J. Martinez, P. Sanchis, V. Polo, J. Corral, A. Marceaux, J. Galiere, J. Lopez, A. Enard, J.-L. Valard, O. Parillaud, E. Estebe, N. Vodjdani, M.-S. Choi, J. den Besten, F. Soares, M. Smit, and J. Marti, "Optically beamformed beam-switched adaptive antennas for fixed and mobile broad-band wireless access networks," *IEEE Trans. Microw. Theory. Tech.*, vol. 54, no. 2, pp. 887–899, Feb. 2006.

[21] B. Vidal, D. Madrid, J. Coffal, and J. Marti, "Novel photonic true-time-delay beamformer based on the free-spectral-range periodicity of arrayed waveguide gratings and fiber dispersion," *IEEE Photon. Technol. Lett.*, vol. 14, no. 11, pp. 1614–1616, Nov. 2002.

[22] L. Jofre, C. Stoltidou, S. Blanch, T. Mengual, B. Vidal, J. Marti, I. McKenzie, and J. M. del Cura, "Optically beamformed wideband array performance," *IEEE Trans. Antennas Propagat.*, vol. 56, no. 6, pp. 1594–1604, Jun. 2008.

[23] R. Esman, M. Frankel, J. Dexter, L. Goldberg, M. Parent, D. Stilwell, and D. Cooper, "Fiber-optic prism true time-delay antenna feed," *IEEE Photon. Technol. Lett.*, vol. 5, no. 11, pp. 1347–1349, Nov. 1993.

[24] B. Zhou, X. Zheng, X. Yu, H. Zhang, Y. Guo, and B. Zhou, "Optical beamforming networks based on broadband optical source and chirped fiber grating," *IEEE Photon. Technol. Lett.*, vol. 20, no. 9, pp. 733–735, Sep. 2008.

[25] K. Prince, A. Chiuchiarelli, M. Presi, I. T. Monroy, and E. Ciaramella, "All-optical delay technique for supporting multiple antennas in a hybrid optical—Wireless transmission system," presented at the 21st Meet. IEEE Lasers Electro-Optics Society, Newport Beach, CA, Nov. 2008.

[26] D. Gesbert, M. Shafi, D.-S. Shiu, P. Smith, and A. Naguib, "From theory to practice: An overview of MIMO space-time coded wireless systems," *IEEE J. Sel. Areas Commun.*, vol. 21, no. 3, pp. 281–302, Apr. 2003.

[27] A. Paulraj, D. Gore, R. Nabar, and H. Bölcskei, "An overview of MIMO communications—A key to gigabit wireless," *Proc. IEEE*, vol. 92, no. 2, pp. 198–218, Feb. 2004.

[28] G. Pendock and D. Sampson, "Transmission performance of high bit rate spectrum-sliced WDM systems," *J. Lightw. Technol.*, vol. 14, no. 10, pp. 2141–2148, Oct. 1996.

[29] G. Foschini and M. Gans, "On limits of wireless communications in a fading environment when using multiple antennas," *Wireless Personal Commun.*, vol. 6, no. 3, pp. 311–335, Mar. 1998.

[30] M. Stoytchev, H. Safar, A. Moustakas, and S. Simon, "Compact antenna arrays for MIMO applications," in *Proc. IEEE Antennas and Propagation Society Int. Symp.*, 2001, vol. 3, pp. 708–711.

[31] A. D. McCoy, B. C. Thomsen, M. Ibsen, and D. J. Richardson, "Experimental study on receiver filtering effects in a spectrum-sliced incoherent light WDM system using SOA based noise reduction," in *Proc. ECOC*, Rimini, Italy, Sep. 2003, pp. 866–867, WE4P156.

[32] K. Y. Cho, Y. Takushima, K. R. Oh, and Y. C. Chung, "Operating wavelength range of 1.25-Gb/s WDM PON implemented by using uncooled RSOA's," presented at the OFC/NFOEC, San Diego, CA, 2008, oTuH3, unpublished.

[33] L. K. Oxenløwe, "Optical Signal Processing With Semiconductor Components," Ph.D. dissertation, Tech. Univ. Denmark, Kgs. Lyngby, Denmark, 2002.

[34] J. Hargreaves, P. Juodawlkis, J. Plant, J. Donnelly, J. Twichell, F. Rana, and R. Ram, "Residual phase-noise measurements of actively mode-locked fiber and semiconductor lasers," in *Proc. LEOS*, 2001, pp. 115–116.

[35] C. H. Cox, III, H. Roussell, R. Ram, and R. Helkey, "Broadband, directly modulated analog fiber link with positive intrinsic gain and reduced noise figure," in *Proc. Int. Topical Mtg. on Microw. Phot.*, 1998, pp. 157–160.

[36] C. H. Cox, III, E. I. Ackerman, G. E. Betts, and J. E. Prince, "Limits on the performance of RF-over-fiber links and their impact on device design," *IEEE Trans. Microw. Theory Tech.*, vol. 54, no. 2, pp. 906–920, Feb. 2006.

[37] C. H. Cox, III, *Analog Optical Links: Theory and Practice*. Cambridge, U.K.: Cambridge Univ. Press, 2004, ch. 6.2.2, pp. 205–217.

[38] H.-H. Lu, S.-J. Tzeng, and Y.-L. Liu, "Intermodulation distortion suppression in a full-duplex radio-on-fiber ring network," *IEEE Photon. Technol. Lett.*, vol. 16, no. 2, pp. 602–604, Feb. 2004.

[39] L. A. Johansson, Y. A. Akulova, C. Coldren, and L. A. Coldren, "Improving the performance of sampled-grating DBR laser-based analog optical transmitters," *J. Lightw. Technol.*, vol. 26, no. 7, pp. 807–815, Jul. 2008.

[40] A. Razibul Islam, G. Town, and A. Tariqul Islam, "PAPR and SFDR of an OFDM/RoF link," in *Proc. OECC/ACOFT*, Jul. 2008, pp. 1–2.

Kamau Prince received the B.Sc. degree (first class honours) in electrical engineering from the University of the West Indies, St. Augustine, Trinidad, in 1999, and the Graduate Diploma in telecommunications engineering and the M.Eng.Sci. degree from the University of Melbourne, Victoria, Australia, in 2003 and 2006, respectively. He is currently pursuing the Ph.D. degree in optical communications at DTU Fotonik, Technical University of Denmark.

Marco Presi received the Laurea degree in physics from "La Sapienza" University of Rome, Italy, in 2001, and the Ph.D. degree in applied physics from the University of Pisa, Italy, in 2006.

Since 2007, he has been a Research Associate at the Scuola Superiore Sant'Anna, Pisa, Italy, where he currently works on WDM optical systems. He has coauthored more than 50 papers published in international peer-reviewed journals and in international conferences.

Andrea Chiuchiarelli received the Laurea degree in electronic engineering from the University of L'Aquila, Italy, in March 2005. He is currently pursuing the Ph.D. degree at the Scuola Superiore Sant'Anna in the Optical Systems group of CEIIC (Center of Excellence for Information and Communication Engineering), Pisa, Italy.

From November 2005 to November 2006, he was with the Inter-University National Consortium for Telecommunications (CNIT).

Isabella Cerutti received the "Laurea" degree in electrical engineering from the Politecnico di Torino, Italy, 1998, and the Ph.D. degree from the University of Texas at Dallas (UTD) in 2002.

From 2002 to 2006, she was a postdoctorate research associate at UTD and then at the Scuola Superiore Sant'Anna (SSSUP), Italy. Since 2007, she has been an Assistant Professor at SSSUP. She coauthored more than 50 publications in international journals and conference proceedings.

Giampiero Contestabile received the Laurea degree in physics from "La Sapienza" University of Rome, Italy, in 1998, and the Ph.D. degree in electrical engineering-telecommunications from "Tor Vergata" University of Rome, Italy, in 2001.

Between 1996 and 2000, he was with the Semiconductor Devices Group of "Fondazione Ugo Bordoni", Rome. In 2001, he was with Optospeed Italia. Since September 2002, he has been an Assistant Professor at the "Scuola Superiore Sant'Anna" University of Pisa, Italy. He has coauthored more than 90 papers published in international peer-reviewed journals and presented at leading international conferences. His main research interests are advanced WDM systems, optical packet switched networks, access networks and applications of semiconductor optical amplifiers.

Dr. Contestabile is one of the reviewers of the JOURNAL OF LIGHTWAVE TECHNOLOGY, *Photonics Technology Letters, OpticsExpress, Optics Letters*, and *Optics Communications*.

Idelfonso Tafur Monroy received the M.Sc. degree in multichannel telecommunications from the Bonch-Bruevitch Institute of Communications, St. Petersburg, Russia, in 1992, the Technology Licenciate degree in telecommunications theory from the Royal Institute of Technology, Stockholm, Sweden, and the Ph.D. degree from the Electrical Engineering Department, Eindhoven University of Technology, The Netherlands, in 1999.

He is currently Head of the metro-access and short range communications group of the Department of Photonics Engineering, Technical University of Denmark. He was an Assistant Professor until 2006 at the Eindhoven University of Technology. Currently, he is an Associate Professor at the Technical University of Denmark. He has participated in several European research projects, including the ACTS, FP6, and FP7 frameworks (APEX, STOLAS, LSAGNE, MUFINS). At the moment, he is in involved the ICT European projects GiGaWaM, ALPHA, BONE, and EURO-FOS. His research interests are in hybrid optical-wireless communication systems, coherent detection technologies and digital signal processing receivers for baseband and radio-over-fiber links, optical switching, nanophotonic technologies, and systems for integrated metro and access networks, short range optical links, and communication theory.

Ernesto Ciaramella (M'06) was born in Rome, Italy, in 1967. He received the Laurea degree (*cum laude*) from La Sapienza University, Rome, Italy, in 1991.

In 1992, he was awarded a scholarship by Alcatel. During 1992–1994, he was with Fondazione Ugo Bordoni, working on nonlinear optical effects. From 1994–1998, he was with CSELT, Turin, Italy, concerned with linear and nonlinear propagation effects in optical fibers and with system modeling. From 1998–2000, he was with the Fondazione Ugo Bordoni, working on optical transmission systems and network architectures. In 2001–2002, he was a Research Manager at CNIT, Pisa, Italy. Since 2002, he has been an Associate Professor at the Scuola Superiore Sant'Anna, Pisa, Italy. His present research activity covers optical transmission systems, nonlinear effects, fiber transmission impairments, all-optical processing, and optical packet switching. He has participated in various European research projects, published more than 100 papers, and is the author/coauthor of ten international patents. He is presently serving on the Technical Program Committee of the Optical Fiber Communication Conference (OFC).

Paper G

A. V. Osadchiy, K. Prince, and I. Tafur Monroy, "Converged delivery of WiMAX and wireline services over an extended reach passive optical access network," *Optical Fiber Technology*, vol. 16, pp. 182 – 186, April 2010.

Optical Fiber Technology 16 (2010) 182–186

Contents lists available at ScienceDirect

Optical Fiber Technology

www.elsevier.com/locate/yofte

Converged delivery of WiMAX and wireline services over an extended reach passive optical access network

Alexey V. Osadchiy *, Kamau Prince, Idelfonso Tafur Monroy

DTU Fotonik, Technical University of Denmark, Oersteds Plads 343, DTU Campus, 2800 Kgs. Lyngby, Denmark

ARTICLE INFO

Article history:
Received 28 September 2009
Revised 9 February 2010
Available online 3 April 2010

Keywords:
Radio-over-fiber
WiMAX
Long-reach
Access
Convergence

ABSTRACT

In this paper we present long-reach fiber access links supporting transmission of Worldwide Interoperability for Microwave Access (WiMAX) compliant signals. We present bi-directional full-duplex transmission of 256-state quadrature amplitude modulation (256-QAM) modulated WiMAX-compliant signals on a 2.4-GHz RF carrier over an 80-km long-reach access link at 100 Mb/s (down) and 64 Mb/s (up). Transmission of 64-QAM and 256-QAM-modulated signals on a 5.8-GHz RF carrier over a 118.8-km access link converged with four baseband differential quadrature phase shift keying (DQPSK) modulated wireline channels, along with ultra-wide band (UWB) and phase shift keying (PSK) radio-over-fiber (RoF) wireless signals over a deployed optical fiber link is also presented.

1. Introduction

Network operators are investigating novel methods of extending the reach of optical access networks to reduce the unit delivery cost of data bandwidth to the end-user. Significant cost reduction is expected to come from eliminating intermediate local exchange nodes within the access network and consolidating access infrastructure across existing last-mile network segments into enhanced-range next-generation systems that interface directly with high-bandwidth metro or core network nodes. In such scenarios, the access network is expected to span up to 100 km, a significant increase over the standard 20 km reach of contemporary networks [1,2]. Additionally, the demand for bandwidth from the individual access network user is being stimulated by novel bandwidth-intensive network services like high-definition (HD) video-on-demand, peer-to-peer file sharing and remote access services. Such trends have also driven increases in the data rates supported by wireless data access networks as well, with emerging wireless access technologies, such as Worldwide Interoperability for Microwave access (WiMAX) [3–5] and 3GPP long-term evolution (LTE) [6], offering higher data access speeds and supporting more users. There are several reasons for this interest: wireless access networks solutions allow client mobility, so that interactions to occur in real-time allowing faster information flow across organizations performed on the move, and the precious time is being utilized more efficiently; at the same time, wireless solutions provide on-demand availability of various entertainment services.

Worldwide Interoperability for Microwave Access (WiMAX) [7] is becoming a widespread wireless access technology with standards for fixed as well as mobile coverage. However, the emergence of high-bitrate wireless access standards creates a new challenge – high-bandwidth signals generated by and destined to the customer premises equipment (CPE), has to be delivered from and to the central office (CO). One way of tackling the problem is transport of WiMAX signals over the already-deployed or newly-installed optical fiber infrastructure. Such an approach, generally known as radio-over-fiber (RoF), allows for low-loss distribution of wireless services and simplifies the structure of the base stations, as all complex signal generation and detection-related equipment is consolidated at the CO, and the base station only performs optical-to-radio and radio-to-optical signal conversion. Another advantage provided by RoF transmission is the prospect of transport of both wireless and wireline signals over the same fiber infrastructure, which reduces installation costs for both services and simplifies coverage of the areas with established fiber infrastructure with the wireless services.

In this article, we report the results obtained during a series of experiments with RoF WiMAX transmission, including bi-directional transmission of WiMAX-compliant signals over an 80-km long-reach PON with air transmission between a CPE and a wireless subscriber unit (WSU). Moreover to show the feasibility of convergence over an extended reach access link, we report on a WDM transmission of WiMAX-compliant signals over 78 km of deployed fiber simultaneously with the transmission of four

* Corresponding author. Address: DTU Fotonik, Technical University of Denmark, Oersteds Plads 343, DTU campus, Office 214, 2800 Kgs. Lyngby, Denmark.
E-mail address: avos@fotonik.dtu.dk (A.V. Osadchiy).

1068-5200/$ - see front matter © 2010 Elsevier Inc. All rights reserved.
doi:10.1016/j.yofte.2010.02.009

10.7 Gbaud DQPSK channels, two 1 Gb/s PSK RoF channels and an ultra-wide band (UWB) over fiber channel.

2. Wireline and wireless converged signal transport scenario

High-bandwidth wireless access technologies are gaining recognition from the end-users as convenient and reliable means of access connection, which causes an increase in the amount of traffic generated by wireless sources. This puts up a challenge – an effective solution for transport and distribution of such traffic is required to interconnect the ever-increasing amount of wireless base stations. Current point-to-multipoint wireless access systems have carrier frequencies ranging from 900 MHz (GSM/UMTS networks) to 5 GHz (WiFi and WiMAX), although there are standards being developed for communications with carrier frequencies above 20 GHz [8]. High carrier frequencies enable high capacities but at the same time put significant limitations on the maximum cell size, which is the coverage area serviced by each wireless access point. For this reason, high-frequency systems' cells are sometimes referred to as picocells. Small cell sizes enable efficient frequency reuse, as the signals from the next cells are greatly attenuated, especially indoors, which removes the need for frequency interleaving [9,10]. At the same time due to small cell size, more base stations are required to ensure adequate coverage. This makes RoF technologies very appealing, since the operation costs of a system counting myriads of picocells can be greatly reduced if the complex and power-hungry part of each base station – the signal generation and detection equipment – can be placed at the CO.

Low attenuation of the optical fiber makes such an equipment placement even more beneficent – if the maximal reach of optical links measures tens to hundreds of kilometers, single CO can potentially host equipment providing coverage for an area measuring thousands of square kilometers. Another argument in favor of long-reach access links is the absence of intermediate nodes between the access-level and the metro-level networks, as the CO can serve as both an access and a metro node, including the bridging between the two segments of network hierarchy.

However, installation of fiber links exclusively to support wireless access networks might be rather costly, so convergence of wireline and wireless access networks within the existing or planned fiber infrastructure is very important: such a convergence reduces both systems' installation costs, since the same infrastructure installation costs are shared between two different access systems. Another interesting prospect of such a convergence is possibility to create access surroundings for the user – wherever the user goes, she will have an ability to use her access network, as long as current location is covered by either the wireless or the wireline component of the access system.

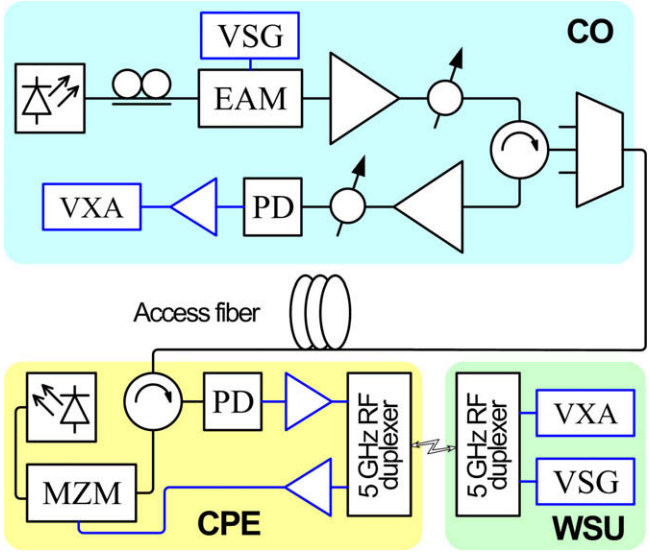

Fig. 1. Long-reach PON link with bi-directional WiMAX transmission. CO – central office; CPE – customer premises equipment; WSU – wireless subscriber unit; VSG – vector signal generator; EAM – electro-absorption modulator; VXA – signal analyzer; MZM – Mach–Zehnder Modulator; and PD – photodiode.

We propose a long-reach access system that implements these design objectives in Fig. 1: a long-reach access link connects the central office (CO) with the customer premises equipment (CPE), which serves as the interface between optical and wireless transmission segments of the communication path between the CO and each wireless subscriber unit (WSU) within each coverage cell. In this work we also demonstrate simultaneous transport of wireless and wireline signals over a common long-reach access link, however, we focus on the performance of signal transport of WiMaX signals. We define the downlink (DL) data path as originating at the CO and terminating at the WSU, and the uplink (UL) data path from the WSU to the CO; and present a series of measurements for WiMaX-compliant signals with a 5.8-GHz RF carrier. The operating frequency was selected for compliance with the European unlicensed 5-GHz communications band.

3. Experimental setup

3.1. Extended reach PON link with bi-directional WiMAX signal transport

The experiment setup is presented in Fig. 1. A 40 GHz electro-absorption modulator (EAM) was used at the CO to modulate the light from a continuous-wave (CW) optical source; the downlink transmit power level was adjusted by an amplifier and a variable optical attenuator (VOA) to limit it to a value that does not introduce non-linear effects. A pre-amplified 10 GHz receiver was used at the CO. The CPE was built with the use of uncooled, commercially-available equipment: 10 GHz photodiode, Mach–Zehnder modulator (MZM) and RF bandpass amplifiers and duplexer. The received signal power at the CPE photodiode was measured to be −5 dBm. Both intensity modulators (EAM and MZM) used in the experiment were biased for operation in the linear regime; input optical power levels into the modulators were +8 dBm and +7 dBm, respectively. The system performance was evaluated for various RF input power levels. The measurements were taken with both transmitters simultaneously active. Results were taken with both transmitters using the same electrical modulation format.

IEEE 802.kd WiMAX-compliant [3,4,11] signals in the unlicensed 2.4 GHz band were obtained from independent Agilent E4438C signal generators operating at unequal carrier frequencies, and signal quality after transmission was assessed using Agilent N9020A-MXA signal analyzers. Signal quality was assessed for bi-directional transmission conditions and evaluated in terms of RMS error-vector magnitude (EVM); uplink (UL) and downlink (DL) signal paths were simultaneously observed.

3.2. Converged transport of WiMAX over a long-reach link

The experiment layout of the converged signal transport is presented in Fig. 2. Field-deployed standard single mode fiber connecting the campus of the Technical University of Denmark (DTU) and facilities located in the suburb of Taastrup was used in this experiment. The total link loss was measured at 25 dB. The eight channels were wavelength-division multiplexed at a 200-GHz channel separation, occupying ITU-compliant wavelengths, denoted λ_1 = 1549.3 nm through λ_8 = 1560.0 nm: four wavelengths (λ_5–λ_8) were used for the 21.4 Gb/s NRZ-DQPSK channels; two (λ_2 and λ_4) for the 250 Mb/s RoF channels with an RF carrier frequency

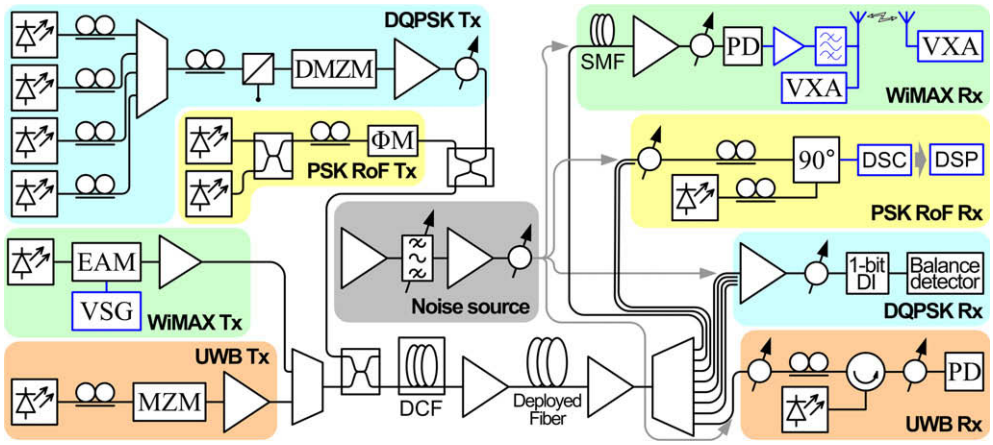

Fig. 2. Converged WiMAX transport experiment setup. (D)MZM – (double) Mach–Zehnder modulator; EAM – electro-absorption modulator; VSG – vector signal generator; VXA – signal analyzer; 1-bit DI – one-bit delay interferometer; DSC – digital sampling scope; and DSP – software-based digital signal processing.

of 5 GHz; a 3.125-Gb/s impulse ultra-wide band (UWB) channel and a 100-Mb/s 256-QAM WiMAX-over-fiber channel with an RF carrier frequency of 2.4 GHz – a single wavelength used for each (λ_3 and λ_1, respectively).

Launch power into the deployed fiber was set to 0 dBm for each of the eight channels. Dispersion compensating fiber (DCF) of length 13-km was used at the transmitter, to match the dispersion of the deployed fiber; the DCF also ensured signal decorrelation at the input of the transmission fiber. An erbium doped fiber amplifier (EDFA) pre-amplifier was used to compensate for the transmission losses before wavelength demultiplexing in an arrayed waveguide grating (AWG). The channel spacing in the system was dictated by the equipment availability, and we expect the system to function properly with a narrower channel spacing [12].

An EAM fed by an optical carrier at λ_2 was modulated with a 256-QAM RF signal, centered at 5.8 GHz, obtained from an Agilent E4438C vector signal generator (VSG); a boost EDFA and VOA controlled the launch power. A pre-amplified receiver was implemented with a 30 dB gain EDFA, optical bandpass filter (BPF) and a 10 GHz PIN photodiode. The electrical signal obtained was amplified by 35 dB, filtered by 25 MHz RF duplexers for 5 GHz unlicensed ISM band operation and radiated by 12 dBi omni-directional 5 GHz antenna. The wireless signal was detected with an identical antenna at 40 cm separation, amplified and assessed with an Agilent 9020 MXA vector signal analyzer (VXA) with the 89600 VSA signal analyzer software. We report error-vector magnitude (EVM) sensitivity to RF source power at both ends of the wireless link for the single active wavelength, and for all WDM transmitters active. We additionally assessed the performance with extra 40 km of uncompensated SMF, after DF and preamp and the post-detection eye diagram.

4. Results

4.1. Extended reach PON link with bi-directional WiMAX signal transport

We assessed the performance with 35-km NZDSF access fiber (Fig. 1): for this case, the OSNR at the CO for the UL was sufficient for reliable measurements to be taken with a received power level of −18 dBm. We report on an un-amplified UL, and bypassed array waveguide (AWG) at the CO. We used DL wavelength (λ_{DL}) of 1549.5 nm and UL at (λ_{UL}) of 1550.6 nm: we assessed full-duplex transmission of 64-QAM at 8 Mb/s (1 Mbaud) for UL and DL and report the results in Fig. 3: the 3.1% IEEE 802.16d EVM threshold for 64-QAM is shown. These results indicate at a bitrate of 6 Mb/s (1 Mbaud), the WiMAX EVM threshold for 4-QAM is satisfied with launch RF power in the range $[-18, 4]$ dBm and $[-31, -9]$ dBm for the DL and UL, respectively. We observed a difference of less than 0.2% between the best-case RMS EVM for UL and DL. We also present results for full-duplex 256-QAM transmission: at 8 Mb/s (1 Mbaud), DL performance closely followed that observed for the 64-QAM transmission at 6 Mb/s. At 64 Mb/s, the 256-QAM UL yielded better than 3.1% EVM for launch RF power values within the range $[-19, -11]$ dBm.

We extended our fiber link in Fig. 1 to 80 km NZDSF: in this case, system losses resulted in insufficient received optical power level at the CO. We thus implemented a pre-amplified CO receiver with −5 dBm into the lightwave converter and inserted AWG to improve OSNR. We assessed full-duplex operation using a single optical wavelength ($\lambda_{DL} = \lambda_{UL} = 1549.5$ nm), and present the results in Fig. 3. With full-duplex 256-QAM transmission at 64 Mb/s (8 Mbaud), the RMS EVM was below 3.1% for launch power in the range $[-11, 1]$ dBm and $[-25, -23]$ dBm for the DL and UL, respectively. When the DL bitrate was increased to 100 Mb/s, this EVM threshold was satisfied with launch power within the range $[-7, 0]$ dBm.

4.2. Converged transport of WiMAX over a long-reach link

The 256-QAM signals at 12 Mbaud were successfully transmitted over the deployed fiber and an additional 40 km of distribution SMF with no further optical amplification, Fig. 2. The assessment of the error-vector magnitude (EVM) at the remote transmit antenna showed a value below 3% – within the standard specifications – as shown in Fig. 4.

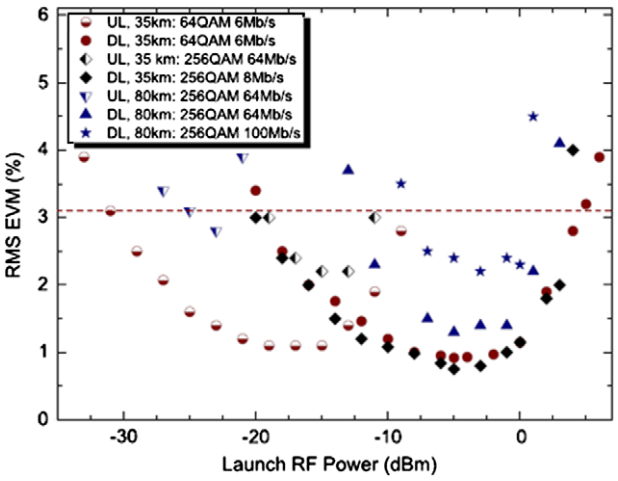

Fig. 3. RMS EVM obtained for 64-QAM and 256-QAM WiMAX-compliant signals.

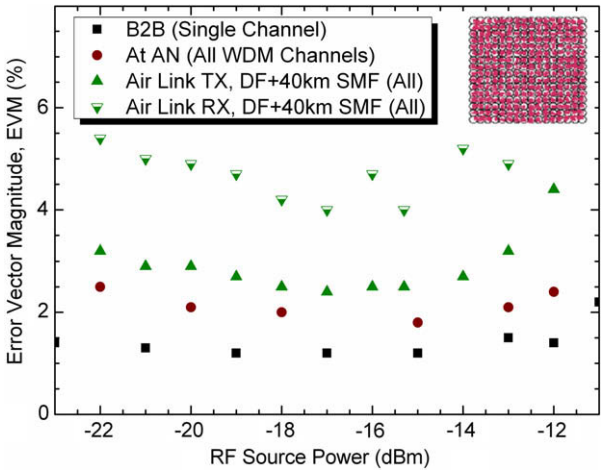

Fig. 4. RMS EVM obtained for the 100 Mb/s 256-QAM channel.

In this article, we focus on the performance of the WiMaX channel and will review briefly the performance of the other channels' propagating simultaneously over the same deployed fiber. The co-existent channels were successfully received at their respective receivers. For the DQPSK channels, a BER of 10^{-9} was observed for OSNRs of between 22 dB (λ_5) and 23.3 dB (λ_8), with transmission penalties not exceeding 0.3 dB. A BER of 10^{-3} was achieved for the coherent-detected RoF PSK channels at OSNRs of approximately 9.6 and 11 dB, and transmission penalties of 0.5 and 2 dB, for channels 2 and 4, respectively. The UWB signal was recorded in form of samples, and then digitally processed offline: a BER of 10^{-3} was obtained for 13 dB OSNR, and transmission penalty comprised only 0.5 dB.

5. Conclusion

We have demonstrated a bi-directional WiMAX-over-fiber signal transmission scheme. The presented scheme supports IEEE 802.16d-compliant signal transmission on a 2.4 GHz carrier: for 256-QAM signals, full-duplex operation at a bit rate of 100 Mb/s in downlink direction and 64 Mb/s in the uplink direction was demonstrated in an 80-km access fiber link. No RF signal processing was performed at CPE, and the use of commercially-available optical transceivers facilitates the implementation of such links.

We also demonstrated successful converged transport of 100 Mb/s WiMAX-compliant signals with a 5.8 GHz RF carrier over a 78.8-km deployed SMF and a 40-km distribution SMF: in total the WiMAX signal stayed within 5% RMS EVM after 118.8-km fiber link transmission and air transmission. Co-existing channels transmitted together with the WiMAX-over-fiber channel over the deployed fiber were also received successfully.

The presented demonstrations of WiMAX signals transport over fiber show prospects for efficient converged transport of high-bandwidth wireless and wireline signals over long-reach links. This enables a new type of access networks to be created or built over the existing fiber-based ones – hybrid wireless-fixed access networks with significantly greater coverage then the currently deployed ones.

Acknowledgments

This work was partly supported by the European Community's Seventh Framework Programme (FP7/2007-2013) within the project ICT ALPHA under Grant agreement 212 352 and ICT GigaWAM under Grant agreement 224 409. We would like to acknowledge Agilent Technologies Denmark for providing access to the WiMAX signal analysis equipment used in the experiment.

References

[1] R.P. Davey, D.B. Grossman, M. Rasztovits-Wiech, D.B. Payne, D. Nesset, A.E. Kelly, A. Rafel, S. Appathurai, Yang Sheng-Hui, Long-reach passive optical networks, J. Lightw. Technol. 27 (3) (2009) 273–291.
[2] C. Lin, Broadband Optical Access Networks and Fiber-to-the-Home, John Wiley & Sons, Inc., 2006.
[3] S.J. Vaughan-Nichols, Achieving wireless broadband with WiMAX, Computer 37 (6) (2004) 10–13.
[4] IEEE Std. 802.16-2004, IEEE LAN/MAN Standards Committee Std., October 2004.
[5] IEEE Std. 802.16e-2005, IEEE LAN/MAN Standards Committee Std., 2006.
[6] D. Mcqueen, The momentum behind LTE adoption [3GPP LTE], IEEE Commun. Mag. 47 (2009) 44–45.
[7] K.H. Teo, Z. Tao, J. Zhang, The mobile broadband WiMAX standard [Standards in a Nutshell], IEEE Signal Proc. Mag. 24 (5) (2007) 144–148.
[8] A.M.J. Koonen, M.G. Larrode, A. Ng'oma, K. Wang, H. Yang, Y. Zheng, E. Tangdiongga, Perspectives of radio over fiber technologies, in: OFC/NFOEC Proceedings, 2008.
[9] C. Park, T.S. Rappaport, Short-range wireless communications for next-generation networks: UWB, 60 GHz millimeter-wave WPAN, and ZigBee, IEEE Wireless Commun. 14 (4) (2007) 70–78.
[10] M. Sauer, A. Kobyakov, J. George, Radio over fiber for picocellular network architectures, J. Lightw. Technol. 25 (11) (2007) 3301–3320.
[11] W. Konhauser, Broadband wireless access solutions – progressive challenges and potential value of next generation mobile networks, Wireless Pers. Commun. 37 (3–4) (2006) 243–259.
[12] D. Zibar, X. Yu, C. Peucheret, P. Jeppesen, I. Tafur Monroy, Digital coherent receiver for phase-modulated radio-over-fiber optical links, IEEE Photon. Technol. Lett. 21 (3) (2009) 155–157.

Alexey V. Osadchiy received the M.Sc. degree in fiber optical communications from the Bonch-Bruevich State University of Communications, St. Petersburg, Russia, in 2006. He is currently pursuing a Ph.D. in optical communications engineering at DTU Fotonik, Technical University of Denmark, with main focus on access networks and interaction between access networks and higher level of network hierarchy networks, namely, metro-access interfacing.

Kamau Prince received the B.Sc. degree (first class honours) in electrical engineering from the University of the West Indies, St. Augustine, Trinidad, in 1999; a Graduate Diploma in telecommunications engineering and M.Eng.Sci. degree from the University of Melbourne, Victoria, Australia, in 2003 and 2006, respectively. He is currently pursuing a Ph.D. in optical communications engineering at DTU Fotonik, Technical University of Denmark.

Idelfonso Tafur Monroy received the M.Sc. degree in multichannel telecommunications from the Bonch-Bruevitch Institute of Communications, St. Petersburg, Russia, in 1992, the Technology Licenciate degree in telecommunications theory from the Royal Institute of Technology, Stockholm, Sweden, and the Ph.D. degree from the Electrical Engineering Department, Eindhoven University of Technology, The Netherlands, in 1999. He is currently Head of the metro-access and short range communications group of the Department of Photonics Engineering, Technical University of Denmark. He was an Assistant Professor until 2006 at the Eindhoven University of Technology. Currently, he is an Associate Professor at the Technical University of Denmark. He has participated in several European research projects, including the ACTS, FP6, and FP7 frameworks (APEX, STOLAS, LSAGNE, MUFINS).

At the moment, he is in involved the ICT European projects Gi-GaWaM, ALPHA, BONE, and EURO-FOS. His research interests are in hybrid optical–wireless communication systems, coherent detection technologies and digital signal processing receivers for baseband and radio-over-fiber links, optical switching, nanophotonic technologies, and systems for integrated metro and access networks, short range optical links, and communication theory.

Paper H

K. Prince, M. Ma, T. B. Gibbon, C. Neumeyr, E. Rönneberg, M. Ortsiefer and I. Tafur Monroy, "10.7-Gb/s passive optical network uplink with uncooled, free-running, directly-modulated 1550-nm VCSEL and inverse dispersion fiber." In preparation for submission to Journal of Optical Networking, April 2010.

10.7-Gb/s Passive Optical Network uplink with Uncooled, Free-running, Directly-Modulated 1550-nm VCSEL and Inverse Dispersion Fiber.

Kamau Prince, Ming Ma, Timothy B. Gibbon, Christian Neumeyr,
Enno Rönneberg, Markus Ortsiefer and I. Tafur Monroy,

***Abstract*—We present a cooler-less, free-running 1550 nm vertical cavity surface emitting laser (VCSEL) directly modulated at 10.7 Gb/s. Optical transmission of the optical output of this device has produced error-free transmission through 40 km of uncompensated singlemode optical fiber. Inverse-dispersion fiber was utilized in the achievement of 99.7 km optical access uplink with 61.7 km SMF and 38 km inverse dispersion fiber, achieving error-free transmission with 24 dB loss margin. These results indicate the feasibility of implementing cooler-less long-wavelength VCSEL devices in a long-reach PON.**

***Index Terms*—passive optical network (PON); vertical cavity surface emitting laser (VCSEL).**

I. Introduction

SUSTAINED increase in demand for broadband data services has motivated the expansion of modern data communications networks [1]. Additionally, bandwidth limitations of traditional copper-based or wireless data transmission schemes have encouraged the deployment of broadband optical transmission technologies in the access networking environment. Sustainable deployment of optical access networks requires reliable, inexpensive and energy-efficient broadband optical sources [3,4]; this has encouraged the development of low-cost laser sources for directly-modulated optical links. Vertical cavity surface emitting laser (VCSEL) technology is a potential candidate for realizing low-cost, broadband signaling sources. Un-cooled VCSEL units have been demonstrated supporting data rates of 10 Gb/s [5-7] and 20 Gb/s[8]; cooled VCSEL sources operating at 38 Gb/s [2] have also been presented. Injection-locking has also been used to extend the transmission range achieved with directly-modulated VCSEL devices VCSEL sources have been operated at 10 Gb/s and demonstrated at 40 km [9]; longer-range transmission has also been reported [7, 10] with more sophisticated control of the chirp of the locked laser source.

This paper reports on the demonstration of a cooler-less 1550 nm VCSEL directly-modulated at 10.7 Gb/s. The output of this device was successfully transmitted over an un-amplified 99.7 km dispersion-matched transmission link in which a field-deployable inverse dispersion fiber (IDF), having an inverse-dispersion profile in the 1550 nm region, was used to compensate for the dispersion introduced by G.652 standard single-mode fiber (SMF). We obtained error-free transmission of this data signal, with a bit error rate (BER) below 10^{-9}. Data transmission was emulated using pseudorandom binary sequence (PRBS) of varying lengths, to assess the robustness of the optical signal obtained to pattern-length dependencies. For uncompensated transmission over 35 km and 40 km, we obtained error-free results with the shortest PRBS, at received power levels of approximately -19 dBm; this is similar to the sensitivity levels reported by injection-locked systems operating at 10 Gb/s [9]. Error-free transmission was also achieved over the dispersion-matched 99.7 km uplink when a PRBS of length 2^{31}-1 was used. Our results show the feasibility of long-wavelength VCSELS in the deployment of enhanced-range passive optical network (PON) systems, and also highlight the applicability of IDF in extending the range of broadband optical access networks.

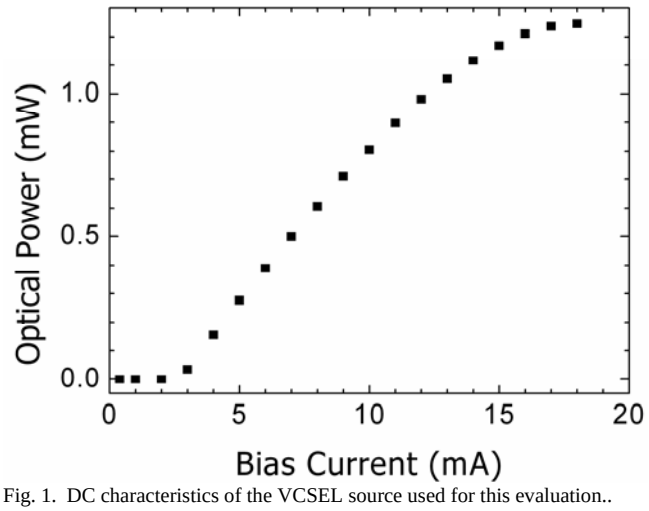

Fig. 1. DC characteristics of the VCSEL source used for this evaluation..

Manuscript received July 9, 2010.

K. Prince, M. Ma, T.B. Gibbon and I. Tafur Monroy are with DTU Fotonik research institute, Technical University of Denmark, Kgs. Lyngby 2880 Denmark. (kpri@fotonik.dtu.dk)

C. Neumeyr, E. Rönneberg and M. Ortsiefer are with Vertilas GmbH, Garching D-85748, Germany.

Digital Object Identifier:

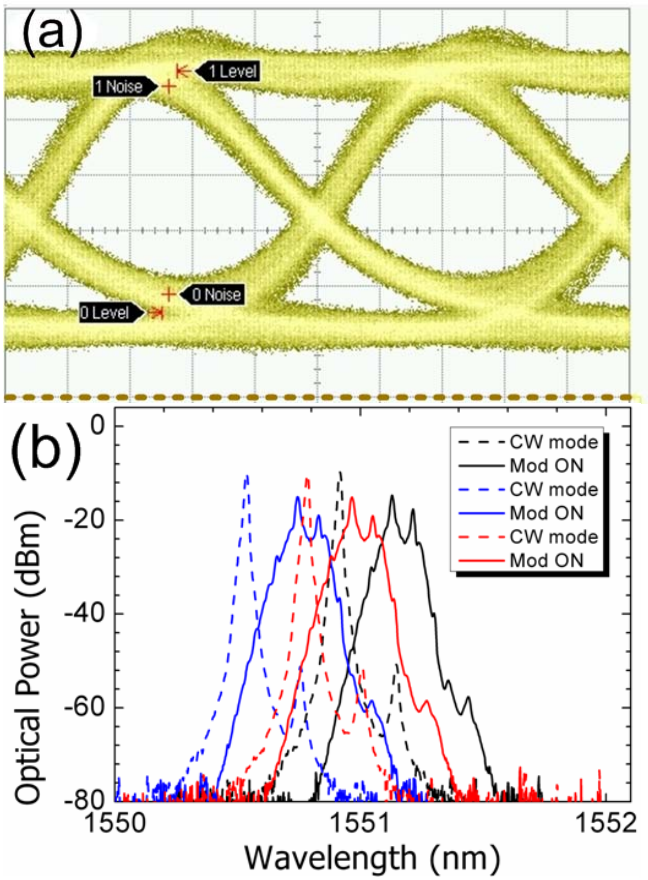

Fig. 2. VCSEL response when modulated with 10.7Gb/s NRZ-OOK modulated signal:(a, top) eye diagram (Scale v:50 µW/div, h:20 ps/div. Dotted line indicates zero level;) and (b, lower) optical spectrum drifts observed during experimental evaluation (measurement resolution: 0.01 nm).

The remainder of this paper is structured as follows: we present the characterization of the VCSEL in Section II, and present the description of the PON uplink evaluation in Section III. Significant system results are presented in Section IV; concluding remarks are presented in Section V.

II. VCSEL Characterization

We assessed the DC characteristics of the VCSEL source and obtained the power vs. bias current response presented in Fig. 1. The maximum rated bias current for this device was specified at 19 mA, we observed a lasing threshold current of 4 mA. When a bias current of 18 mA was applied, the VCSEL provided +1 dBm average optical output power.

When we applied a 10.7 Gb/s NRZ-OOK modulating signal to this device, we observed that the optical output obtained had an optical extinction ratio of 5.85 dB and an optical signal-to-noise ratio (OSNR) of 7.43 dB; a typical eye diagram observation is presented in Fig. 2(a).

During the course of the experiment, the continuous-wave (CW) lasing wavelength of the un-cooled device varied between 1550.5 nm and 1550.9 nm; when modulation was applied, the peak wavelength increased by approximately 0.3 nm and was observed to vary between 1550.8 nm and 1560.1 nm over the course of the experiment. Figure 2(b) presents typical optical spectra of the laser output observed over the course of the experiment; the blue and black traces represent extreme values observed in the excursion of the laser output wavelength, red trace indicates median observations. Dashed traces indicate CW mode operation and the solid lines reflect laser output when modulation was activated (Mod ON).

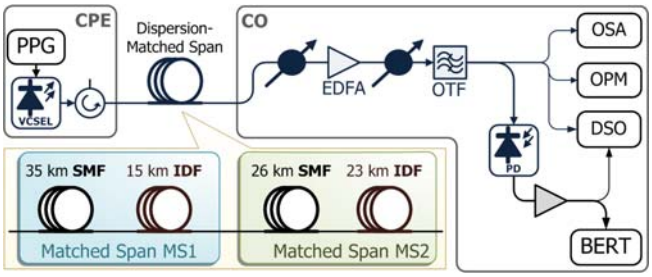

Fig. 3. System layout: free-running cooler-less VCSEL within customer premises equipment (CPE) transmits at 10.7 Gbps to receiver at central office (CO) via dispersion-matched spans (MS1 and MS2) of transmission fiber. BERT, bit error-rate test; DSO, digital storage oscilloscope; OSA, optical spectrum analyzer; OTF, tunable optical bandpass filter (0.9 nm FWHM); PPG, pulse pattern generator.

III. Passive Optical Network (PON) Uplink

We emulated the uplink of an extended-reach passive optical network using the setup shown in Fig. 3. The customer premises equipment (CPE) consisted of a free-running VCSEL that was directly modulated by a NRZ-OOK data signal from a pulse pattern generator (PPG). The VCSEL used in this experiment had a threshold current of 3 mA, a maximum rated bias current of 19mA, and operated without temperature stabilization controls. A circulator was used to prevent back-scattered optical energy from entering the laser cavity: in practical systems, this circulator would facilitate bidirectional communication over a single fiber.

Two types of transmission fiber were implemented in dispersion-matched sets of SMF and IDF. The SMF used in this evaluation had a specified unit dispersion of 17 ps/nm.km at 1550 nm wavelength. The first matched span, MS1, comprised of 35.3 km SMF and 14.8 km IDF; the total dispersion (D) of MS1 was -0.59 ps/nm (at 1550 nm wavelength). The second matched span, MS2, consisted of 26.4 km SMF and 23.3 km IDF; D was -1.7 ps/nm (at 1550 nm). We implemented a pre-amplified receiver at the central office (CO) using an EDFA with 35 dB gain and a noise figure of 4.2 dB. An optical tunable filter (OTF) with 0.9 nm full width at half-maximum (FWHM) was used to remove unwanted spontaneous emission noise and improve the OSNR at the 10 GHz PIN photodetector (PD); the OTF was tuned to allow maximum transmitted signal energy to the PD. The average optical power into the PD was maintained at -9 dBm, which was well within its linear response range.

IV. Key Results

We assessed the optical signal obtained at key points within the system, and utilized PRBS of varying length to

assess system sensitivity to pattern-length dependent effects. Observations of the propagating signal were made after 35 km SMF, 40 km SMF and after dispersion-compensated transmission over 50 km (MS1) and 99.7 km (MS1 and MS2) of optical fiber. The eye diagrams obtained were not observed to vary significantly with change in the PRBS used. Samples

TABLE I
EXTINCTION RATIO AND OSNR AT KEY POINTS ALONG THE PON UPLINK

Observation Point	Extinction Ratio (dB)	OSNR (dB)
CPE output	5.88	7.45
35 km SMF	4.73	2.80
40 km SMF	4.61	2.70
MS1 (50 km total)	5.79	5.07
MS1 + MS2 (99.7 km total)	6.01	4.71

OSNR was assessed using signal eye observations on DSO.

obtained for sequence length 2^7-1 bits are presented in Fig. 4; all samples were obtained after receiver pre-amplification as shown in Fig. 3. Table 1 presents the optical extinction ratio and optical signal to noise ratio observations at these key points within the transmission uplink.

A clear open eye was observed at the ONU output, as shown in Fig. 2(a). We observed the degradation in OSNR associated with transmission over uncompensated SMF, as shown in Fig. 4(a) and Fig 4(b) for 35 km and 40 km lengths, respectively. Although clear distinction can be made between low and high levels in the diagram, the eye of the propagating signal waveform was closed by ringing effects which introduced vertical transitions close to the center of the bit period; these effects are a result of dispersion-induced inter-symbol interference. Signals observations at the outputs of the 50 km (MS1) and 99.7 km (cascaded MS1 and MS2) lengths of dispersion-matched fiber indicate good signal recovery at the receiver; clear open eyes and good OSNR were observed. Improved extinction ratio was observed after the 99.7 km of cascaded fiber: the net negative chromatic dispersion of the link improves the directly-modulated optical signal from the laser, as previously reported in [9]. The OSNR was however degraded by 3.38 dB by transmission along MS1; and a further 0.36 dB along transmission over the second matched span (MS2). These results indicate feasibility of transmission over the cascaded 99.7 km matched span, we assessed BER sensitivity to received signal power.

We also assessed data transmission through this uplink using a bit error rate sensitivity assessment; again, PRBS of varying lengths were used to evaluate pattern length-dependent system response. The results of the BER sensitivity assessment are presented in Fig. 5. We used solid black symbols to represent the results obtained at the CPE output, and distinguish between PRBS of various lengths by using the same geometric shape for each PRBS length to easily differentiate the results for PRBS lengths of 2^7-1 (circle), 2^{15}-1 (square), 2^{23}-1 (upward pointing triangle) and 2^{31}-1 bits (downward pointing triangle). We used unfilled (blue) symbols for results after 35 km SMF, and (blue) symbols with crosses for results after 40 km SMF. Red (top half-filled) symbols indicate results at the output of MS1, and green (left half-filled) symbols indicate results after 99.7 km cascaded MS1 and MS2.

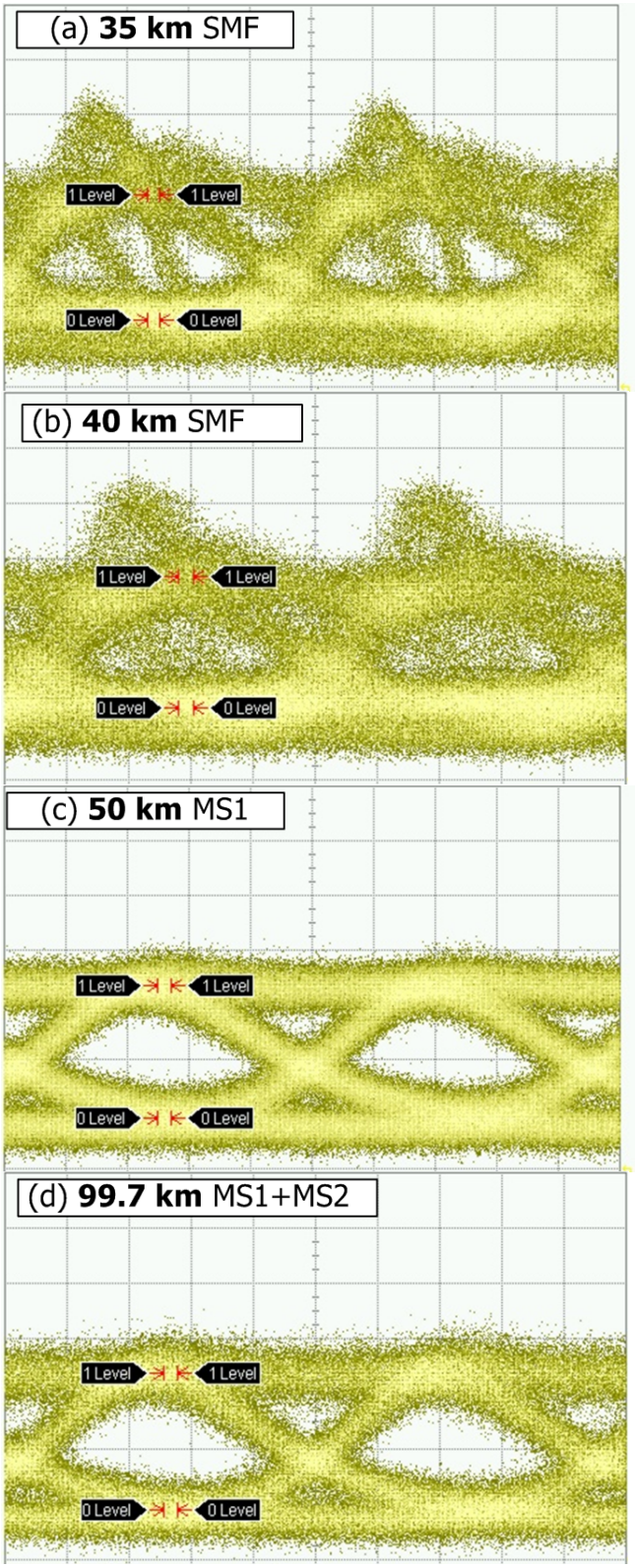

Fig. 4. Eye observations for 10.7 Gb/s NRZ-OOK waveform, at key points: (a) 35 km SMF, (b) 40 km SMF, (c) 50 km of MS1, and (d) 99.7 km of MS1 + MS2. Dotted line indicates zero level. Scale V: 50 μW/div, H: 20 ps/div.

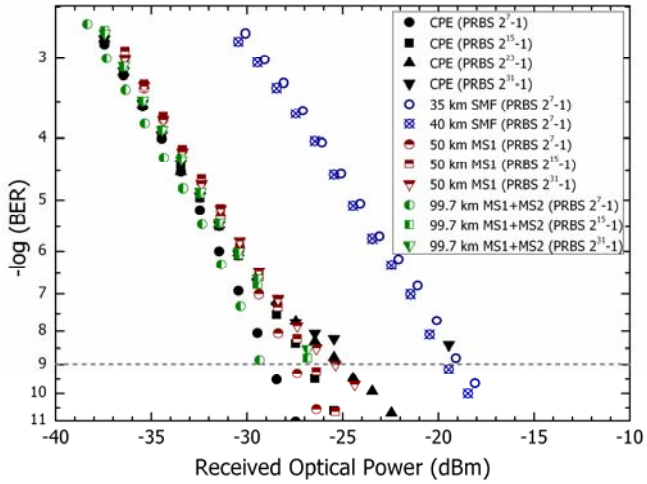

Fig. 5. BER sensitivity for 10.7 Gb/s signal at key points throughout the transmission link. PRBS of various lengths (2^7-1,2^{15}-1, 2^{31}-1) were used to evaluate system. (Dotted line indicates error-free threshold at BER=10^{-9})

For the signal obtained directly from the CPE, error-free results were obtained with -29 dBm of received optical power, when a PRBS of length 2^7-1 bits was used. Approximately 2 dB of power penalty was observed with a PRBS of length 2^{15}-1 bits, and 4 dB of penalty was observed with a PRBS of length 2^{23}-1 bits. A BER floor close to $5x10^{-8}$ was observed with PRBS length 2^{31}-1 bits: this indicates that the transmitter is susceptible to pattern-length dependent effects, this is probably due to the presence of long runs of successive ones and zeros in the modulating signal waveform. These cumulatively vary the bias point of the device around the desired value, thus distorting the optical properties of the laser output waveform.

The inclusion of IDF into the link was observed to improve system performance, with increased receiver sensitivity over the uncompensated transmission. For the uncompensated transmission over 35 km and 40 km, we obtained error-free results with only the shortest PRBS, at received power levels of approximately -19 dBm. These results compare favorably with the sensitivity levels reported by the injection locked results [9], which is encouraging as our system did not require any injection locking. However, when the IDF was used, we were able to recover error-free transmissions for all PRBS used. The net negative dispersion of the matched transmission spans was observed to improve transmission performance beyond that obtained at the transmitter output; this result does not conflict with previously-reported results for transmission of directly-modulated laser signals over links with net negative chromatic dispersion [11].

V. Conclusion

We have presented results of the characterization of a novel VCSEL device, that can be directly-modulated at 10.7 Gb/s and the output signal can be transmitted error-free over a 40 km of uncompensated SMF with a receiver sensitivity of -29 dBm when a PRBS of length 2^7-1 was used. Field-deployable IDF fiber was used to implement an extended-range 99.7 km PON uplink; error-free transmission was also achieved over this link. Less than 3 dB penalty was observed when a PRBS of length 2^{31}-1 bits was used over the same length transmission span, which is consistent with reported assessments of optical transmission over negatively dispersive transmission media.

Acknowledgment

The research leading to these results received funding from the European Commission Seventh Framework Program FP7-ICT-2007-2 within the ICT project GigaWaM. K. Prince acknowledges an International PhD scholarship from the Danish Ministry for Science, Technology and Innovation.

References

[1] S. Cherry, "Edholm's law of bandwidth," *IEEE Spectr*. vol. 41, pp. 58-60, July 2004.

[2] D. Bimberg, "Ultrafast VCELs for datacom," *IEEE Photonics J*. vol. 2, pp. 273-275, April 2010.

[3] E. Kapon and A. Sirbu, "Long-wavelength VCSELs: Power-efficient answer," *Nature Photon*., vol. 3, pp 27-29, Jan. 2009.

[4] F. Koyama, "Recent Advances of VCSEL Photonics," *J. Lightw. Technol*., vol. 24, pp. 4502-4513, Dec. 2006.

[5] J. Jewell, L. Graham, M. Crom, K. Maranowski, J. Smith and T. Fanning, "1310nm VCSELs in 1-10Gb/s commercial applications," *Proc SPIE*, vol. 6132, no. 613204-1, Feb. 2006.

[6] X. Cheng, Y. Wen, Z. Xu, X. Shao, Y. Wang and Y. Yeo, "10-Gb/s WDM-PON transmission using uncooled, directly modulated free-running 1.55μm VCSELs," in *Proc 34th European Conf. on Optical Comm*,. Brussels, Belgium Sep. 2008.

[7] D. Parekh, B. Zhang, X. Zhao, Y. Yue, W. Hofmann, M Amann, A. Willner and C. Chang-Hasnain, "90-km Single-Mode Fiber Transmission of 10-Gbs Multimode VCSELs under Optical Injection Locking" in *Proc. Optical Fiber Conference (OFC).* San Diego, CA. March 2009. Paper OTuK7.

[8] L. Xu, W. Hofmann, H. Tsang, R. Penty, I. White and M. Amann, "1.55μm VCSEL Transmission Performance up to 20 Gb/s for Access Networks," in *Proc. Opto-Electronics and Communications Conference, (OECC).* Hong Kong, 2009. Paper ThPD1.

[9] P. Boffi, A. Boletti, A. Gatto and M. Martinell, "VCSEL to VCSEL Injection Locking for Uncompensated 40-km Transmission at 10 Gb/s," in *Proc. OFC*. March 2009. Paper JThA32.

[10] B. Zhang, X. Zhao, L. Christen, D. Parekh, W. Hofmann, M. Wu, M. Amann, C. Chang-Hasnain, and A. Willner, "Adjustable Chirp Injection-Locked 1.55-μm VCSELs for Enhanced Chromatic Dispersion Compensation at 10-Gbit/s," in *Proc. OFC*. 2008. Paper OWT7.

[11] I. Tomkos, D. Chowdhury, J. Conradi, D. Culverhouse, K. Ennser, C. Giroux, B. Hallock, T. Kennedy, A. Kruse, S. Kumar, N. Lascar, I. Roudas, M. Sharma, R. Vodhanel and R. C. Wang, "Demonstration of negative dispersion fibers for DWDM metropolitan area networks," *IEEE J. Sel. Topics in Q. Electron*., vol. 7, pp. 439-60. May 2001.

Chapter 6

Outlook

During the life of this project, significant achievements supporting a paradigm for converged fixed and wireless services delivery over a common optical infrastructure have been implemented and reported in peer-reviewed publications. These applications of the framework have allowed repeatable, reliable implementation of standards-compliant signal delivery, through the application of sound engineering principles. Results supporting this paradigm of low-complexity cross-platform support for fixed and wireless signal transport via a unified optical access infrastructure have also been encouraging. The demonstration of fixed, wireless and converged signal delivery through the optical access environment, using only common, commercially-available optical network components. In addition to extending the known limits of current optical access systems and signaling technology, support for next-generation RF access networking in next-generation long-reach WDM optical access infrastructure has also been demonstrated.

In order to fulfil the previously-articulated motivation for the simplification of field-installed networking equipment, efforts have been made as far as possible to use an all-passive distribution plant, for network lengths within 60 km of the CO node. Additionally, the framework has allowed the concentration of most advanced networking functionalities (including signal processing and routing, for example) at the CO, leading to a flexible overall network architecture. It is anticipated that the successes that were achieved with such network configurations will guide the implementation of future long-range and converged optical networks.

6.1 Future work

Developments in optical and radiowave signaling technology, as well as their use in the provisioning of greater levels of broadband access have been examined. On the demand side, trends indicating the continued demand for increasingly greater levels of connectivity in both fixed and wireless networks have been noted. These trends indicate the continuation of efforts to integrate baseband and RF connectivity via optical access infrastructure. A significant concern, however, remains with the competing requirements of high-linearity support and low-complexity imposed on the optoelectronic transceivers, and we have noted efforts to define baseband optical transport methods, such as the Common Public Radio Interface (CPRI)[274] and other methods of provisioning digital baseband radio over fiber.[275,276]

Such digital transmission schemes, while allowing long-haul antenna remoting without the dispersion-induced power loss, requires high-precision electronics to be installed at the wireless base transceiver stations. It may well be that the costs associated with this make these schemes feasible in high-density areas, but it appears unlikely that such schemes will allow for low-complexity multiple-protocol RF service delivery across entire OAN installations. It is therefore anticipated that the final solution realized for such converged access systems will be realized with colorless, uncooled, low-cost optelectronic transceivers, which will allow the high-linearity, broadband RF signal delivery required to support future generations of fixed and wireless access networking technologies. Encouraging results have been obtained with RSOA[143] and VCSEL[241] devices, indicating that these may well be lines for continued investigation.

It has already been additionally noted[277] that the low-loss link extension allowed by radio over fiber antenna remoting systems allows transceiver separation distances exceeding the path lengths anticipated by wireless standards designers, leading to protocol time-out issues beyond a certain optical path length. In addition to the examination of these new issues, we anticipate that the simultaneous collapse of metro- and access-level network hierarchies into the long-range OAN schemes being proposed, as well as the convergence of baseband and microwave RF signal delivery via fixed optical access infrastructure will pose new challenges to systems developers. It is anticipated that the reduction in complexity of outside plant infrastructure in such long-reach converged OAN implementations can allow

enhanced network efficiencies, and that the concentration of network processing load at the CO node will open the door for future system optimization.

Bibliography

[1] Berkman Center for Internet & Society. Next generation connectivity: A review of broadband internet transitions and policy from around the world. http://www.fcc.gov/stage/pdf/Berkman_Center_Broadband_Study_13Oct09.pdf, Harvard University, Oct. 2009.

[2] S. Cherry. Edholm's law of bandwidth. *IEEE Spectrum*, 41(7):58–60, July 2004. ISSN 0018-9235. doi: 10.1109/MSPEC.2004.1309810.

[3] Computerworld Executive Briefing. The frenetic pace of wireless. online, March 2007. URL http://whitepapers.zdnet.com/abstract.aspx?docid=308092.

[4] Paul E. Green. Fiber to the home: the next big broadband thing. *IEEE Communications Magazine*, 42(9):100 – 106, Sept. 2004. ISSN 0163-6804. doi: 10.1109/MCOM.2004.1336726.

[5] Jeff Halpern, George Garceau, and Sammy Thomas. Fiber: Revolutionizing the Bells' telecom networks. Technical report, Bernstein Research and Telcordia Technologies, May 2004. URL http://www.telcordia.com/products/fttp/bernstein-telcordia.pdf.

[6] P.E. Green, Jr. Paving the last mile with glass. *IEEE Spectrum*, 39(12):13 – 14, Dec. 2002. ISSN 0018-9235. doi: 10.1109/MSPEC.2002.1088446.

[7] R. E. Wagner, J. R. Igel, R. Whitman, M. D. Vaughn, A. B. Ruffin, and S. Bickham. Fiber-based broadband-access deployment in the United States. *J. Lightwave Technol.*, 24(12):4526–4540, Dec. 2006. ISSN 0733-8724. doi: 10.1109/JLT.2006.886067.

[8] H. Shinohara. Broadband access in Japan: rapidly growing FTTH market. *IEEE Communications Magazine*, 43(9):72 – 78, Sept. 2005. ISSN 0163-6804. doi: 10.1109/MCOM.2005.1509970.

[9] R. Kompfner. Optics at Bell laboratories—optical communications. *Appl. Opt.*, 11(11):2412–2425, 1972. doi: 10.1364/AO.11.002412. URL http://ao.osa.org/abstract.cfm?URI=ao-11-11-2412.

[10] Tingye Li. Advances in optical fiber communications: An historical perspective. *IEEE J. Sel. Areas Commun.*, 1(3):356 – 372, April 1983. ISSN 0733-8716.

[11] Jeff Hecht. *City of Light: The Story of Fiber Optics*. Oxford University Press, New York, USA, 1999. ISBN 0-19-510818-3.

[12] Ming-Jun Li and Daniel A. Nolan. Optical transmission fiber design evolution. *J. Lightwave Technol.*, 26(9):1079–1092, 2008. URL http://jlt.osa.org/abstract.cfm?URI=JLT-26-9-1079.

[13] Donald B. Keck. *Optical Fiber Spans 30 Years*. Corning Inc, 2000. URL http://www.corning.com/docs/opticalfiber/r3461.pdf.

[14] Albert Einstein. Zur Quantentheorie der Strahlung (On the Quantum Theory of Radiation). *Physik. Zeitschr.*, 18:121–128, 1917. URL http://www.ecse.rpi.edu/~schubert/More-reprints/1917%20Einstein%20(Physikalische%20Zeitschrift)%20Zur%20Quantentheorie%20der%20Strahlung.pdf.

[15] B. L. van der Waerden. *Sources of Quantum Physics*, volume 5. North-Holland Publishing Co., 1967.

[16] J. P. Gordon, H. J. Zeiger, and C. H. Townes. The maser—new type of microwave amplifier, frequency standard, and spectrometer. *Phys. Rev.*, 99 (4):1264–1274, Aug 1955. doi: 10.1103/PhysRev.99.1264.

[17] A. L. Schawlow and C. H. Townes. Infrared and optical masers. *Phys. Rev.*, 112(6):1940–1949, Dec 1958. doi: 10.1103/PhysRev.112.1940.

[18] T. Maiman. Stimulated optical radiation in ruby. *Nature*, 187(4736):493–494, Aug. 1960. doi: 10.1038/187493a0.

[19] A. Javan, W. R. Bennett, and D. R. Herriott. Population inversion and continuous optical maser oscillation in a gas discharge containing a He-Ne mixture. *Phys. Rev. Lett.*, 6(3):106–110, Feb 1961. doi: 10.1103/PhysRevLett.6.106.

[20] R. N. Hall, G. E. Fenner, J. D. Kingsley, T. J. Soltys, and R. O. Carlson. Coherent light emission from GaAs junctions. *Phys. Rev. Lett.*, 9(9):366–368, Nov 1962. doi: 10.1103/PhysRevLett.9.366.

[21] Z. I. Alferov, V. M. Andreev, D. Z. Garbuzov, Y. V. Zhilyaev, E. P. Morozov, E. L. Portnoi, and V. G. Trofim. Investigation of the influence of the AlAs–GaAs heterostructure parameters on the laser threshold current and the realization of continuous emission at the room temperature. In *Fiz. Tekh. Poluprovodn.*, volume 4, pages 1826–1829, 1970.

[22] Z. I. Alferov, V. M. Andreev, D. Z. Garbuzov, Y. V. Zhilyaev, E. P. Morozov, E. L. Portnoi, and V. G. Trofim. Investigation of the influence of the AlAs–GaAs heterostructure parameters on the laser threshold current and the realization of continuous emission at the room temperature. In *Sov. Phys. Semicond.*, volume 4, pages 1573–1575, 1971.

[23] I. Hayashi, M. B. Panish, P. W. Foy, and S. Sumski. Junction lasers which operate continuously at room temperature. *Applied Physics Letters*, 17(3): 109–111, 1970. doi: 10.1063/1.1653326. URL http://link.aip.org/link/?APL/17/109/1.

[24] L. V. Keldysh. Behavior of non-metallic crystals in strong electric fields. *Soviet Journal of Experimental and Theoretical Physics*, 6, 1958.

[25] Ludwig Zehnder. Ein neuer Interferenzrefraktor. *Zeitschrift für Instrumentenkunde*, 11:275–285, Aug. 1891.

[26] Ludwig Mach. Ueber einen Interferenzrefraktor. *Zeitschrift für Instrumentenkunde*, 12:89–94, March 1892.

[27] Eugen Lach, Karsten Schuh, and Michael Schmidt. Application of electroabsorption modulators for high-speed transmission systems. *Journal of Optical and Fiber Communications Research*, 2(2):140–170, June 2005.

[28] Charles J. Koester and Elias Snitzer. Amplification in a fiber laser. *Appl. Opt.*, 3(10):1182–1186, 1964. URL http://ao.osa.org/abstract.cfm?URI=ao-3-10-1182.

[29] R.J. Mears, L. Reekie, I.M. Jauncey, and D.N. Payne. Low-noise erbium-doped fibre amplifier operating at 1.54μm. *Electron. Lett.*, 23(19):1026–1028, Sept. 1987. ISSN 0013-5194. doi: 10.1049/el:19870719.

[30] E. Desurvire, J. R. Simpson, and P. C. Becker. High-gain erbium-doped traveling-wave fiber amplifier. *Opt. Lett.*, 12(11):888–890, 1987. URL http://ol.osa.org/abstract.cfm?URI=ol-12-11-888.

[31] M. Öberg, B. Broberg, and S. Lindgren. InGaAsP-InP laser amplifier with integrated passive waveguides. *IEEE J. Quantum Electron.*, 23(6):1021 – 1026, June 1987. ISSN 0018-9197.

[32] M. Riordan and L. Hoddeson. The origins of the PN junction. *IEEE Spectrum*, 34(6):46 –51, June 1997. ISSN 0018-9235. doi: 10.1109/6.591664.

[33] R. P. Reisz. High-speed semiconductor photodiodes. *Rev. Sci. Instrum*, 33 (994):994–998, Sept. 1962.

[34] E. Snitzer. Cylindrical dielectric waveguide modes. *J. Opt. Soc. Am.*, 51(5):491–498, 1961. URL http://www.opticsinfobase.org/abstract.cfm?URI=josa-51-5-491.

[35] K.C. Kao and G.A. Hockham. Dielectric-fibre surface waveguides for optical frequencies. *Proc. IEEE*, 113(7):1151 –1158, July 1966. ISSN 0020-3270. doi: 10.1049/piee.1966.0189.

[36] F. P. Kapron, D. B. Keck, and R. D. Maurer. Radiation losses in glass optical waveguides. *Applied Physics Letters*, 17(10):423–425, 1970. doi: 10.1063/1.1653255. URL http://link.aip.org/link/?APL/17/423/1.

[37] D. B. Keck and R. Tynes. Spectral response of low-loss optical waveguides. *Applied Optics*, 11(7):1502–1506, 1972. URL http://ao.osa.org/abstract.cfm?URI=ao-11-7-1502.

[38] D.B. Keck, R.D. Maurer, and P.C. Schultz. On the ultimate lower limit of attenuation in glass optical waveguides. *Applied Physics Letters*, 22(7): 307–309, 1973. doi: 10.1063/1.1654649. URL http://link.aip.org/link/?APL/22/307/1.

[39] P. Kaiser, A. R. Tynes, H. W. Astle, A. D. Pearson, W. G. French, R. E. Jaeger, and A. H. Cherin. Spectral losses of unclad vitreous silica and soda-lime-silicate fibers. *J. Optical Society of America*, 63(9):1141–1148, 1973. URL http://www.opticsinfobase.org/abstract.cfm?URI=josa-63-9-1141.

[40] M. Horiguchi and H. Osanai. Spectral losses of low-OH-content optical fibres. *Electronics Letters*, 12(12):310 –312, June 1976. ISSN 0013-5194. doi: 10.1049/el:19760239.

[41] H. Osanai, T. Shioda, T. Moriyama, S. Araki, M. Horiguchi, T. Izawa, and H. Takata. Effect of dopants on transmission loss of low-OH-content optical fibres. *Electronics Letters*, 12(21):549 –550, Oct. 1976. ISSN 0013-5194. doi: 10.1049/el:19760418.

[42] Tatsuya Kimura and Kazuhiro Daikoku. A proposal on optical fibre transmission systems in a low-loss 1.0–1.4 μm wavelength region. *Optical and Quantum Electronics*, 9(1):33–42, January 1977.

[43] T. Miya, Y. Terunuma, T. Hosaka, and T. Miyashita. Ultimate low-loss single-mode fibre at 1.55 μm. *Electronics Letters*, 15(4):106 –108, 15 1979. ISSN 0013-5194. doi: 10.1049/el:19790077.

[44] ITU-T. Recommendation G.652 – characteristics of a single-mode optical fibre and cable. URL http://www.itu.int/rec/T-REC-G.652/en, Nov. 2009.

[45] J.R. Stern, D.B. Payne, D.J. McCartney, P. Healey, P. Lindsey, D.M. Russ, and J.H. Stewart. Field installation of a 31.5 km monomode optical fibre system operated at 140 Mbit/s and 650 Mbit/s. *Electronics Letters*, 18(14): 631 –632, 8 1982. ISSN 0013-5194. doi: 10.1049/el:19820431.

[46] R. Hooper, J. Midwinter, D. Smith, and I. Stanley. Progress in monomode transmission techniques in the United Kingdom. *J. Lightwave Technol.*, 1 (4):596 – 611, Dec. 1983. ISSN 0733-8724.

[47] A.J. Barlow, D.N. Payne, M.R. Hadley, and R.J. Mansfield. Production of single-mode fibres with negligible intrinsic birefringence and polarisation mode dispersion. *Electronics Letters*, 17(20):725 –726, Oct. 1981. ISSN 0013-5194. doi: 10.1049/el:19810509.

[48] J. M. Dugan, A. J. Price, M. Ramadan, D. L. Wolf, E. F. Murphy, A. J. Antos, D. K. Smith, and D. W. Hall. All-optical, fiber-based 1550 nm dispersion compensation in a 10 Gbit/s, 150 km transmission experiment over 1310 nm optimized fiber. In *Digest of Conference on Optical Fiber Communication*, pages 363–366, San Jose, California, Feb. 1992. Optical Society

of America. URL http://www.opticsinfobase.org/abstract.cfm?URI=OFC-1992-PD14. Paper PD14.

[49] ITU-T. Recommendation G.653 – characteristics of a dispersion-shifted single-mode optical fibre and cable. URL http://www.itu.int/rec/T-REC-G.653/en, Dec. 2006.

[50] ITU-T. Recommendation G.655 – characteristics of a non-zero dispersion-shifted single-mode optical fibre and cable. URL http://www.itu.int/rec/T-REC-G.655/en, Nov. 2009.

[51] S.N. Knudsen, M.O. Pedersen, and L. Gruner-Nielsen. Optimisation of dispersion compensating fibres for cabled long-haul applications. *Electronics Letters*, 36(25):2067 –2068, Dec. 2000. ISSN 0013-5194. doi: 10.1049/el:20001445.

[52] M.O. Pedersen, S.N. Knudsen, T. Geisler, T. Veng, and L. Gruner-Nielsen. New low-loss inverse dispersion fiber for dispersion matched fiber sets. In *Proc. 28th European Conference on Optical Communication (ECOC)*, volume 2, pages 1 –2, 2002. doi: 10.1109/ECOC.2002.204467.

[53] L.J. Bottino. Optical communications-the origins of the state of the art. In *Proc. 22nd Digital Avionics Systems Conference (DASC)*, volume 2, pages 6.B.5 – 61–13 vol.2, Oct. 2003. doi: 10.1109/DASC.2003.1245883.

[54] Jeff Hecht. Fiber to the home why "the last mile" is truly the hardest. *Opt. Photon. News*, 14(3):26–31, 2003. URL http://www.osa-opn.org/abstract.cfm?URI=OPN-14-3-26.

[55] J.E. Midwinter. The start of optical fiber communications as seen from a U.K. perspective. *IEEE J. Sel. Topics Quantum Electron.*, 6(6):1307 –1311, Nov.-Dec. 2000. ISSN 1077-260X. doi: 10.1109/2944.902183.

[56] Laser Focus. PS-noted in passing: communication applications, July 1977.

[57] S.D. Personick, N.L. Rhodes, D.C. Hanson, and K.H. Chan. Contrasting fiber-optic-component-design requirements in telecommunications, analog, and local data communications applications. *Proc. IEEE*, 68(10):1254 – 1262, Oct. 1980. ISSN 0018-9219.

[58] Yoneji Masuda. *The information society as post-industrial society*, page 22. Transaction Publishers, second edition, January 1980.

[59] M. Kawahata. Hi-OVIS (Higashi Ikoma Optical Visual Information System) development project. In *Proc. Integ. Optics and Optical Comun. (IOOC)*, pages 467–471, Tokyo, Japan, 1977.

[60] Masahiro Kawahata. Hi-OVIS. In Kenneth L. Kraemer and Jay G. Blumler, editors, *Wired cities: shaping the future of communications*, pages 179–200. G. K. Hall & Co, Boston, MA, USA, 1987.

[61] K. Sakurai and K. Asatani. A review of broad-band fiber system activity in Japan. *IEEE J. Sel. Areas Commun.*, 1(3):428 – 435, April 1983. ISSN 0733-8716.

[62] Anthony Newstead. Future information cities: Japan's vision. *Futures*, 21(3):263 – 276, 1989. ISSN 0016-3287. doi: 10.1016/0016-3287(89)90023-2. URL http://www.sciencedirect.com/science/article/B6V65-463XX5G-3/2/25975e3bade600ab110aa42c642779fa.

[63] Jeff Hecht. Building a fiber-optic communication industry. *Opt. Photon. News*, 12(3):22–26, 2001. URL http://www.osa-opn.org/abstract.cfm?URI=OPN-12-3-22.

[64] Alexander Graham Bell. Apparatus for signaling and communicating, called "Photophone". U.S. Patent No. 235199, Dec. 1880.

[65] FSAN website. http://www.fsanweb.org/, Feb. 2010.

[66] IEEE. 802.3 Ethernet working group. http://www.ieee802.org/3/, March 2010.

[67] Paul W. Shumate. Fiber-to-the-home: 1977–2007. *J. Lightwave Technol.*, 26(9):1093–1103, 2008. URL http://jlt.osa.org/abstract.cfm?URI=JLT-26-9-1093.

[68] Anpeng Huang, Liang Shan, Wei Li, Anshi Xu, and Linzhen Xie. Solutions to challenges of FTTH deployment in China. In *IEEE Globecom Workshops*, pages 1 –3, Nov. 2007. doi: 10.1109/GLOCOMW.2007.4437843.

[69] Hiromichi Shinohara. FTTH experiences in Japan (invited). *J. Opt. Netw.*, 6(6):616–623, 2007. URL http://jon.osa.org/abstract.cfm?URI=JON-6-6-616.

[70] D. Payne and J. Stern. Transparent single-mode fiber optical networks. *J. Lightwave Technol.*, 4(7):864 – 869, jul 1986. ISSN 0733-8724.

[71] J.R. Stern, J.W. Ballance, D.W. Faulkner, S. Hornung, D.B. Payne, and K. Oakley. Passive optical local networks for telephony applications and beyond. *Electronics Letters*, 23(24):1255–1256, 1987. doi: 10.1049/el:19870872. URL http://link.aip.org/link/?ELL/23/1255/1.

[72] S.S. Wagner, H. Kobrinski, T.J. Robe, H.L. Lemberg, and L.S. Smoot. Experimental demonstration of a passive optical subscriber loop architecture. *Electronics Letters*, 24(6):344–346, Mar 1988. ISSN 0013-5194.

[73] J.A. Salehi and C.A. Brackett. Code division multiple-access techniques in optical fiber networks. II. systems performance analysis. *IEEE Trans. Commun.*, 37(8):834–842, Aug 1989. ISSN 0090-6778. doi: 10.1109/26.31182.

[74] J.A. Salehi. Code division multiple-access techniques in optical fiber networks. I. fundamental principles. *IEEE Trans. Commun.*, 37(8):824–833, Aug 1989. ISSN 0090-6778. doi: 10.1109/26.31181.

[75] T.E. Darcie. Subcarrier multiplexing for lightwave networks and video distribution systems. *IEEE J. Sel. Areas Commun.*, 8(7):1240–1248, Sep 1990. ISSN 0733-8716. doi: 10.1109/49.59123.

[76] T.E. Darcie and G.E. Bodeep. Lightwave subcarrier CATV transmission systems. *IEEE Trans. Microw. Theory Tech.*, 38(5):524–533, May 1990. ISSN 0000-0000. doi: 10.1109/22.54920.

[77] R. Olshansky, V.A. Lanzisera, and P.M. Hill. Subcarrier multiplexed lightwave systems for broad-band distribution. *J. Lightwave Technol.*, 7(9):1329–1342, Sep 1989. ISSN 0733-8724. doi: 10.1109/50.50712.

[78] Arthur James Lowery. Optical OFDM. In *Proc. Conference on Lasers and Electro-Optics and Quantum Electronics and Laser Science (CLEO/QELS)*, pages 1 –2, May 2008. Paper CWN1.

[79] J. Armstrong. OFDM for next generation optical communication systems. In *Proc. 7th International Conference on Optical Internet (COIN)*, pages 1–2, Tokyo, Japan, Oct. 2008.

[80] J. Armstrong. OFDM for optical communications. *J. Lightwave Technol.*, 27 (3):189–204, Feb.1, 2009. ISSN 0733-8724. doi: 10.1109/JLT.2008.2010061.

[81] A.J. Lowery, Liang Du, and J. Armstrong. Orthogonal frequency division multiplexing for adaptive dispersion compensation in long haul WDM systems. In *Proc. Optical Fiber Communication/National Fiber Optic Engineers Conference (OFC/NFOEC)*, pages 1 – 3, March 2006.

[82] A.J. Lowery, Liang Bangyuan Du, and J. Armstrong. Performance of optical OFDM in ultralong-haul WDM lightwave systems. *J. Lightwave Technol.*, 25 (1):131 –138, January 2007. ISSN 0733-8724. doi: 10.1109/JLT.2006.888161.

[83] Kevin D. Stalley, Donald E. A. Clarke, and Paul A. Rosher. Optical fibre communications system. U.S. Patent No. 5,479,286, Dec. 1995.

[84] Chang-Hee Lee, Sang-Mook Lee, Ki-Man Choi, Jung-Hyung Moon, Sil-Gu Mun, Ki-Tae Jeong, Jin Hee Kim, and Byoungwhi Kim. WDM-PON experiences in Korea (invited). *J. Opt. Netw.*, 6(5):451–464, 2007. URL http://jon.osa.org/abstract.cfm?URI=JON-6-5-451.

[85] ITU-T. Recommendation G.983.1 - broadband optical access systems based on passive optical networks (PON). URL http://www.itu.int/rec/T-REC-G.983.1/en, January 2005.

[86] Kiyoshi Yokota, Kazuho Kawaguchi, Shinya Iko, Noboru Yamamichi, and Ryuji Tanaka. ATM-PON. *OKI Technical Review*, 67(182):9–12, May 2000.

[87] ITU-T. Recommendation G.983.4: A broadband optical access system with increased service capability using dynamic bandwidth assignment (DBA). URL http://www.itu.int/rec/T-REC-G.983.4/en, January 2005.

[88] IEEE. Standard 802.3ah-2004. http://ieeexplore.ieee.org.globalproxy.cvt.dk/servlet/opac?punumber=9283, 2004.

[89] IEEE. 802.3ah. http://standards.ieee.org/getieee802/download/802.3-2008_section5.pdf, 2008.

[90] ITU-T. Recommendation G.984.1 : Gigabit-capable passive optical networks (GPON): General characteristics. URL http://www.itu.int/rec/T-REC-G.984.1/en, Oct. 2009.

[91] ITU-T. Recommendation G.984.2 gigabit-capable passive optical networks (G-PON): Physical media dependent (pmd) layer specification. URL http://www.itu.int/rec/T-REC-G.984.2/en, March 2008.

[92] ITU-T. Recommendation G.984.3 : Gigabit-capable passive optical networks (G-PON): Transmission convergence layer specification. URL http://www.itu.int/rec/T-REC-G.984.3/en, March 2008.

[93] ITU-T. Recommendation G.984.4: Gigabit-capable passive optical networks (G-PON): Ont management and control interface specification. URL http://www.itu.int/rec/T-REC-G.984.4/en, Feb. 2008.

[94] ITU-T. Recommendation G.984.5 gigabit-capable passive optical networks (G-PON): Enhancement band. URL http://www.itu.int/rec/T-REC-G.984.5/en, Oct. 2009.

[95] Ethernet Alliance. Overview of 10Gb/s EPON status, requirements and applications. http://www.ethernetalliance.org/about_us/technology_overview/10g_epon, May 2009. Version 2.4.

[96] IEEE. Standard 802.3av-2009. http://www.ieee802.org/3/av/, Sept. 2009.

[97] "IEEE Approves 10G-EPON Standard". URL http://standards.ieee.org/announcements/stdbd_approves_ieee802.3av.html, Sept. 2009.

[98] Junichi Nagagawa, Masaki Noda, Naoki Suzuki, Satoshi Yoshima, Kenichi Nakura, and Masamichi Nogami. First demonstration of 10G-EPON and GE-PON co-existing system employing dual-rate burst-mode 3r transceiver. In *Technical Digest Optical Fiber Communication Conference and Exhibit (OFC)*, San Diego, CA, USA, March 2010. Paper PDPD10.

[99] M. Chacinski, U. Westergren, L. Thylen, B. Stoltz, J. Rosenzweig, R. Driad, R. E. Makon, J. Li, and A. Steffan. ETDM transmitter module for 100-Gb/s Ethernet. *IEEE Photon. Technol. Lett.*, 22(2):70–72, January 2010. ISSN 1041-1135. doi: 10.1109/LPT.2009.2036146.

[100] Frank J. Effenberger. Tutorial: XG-PON. In *Technical Digest Optical Fiber Communication Conference and Exhibit (OFC)*, San Diego, CA, USA, March 2010. Paper OWX4.

[101] E.K. Lau, Hyuk-Kee Sung, and M.C. Wu. Ultra-high, 72 GHz resonance frequency and 44 GHz bandwidth of injection-locked 1.55-μm DFB lasers. In *Proc. Optical Fiber Communication Conference (OFC)*, page 3 pp., March 2006. doi: 10.1109/OFC.2006.215716. Paper OThG2.

[102] L. Chrostowski, X. Zhao, C.J. Chang-Hasnain, R. Shau, M. Ortsiefer, and M.-C. Amann. 50-GHz optically injection-locked 1.55-μm VCSELs. *IEEE Photon. Technol. Lett.*, 18(2):367 –369, January 2006. ISSN 1041-1135. doi: 10.1109/LPT.2005.862370.

[103] A. Beling, H.-G. Bach, G.G. Mekonnen, R. Kunkel, and D. Schmidt. Miniaturized waveguide-integrated p-i-n photodetector with 120-GHz bandwidth and high responsivity. *IEEE Photon. Technol. Lett.*, 17(10):2152 – 2154, oct. 2005. ISSN 1041-1135. doi: 10.1109/LPT.2005.856370.

[104] J.H. Sinsky, A. Adamiecki, L. Buhl, G. Raybon, P. Winzer, O. Wohlgemuth, M. Duelk, C.R. Doerr, A. Umbach, H.-G. Bach, and D. Schmidt. A 107-Gbit/s optoelectronic receiver utilizing hybrid integration of a photodetector and electronic demultiplexer. *J. Lightwave Technol.*, 26(1):114 –120, January 2008. ISSN 0733-8724. doi: 10.1109/JLT.2007.913065.

[105] R. Driad, R.E. Makon, V. Hurm, K. Schneider, F. Benkhelifa, R. Losch, and J. Rosenzweig. InP DHBT-based ICs for 100 Gbit/s data transmission. In *Proc. 20th International Conference on Indium Phosphide and Related Materials (IPRM)*, pages 1–4, May 2008. doi: 10.1109/ICIPRM.2008.4702960.

[106] A. Beling and J.C. Campbell. InP-based high-speed photodetectors. *J. Lightwave Technol.*, 27(3):343 –355, Feb. 2009. ISSN 0733-8724. doi: 10.1109/JLT.2008.2008399.

[107] G. Grasso, P. Galli, M. Romagnoli, E. Iannone, and A. Bogoni. Role of integrated photonics technologies in the realization of terabit nodes [invited]. *IEEE/OSA Journal of Optical Communications and Networking*, 1(3):B111 –B119, Aug. 2009. ISSN 1943-0620. doi: 10.1364/JOCN.1.00B111.

[108] S. Kakehashi, H. Hasegawa, K. Sato, O. Moriwaki, S. Kamei, Y. Jinnouchi, and M. Okuno. Performance of waveband MUX/DEMUX using concatenated AWGs. *IEEE Photonics Technology Letters*, 19(16):1197 –1199, Aug. 15 2007. ISSN 1041-1135. doi: 10.1109/LPT.2007.901602.

[109] E.I. Ackerman and C.H. Cox. Optimization of photonic transmit/receive module performance. In *Proc. International Topical Meeting on Microwave Photonics (MWP)*, pages 1–4, Oct. 2009.

[110] T. Kuri, K. Kitayama, and Y. Takahashi. 60-GHz-band full-duplex radio-on-fiber system using two-RF-port electroabsorption transceiver. *IEEE Photon. Technol. Lett.*, 12(4):419–421, April 2000. ISSN 0000-0000. doi: 10.1109/68.839038.

[111] D. Torrientes, P. Chanclou, F. Laurent, S. Tsyier, Y. Chang, B. Charbonnier, and C. Kazmierski. 10Gbit/s for next generation PON with electronic equalization using un-cooled 1.55 μm directly modulated laser. In *Proc. 35th. European Conference on Optical Communication (ECOC)*, pages 1 –2, Sept. 2009. Paper PD3.5.

[112] D.J. Shin, D.K. Jung, J.K. Lee, J.H. Lee, Y.H. Choi, Y.C. Bang, H.S. Shin, J. Lee, S.T. Hwang, and Y.J. Oh. 155 Mbit/s transmission using ASE-injected Fabry-Perot laser diode in WDM-PON over 70 °C temperature range. *Electronics Letters*, 39(18):1331–1332, Sept. 2003. ISSN 0013-5194. doi: 10.1049/el:20030850.

[113] Shweta Jain, Frank J. Effenberger, Andrea Szabo, Zhishan Feng, Albert Forcucci, Wei Guo, Yuanqiu Luo, Robert Mapes, Yixin Zhang, and Vincent O'Byrne. World's first XG-PON field trial. In *Technical Digest Optical Fiber Communication Conference and Exhibit (OFC)*, San Diego, CA, USA, March 2010. Paper PDPD6.

[114] R.P. Davey, D.B. Grossman, M. Rasztovits-Wiech, D.B. Payne, D. Nesset, A.E. Kelly, A. Rafel, S. Appathurai, and Sheng-Hui Yang. Long-reach passive optical networks. *J. Lightwave Technol.*, 27(3):273–291, Feb.1, 2009. ISSN 0733-8724. doi: 10.1109/JLT.2008.2006991.

[115] Ken-Ichi Suzuki, Youichi Fukada, Derek Nesset, and Russell Davey. Amplified gigabit PON systems (invited). *J. Opt. Netw.*, 6(5):422–433, 2007. URL http://jon.osa.org/abstract.cfm?URI=JON-6-5-422.

[116] Derek Nesset and Paul Wright. Raman extended GPON using 1240 nm semiconductor quantum-dot lasers. In *Technical Digest Optical Fiber Communication Conference and Exhibit (OFC)*, San Diego, CA, USA, March 2010. Paper OThW6.

[117] R.P. Davey, P. Healey, I. Hope, P. Watkinson, D.B. Payne, O. Marmur, J. Ruhmann, and Y. Zuiderveld. DWDM reach extension of a GPON to 135 km. *Lightwave Technology, Journal of*, 24(1):29–31, Jan. 2006. ISSN 0733-8724. doi: 10.1109/JLT.2005.861140.

[118] K. Grobe and J.-P. Elbers. PON in adolescence: from TDMA to WDM-PON. *IEEE Commun. Mag.*, 46(1):26–34, January 2008. ISSN 0163-6804. doi: 10.1109/MCOM.2008.4427227.

[119] Fu-Tai An, D. Gutierrez, Kyeong Soo Kim, Jung Woo Lee, and L.G. Kazovsky. SUCCESS-HPON: A next-generation optical access architecture for smooth migration from TDM-PON to WDM-PON. *IEEE Commun. Mag.*, 43(11):S40–S47, Nov. 2005. ISSN 0163-6804. doi: 10.1109/MCOM.2005.1541698.

[120] Xu Wang. Recent progresses in OCDMA. In *Proc. 10th Annivarsary International Conference on Transparent Optical Networks (ICTON)*, volume 1, pages 39 –42, june 2008. doi: 10.1109/ICTON.2008.4598365.

[121] G. Cincotti, N. Kataoka, N. Wada, Xu Wang, T. Miyazaki, and K.-i. Kitayama. Demonstration of asynchronous, 10Gbps OCDMA PON system with colorless and sourceless ONUs. In *Proc. 35th. European Conference on Optical Communication (ECOC)*, pages 1 –2, sept. 2009.

[122] K. Kitayama, Xu Wang, and Naoya Wada. OCDMA over WDM PON-solution path to gigabit-symmetric FTTH. *J. Lightwave Technol.*, 24(4): 1654 – 1662, April 2006. ISSN 0733-8724. doi: 10.1109/JLT.2006.871030.

[123] N. Kataoka, Xu Wang, N. Wada, G. Cincotti, Y. Terada, and K.-i. Kitayama. 8x8 full-duplex demonstration of asynchronous, 10Gbps, DPSK-OCDMA system using apodized SSFBG and multi-port en/decoder. In *Proc. 35th. European Conference on Optical Communication (ECOC)*, Vienna, Austria, Sept. 2009. Paper 6.5.5.

[124] Chang-Hee Lee, Sil-Gu Mun, and Jung-Hyung Moon. WDM-PON overview. In *Proc. 35th. European Conference on Optical Communication (ECOC)*, Vienna, Austria, Sep 2009.

[125] Robert D. Feldman, E. E. Harstead, S. Jiang, Thomas H. Wood, and Martin Zirngibl. An evaluation of architectures incorporating wavelength division

multiplexing for broad-band fiber access. *J. Lightwave Technol.*, 16(9):1546, 1998. URL http://jlt.osa.org/abstract.cfm?URI=JLT-16-9-1546.

[126] Amitabha Banerjee, Youngil Park, Frederick Clarke, Huan Song, Sunhee Yang, Glen Kramer, Kwangjoon Kim, and Biswanath Mukherjee. Wavelength-division-multiplexed passive optical network (WDM-PON) technologies for broadband access: a review (invited). *J. Opt. Netw.*, 4 (11):737–758, Nov. 2005. URL http://jon.osa.org/abstract.cfm?URI=JON-4-11-737.

[127] E.L. Goldstein, L. Eskildsen, and A.F. Elrefaie. Performance implications of component crosstalk in transparent lightwave networks. *IEEE Photon. Technol. Lett.*, 6(5):657–660, May 1994. ISSN 1041-1135. doi: 10.1109/68.285571.

[128] Junichi Hasegawa and Kazutaka Nara. Low loss 50 GHz 80 ch athermal AWG module. In *Technical Digest, 10th. OptoElectronics and Commun. Conf. (OECC)*, pages 458–459, Seoul, South Korea, Jul 2005. Paper 7E3-3.

[129] Junichi Hasegawa and Kazutaka Nara. Ultra-wide temperature range (-30 $\sim$ 70°C) operation of athermal AWG module using pure aluminum plate. In *Proc. Optical Fiber Communication Conference (OFC)*, March 2006. Paper OWI68.

[130] Junichi Hasegawa and Kazutaka Nara. Athermal AWG module with extremely low temperature dependence ($\ll +/-5$pm) of center wavelength using multi-compensating plates. In *Proc. 32rd European Conference and Exhibition on Optical Communication (ECOC)*, pages 1 –2, Cannes, France, Sept. 2006. doi: 10.1109/ECOC.2006.4801038.

[131] Fu-Tai An, Kyeong Soo Kim, David Gutierrez, Scott Yam, Eric (Shih-Tse) Hu, Kapil Shrikhande, and Leonid G. Kazovsky. SUCCESS: a next-generation hybrid WDM/TDM optical access network architecture. *J. Lightwave Technol.*, 22(11):2557, 2004. URL http://jlt.osa.org/abstract.cfm?URI=JLT-22-11-2557.

[132] J. A. Lazaro, J. Prat, P. Chanclou, G. M. Tosi Beleffi, A. Teixeira, I. Tomkos, R. Soila, and V. Koratzinos. Scalable extended reach PON. In *Proc. Optical Fiber Communication Conference (OFC)*, 2008. OThL2.

[133] Josep Prat, Jose Lazaro, Philippe Chanclou, Risto Soila, Ana M. Gallardo, Antonio Teixeira, Giorgio M. TosiBeleffi, and Ioannis Tomkos. Results from EU project SARDANA on 10G extended reach WDM PONs. In *Technical Digest Optical Fiber Communication Conference and Exhibit (OFC)*, San Diego, CA, USA, March 2010. Paper OThG5.

[134] L.-S. Yan, Y. Wang, B. Zhang, C. Yu, J. McGeehan, L. Paraschis, and A. E. Willner. Reach extension in 10-Gb/s directly modulated transmission systems using asymmetric and narrowband optical filtering. *Opt. Express*, 13(13):5106–5115, 2005. URL http://www.opticsexpress.org/abstract.cfm?URI=oe-13-13-5106.

[135] O. Akanbi, Jianjun Yu, and Gee-Kung Chang. A new scheme for bidirectional wdm-pon using upstream and downstream channels generated by optical carrier suppression and separation technique. *IEEE Photon. Technol. Lett.*, 18(2):340–342, 15, 2006. ISSN 1041-1135. doi: 10.1109/LPT.2005.861975.

[136] A. Chowdhury, Hung-Chang Chien, Ming-Fang Huang, Jianjun Yu, and Gee-Kung Chang. Rayleigh backscattering noise-eliminated 115-km long-reach bidirectional centralized WDM-PON with 10-Gb/s DPSK downstream and remodulated 2.5-Gb/s OCS-SCM upstream signal. *IEEE Photon. Technol. Lett.*, 20(24):2081–2083, Dec.15, 2008. ISSN 1041-1135. doi: 10.1109/LPT.2008.2006630.

[137] Neda Cvijetic, Dayou Qian, Junqiang Hu, and Ting Wang. 44-Gb/s/λ upstream OFDMA-PON transmission with polarization- insensitive source-free ONUs. In *Technical Digest Optical Fiber Communication Conference and Exhibit (OFC)*, San Diego, CA, USA, March 2010. Paper OTuO2.

[138] Dayou Qian, Neda Cvijetic, Junqiang Hu, and Ting Wang. 108 gb/s ofdma-pon with polarization multiplexing and direct detection. *J. Lightwave Technol.*, 28(4):484–493, Feb. 2010. URL http://jlt.osa.org/abstract.cfm?URI=JLT-28-4-484.

[139] Marco Presi, Roberto Proietti, Kamau Prince, Giampiero Contestabile, and Ernesto Ciaramella. A 80 km reach fully passive WDM-PON based on reflective ONUs. *Opt. Express*, 16(23):19043–19048, Nov. 2008. doi: 10.1364/OE.16.019043. URL http://www.opticsexpress.org/abstract.cfm?URI=oe-16-23-19043.

[140] Q. T. Nguyen, P. Besnard, L. Bramerie, A. Shen, G. H. Duan, C. Kazmierski, and J.-C. Simon. Bidirectional transmission in colourless WDM-PON based on injection-locked fabry-perot laser at 2.5 Gbit/s using low-cost seeding source. In *Proc. 35th. European Conference on Optical Communication (ECOC)*, Vienna, Austria, Sep. 2009. Paper 6.5.1.

[141] Q.T. Nguyen, L. Bramerie, P. Besnard, A. Shen, A. Garreau, C. Kazmierski, G.H. Duan, and J.C. Simon. 24 channels colorless WDM-PON with L-band 10 Gb/s downstream and C-band 2.5 Gb/s upstream using multiple-wavelengths seeding sources based on mode-locked lasers. In *Technical Digest Optical Fiber Communication Conference and Exhibit (OFC)*, San Diego, CA, USA, March 2010. Paper OThG6.

[142] Mireia Omella, Ioannis Papagiannakis, Bernhard Schrenk, Dimitrios Klonidis, Jose A. Lázaro, Alexios N. Birbas, John Kikidis, Josep Prat, and Ioannis Tomkos. 10 Gb/s full-duplex bidirectional transmission with RSOA-based ONU using detuned optical filtering and decision feedback equalization. *Opt. Express*, 17(7):5008–5013, 2009. URL http://www.opticsexpress.org/abstract.cfm?URI=oe-17-7-5008.

[143] M. Omella, J. A. Lazaro, I. Papagiannakis, A. N. Birbas, D Klonidis, J. Kikidis, I. Tomkos, and J. Prat. Design optimization for 10 Gb/s full-duplex transmission using RSOA based ONU with electrical and optical filtering and equalization. In *Proc. 35th. European Conference on Optical Communication (ECOC)*, 2009. Paper 7.5.5.

[144] Robert Olshansky, Richard Gross, and Mark Schmidt. Subcarrier multiplexed coherent lightwave systems for video distribution. *IEEE J. Sel. Areas Commun.*, 8(7):1268–1275, Sep 1990. ISSN 0733-8716. doi: 10.1109/49.59126.

[145] Jeung-Mo Kang and Sang-Kook Han. A novel hybrid WDM/SCM-PON sharing wavelength for up- and down-link using reflective semiconductor optical amplifier. *IEEE Photon. Technol. Lett.*, 18(3):502–504, January 2006. ISSN 1041-1135. doi: 10.1109/LPT.2005.863632.

[146] J.G. Proakis. *Digital Communication*, chapter 5, pages 152–223. McGraw-Hill, New York, 4th edition, 1995.

[147] Robert G. Gallager. Low-density parity-check codes. *IRE Transactions on Information Theory*, 8(1):21 –28, January 1962. ISSN 0096-1000. doi: 10.1109/TIT.1962.1057683.

[148] Robert G. Gallager. *Low-Density Parity-Check codes*. M.I.T. Press, 1963.

[149] C. Berrou, A. Glavieux, and P. Thitimajshima. Near Shannon limit error-correcting coding and decoding: Turbo-codes. 1. In *Technical Program, Conference Record, IEEE International Conference on Communications (ICC)*, volume 2, pages 1064 –1070, Geneva, Switzerland, May 1993. doi: 10.1109/ICC.1993.397441.

[150] E. Guizzo. Closing in on the perfect code [turbo codes]. *IEEE Spectrum*, 41(3):36 – 42, March 2004. ISSN 0018-9235. doi: 10.1109/MSPEC.2004.1270546.

[151] E. E. Altshuler, V. J. Falcone, and K. N. Wulfsberg. Atmospheric effects on propagation at millimeter wavelengths. *IEEE Spectrum*, 5(7):83–90, July 1968. ISSN 0018-9235. doi: 10.1109/MSPEC.1968.5214540.

[152] A.W. Straiton and C.W. Tolbert. Anomalies in the absorption of radio waves by atmospheric gases. *Proceedings of the IRE*, 48(5):898–903, May 1960. ISSN 0096-8390. doi: 10.1109/JRPROC.1960.287627.

[153] A. Straiton. The absorption and reradiation of radio waves by oxygen and water vapor in the atmosphere. *IEEE Trans. Antennas Propag.*, 23(4):595–597, Jul 1975. ISSN 0018-926X.

[154] J. H. van Vleck. The absorption of microwaves by oxygen. *Phys. Rev.*, 71 (7):413–424, Apr 1947. doi: 10.1103/PhysRev.71.413.

[155] J. H. van Vleck. The absorption of microwaves by uncondensed water vapor. *Phys. Rev.*, 71(7):425–433, Apr 1947. doi: 10.1103/PhysRev.71.425.

[156] T.S. Rappaport. *Wireless Communications: Principles and Practice*. IEEE Press, Piscataway, NJ, USA, 1996.

[157] Marvin K. Simon and Mohamed-Slim Alouini. *Digital Communication over Fading Channels: A Unified Approach to Performance Analysis*. John Wiley & Sons, Inc., New York, 2000.

[158] W.C.Y. Lee. Future vision for wireless communications. In *Proc. Seventh IEEE International Symposium on Personal, Indoor and Mobile Radio Communications (PIMRC)*, volume 1, Oct 1996. doi: 10.1109/PIMRC.1996.567501.

[159] S.M. Cherry. The wireless last mile. *IEEE Spectrum*, 40(9):18 – 22, Sept. 2003. ISSN 0018-9235. doi: 10.1109/MSPEC.2003.1228003.

[160] IEEE. Std 802.11n-2009. http://ieeexplore.ieee.org/servlet/opac?punumber=5307291, Oct. 2009. doi: 10.1109/IEEESTD.2009.5307322.

[161] Richard Nee, V. K. Jones, Geert Awater, Allert Zelst, James Gardner, and Greg Steele. The 802.11n MIMO-OFDM Standard for Wireless LAN and Beyond. *Wirel. Pers. Commun.*, 37(3-4):445–453, 2006. ISSN 0929-6212. doi: http://dx.doi.org/10.1007/s11277-006-9073-2.

[162] T.K. Paul and T. Ogunfunmi. Wireless LAN comes of age: Understanding the IEEE 802.11n amendment. *IEEE Circuits and Systems Magazine*, 8(1): 28–54, Quarter 2008. ISSN 1531-636X. doi: 10.1109/MCAS.2008.915504.

[163] IEEE. Standard 802.16e-2005. http://standards.ieee.org/getieee802/download/802.16e-2005.pdf, Feb. 2006.

[164] IEEE. Standard 802.16-2009. http://ieeexplore.ieee.org.globalproxy.cvt.dk/servlet/opac?punumber=5062428, May 2009.

[165] Koon Hoo Teo, Zhifeng Tao, and Jinyun Zhang. The mobile broadband WiMAX standard [standards in a nutshell]. *IEEE Signal Processing Mag*, 24(5):144–148, Sept. 2007. ISSN 1053-5888. doi: 10.1109/MSP.2007.904740.

[166] Steven J. Vaughan-Nichols. Achieving wireless broadband with WiMAX. *Computer*, 37(6):10–13, 2004. ISSN 0018-9162. doi: http://doi.ieeecomputersociety.org/10.1109/MC.2004.4.

[167] Steven J. Vaughan-Nichols. Mobile WiMAX: The next wireless battle ground. *Computer*, 41(6):16–18, 2008. ISSN 0018-9162. doi: http://doi.ieeecomputersociety.org/10.1109/MC.2008.201.

[168] D. Astely, E. Dahlman, A. Furuskar, Y. Jading, M. Lindstrom, and S. Parkvall. LTE: the evolution of mobile broadband. *IEEE Commun. Mag.*, 47(4): 44–51, April 2009. ISSN 0163-6804. doi: 10.1109/MCOM.2009.4907406.

[169] A. Furuskar, T. Jonsson, and M. Lundevall. The LTE radio interface - key characteristics and performance. In *Proc. IEEE 19th. International Symposium on Personal, Indoor and Mobile Radio Communications (PIMRC)*, pages 1–5, Sept. 2008. doi: 10.1109/PIMRC.2008.4699492.

[170] Darren McQueen. The momentum behind LTE adoption [3GPP LTE]. *IEEE Commun. Mag.*, 47(2):44–45, Feb. 2009. ISSN 0163-6804. doi: 10.1109/MCOM.2009.4785379.

[171] V. Kukshya, T.S. Rappaport, H. Izadpanah, G. Tangonan, R.A. Guerrero, J.K. Mendoza, and B. Lee. Free-space optics and high-speed RF for next generation networks - propagation measurements. In *Proc. IEEE 56th. Vehicular Technology Conference (VTC)*, volume 1, pages 616 – 620, Dec. 2002. doi: 10.1109/VETECF.2002.1040418.

[172] A.M. Mahdy and J.S. Deogun. Optimizing free space optics for city-wide wireless networks. In *Proc. 6th. International Conference on Networking (ICN)*, pages 66 –66, April 2007. doi: 10.1109/ICN.2007.66.

[173] Ernesto Ciaramella, Yoshinori Arimoto, Giampiero Contestabile, Marco Presi, Antonio D'Errico, Vincenzo Guarino, and Mitsuji Matsumoto. 1.28 Terabit/s (32x40 Gbit/s) WDM transmission over a double-pass free space optical link. In *Proc. Optical Fiber Communication Conference (OFC)*. Optical Society of America, 2009. URL http://www.opticsinfobase.org/abstract.cfm?URI=OFC-2009-OMN7. Paper OMN7.

[174] Homayoun Nikookar and Ramjee Prasad. UWB regulation. In *Introduction to Ultra Wideband for Wireless Communications*, pages 163–171. Springer Netherlands, 2008. doi: 10.1007/978-1-4020-6633-7_10.

[175] B. Allen, T. Brown, K. Schwieger, E. Zimmermann, W. Malik, D. Edwards, L. Ouvry, and I. Oppermann. Ultra wideband: Applications, technology and future perspectives. In *Proc. International Workshop on Convergent Technologies (IWCT)*. Citeseer, 2005.

[176] Copps and Martin. Revision of part 15 of the commission's rules regarding ultra-wideband transmission systems. Technical report, Federal Communications Commission, Washington, D.C., April 2002. URL http://www.fcc.gov/Bureaus/Engineering_Technology/Orders/2002/fcc02048.pdf. ET-Docket 98-153, FCC02-48.

[177] ETSI. EN 302 065 v 1.1.1: Harmonized european standard for UWB communications, Feb. 2008.

[178] ECMA. ECMA-368: High rate ultra wideband PHY and MAC standard. http://www.ecma-international.org/publications/files/ECMA-ST/ECMA-368.pdf, Geneva, Switzerland, Dec. 2008.

[179] ECMA. ECMA-369: MAC-PHY interface for ECMA-368. http://www.ecma-international.org/publications/files/ECMA-ST/ECMA-369.pdf, Geneva, Switzerland, Dec. 2008.

[180] ISO/IEC. Standard 26907. http://www,iso.org, Geneva, Switzerland, Nov. 2009.

[181] IEEE. Standard 802.16-2004. http://standards.ieee.org/getieee802/download/802.16-2004.pdf, Oct. 2004.

[182] IEEE. Standard 802.16j-2009. http://ieeexplore.ieee.org.globalproxy.cvt.dk/servlet/opac?punumber=5167146, June 2009.

[183] A. Goldsmith, S.A. Jafar, N. Jindal, and S. Vishwanath. Capacity limits of MIMO channels. *IEEE J. Sel. Areas Commun.*, 21(5):684–702, June 2003. ISSN 0733-8716. doi: 10.1109/JSAC.2003.810294.

[184] J.H. Winters. Smart antennas for wireless systems. *IEEE Pers. Commun.*, 5(1):23–27, Feb 1998. ISSN 1070-9916. doi: 10.1109/98.656155.

[185] D. Gesbert, M. Shafi, Da-Shan Shiu, P.J. Smith, and A. Naguib. From theory to practice: an overview of MIMO space-time coded wireless systems. *IEEE J. Sel. Areas Commun.*, 21(3):281–302, Apr 2003. ISSN 0733-8716. doi: 10.1109/JSAC.2003.809458.

[186] Arogyaswami Paulraj, Dhananjay Gore, Rohit Nabar, and Helmut Bölcskei. An overview of MIMO communications - a key to gigabit wireless. *Proc. IEEE*, 92(2):198–218, Feb 2004. ISSN 0018-9219. doi: 10.1109/JPROC.2003.821915.

[187] E. Ackerman, S. Wanuga, D. Kasemset, A.S. Daryoush, and N.R. Samant. Maximum dynamic range operation of a microwave external modulation fiber-optic link. *IEEE Trans. Microw. Theory Tech.*, 41(8):1299–1306, Aug. 1993. ISSN 0018-9480. doi: 10.1109/22.241670.

[188] A.S. Daryoush, E. Ackerman, N.R. Samant, S. Wanuga, and D. Kasemset. Interfaces for high speed fiber-optic links: analysis and experiment. *IEEE Trans. Microw. Theory Tech.*, 39(12):2031–2044, Dec. 1991. ISSN 0018-9480. doi: 10.1109/22.106543.

[189] Charles H. Cox, III, Edward I. Ackerman, Gary E. Betts, and Joelle E. Prince. Limits on the performance of RF-over-fiber links and their impact on device design. *IEEE Trans. Microw. Theory Tech.*, 54(2):906–920, Feb. 2006. doi: 10.1109/TMTT.2005.863818.

[190] Charles H. Cox, III, Edward I. Ackerman, and Gary E. Betts. Some limits on the performance of an analog optical link. In *Proc. International Topical Meeting on Microwave Photonics (MWP)*, pages 33–36, Dec 1996. doi: 10.1109/MWP.1996.662060.

[191] C.H. Cox, III, E. Ackerman, R. Helkey, and G.E. Betts. Techniques and performance of intensity-modulation direct-detection analog optical links. *IEEE Trans. Microw. Theory Tech.*, 45(8):1375–1383, Aug 1997. ISSN 0018-9480. doi: 10.1109/22.618439.

[192] Charles H. Cox, III, Edward I. Ackerman, Gary E. Betts, and Joelle L. Prince. Corrections to "Limits on the performance of RF-over-fiber links and their impact on device design". *IEEE Trans. Microw. Theory Tech.*, 55 (2):351–351, Feb. 2007. ISSN 0000-0000. doi: 10.1109/TMTT.2006.890072.

[193] Kamau Prince, Alexey V. Osadchiy, and I. Tafur Monroy. WiMAX radio-on-fibre in 118-km long-reach PON with deployed fibre. In *Proc. 35th. European Conference on Optical Communication (ECOC)*, Vienna, Austria, September 2009. Paper 2.4.1.

[194] Kamau Prince, Alexey V. Osadchiy, and Idelfonso Tafur Monroy. Full-duplex transmission of 256-QAM WiMAX signals over an 80-km long-reach PON. In *Proc. 22nd. Annual Mtg of the IEEE Photonics Society*, Belek-Antalya, Turkey, Oct. 2009. Paper WS1.

[195] Alexey V. Osadchiy, Kamau Prince, and Idelfonso Tafur Monroy. Converged delivery of WiMAX and wireline services over an extended reach passive optical access network. *Optical Fiber Technology*, 16 (3):182 – 186, April 2010. ISSN 2009.11.09. doi: 10.1016/j.yofte.

2010.02.009. URL http://www.sciencedirect.com/science/article/B6WP0-4YS6PC0-1/2/202df28d4a661433e5ba1396bfa937a3.

[196] Agilent Application note. Using error vector magnitude measurements to analyze and troubleshoot vector modulated signals: PN 89400-14. http://cp.literature.agilent.com/litweb/pdf/5965-2898E.pdf, Oct. 2000. Product Note.

[197] Agilent Application note. Intermodulation distortion (IMD) measurements: Scorpion option 3. http://www.us.anritsu.com/downloads/files/IMDanREVc.pdf, Morgan Hill, CA, USA, April 2000.

[198] Agilent Application note. Intermodulation distortion (IMD) measurements: Using the 37300 series vector network analyzer. http://www.us.anritsu.com/downloads/files/11410-00257a.pdf, Morgan Hill, CA, USA, Sept. 2000.

[199] G. Agrawal. *Fiber-Optic Communication Systems*, chapter 2, pages 23–72. John Wiley & Sons, Inc., 2002.

[200] X.N. Fernando and A. Anpalagan. On the design of optical fiber based wireless access systems. In *Proc. IEEE International Conference on Communications (ICC)*, volume 6, pages 3550–3555, Paris, France, June 2004. doi: 10.1109/ICC.2004.1313205.

[201] Anthony Ng'oma. *Radio-over-Fibre Technology for Broadband Wireless Communication Systems*. Doctoral thesis, Tech. Univ. Eindhoven, June 2005. URL http://alexandria.tue.nl/extra2/200512106.pdf.

[202] Andreas Wiberg. *Generation, Modulation, and Detection of Signals in Microwave Photonic Systems*. Doctoral thesis, Chalmers University of Technology, Department of Microtechnology and Nanoscience, Photonics, March 2008.

[203] T. Koonen. Fiber to the home/fiber to the premises: What, where, and when? *Proc. IEEE*, 94(5):911–934, May 2006. ISSN 0018-9219. doi: 10.1109/JPROC.2006.873435.

[204] Christina Lim, Ampalavanapillai Nirmalathas, Dalma Novak, Rod Waterhouse, and Gideon Yoffe. Millimeter-wave broad-band fiber-wireless system

incorporating baseband data transmission over fiber and remote LO delivery. *J. Lightwave Technol.*, 18(10):1355, 2000. URL http://jlt.osa.org/abstract.cfm?URI=JLT-18-10-1355.

[205] R. Hofstetter, H. Schmuck, and R. Heidemann. Dispersion effects in optical millimeter-wave systems using self-heterodyne method for transport and generation. *IEEE Trans Microw Theory Tech*, 43(9):2263–2269, Sep 1995. ISSN 0018-9480. doi: 10.1109/22.414574.

[206] E. Vourc'h, B. Della, D. Le Berre, and D. Herve. Millimeter-wave power-fading compensation for wdm fiber-radio transmission using a wavelength-self-tunable single-sideband filter. *IEEE Trans. Microw. Theory Tech.*, 50 (12):3009–3015, Dec. 2002. ISSN 0018-9480. doi: 10.1109/TMTT.2002.805167.

[207] U. Gliese, S. Norskov, and T.N. Nielsen. Chromatic dispersion in fiber-optic microwave and millimeter-wave links. *IEEE Trans. Microw. Theory. Tech.*, 44(10):1716–1724, Oct 1996. ISSN 0018-9480. doi: 10.1109/22.538964.

[208] H. Schmuck. Effect of polarisation-mode-dispersion in fibre-optic millimetre-wave systems. *Electronics Letters*, 30(18):1503–1504, Sep 1994. ISSN 0013-5194.

[209] K. J. Williams and R. D. Esman. Stimulated brillouin scattering for improvement of microwave fibre-optic link efficiency. *Electronics Letters*, 30 (23):1965 –1966, Nov. 1994. ISSN 0013-5194.

[210] M.J. LaGasse, W. Charczenko, M.C. Hamilton, and S. Thaniyavarn. Optical carrier filtering for high dynamic range fibre optic links. *Electronics Letters*, 30(25):2157 –2158, Dec. 1994. ISSN 0013-5194.

[211] M. Attygalle, C. Lim, G.J. Pendock, A. Nirmalathas, and G. Edvell. Transmission improvement in fiber wireless links using fiber bragg gratings. *IEEE Photon. Technol. Lett.*, 17(1):190 –192, January 2005. ISSN 1041-1135. doi: 10.1109/LPT.2004.836901.

[212] K. Kitayama and H. Sotobayashi. Fading-free fiber-optic transport of 60 GHz-optical DSB signal by using in-line phase conjugator. In *Technical Digest, Optical Fiber Communication Conference & the International Conference on Integrated Optics and Optical Fiber Communication (OFC/IOOC)*, volume 2, pages 64 –66, 1999. doi: 10.1109/OFC.1999.766337.

[213] H. Toda, T. Yamashita, T. Kuri, and K. Kitayama. Demultiplexing using an arrayed-waveguide grating for frequency-interleaved DWDM millimeter-wave radio-on-fiber systems. *J. Lightwave Technol.*, 21(8):1735–1741, Aug. 2003. ISSN 0733-8724. doi: 10.1109/JLT.2003.815650.

[214] Ming-Tuo Zhou, Qi Je Wang, Yan Zhang, Y. Zhang, Y.C. Soh, and M. Fujise. Cost-effective optical modulation depth enhancement and optical carrier recovery in millimeter-wave fiber-wireless links using an all-fiber optical interleaver. In *Proc. International Topical Meeting on Microwave Photonics (MWP)*, pages 1 –4, Oct. 2006. doi: 10.1109/MWP.2006.346574.

[215] G.H. Smith, D. Novak, and Z. Ahmed. Overcoming chromatic-dispersion effects in fiber-wireless systems incorporating external modulators. *IEEE Trans. Microw. Theory Tech.*, 45(8):1410–1415, Aug 1997. ISSN 0018-9480. doi: 10.1109/22.618444.

[216] W. Ng, A.A. Walston, G.L. Tangonan, J.J. Lee, I.L. Newberg, and N. Bernstein. The first demonstration of an optically steered microwave phased array antenna using true-time-delay. *J. Lightwave Technol.*, 9(9):1124–1131, Sep 1991. ISSN 0733-8724. doi: 10.1109/50.85809.

[217] Jose Capmany and Dalma Novak. Microwave photonics combines two worlds. *Nature Photon.*, 1(6):319–330, June 2007. ISSN 1749-4885. URL http://dx.doi.org/10.1038/nphoton.2007.89.

[218] Vincent J. Urick. Long-haul analog links tutorial. In *Technical Digest Optical Fiber Communication Conference and Exhibit (OFC)*, San Diego, CA, USA, March 2010. Paper OML5.

[219] L. Roselli, V. Borgioni, F. Zepparelli, F. Ambrosi, M. Comez, P. Faccin, and A. Casini. Analog laser predistortion for multiservice radio-over-fiber systems. *J. Lightwave Technol.*, 21(5):1211–1223, May 2003. ISSN 0733-8724. doi: 10.1109/JLT.2003.810931.

[220] A.R. Shah and B. Jalali. Adaptive equalisation for broadband predistortion linearisation of optical transmitters. *IEE Proceedings: Optoelectronics*, 152 (1):16–32, Feb. 2005. ISSN 1350-2433. doi: 10.1049/ip-opt:20051093.

[221] Tabassam Ismail, Chin-Pang Liu, John E. Mitchell, and Alwyn J. Seeds. High-dynamic-range wireless-over-fiber link using feedforward linearization.

J. Lightwave Technol., 25(11):3274–3282, 2007. URL http://jlt.osa.org/abstract.cfm?URI=JLT-25-11-3274.

[222] G.E. Betts and F.J. O'Donnell. Microwave analog optical links using suboctave linearized modulators. *IEEE Photon. Technol. Lett.*, 8(9):1273 –1275, Sept. 1996. ISSN 1041-1135. doi: 10.1109/68.531860.

[223] Adil Karim and Jason Devenport. High dynamic range microwave photonic links for RF signal transport and RF-IF conversion. *J. Lightwave Technol.*, 26(15):2718–2724, 2008. URL http://jlt.osa.org/abstract.cfm?URI=JLT-26-15-2718.

[224] X.N. Fernando and A.B. Sesay. A hammerstein type equalizer for the wiener type fiber-wireless channel. In *Proc. IEEE Pacific Rim Conference on Communications, Computers and Signal Processing (PACRIM)*, volume 2, pages 546–549, Victoria, BC, Canada, Aug. 2001. doi: 10.1109/PACRIM.2001.953691.

[225] R.E. Schuh. Hybrid fiber radio for second and third generation wireless systems. In *Proc. International Topical Meeting on Microwave Photonics (MWP)*, volume 1, pages 213–216, 1999. doi: 10.1109/MWP.1999.819688.

[226] Nathan J. Gomes, Maria Morant, Arokiaswami Alphones, Béatrice Cabon, John E. Mitchell, Christophe Lethien, Mark Csörnyei, Andreas Stöhr, and Stavros Iezekiel. Radio-over-fiber transport for the support of wireless broadband services (Invited). *J. Opt. Netw.*, 8(2):156–178, 2009. URL http://jon.osa.org/abstract.cfm?URI=JON-8-2-156.

[227] K.-A. Persson, C. Carlsson, A. Alping, A. Haglund, J.S. Gustavsson, P. Modh, and A. Larsson. WCDMA radio-over-fibre transmission experiment using singlemode VCSEL and multimode fibre. *Electron. Lett.*, 42(6): 372–374, March 2006. ISSN 0013-5194. doi: 10.1049/el:20064130.

[228] K. Fang, M.J. Crisp, F. Yang, R.V. Penty, and I.H. White. Demonstration of distributed antenna system using optical multicast radio-over-fibre links. In *Proc. International Topical Meeting on Microwave Photonics (MWP)*, pages 1–4, Oct. 2009.

[229] Francisca Martínez, Jaime Campos, Antonio Ramírez, Valentín Polo, Alejandro Martínez, David Zorrilla, and Javier Martí. Transmission of IEEE

802.16d WiMAX signals over radio-over-fibre IMDD links. In *Proc. 5th International Conference on Wired/Wireless Internet Communications (WWIC)*, Coimbra, Portugal, May 2007.

[230] Navid Ghazisaidi, Francesco Paolucci, and Martin Maier. SuperMAN: Optical-wireless integration of RPR and WiMAX. *J. Opt. Netw.*, 8(3):249–271, 2009. URL http://jon.osa.org/abstract.cfm?URI=JON-8-3-249.

[231] F. Smyth and L. P. Barry. Overcoming distortion limitations in hybrid radio/photonic systems for the distribution of WCDMA signals. *Electrical Engineering (Archiv fur Elektrotechnik)*, 85(4):191–194, Sept. 2003. doi: 10.1007/s00202-003-0162-x.

[232] Chia-Kai Weng, Yu-Min Lin, and Winston I. Way. Radio-over-fiber 16-QAM, 100-km transmission at 5 Gb/s using DSB-SC transmitter and remote heterodyne detection. *J. Lightwave Technol.*, 26(6):643–653, March 2008.

[233] Jesper Bevensee Jensen, Roberto Rodes, Antonio Caballero, Xianbin Yu, Timothy Braidwood Gibbon, and Idelfonso Tafur Monroy. 4 Gbps impulse radio (IR) ultra-wideband (UWB) transmission over 100 meters multi mode fiber with 4 meters wireless transmission. *Optics Express*, 17(19):16898–16903, 2009. URL http://www.opticsexpress.org/abstract.cfm?URI=oe-17-19-16898.

[234] M. Morant, J. Perez, R. Llorente, and J. Marti. Combined analysis of OFDM-UWB transmission in hybrid wireless-optical access networks. *IEEE Photon. Technol. Lett.*, 21(19):1378 –1380, Oct. 2009. ISSN 1041-1135. doi: 10.1109/LPT.2009.2026182.

[235] Ignacio González Insua, Dirk Plettemeier, and Christian G. Schäffer. Broadband radio-over-fiber-based wireless access with 10 gbits/s data rates. *J. Opt. Netw.*, 8(1):77–83, 2009. URL http://jon.osa.org/abstract.cfm?URI=JON-8-1-77.

[236] Ignacio González Insua, Dirk Plettemeier, and Christian G. Schäffer. Simple remote heterodyne rof system for Gbps wireless access. In *Proc. International Topical Meeting on Microwave Photonics (MWP)*, Oct. 2009.

[237] Su Khiong Yong and Chia-Chin Chong. An overview of multigigabit wireless through millimeter wave technology: Potentials and technical challenges. *EURASIP Journal on Wireless Communications and Networking*, 2007, 2007. Article ID 78907.

[238] R.C. Daniels and R.W. Heath. 60 GHz wireless communications: emerging requirements and design recommendations. *IEEE Vehicular Technology Magazine*, 2(3):41–50, Sept. 2007. ISSN 1556-6072. doi: 10.1109/MVT.2008.915320.

[239] A. Ng'oma, M. Sauer, F. Annunziata, Wen-Jr Jiang, Po-Tsung Shih, Chun-Ting Lin, Jyehong Chen, and Sien Chi. 14 Gbps 60 GHz RoF link employing a simple system architecture and OFDM modulation. In *Proc. International Topical Meeting on Microwave Photonics (MWP)*, pages 1–4, Oct. 2009.

[240] Anthony Ng'oma, Po-Tsung Shih, Jacob George, Frank Annunziata, Michael Sauer, Chun-Ting Lin, Wen-Jr Jiang, Jyehong Chen, and Sien Chi. 21 Gbps OFDM wireless signal transmission at 60 GHz using a simple IMDD radio-over-fiber system. In *Technical Digest Optical Fiber Communication Conference and Exhibit (OFC)*, San Diego, CA, USA, March 2010. Paper OTuF4.

[241] Devang Parekh, Weijian Yang, Anthony Ng'Oma, Davide Fortusini, Michael Sauer, Seldon Benjamin, Werner Hofmann, Markus C. Amann, and Connie J. Chang-Hasnain. Multi-Gbps ASK and QPSK-modulated 60 GHz rof link using an optically injection locked VCSEL. In *Technical Digest Optical Fiber Communication Conference and Exhibit (OFC)*, San Diego, CA, USA, March 2010. Paper OTuF5.

[242] Hyun-Seung Kim, Yong-Yuk Won, Yong-Hwan Son, and Sang-Kook Han. Full colorless WDM-RoF system with simultaneous transmission of 63-GHz and baseband 1.25-Gbps data by sideband separation. In *Technical Digest Optical Fiber Communication Conference and Exhibit (OFC)*, San Diego, CA, USA, March 2010. Paper OThO2.

[243] Benoît Charbonnier, Frédéric Lecoche, Mario Weiß, Andreas Stöhr, F. van Dijk, A. Enard, F. Blache, M. Goix, F. Mallecot, D.G. Moodie, A. Borghesani, and C.W.Ford. Ultra-wideband radio-over-fiber techniques and networks. In *Technical Digest Optical Fiber Communication Conference and Exhibit (OFC)*, San Diego, CA, USA, March 2010. Paper OThO3.

[244] T. Nagatsuma and A. Hirata. 10-Gbit/s wireless link technology using the 120-GHz band. *NTT Technical Review*, 2(11):58–62, 2004.

[245] A. Hirata, T. Kosugi, H. Takahashi, R. Yamaguchi, F. Nakajima, T. Furuta, H. Ito, H. Sugahara, Y. Sato, and T. Nagatsuma. 120-GHz-band millimeter-wave photonic wireless link for 10-Gb/s data transmission. *IEEE Trans. Microw. Theory Tech.*, 54(5):1937–1944, May 2006. ISSN 0018-9480. doi: 10.1109/TMTT.2006.872798.

[246] T. Nagatsuma, H.-J. Song, Y. Fujimoto, K. Miyake, A. Hirata, K. Ajito, A. Wakatsuki, T. Furuta, N. Kukutsu, and Y. Kado. Giga-bit wireless link using 300–400 GHz bands. In *Proc. International Topical Meeting on Microwave Photonics (MWP)*, pages 1–4, Oct. 2009.

[247] A. Martinez, V. Polo, and J. Marti. Simultaneous baseband and RF optical modulation scheme for feeding wireless and wireline heterogeneous access networks. *IEEE Trans. Microw. Theory Tech.*, 49(10):2018–2024, Oct 2001. ISSN 0000-0000. doi: 10.1109/22.954824.

[248] Chun-Ting Lin, Jason Jyehong Chen, Peng-Chun Peng, Cheng-Feng Peng, Wei-Ren Peng, Bi-Shiou Chiou, and Sien Chi. Hybrid optical access network integrating fiber-to-the-home and radio-over-fiber systems. *IEEE Photon. Technol. Lett.*, 19(8):610–612, Apr 2007. ISSN 1041-1135. doi: 10.1109/LPT.2007.894326.

[249] H. Kosek, Yifeng He, Xijia Gu, and X.N. Fernando. All-optical demultiplexing of WLAN and Cellular CDMA Radio Signals. *J. Lightwave Technol.*, 25 (6):1401 –1409, June 2007. ISSN 0733-8724. doi: 10.1109/JLT.2007.896767.

[250] K. Ikeda, T. Kuri, and K. Kitayama. Simultaneous three-band modulation and fiber-optic transmission of 2.5-Gb/s baseband, microwave-, and 60-GHz-band signals on a single wavelength. *J. Lightwave Technol.*, 21(12):3194–3202, Dec 2003. ISSN 0733-8724. doi: 10.1109/JLT.2003.821739.

[251] H. Le Bras and M. Moignard. Distribution of 3G base stations on passive optical network architecture. In *Proc. Int'l Topical Meeting on Microwave Photonics (MWP)*, pages 1 –4, Oct. 2006. doi: 10.1109/MWP.2006.346567.

[252] Zhensheng Jia, Jianjun Yu, Yu-Ting Hsueh, A. Chowdhury, Hung-Chang Chien, J.A. Buck, and Gee-Kung Chang. Multiband signal generation and

dispersion-tolerant transmission based on photonic frequency tripling technology for 60-GHz radio-over-fiber systems. *IEEE Photon. Technol. Lett.*, 20(17):1470 –1472, Sept. 2008. ISSN 1041-1135. doi: 10.1109/LPT.2008.927901.

[253] M. Chacinski, A. Djupsjobacka, U. Westergren, R. Schatz, P.-Y. Fonjallaz, E. Tipsuwannakul, and E. Udvary. 400km transmission of STM-16 data on baseband and DVBT on 40GHz subcarrier. In *Proc. International Conference on Telecommunications (ICT)*, pages 1 –3, june 2008. doi: 10.1109/ICTEL.2008.4652670.

[254] I.H. White, R.V. Penty, M. Crisp, and S. Sabesan. Wideband wireless over fiber systems. In *Technical Digest Optical Fiber Communication Conference and Exhibit (OFC)*, San Diego, CA, USA, March 2010. Paper OTuF1.

[255] J. Perez, M. Morant, R. Llorente, and J. Marti. Joint distribution of polarization-multiplexed UWB and WiMAX Radio in PON. *J. Lightwave Technol.*, 27(12):1912 –1919, June 2009. ISSN 0733-8724. doi: 10.1109/JLT.2009.2022342.

[256] Eli Kapon and Alexei Sirbu. Long-wavelength VCSELs: Power-efficient answer. *Nature Photon.*, 3(1), Jan 2009. doi: 10.1038/nphoton.2008.266. URL http://dx.doi.org/10.1038/nphoton.2008.266.

[257] F. Koyama. Recent advances of VCSEL photonics. *J. Lightwave Technol.*, 24 (12):4502–4513, Dec. 2006. ISSN 0733-8724. doi: 10.1109/JLT.2006.886064.

[258] Pierpaolo Boffi, Anna Boletti, Alberto Gatto, and Mario Martinelli. VCSEL to VCSEL injection locking for uncompensated 40-km transmission at 10 Gb/s. In *Technical Digest Optical Fiber Communication Conference and Exhibit (OFC)*. Optical Society of America, 2009. URL http://www.opticsinfobase.org/abstract.cfm?URI=OFC-2009-JThA32. Paper JThA32.

[259] Bo Zhang, Xiaoxue Zhao, Louis Christen, Devang Parekh, Werner Hofmann, Ming C. Wu, Markus C. Amann, Connie J. Chang-Hasnain, and Alan E. Willner. Adjustable chirp injection-locked 1.55-μm VCSELs for enhanced chromatic dispersion compensation at 10-Gbit/s. In *Proc. OFC*, page OWT7. Optical Society of America, 2008. URL http://www.opticsinfobase.org/abstract.cfm?URI=OFC-2008-OWT7.

[260] Xiaoxue Zhao, Bo Zhang, Louis Christen, Devang Parekh, Werner Hofmann, Markus C. Amann, Fumio Koyama, Alan E. Willner, and Connie J. Chang-Hasnain. Greatly increased fiber transmission distance with an optically injection-locked vertical-cavity surface-emitting laser. *Opt. Express*, 17(16): 13785–13791, 2009. URL http://www.opticsexpress.org/abstract.cfm?URI=oe-17-16-13785.

[261] GigaWaM website. URL http://www.gigawam.com/, March 2010.

[262] Timothy Braidwood Gibbon, Kamau Prince, C. Neumeyr, E. Rönneberg, M. Ortsiefer, and I Tafur Monroy. 10 Gb/s 1550 nm VCSEL transmission over 23.6 km single mode fiber with no dispersion compensation and no injection locking for WDM PONs. In *Proc. Optical Fiber Communication/-National Fiber Optic Engineers Conference (OFC/NFOEC)*, San Diego, CA, USA, March 2010. Paper JThA30.

[263] Kamau Prince, Ming Ma, Timothy Braidwood Gibbon, and Idelfonso Tafur Monroy. Demonstration of 10.7-gb/s transmission in 50-km pon with uncooled free-running 1550-nm vcsel. In *Proc. Conference on Lasers and Electro-Optics and Quantum Electronics and Laser Science (CLEO/QELS)*, May 2010. Paper ATuA2.

[264] B. Allen, S.A. Ghorashi, and M. Ghavarm. A review of pulse design for impulse radio. In *Proc. IEE Seminar on Ultra Wideband Communications Technologies and System Design*, pages 93 – 97, July 2004.

[265] Victor Torres-Company, Kamau Prince, and I. Tafur Monroy. Fiber transmission and generation of ultrawideband pulses by direct current modulation of semiconductor lasers and chirp-to-intensity conversion. *Virtual Journal of Ultrafast Science*, 7(3), March 2008. doi: 10.1364/OL.33.000222. Source: Opt. Lett. **33**, 222 (2008).

[266] Victor Torres-Company, Kamau Prince, Xianbin Yu, Timothy Braidwood Gibbon, and I Tafur Monroy. Ultrawideband-over-fiber technologies with directly-modulated semiconductor lasers. In Christophe Lethien, editor, *Optical fibre, new developments*, chapter 17, pages 407–424. INTEH, 2009. ISBN 978-953-7619-50-3.

[267] Alwyn Seeds. Optical technologies for phased array antennas. *IEICE Transactions on Electronics*, 76(2):198–206, 1993.

[268] B. Vidal, D. Madrid, J.L. Corral, V. Polo, A. Martinez, J.H. den Besten, F. Soares, J. Marti, and M.K. Smit. Photonic true-time delay beamformer for broadband wireless access networks at 40 GHz band. *IEEE MTT-S International Microwave Symposium Digest*, 3:1949–1952, 2002. doi: 10.1109/MWSYM.2002.1012246.

[269] E.N. Toughlian and H. Zmuda. A photonic variable RF delay line for phased array antennas. *J. Lightw. Technol.*, 8(12):1824–1828, Dec 1990. ISSN 0733-8724. doi: 10.1109/50.62877.

[270] National Instruments. Modulation error ratio (MER) and error vector magnitude (EVM). http://zone.ni.com/devzone/cda/tut/p/id/3652, 2008.

[271] Kamau Prince, Andrea Chiuchiarelli, Marco Presi, I. Tafur Monroy, and Ernesto Ciaramella. All-optical delay technique for supporting multiple antennas in a hybrid optical - wireless transmission system. In *Proc. 21st Ann. Mtg. of IEEE Lasers & Electro-Optics Society (LEOS)*, pages 85–86, Newport Beach, CA, USA, Nov. 2008. doi: 10.1109/LEOS.2008.4688500. Paper MJ3.

[272] M. Presi, K. Prince, A. Chiuchiarelli, I. Cerutti, G. Contestabile, I. Tafur Monroy, and E. Ciaramella. Adaptive antenna system for OFDMA WiMAX radio-over-fiber links using a directly modulated R-SOA and optical filtering. In *Proc. Optical Fiber Communication/National Fiber Optic Engineers Conference (OFC/NFOEC)*, San Diego, CA, USA, March 2009. JWA74.

[273] I. Tafur Monroy, Kamau Prince, Jorge Seoane, and Xianbin Yu. Optically envelope detected QAM and QPSK RF modulated signals in hybrid wireless-fiber systems. *Microwave and Optical Technology Letters*, 51(3):864–866, March 2009. doi: 10.1002/mop.24182.

[274] CPRI. URL http://www.cpri.info/, March 2010.

[275] A. Nirmalathas, P. Gamage, C. Lim, D. Novak, R. Waterhouse, and Yizhuo Yang. Digitized RF transmission over fiber. *IEEE Microw. Mag.*, 10(4): 75–81, June 2009. ISSN 1527-3342. doi: 10.1109/MMM.2009.932284.

[276] A. Nirmalathas, P.A. Gamage, Yizhuo Yang, C. Lim, D. Novak, and R. Waterhouse. Cost-effective optical backhaul for broadband wireless. In *IEEE*

LEOS Annual Meeting Conference Proceedings (LEOS), pages 440–441, Belek-Antalya, Turkey, Oct. 2009. doi: 10.1109/LEOS.2009.5343211.

[277] J.E. Mitchell. Radio over fibre networks: Advances and challenges. In *Proc. 35th. European Conference on Optical Communication (ECOC)*, pages 1 –4, Vienna, Austria, Sept. 2009. Paper 2.4.5.